UNIVERSITY OF SOUTHAMPTON

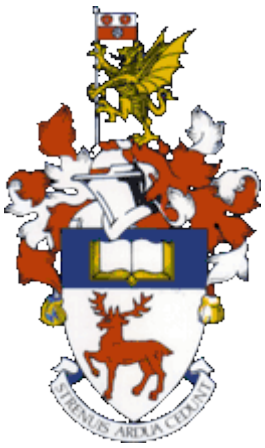

Environmental effects on the physiology of calcification in the Pacific oyster *Crassostrea gigas* Thunberg, 1793

by

FRAUKE BAGUSCHE

A thesis submitted in partial fulfilment for the degree of

Doctor of Philosophy

in the

Faculty of Natural and Environmental Sciences

School of Ocean and Earth Science

February 2013

“It always seems impossible until it’s done”

Nelson Mandela

TO MY FAMILY

UNIVERSITY OF SOUTHAMPTON

Abstract

FACULTY OF NATURAL AND ENVIRONMENTAL SCIENCES

SCHOOL OF OCEAN AND EARTH SCIENCE

Doctor of Philosophy

ENVIRONMEMTAL EFFECTS ON THE PHYSIOLOGY OF CALCIFICATION IN THE PACIFIC OYSTER *CRASSOSTREA GIGAS* THUNBERG, 1793

by Frauke Bagusche

The aim of this study was to investigate the impacts of ocean warming and CO_2-driven ocean acidification on biomineralisation of the Pacific oyster *Crassostrea gigas* during ontogeny. Changing environmental conditions have been found to impact development of marine calcifiers such as bivalves. As a commercially important bivalve species harvested worldwide and supporting a global industry, development of the Pacific oyster may be at risk. Thus, it is important to fully understand the physiology of calcification of *C. gigas* during ontogeny, from a molecular to mineralogical level.

Two *in vivo* lab experiments were designed to study growth of *C. gigas* under future ocean scenarios. The first experiment was performed to test the effects of low pH (pH 7.5) on development of adult and juvenile *C. gigas*. It was shown that growth of juveniles and adults was significantly retarded at low pH compared to the control (pH 8.3). Quantitative real-time PCR analyses revealed a significant effect of low pH on gene expression of the biomineralisation-related genes *CGCam*, *CGPerl* and *CGMG4*, suggesting a possible reduction in Ca-binding activity and $CaCO_3$ precipitation, which ultimately could result in retarded shell growth. With the second experiment the effects of pH (pH 8.1 & pH 7.4) and temperature (20°C & 24 °C) and their synergistic effects on larval development were investigated including shell growth, gene expression and shell mineralogy. Though $CaCO_3$ polymorph precipitation was not affected, regardless of pH and temperature, significant effects on the expression of *CGCam*, *CGPerl, CGDent* and *CGMG4*, shell structure and crystal disorder were observed. Even though elevated temperature seemed to diminish the effects of low pH in terms of shell size, Fourier Transform Infrared spectroscopy revealed an increase in crystal disorder, indicated by higher ν_2/ν_4 ratios and lower FWHM values, which may lead to an increase in shell dissolution. Using scanning electron microscopy it was shown that larval shells at 24°C pH 7.4 showed the greatest signs of dissolution and increased malformations, supporting the results of the FTIR analyses. Significant differences in gene expression levels were identified, specific for each gene of interest and developmental stage.

This study demonstrates that the effects of temperature and pH, alone and in combination, have overall negative effects on *C. gigas* development, based on decreased growth rates, increased mineral disorder and altered gene expression of skeletogenesis-related genes. Under the conditions of this experiment, low pH is a greater single stressor than high temperature, whereas the combination of these two factors produces greater changes in physiology and shell properties in *C. gigas* than each of the factors alone. Impaired shell growth including corrosions, malformations and increased mineral disorder are likely to jeopardise the survival of larvae and may lead to reductions in both natural and commercial oyster populations.

Table of Contents

List of Figures

List of Figures

List of Tables

Declaration of Authorship

I, FRAUKE BAGUSCHE, declare that the thesis entitled "Environmental effects on the physiology of calcification in the Pacific oyster *Crassostrea gigas* Thunberg, 1793" and the work presented in the thesis are both my own, and have been generated by me as the result of my own original research. I confirm that:

- This work was done wholly or mainly while in candidature for a research degree at this University
- Where any part of this thesis has previously been submitted for a degree or any other qualification at this University or any other institution, this has been clearly stated
- Where I have consulted the published work of others, this is always clearly attributed
- Where I have quoted from the work of others, the source is always given. With the exception of such quotations, this thesis is entirely my own work
- I have acknowledged all main sources of help
- Where the thesis is based on work done by myself jointly with others, I have made clear exactly what was done by others and what I have contributed myself
- None of this work has been published before submission

Signed: ……..

Date:…….

Acknowledgments

I would like to thank my supervisors at the National Oceanography Centre, Dr. Chris Hauton and Dr. Clive Trueman for their support throughout my Ph.D. Particular thanks is due to Dr. Chris Hauton for his personal tuition in the lab, his patience, his valuable input to get me back on track and for his thorough reviews of my writing. I couldn't have wished for a better supervisor. I would also like to thank my panel chair Dr. Sven Thatje for his support and advice.

A special thank you to my external supervisor Dr. Stéphane Pouvreau at the French Research Institute for Exploitation of the Sea (Ifremer), Station d'Argenton. I very much appreciate his input, ideas, his help with the experiments and his high spirits. I'm very grateful for the help of Pierrick LeSouchu, who never runs out of good ideas and who is the true Gyro Gearloose (Géo Trouvetou) in science. I thank the entire staff of Ifremer, Station d'Argenton for their assistance, knowledge and the good times they gave me during the duration of my experiments.

A massive thank you to Sarah Long for conducting the FTIR analyses and supplying me with spectra and support. Her involvement with my project was very valuable and of great help. Thank you to a great deal of support staff within NOCS for their time and knowledge, particularly Dr. John Gittins and Dr. Richard Pearce. Thank you to Ross Williams, Dave Spanner, and Bob and John.

Lastly, I could not have completed my project or maintained my sanity without the support and encouragement of my family and friends. Thank you to my parents for their support, financially and mentally, and to my brothers Tobias and Fabian who always cheered me up when I needed a laugh. Thank you to George who was there when times were dark and I was about to give up. Without his support I wouldn't be there where I am now. Thank you to my dear friends Hanna, Lauren, Jo and Sophie who held me up during hard times, who were there when I needed them and which whom I shared many wonderful moments. A huge thank you to Holger, who never gave up on me, supported me, listened to me, motivated me and helped me whenever he could. Due to his support I was able to rediscover my creativity and my dreams. Thank you for believing in me.
Thank you to Judith Brunson who certainly is the best landlady I've ever had.

This work was founded by the FP7 Marie Curie Initial Training Network Cal.Mar.O (http://www.calmaro.eu) and supported by the project Velyger (http://wwz.ifremer.fr/velyger).

Abbreviations

ACC	Amorphous Calcium Carbonate
ACP	Annealing Control Primer
APM	Antero-Posterior Measurement
BCM	Biologically Controlled Biomineralisation
BIM	Biologically Induced Biomineralisation
BLAST	Basic Local Alignment Search Tool
bp	Base pairs
Ca^{2+}	Calcium
$CaCO_3$	Calcium carbonate
CaM	Calmodulin
cDNA	Complementary DNA
CG18S	*Crassostrea gigas* 18S
CGAct	*Crassostrea gigas* actin
CGCaM	*Crassostrea gigas* calmodulin
CGCyclo	*Crassostrea gigas* cyclophilin
CGDent	*Crassostrea gigas* dentin
CGMG4	*Crassostrea gigas* mantle gene 4
CGPerl	*Crassostrea gigas* perlucin
CGTub	*Crassostrea gigas* tubulin
C_q	Quantitation cycle
CV	Coccolith Vesicle
DEG	Differentially Expressed Genes
DEPC	Diethyl-pyrocarbonate
DM	Dorsal Mantle
DPP	Dentin phosphoprotein
DSP	Dentin sialoprotein
DSPP	Dentin sialophosphoprotein
DVM	Dorso-Ventral Measurement
ERG	Endogenous reference gene
EST	Expressed Sequence Tag
FTIR	Fourier Transform Infrared spectroscopy
FWHM	Full Width at Half Maximum

GOI	Gene of Interest
HCO_3^-	Bicarbonate ions
IF	Inner Mantle Fold
IRC	Inter Run Calibrator
MF	Middle Mantle Fold
MIQE	Minimum standard for the provision of Information for QPCR Experiments
mRNA	Messenger RNA
NCBI	National Center for Biotechnology Information
NRQ	Normalised Relative Quantities
NTC	No Template Control
OF	Outer Mantle Fold
ORF	Open Reading Frame
PI	Prodissoconch I
PII	Prodissoconch II
PMC	Primary Mesenchyme Cells
qPCR	Quantitative real-time PCR
REF	Refractive Granulocytes
RQI	RNA Quality Indicator
RLV	Relative Linear Values
rRNA	Ribosomal RNA
SEM	Scanning Electron Microscopy
SST	Sea Surface Temperature
T-ISO	*Isochrysis* T-ISO *galbana*
VM	Ventral Mantle
XRD	X-Ray Diffraction

1 - General Introduction

"We, and the rest of life with whom we share this planet, will have to survive in the future with an ocean that is hotter, higher, and more acidic than at any time in the recent evolutionary past"

James W. Porter (2012)

Crassostrea gigas, also called Japanese oyster, Miyagi oyster, Pacific cupped oyster, or Pacific rock oyster is economically a very important oyster species and relatively easy to produce for laboratory experiments. For these reasons it has become an ideal candidate to function as a model organism for researchers investigating larval biology and development in bivalve molluscs. In the last twenty to thirty years many studies have been conducted using *C. gigas* as a model species, with a particular focus being the impacts of environmental change (including elevated pCO_2, toxins, pollutants, and hypoxia stress) on shell composition, metabolism and calcification (Almeida et al., 1998; David et al., 2010; Gazeau et al., 2007; Grangeré et al., 2009; Kurihara et al., 2007).

1.1 Biogeography & Economic Value

C. gigas is thought to have originated in Japan and was first introduced into the USA in 1903 and into France in the 1969 as a commercial species for aquaculture and as a replacement for collapsed fisheries of native and farmed oyster *Ostrea edulis* (Enríquez-Díaz et al., 2009). Today it is a cosmopolitan bivalve species and widely cultivated in more than 40 countries including Canada, US, Mexico, Argentina, Norway, Germany, the UK south to Portugal and in the Mediterranean, Japan, China, Taiwan, New Zealand, Australia, South Africa (FAO, 2012; Minchin and Gollasch, 2008). Besides these countries, *C. gigas* has been also introduced to countries such as Israel, the Philippines, Malaysia, the Seychelles, Fiji and French Polynesia (FAO, 2012) reflecting the successful survival in a broad spectrum of very different environments. *C. gigas* has been recognised in many countries such as in the Wadden Sea (North Sea) of Denmark, the Netherlands and Germany as an invasive species where it overgrows beds of the blue mussel *Mytilus edulis* turning them into oyster reefs (Diederich, 2000; Diederich et al., 2004; Minchin and Gollasch, 2008; Nehls and Büttger, 2007; Nehls et al., 2006).

In the past 60 years global aquaculture production of *Crassostrea gigas* has increased by 444% from 149163 metric tonnes (mt) in the 1950s to 662513 mt in 2010 yielding a 1 262 608 USD market value (FAO, 2012) (Figure 1). As the main producer country in Europe, France harvests annually about 150 000 mt of *C. gigas* (Nehls and Büttger, 2007).

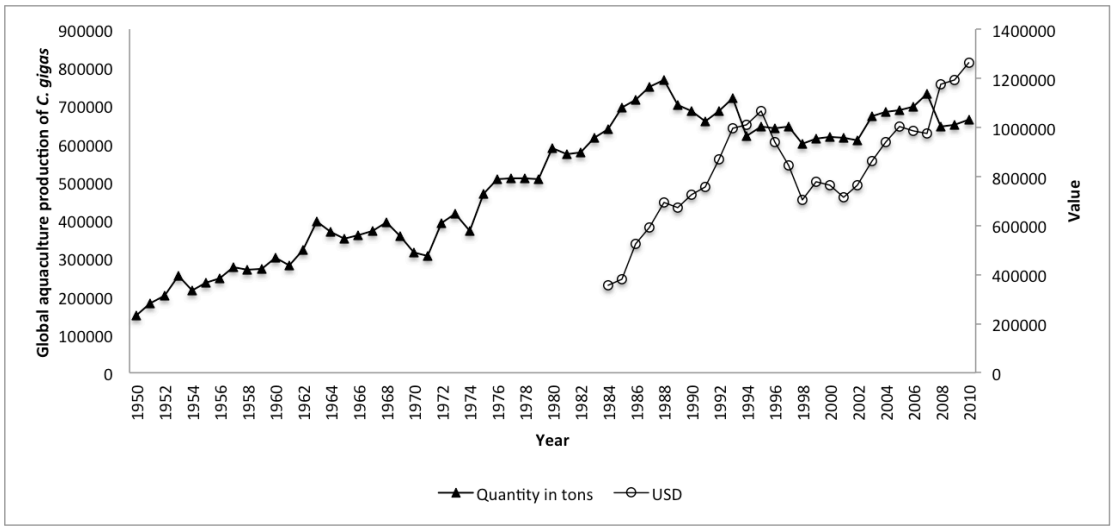

Figure 1: Global aquaculture production of *Crassostrea gigas*. Plot based on data taken from FAO Fishery Statistic (2012).

1.2 Biology & Habitat

Pacific oysters are protandrous hermaphrodites, which means that they have separate sexes but change sexes seasonally. *C. gigas* begins life as a male oyster and changes sex after a year. This change takes place after spawning during the indifferent phase of gonad development (Galtsoff, 1964). Spawning is temperature dependent and occurs if the water temperature rises above 18°C (FAO, 2012). In the natural environment gametogenesis proceeds over the winter months, accelerates in spring, and several intensive spawnings occur between July and September (Gosling, 2003). Oysters are broadcast spawners with pelagic embryonic larval stages, followed by benthic sessile adult stages. Gametes are released into the water column where they act as a trigger and activate other animals to spawn. Typically, Pacific oysters produce between 50-100 million eggs in a single spawning (FAO, 2012). After the egg has been fertilized it undergoes a spiral cleavage and within 12 h (at a given temperature of 24°C) it passes through the multi-cellular blastula and gastrula stages and transforms into a ciliated, motile planktotrophic larva- the "trochophora" (Figure 2). 20 h after fertilisation the trochophore larva develops into a swimming veliger, the "prodissoconch I" stage. This stage is also referred as D-veliger due to the distinctive D-shape of the shell (Moltschaniwskyj, 2006). Approximately 48 h after fertilisation the second larval shell "prodissoconch II" has been developed. The duration of the veliger stage varies and is affected by environmental factors such as temperature and food supply; but in *C. gigas* at 24°C it can be between 14-19 days. The swimming veliger, also called pediveliger later in its development, settles down by losing the velum, cements itself onto hard substrate, and starts its metamorphosis to become a juvenile individual, the so-called "spat".

Prodissoconch I and II are preserved during metamorphosis and integrated into the juvenile shell called "dissoconch".

Pacific oyster larvae prefer to settle onto hard or rocky surfaces in estuaries as well as in intertidal and subtidal zones up to 40 m depth. They also can also be found in sandy or muddy environments like the Wadden Sea (North Sea) attached to boulders or other bivalve shells where they can form vast oyster reefs with dense layers of shells cemented onto each other (Diederich, 2005; FAO, 2012; Nehls et al., 2006).

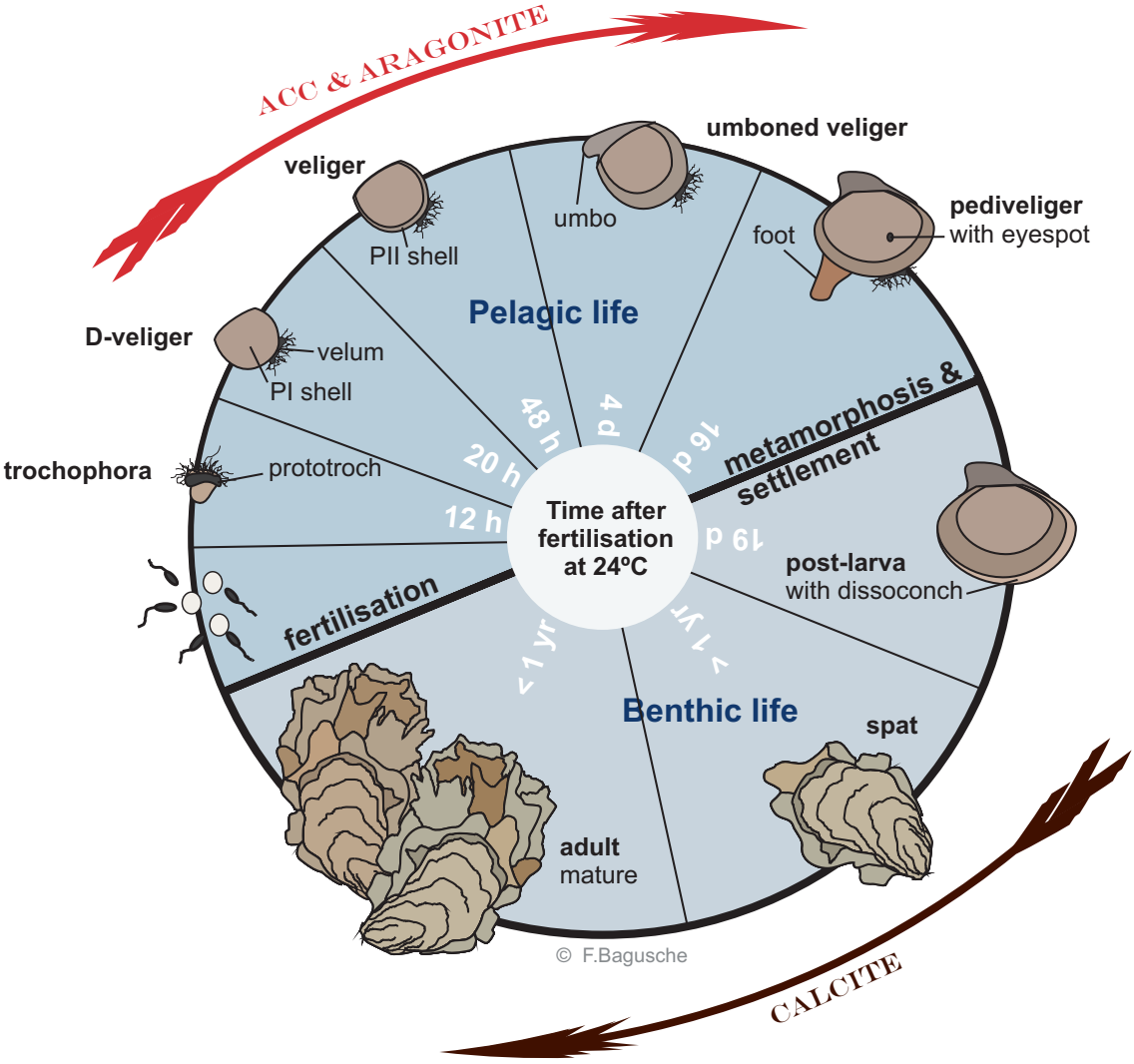

Figure 2: Life cycle of *C. gigas* at 24°C pH 8.1. Mineralogical changes are indicated with arrows. PI: Prodissoconch I; Prodissoconch II.

1.3 Biomineralisation

Biomineralisation is a fascinating phenomenon among different phyla and can be described as the process, by which living organisms produce minerals, often to protect or support their soft tissue. A biomineral is composed of both, mineral and organic components (Lowenstam and Weiner, 1989; Weiner and Dove, 2003). The most abundant biogenic minerals are calcium carbonates with eight polymorphs including calcite, aragonite, vaterite, magnesium calcite (Mg-calcite), monohydrocalcite, protodolomite, hydrocerussite and amorphous calcium carbonate (ACC). Except for the ACC, all other polymorphs of calcium carbonate are crystalline (Addadi et al., 2003).

The mechanisms of shell formation are still not fully understood and continue to be controversially discussed. In the following, different actual concepts of the mechanisms of biomineralisation will be briefly introduced.

Biologically Induced Mineralisation and Biologically Controlled Mineralisation

According to Lowenstam (1981) and Lowenstam and Weiner (1989) biomineralisation processes can be divided into two different mineralisation strategies: 1) Biologically Induced Mineralisation (BIM) and 2) Biologically Controlled Mineralisation (BCM) - the latter being subdivided into biologically controlled extracellular mineralisation, biologically controlled intracellular mineralisation and biologically controlled intercellular mineralisation.

The BIM is characterised by passive mineralisation processes where the cells of the organisms, such as some anaerobic prokaryotes, have no or just minor control on mineral precipitation. Minerals are deposited extracellularly, in an open environment, by interactions of secreted metabolic products with compounds or ions in the environment and therefore are a product of uncontrolled and unintended metabolic activity (Frankel and Bazylinzki, 2003). One characteristic feature of BIM is that "the type of mineral formed is a function just as much of the environmental conditions in which the organism lives as it is of the biological processes involved in its formation. The same organism in different environments can form different minerals" (Lowenstam and Weiner, 1989).

In contrast, the BCM, also called organic matrix-mediated mineralisation (Lowenstam, 1981), is identified by controlled nucleation, morphology, growth and location of mineral deposition by cellular activities of organisms such as magnetotactic bacteria (Frankel and Bazylinzki, 2003) and eukaryotic calcifiers like scleractinian corals (Langdon and Atkinson, 2005), foraminifera (Erez, 2003), coccolithophores (Weiner and Dove, 2003), mammals (Veis, 2003) and molluscs (Addadi et al., 2006; Weiss et al., 2002). Even though BCM can be differentiated into extracellular, intercellular, and intracellular mineralisation all three mineralisation strategies

take place within an isolated environment (Lowenstam and Weiner, 1989; Veis, 2003; Weiner and Dove, 2003).

In biologically controlled extracellular mineralisation, organisms either actively pump cations across the cell membrane followed by passive diffusion through extracellular fluids to the site of nucleation, or secrete vesicles containing cations which release their contents as a result of compartment breakdown at the site of nucleation (Weiner and Dove, 2003). Mammals, for example, use this strategy to precipitate minerals for teeth and bone development (Buckwalter et al., 1995; Veis, 2003) as well as molluscs, such as *Crassostrea gigas* for shell development (Weiss et al., 2002) or scleractinian corals to develop their skeletons (Langdon and Atkinson, 2005; Tambutté et al., 2011).

Most haptophyte algae, the coccolithophores, calcify via biologically controlled intracellular mineralisation where biominerals are nucleated intracellularly within compartments, such as vesicles. Intracellular assembly of the growth units and subsequent secretion into the organic matrix or direct secretion of the growth units into the extracellular organic matrix are two possible strategies (Weiner and Dove, 2003). Another possible strategy, but less frequently used, is by magnetotactic bacteria (Frankel and Bazylinzki, 2003), where the biomineral remains within the cell either as a single growth unit or is organised intracellularly into a higher order structure (Weiner and Dove, 2003).
Biologically controlled intercellular mineralisation is the strategy of choice for calcareous algae like *Amphiroa anceps.* The epithelial surfaces of the adjacent cells are used as a nucleation side and calcite is deposited within the organic material of the cell walls (Borowitzka, 1981; Weiner and Dove, 2003).

Haemocyte –mediated mineralisation

Mount et al. (2004) hypothesised a mechanism of haemocyte-mediated shell mineralisation in the adult eastern oyster *Crassostrea virginica* Gmelin, 1791 driven by granulocytic haemocytes, or refractive granulocytes (REF cells), which seem to contain calcium carbonate crystals. Their studies revealed an increase of REF cells from 5 to 15 % of the total haemocyte population 48 h after notching the shells. According to their study, the crystal-bearing REF cells appear to release their crystals at the mineralisation front. SEM images of regenerated shell pieces revealed REF cells, associated with calcitic crystals, on the surface of the prismatic layer. The authors supposed that crystals essentially developed from nascent crystal secretions of REF cells and grew after deposition onto the surface of the outer mantle epithelium. This hypothesis has since been accepted by a number of research groups, including Liu et al. (2007) and Kádár (2008 and 2009) and Zhang et al. (2012).

1.3.1 Biomineralisation in different organisms

Biomineralisation based on $CaCO_3$ is almost universal within Kingdom Animalia, especially within the invertebrates such as molluscs, cnidarians, arthropods, and echinoderms. To give a better idea of how common biomineralisation is, a few examples of calcifying taxa and their biomineralisation strategies will be presented below.

Biomineralisation is very common in the different Protista phyla, such as in Foraminifera, Heterokontophyta, including diatoms and in Haptophyta, including coccolithophores. The most abundant calcifying species in the world's oceans are coccolithophores, with *Emiliania huxleyi* as one of its best-studied species. These unicellular haptophyte algae produce exoskeletons of tiny interconnected calcitic plates, called coccoliths that envelop the cell membrane creating the coccosphere. In general, coccoliths can fall into two categories, heterococcoliths and holococcoliths. The latter exhibit, compared to heterococcoliths, a less complex morphology comprised of uniform-shaped crystals that are thought to be produced extracellularly during certain life-cycle stages (Young et al., 1999). Heterococcoliths, the more widely abundant coccolith form, are produced intracellularly and consist of complex calcite crystal elements that are routinely used for coccolithophore taxonomy (Young et al., 1992).
Mineralisation of (hetero-) coccoliths in *E. huxleyi* occurs in an intracellular, Golgi-derived compartment, namely the coccolith vesicle (CV), which is located next to the nucleus. Throughout the calcification process the CV is connected to the reticular body that is expected to provide rapid ion transport and supersaturated conditions inside the CV (Brownlee and Taylor, 2004). Mineralisation starts inside the CV by formation of a proto-coccolith ring around an organic base plate of highly acidic polysaccharides such as galacturonomannan (Marsh et al., 1992; Westbroek et al., 1984). Subsequently, the vesicle gradually expands, while the crystal grows up- and outwards to form a complete coccolith (Young and Henriksen, 2003). In an extrusion process, the mature coccolith is then transferred to the exterior surface of the cell. During this process, the coccolith-vesicle moves away from the nucleus, CV membrane and plasma membrane fuse, and the coccolith then penetrates to the cell surface through the layer of organic scales, subsequently interlocking with adjacent coccoliths (Marsh, 2003; Taylor et al., 2007).

The mechanisms of biomineralisation and environmental impacts on calcification have been studied in echinoderms thoroughly. Echinoidea, or sea urchins, have served as model organisms for developmental studies and calcification mechanisms from a molecular (Hammond and Hofmann, 2012; Livingston et al., 2006; Martin et al., 2011) to a microstructural level (Beniash et al., 1997; Politi, 2004; Wilt, 2002) for at least a century. Skeletogenesis in sea urchin

embryos will be very briefly summarised in the following. For more details of sea urchin skeletogenesis please see for example Decker and Lennarz (1988) and Wilt (2002).
During the blastula and gastrula stage, specialised cells, the so-called primary mesenchyme cells (PMC) fuse and form a syncytium including a vacuole. Within this vacuole defined crystalline calcite spicules (Decker and Lennarz, 1988) transforming from a transient ACC phase are deposited. Most probably, ACC is introduced to the mineralisation site by vesicles secreted by the PMCs and stabilised through organic macromolecules incorporated within the mineral (Beniash et al., 1997; Politi, 2004; Politi et al., 2008). Within each spicule, two types of organic matrices are present - an extracellular matrix, which surrounds each spicule and a proteinaceous matrix that is occluded within the spicule (Wilt, 2002). The mature sea urchin larval spicule, composed of a single optical crystal of high magnesium calcite and small amounts of organic macromolecules (0.1 wt %) (Politi, 2004), is a model system for biominerals, and the first one in which the amorphous calcium carbonate precursor was discovered (Beniash et al., 1997). As stated above, high Mg-calcite is with aragonite the most soluble calcium carbonate polymorph (Mucci, 1983) which makes sea urchins interesting candidates to test if their development is affected by changing environmental conditions such as ocean acidification and ocean warming (Brennand et al., 2010; Martin et al., 2011; O'Donnell et al., 2010; Stumpp et al., 2011a; Stumpp et al., 2011b).

In the field of biomineralisation the Chordata, including humans, is the most intensively studied phylum (Lowenstam and Weiner, 1989). Unlike the molluscs for example, human biominerals consist of hydroxyapatite ($Ca_5(PO_4)_3(OH)$), a calcium phosphate (Killian et al., 2010) rather than of calcium carbonate. Osteogenesis or ossification (= bone tissue formation) can be classified into two different mineralisation processes- endochondral and intramembranous ossification. While during endochondral ossification cartilage tissue from aggregated mesenchymal cells serves as a precursor, bone mineral is directly deposited into the mesenchyme during intramembranous ossification (Gilbert, 2000). In endochondral ossification the cartilage is surrounded by an irregular collagenous connective tissue - the perichondrium, which when vascularised, becomes the periostreum. As the name already implies (Greek *Peri-* meaning "surrounding" and *-osteon*, meaning "bone), the periostreum envelops the exterior surface of the bones. Osteoblasts, synthesised by the periostreum, precipitate a collagenous matrix within which mineral nucleation and mineral deposition take place. Subsequently, the cartilage tissue is then replaced by bone. A very striking feature of bone mineral is the small size of the crystals, which have been reported to be the smallest biologically formed crystals known (Lowenstam and Weiner, 1989). However, the mechanisms triggering bone development in humans and how mineral is deposited within the organic matrix still remain uncertain and is subject of many on-going research projects (Buckwalter et al., 1995; Gilbert, 2000).

1.3.2 Biomineralisation in molluscs

Molluscs are soft-bodied metazoans that have developed external structures of calcium carbonate to protect themselves against predators and support their living tissue. These protective biominerals form a wide range of morphologies, including spicules or scales in solenogaster and caudofoveate molluscs (Eyster and Morse, 1984), calcareous plates in polyplacophorans and rigid shells in the Conchifera (Monoplacophora, Bivalvia, Gastropoda, Cephalopoda) (Marin and Luquet, 2004). The Molluscan shell is composed of 95-99% of calcium carbonate ($CaCO_3$) by weight and less than 1-5% organic matrix. The minor part of the shell, the organic matrix has been thought to be the controller of shell formation by directing crystal nucleation, growth and morphology of the shell microstructure (Addadi et al., 2006; Takeuchi and Endo, 2006; Zhang et al., 2006). The major biogenic forms of $CaCO_3$ in molluscs and other marine calcifiers are aragonite and calcite (Bøggild, 1930; Talmage and Gobler, 2009). According to Bøggild (1930) all aragonitic shells are non-magnesium whilst calcitic shells may be divided in to two groups - the magnesium and non-magnesium shells. Calcite is the most stable polymorph while aragonite and magnesium calcite (Mg-calcite) are at least 50% more soluble in seawater (Mucci, 1983), suggesting that organisms which build up their shells with these types of $CaCO_3$ may be affected by increasing pCO_2 (Feely, 2004).

1.3.2.1 Shell development in bivalves

Molluscan shell growth starts at an early developmental stage, the so-called veliger stage and has an ectodermic origin as with all the exoskeletons of calcifying protostomes (Eyster and Morse, 1984; Marin and Luquet, 2004). Compared to crustaceans, whose calcified exoskeletons are replaced periodically by ecdysis, mollusc shells grow continuously during all life stages (Eyster and Morse, 1984; Marin and Luquet, 2004). The following sections will summarise shell development from larval to adult stages in different bivalve taxa.

Early shell formation - The larval shell

Shell formation is initiated by the shell field, a group of specialized ectodermal cells at the end of gastrulation (Kniprath, 1980). When the central part of the shell field invaginates to build the shell gland, the remaining peripheral cells start to produce the outer organic shell layer, the periostracum (Eyster and Morse, 1984; Marin and Luquet, 2004).Then the inner part of the shell gland everts and transforms into the calcifying mantle epithelium (Kniprath, 1980; Marin and Luquet, 2004). During this process the lateral extension of the periostracum is initiated. The periostracum isolates an internal environment, the site of biomineralisation, from the external environment (Addadi et al., 2006). Primary mineralisation takes place between the periostracum and the shell field (Marin and Luquet, 2004). As mentioned above, the early shell is called

prodissoconch I, later prodissoconch II, and is aragonitic in all bivalve larvae studied so far (Kudo et al., 2009; LaBarbera, 1974; Weiss et al., 2002). Weiss and co-authors (2002) identified three larval shell layers in *Mercenaria mercenaria* Schumacher, 1817 and *Crassostrea gigas*. These layers are an inner prismatic layer, overlain by a homogenous layer with globular structures and an outer prismatic layer at some locations, which is adjacent to the periostracum. They suggested an occurrence of ACC in prodissoconch I as a precursor phase of crystalline aragonite in prodissoconch II. In contrast, Kudo et al. (2009) argued that in *Crassostrea nippona* Seki, 1934 there are just two aragonitic layers in the larval shell, without the inner prismatic one. Also they did not find any evidence for ACC. These differences in shell structure may be due to species-specific differences in the bivalve species investigated or the different methods applied. In any case it reflects the complex shape of the larval shell and it gives impetus for further investigations. The metamorphosis from the larval to the juvenile stage is identified by a distinct transition, which links the larval prodissoconch with the juvenile dissoconch shell (Marin and Luquet, 2004).

Shell formation – The adult shell

The shell of adult molluscs is highly variable and consists of calcite or aragonite, or both and is built up of one or more shell layers (Weiss et al., 2002), each with its own unique microstructure. As a rule, the upper part (prismatic layer) of the shell consists of calcite and the lower part (foliated and nacreous layer) of aragonite in the majority of the Mollusca (Bøggild, 1930), but in a few species like *Crassostrea gigas* mature shells are composed almost entirely of calcite with a minor aragonitic part, the so called 'myostracum' (Lee and Choi, 2007a; Lee et al., 2006b; MacDonald et al., 2010; Walne, 1979; Weiss et al., 2002). The shell of adult *C. gigas* consists of two elongated valves unequal in shape and size. While the left valve is deeply cupped, the right valve is slightly convex or flat and usually cemented onto substrate. Both valves are very solid, rough and sculptured with irregular, large radial folds. While the shape of the shells can vary with the environment, the colour of the external shell is usually beige-brownish with dark purple/brown radial bands or spots. The internal shell is whitish with a purplish/brownish muscle scar. Shell length varies, but can reach up to 30 cm (Miossec et al., 2009).

The primary mineralisation of a post-metamorphosed shell takes place in a tiny, insulated compartment, the extrapallial space (EPS) filled with the extrapallial fluid (Figure 3), which is bounded by the growing shell, the periostracum and the mantle epithelium (Marin and Luquet, 2004). The epithelial cells of mantle and periostracum are directly responsible for shell formation. They elaborate a matrix within this space, comprising various macromolecules such

as β-chitin, silk-fibroin-like proteins and an assemblage of relative hydrophilic macromolecules rich in aspartic acid (Asp). Within this organic framework, which is thought to be the controller of crystal formation, the minerals are deposited (Addadi et al., 2006; Levi-Kalisman et al., 2001; Lowenstam and Weiner, 1989). Genes involved in shell formation, precisely control the secretion of the organic matrix (Kobayashi and Samata, 2006). Formation, composition and function of the organic matrix will be explained in more detail in Section 1.3.3.

The main functions of the periostracum are the sealing of the EPS and the initial support of the calcium carbonate crystals (Marin and Luquet, 2004). The periostracum, a proteinaceous, water-insoluble layer which covers the external surface of the post-metamorphosed shell, originates from a row of basal periostracum secreting cells (psc), located at the base of the periostracal groove (Figure 3). This thin layer, composed of quinone-tanned proteins, lipids and mucopolysaccharides protects the shell from dissolution (Lowenstam and Weiner, 1989; Salas et al., 2012) and acts as a substrate for mineralisation and crystal growth (Kennedy, 1969). The primary organ responsible for mineralisation is the mantle (Lowenstam and Weiner, 1989), which can be roughly subdivided into two zones- the dorsal mantle (DM) or mantle pallial and the ventral mantle (VM) or mantle edge (Figure 3). The mantle edge is characterised by three folds – the outer fold (OF), the middle fold (MF) and the inner fold (IF). Generally, the outer prismatic layer (calcite) is always related to the proteins secreted from outer epithelia of the mantle edge, the OF. The inner nacreous layer (aragonite) is related to proteins secreted from the pallial or dorsal region of the mantle (Baronnet et al., 2008; Kong et al., 2009; Takeuchi and Endo, 2006; Zhang and Zhang, 2006). The recent work of Gardner and co-authors (2011) suggested at least five unique functioning zones in the mantle of the pearl oyster *Pinctada maxima,* the DM, the VM, the IF, the MF and the OF which were related to five clusters (A-E) of differentially expressed sequence tags (ESTs). Each cluster was mapped to a special location within these five zones and linked to the formation of the either the organic parts of the shell or to the different microstructures. Cluster A showed the highest expression in the dorsal mantle and slightly less in the ventral mantle and was linked to the formation of nacre. Cluster D was related to periostracum formation as expression was almost exclusively mapped in the outer fold of the mantle, specifically in the inner epithelium of the OF where the periostracum secreting cells are located (psc, Figure 1). Cluster E was associated with the formation of calcitic prisms and showed its highest expression profile in the OF. The results of Gardner et al. (2011) correspond to the generalised findings above, but revealed more detailed locations of different expression zones in the mantle of the pearl oyster.

As mentioned above, calcification takes place in the EPS, containing the slightly alkaline extrapallial fluid (EPF). According to McConnaughey and Gillikin (2008) the EPF is supersaturated with respect to $CaCO_3$, which is used to assemble the microstructures. The authors suggest that supersaturation of $CaCO_3$ occurs due to adding of Ca^{2+} or carbonate ions

(CO_3^{2-}) or both. CO_3^{2-} potentially derives from several sources. Bicarbonate (HCO_3^-) may enter the EPF by fluid exchange (Figure 3) around the periostracum as well as by entering the mantle. Due to the alkaline nature of the EPF HCO_3^- will be then deprotonated to yield CO_3^{2-}. CO_2 provided by respiration processes will also diffuse from the mantle tissues into the EPF and react with H_2O and OH^- to produce CO_3^{2-}. To maintain the alkaline nature of the EPF and to provide Ca^{2+} an ATP-driven $Ca^{2+}/2H^+$ exchanger pumps protons out of the EPF into the mantle tissue and Ca^{2+}, stored as granules in and between the cells, into the EPF. Additionally, Ca^{2+} enters the EPF my fluid exchange from Ca^{2+}-rich seawater around the periostracum (McConnaughey and Gillikin, 2008).

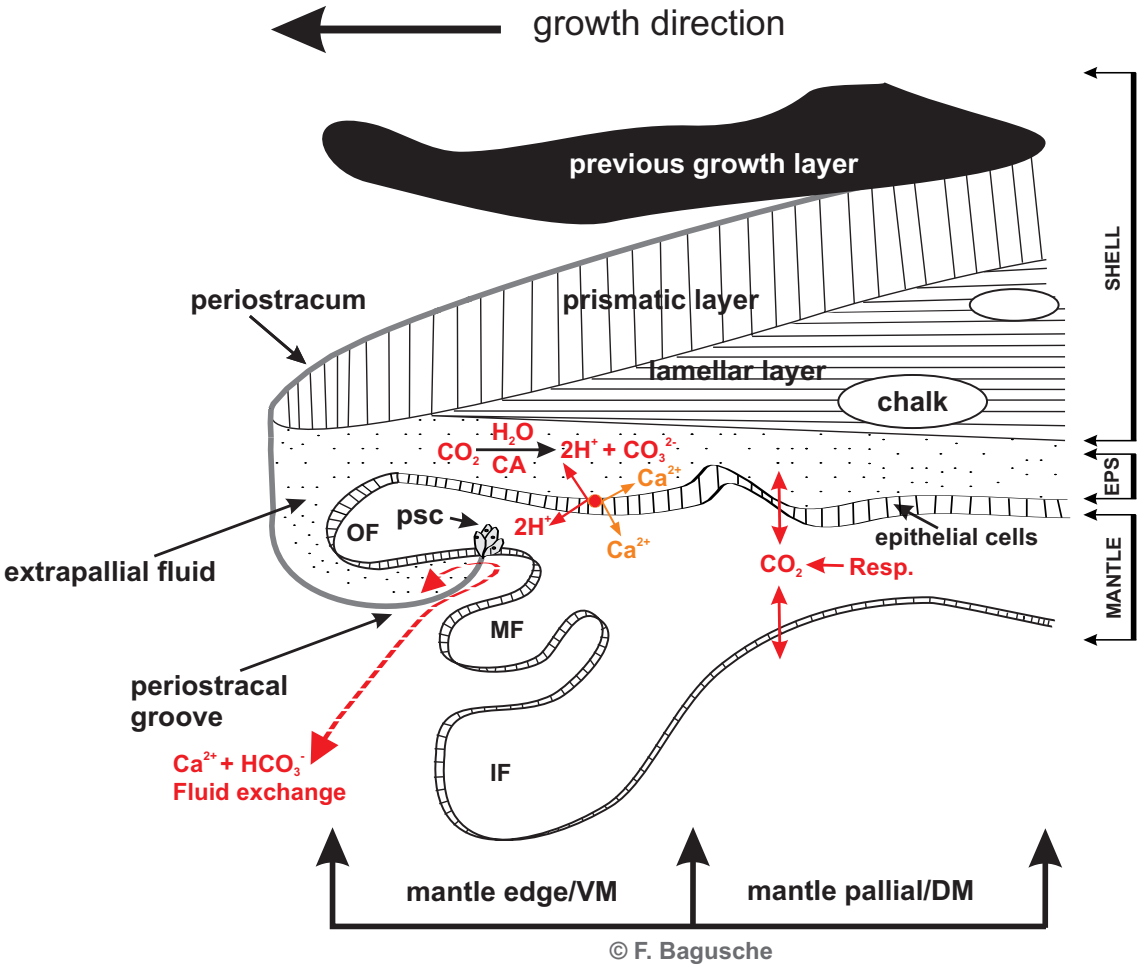

Figure 3: Schematic cross section of the layered adult *C. gigas* shell with adjacent mantle tissue showing likely transport routes for calcium and inorganic carbon. EPS: Extrapallial space; OF: Outer mantle fold; MF: Middle mantle fold; IF: Inner mantle fold; psc: periostracum secreting cells; VM: Ventral mantle; DM: Dorsal mantle. Based on Kennedy et al. (1969), Nakahara (1991), Jacob et al. (2008), McConnaughey and Gillikin (2008), and Kong et al. (2009).

Shell microstructures in adult shells

The main types of microstructures and the distributions of calcite and aragonite were discriminated in the 1930s by Bøggild (1930). To date more than 10 types of shell structures have been determined in adult bivalve shells (Kobayashi and Samata, 2006). Four microstructures have been identified so far for both valves in adult *C. gigas*, the calcitic prismatic layer (Figures 3 & 4), the aragonitic myostracum, the calcitic lamellar layer and the chalky microstructure (Higuera-Ruiz and Elorza, 2009; MacDonald et al., 2010). The microstructures occurring in post-metamorphosed *C. gigas* will be briefly described.

1. Calcitic prismatic layer

Calcitic prisms are usually located below the periostracum and almost perpendicular to it (Figure 2). The simple prismatic structure is an aggregation of polygonal first order prisms in a honeycomb pattern whose longer axes are arranged densely and vertically to the shell surface. Each prism is made of small calcite crystallites arranged perpendicularly the shell surface and is surrounded by an organic matrix (Figure 5) (Kobayashi, 2008; Kobayashi and Samata, 2006; MacDonald et al., 2010). Unlike aragonitic prisms, prisms made of calcite are characterised by transverse striations (Kennedy, 1969). Growth of simple prisms begins with appearance of small spherulite crystals on the periostracum at the shell margin, where they push aside their organic membranes until they lock as a series of carbonate blocks separated by passively formed interprismatic sheets. From then onwards they only can grow inwards, away from the periostracum, resulting in a newly formed prism (Kennedy, 1969).
Higuera-Ruiz and Elorza (2009) found calcitic prisms in both the right and the left valve of adult *C. gigas* shells, although the calcitic prisms of the left valve were found to be less striking compared with calcitic prisms of the right valve. These observations have been supported by various authors (Carriker et al., 1980; Galtsoff, 1964; Stenzel, 1964) who reported calcitic prisms in both valves of *Crassostrea virginica.* According to Higuera-Ruiz and Elorza (2009) the prismatic units of the right valve of *C. gigas* can reach a maximum length of 400 μm (average 100 μm) and an average width of 20 μm. The prisms of the left valve are thinner than those of the right valve and can grow up to 120 μm in length.

2. Myostracum

The myostracum is composed of aragonitic simple prisms (Carriker et al., 1980) that are orientated with their long axis perpendicular to the shell surface. The shape of these first-order, densely packed units are needle-like with no observable inter-prismatic sheets according to MacDonald et al. (2010). However, Lee at al. (2011) describes the myostracum in *C. gigas* as “a

hierarchically complex multilayer composed of a myostracal prisms and organic matrix", made of chitin.

The external surface of the myostracum forms the adductor muscle scar in both valves. Due to shell growth, the adductor muscle moves ventrally and the myostracum becomes overlaid by foliated calcite. Cutting a shell longitudinally, the myostracal prisms become visible as thin line embedded in the foliated structure (Carriker et al., 1980; MacDonald et al., 2010).

3. Foliated layer

This structure is built of more or less regular, parallel elongate, calcitic tablets (also called leaves, laths, or folia), which are orientated horizontally and parallel to the surface of the shell (Bøggild, 1930; Kobayashi and Samata, 2006). According to Higuera-Ruiz and Elorza (2009) the foliated laths of *C. gigas* are densely packed first order lamellae, joined together by organic matrix. Lath thickness ranges from 0.2 to 0.3 μm and length is variable. Every lath consists of sub-units (or second order units) between 10-40 nm thickness and 15-20 nm length.

4. Chalky microstructure

Lenses of chalky, white calcitic structure embedded in the foliated layer occur randomly in both valves. Carriker (Carriker et al., 1980) described for *C. virginica* a spongy, porous pattern, consisting of first order units called 'blades' and 'leaflets'. Blades are larger than leaflets and arranged perpendicular to the inner surface of the valves. Leaflets branch at several angles from the central blades, giving the chalky structure its characteristic spongy appearance (Carriker et al., 1980; Higuera-Ruiz and Elorza, 2009). No organic matrices have been observed in this microstructure so far.

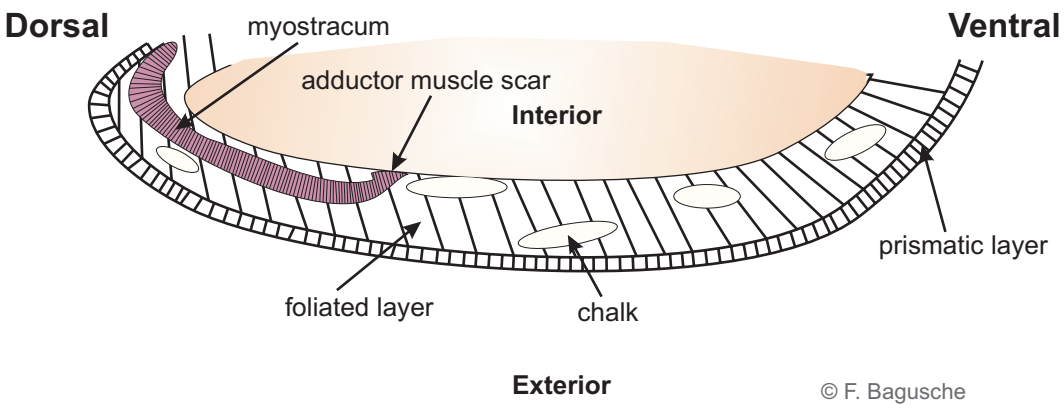

Figure 4: Schematic longitudinal section of an adult *C. gigas* shell with its layered microstructures (not drawn to scale). Redrawn after MacDonald et al. (2010).

5. Nacre

Nacre, or "mother-of-pearl", is the most intensively studied microstructure in molluscs due to its great economical value in pearl production and jewellery (Cartwright and Checa, 2006; Cuif and Dauphin, 1996) and even though it does not occur in *Crassostrea* it will be briefly described. Additionally, nacre has become of great interest for biomedical research because of its strength, resistance and similarity to mammal bone; it could act as an alternative bone substitute material (Lopez et al., 2004). Studies of the water-insoluble matrix of the nacreous layer have identified that nacre is capable of inducing the differentiation of osteoblasts, suggesting that nacre contains certain signal molecules with osteogenic capability and could therefore be used for human bone regeneration (Moutahir-Belqasmi and Balmain, 2001; Zhang and Zhang, 2006).

Nacre is deposited by many mollusc species such as the Polynesian pearl oyster *Pinctada margaritifera* (Cuif and Dauphin, 1996; Dauphin et al., 2008) or the gastropod *Haliotis rufescence* (Nakahara, 1991) to build the inner layer of the shell, or in case of *Pinctada* nacreous pearls. The nacreous structure is an accumulation of aragonitic, polygonal, single-crystal tablets. Theses tablets are orientated horizontally, parallel to the growth lines of the shell. Organic matrices are located in and around the tablets (Bøggild, 1930; Kobayashi and Samata, 2006). In bivalves nacre is deposited as a brick-wall structure (Checa et al., 2006) while in gastropods nacre is arranged as a pyramid-shaped stacks (Nakahara, 1991).

1.3.3 The organic matrix in molluscs and its involvement in biomineralisation

Molluscan shells are built up of polymorphs of $CaCO_3$ and just a minor organic part comprising 1-5% by dry weight (Gong et al., 2008; Sudo et al., 1997; Takeuchi and Endo, 2006; Zhang and Zhang, 2006). This organic part, also called organic matrix, is thought to be the controller of mineralisation processes (Addadi et al., 2006; Takeuchi and Endo, 2006; Zhang and Zhang, 2006). Organic matrices show a great diversity in their molecular weight and amino acid composition across the species and within the different microstructures of species (Table 1) (Kobayashi and Samata, 2006). There are two kinds of organic matrices intensively studied so far, inter- and intra-crystalline matrix occurring in both the prismatic and the nacreous layer. Inter-crystalline matrices envelop the individual crystals (Figure 5), while intra-crystalline matrices are net-like and pervade the crystals. The main components of these cell-free matrices are proteins, glycoproteins, proteoglycans, polysaccharides, and chitin secreted by the external mantle epithelium (Addadi et al., 2006; Joubert et al., 2010; Marin and Luquet, 2004). Precise interactions between proteins and the mineral ions produce crystallites with well-defined shapes

(Marin and Luquet, 2004). Matrix proteins are often classified as soluble or insoluble, in regards to their solubility after decalcification with a weak acid or a calcium-chelating agent such as EDTA (Zhang and Zhang, 2006).

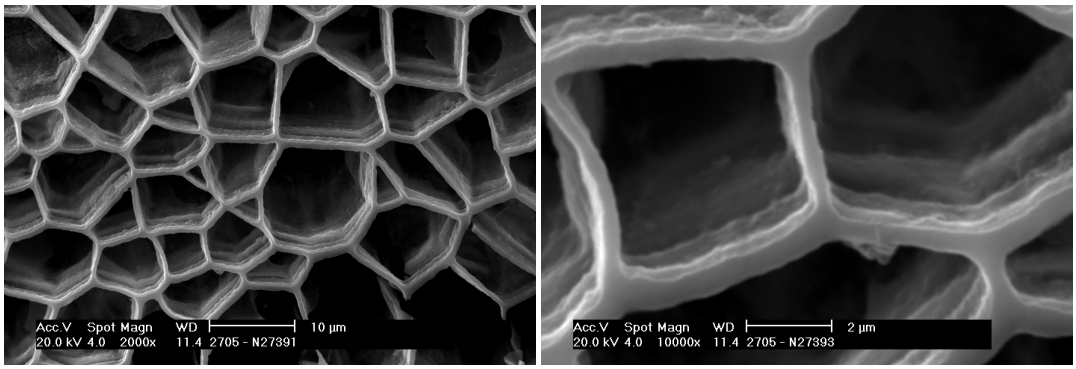

Figure 5: Scanning electron micrograph of a 3-dimensional inter-prismatic organic matrix framework from the demineralised prismatic layer of an adult *C. gigas*. The shape of the matrix defines the shape of each prism. Scale bar in A = 10 µm, B = 2 µm. © F. Bagusche.

In 1984, Weiner et al. (1984) introduced a model of the nacreous inter-lamellar organic matrix based on studies of the nacreous layer of two bivalve species, *Pinctada margaritifera* and *Neotrigonia margariticea*, the gastropod *Tectus dentatus* and the cephalopod *Nautilus repertus*. The matrix was described as a complex of several layers with the hydrophobic polysaccharide β-chitin as the core structural component sandwiched between layers of silk protein and surface coated with acidic macromolecules (Figure 6 A).

The current model of the organic matrix by Levi-Kalisman et al. (2001) (Fig. 6 B) is based on analyses of the nacreous layer in the saw-toothed pen shell *Atrina serrata*. According to this model, the major components involved in biomineralisation are relatively hydrophobic silk proteins and an assemblage of hydrophilic macromolecules rich in aspartic acid, some of them located on the surface of the 3-dimensional scaffold of aligned and layered β-chitin fibres, whilst others are situated within the mineral phase. Nucleation is initiated by Asp-rich glycoproteins absorbed to the matrix surface. The authors suggest that prior to mineralisation the silk fibroin is in a hydrated gel state and not present as a defined layer and that the growth of aragonite crystals takes place within this hydrated gel phase, pushing the gel aside into inter- and intra-crystalline spaces while crystals increase in size.

The models of Levi-Kalisman et al. (2001) and Weiner et al. (1984) differ in the nature and location of the silk proteins. Whilst the latter model suggested silk proteins as a definite layers within the matrix, the recent model explains the silk in the form of a hydrated gel. However, both models propose that molecules rich in aspartic acid are absorbed to the matrix to construct the site of nucleation.

In 2006, Addadi et al. (2006) published a reviewed and updated model of nacre synthesis in the rigid pen shell *Atrina rigida* (Figure 6 D). The authors suggested that first a microenvironment is formed by two layers of β-chitin, eventually filled with gel containing silk-like proteins (Figure 6 D.4). Acidic macromolecules are absorbed onto the β-chitin matrix inducing the nucleation of aragonite tablets. As the crystal grows, the hydrated gel phase is subsequently displaced towards the adjacent tablets and between the crystal and the chitin layer (Figure 5 D.5). The first mineral formed is amorphous calcium carbonate, which eventually matures into aragonitic nacre during growth.

The models mentioned above all describe aragonitic nacre synthesis, but the mechanisms explaining the components that control prism formation are not well understood. In 2007, Nudelman et al. (2007) compared the growth strategies of shell prismatic and nacreous layers in *Atrina rigida,* focussing on structure and formation processes of the prismatic layer (Figure 6 C). According to the model proposed, prism growth starts by deposition of a dense intra-crystalline meshwork of chitinous fibres upon an already formed calcitic layer (Figure 5 C.1). On top of the framework of chitin, amorphous calcium carbonate stabilised by Asprich, an acidic protein of the soluble organic matrix, is then deposited (Figure 6 C.2). Once in contact with the mineral, ACC crystallises and forms a new calcitic layer occluding the chitin fibres (Figure 6 C.3). By repeating these deposition steps, the intra-crystalline matrix appears as growth layers within the prism.

Compared to the growth of the nacreous layer in *Atrina rigida* where chitin forms an inter-crystalline scaffold, chitin is deposited in prisms as an intra-crystalline matrix (Nudelman et al., 2007). Both, the organic matrix of the prismatic layer and the matrix of the nacreous layer, differ in regards to proteins involved in mineralisation processes. While several proteins and their putative functions of the nacreous organic matrix have been identified so far, information on proteins of the organic matrix in calcitic prisms is still relatively rare. In Table 1, proteins and genes involved in biomineralisation processes of both microstructures identified to date, their putative functions and main characteristics have been summarised.

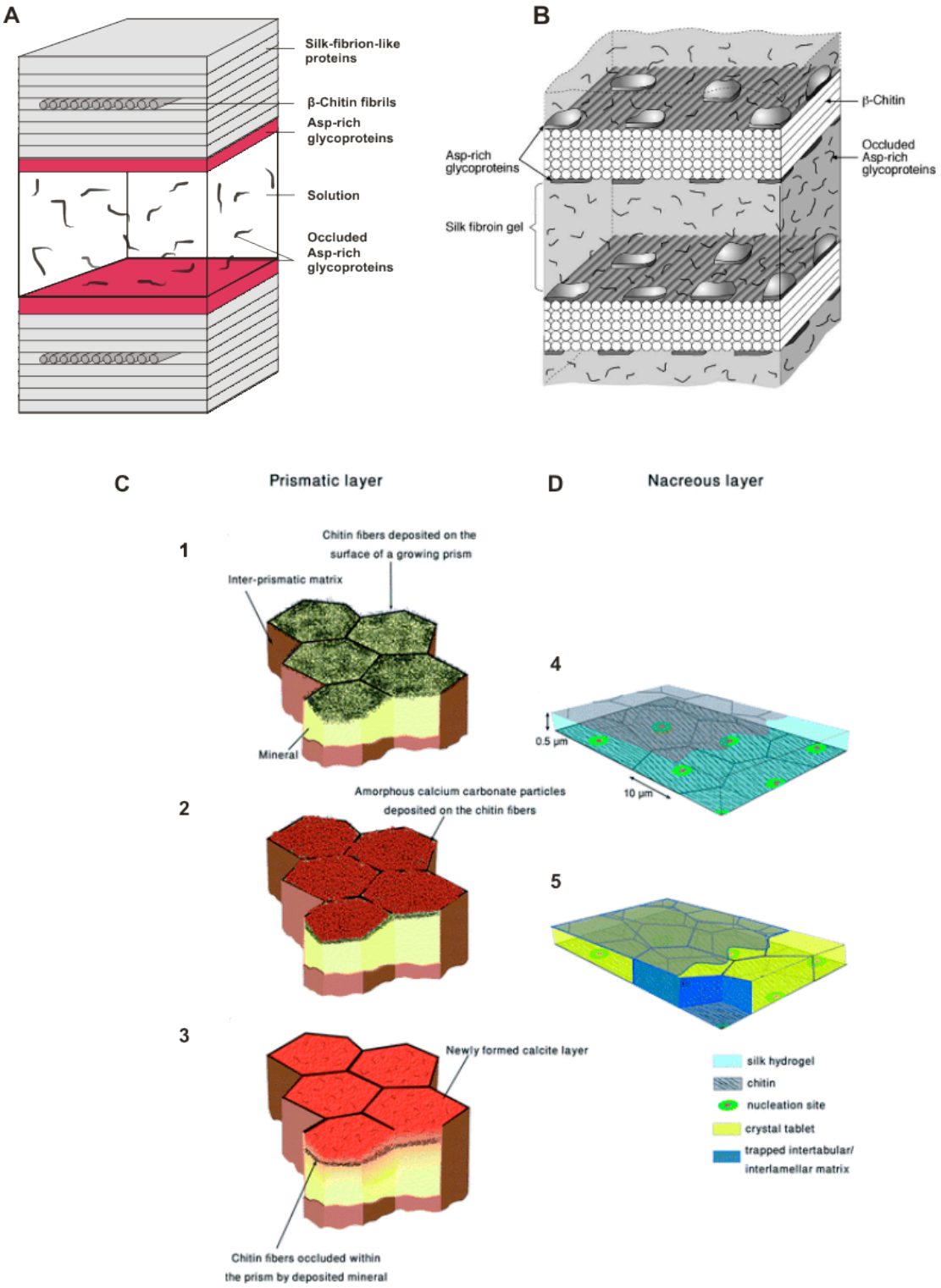

Figure 6: Schematic illustrations of the organic matrix and proposed mechanisms of crystal growth. (A) & (B): Model of the demineralised nacreous layer organic matrix of (A) *Pinctada margaritifera*, *Neotrigonia margariticea*, *Tectus dentatus* and *Nautilus repertus*, redrawn after Weiner & Traub (1984) and (B) *Atrina serrata*, reproduced from Levi-Kalismann et al. (2001). (C) & (D): Proposed mechanisms of crystal growth of the prismatic layer of (C) *Atrina rigida* reproduced from Nudelman et al. (2007) and the nacreous layer of (D) *Atrina rigida* reproduced from Addadi et al. (2006)

1.3.4 Proteins and genes involved in biomineralisation in molluscs

Molluscan shell development at gene transcription level is largely unknown to date, whilst in other invertebrates such as in echinoderms studies of molecular mechanisms of calcification are much developed (Hammond and Hofmann, 2012; Livingston et al., 2006; Martin et al., 2011; Stumpp et al., 2011b). In bivalves, most research on proteins and genes involved in biomineralisation has been done in the pearl oyster *Pinctada* (Table 1) as this genus is of special interest due to its great economic value in regards to pearl production. As an example, in 2004 global marine pearl production had an estimated value of approximately US$ 475 million (Bondad-Reantaso et al., 2007). To increase the quality of pearls in pearl oysters and to understand the molecular pathways of shell growth during oyster development, current research focus on genes and proteins thought to regulate biomineralisation (Fang et al., 2011; Joubert et al., 2010; Miyazaki et al., 2010; Takeuchi and Endo, 2006). Table 1 summarises recent studies of biomineralisation-proteins and genes and gives a brief overview of the main characteristics and functions of these genes and proteins. In Chapter 4, the molecular mechanisms of calcification known to date will be described in more detail.

Table 1: Selected proteins and genes (mRNA) involved in biomineralisation in molluscs. Names, accession numbers, solubility, molecular weight (MW), aa: Amino acids, theoretical isoelectric point (IP), expression localisation, putative function and the microstructure are listed. Matrix proteins are classified as soluble or insoluble, in regards to their solubility after decalcification with a weak acid or a calcium-chelating agent such as EDTA (Zhang and Zhang, 2006). DM: Dorsal mantle, VM: Ventral mantle, NL: Nacreous layer (aragonitic), P: Periostracum, PL: Prismatic layer (calcitic), FL: Foliated layer (calcitic).

Species	mRNA name & GeneBank™ accession no.	Protein name & UniProtKB accession no.	Solubility	MW kDA *(aa)*	IP theor.	Expression localisation	Putative function	Micro-structure	Reference
BIVALVIA									
Pinctada fucata		**MSI 60** D86074	Insoluble	61.7 *738*	4.9	Outer epithelia of mantle pallial (DM)	Framework protein, calcium ion binding, formation of crystalline β-sheets	NL	Sudo et al., 1997
	pMSI 2 D86073	**MSI 31** D86073	Insoluble	32.8 *334*	3.8	Outer epithelia of mantle edge (VM)	Framework protein, calcium-ion binding, formation of disulphide bonds in the prismatic walls	PL	Sudo et al., 1997
	N16/pearlin AB023067	**N16.1 matrix protein** Q9TVT2	Insoluble	16 *131*	4.8	Highly expressed in the DM, very low expression in the VM	Formation of nacreous layer, probably Ca-binding activity	NL & probably PL	Samata et al., 1999
	Nacrein D83523	**Nacrein** Q27908	Soluble	60/48 *447/430*	6.8	Entire mantle tissue (VM + DM)	$CaCO_3$ inhibitor, carbonic anhydrase function, HCO_3^- synthesis	NL, PL & FL	Miyamoto et al., 2005; Miyamoto et al., 2002; Miyamoto et al., 1996
	Pif177 AB236929	**Protein Pif97** C7G0B5 **Protein Pif80** C7G0B5		97 *525* 80 *460*	4.65 4.99	Highly expressed in the DM (Pif97 & Pif80), very low expression in the VM (Pif80)	Initiation of aragonite crystallisation & subsequent stacking of aragonite tablets. Pif80 binds to both, aragonite & calcite, but more specific to aragonite	NL	Suzuki et al., 2009
	Prismalin-14 AB159512	**Prismalin-14** Q6F4C6	Insoluble	13.5 *105*	3.98	Inner side of the OF of the mantle	Inhibition of $CaCO_3$ precipitation, calcium ion binding, chitin-binding	PL	Suzuki et al., 2004 & 2007
	Aspein AB094512	**Shell matrix protein** Q76K52	Soluble	39 *413*	1.45	Outer edge of the mantle (VM)	Ca^{2+} carrier, crystal nucleator inducing calcite precipitation of the prismatic layer	PL	Tsukamoto et al., 2004
	Shemartin-1 - Shemartin-7 AB244419-AB244425	**Shematrin-1-Shematrin-7** Q1MW96-Q1MW90	Insoluble	See ref.	See ref.	Mantle edge (VM)	Framework proteins	PL	Yano et al., 2006
	n/a	**PFMG4** DQ104258	n/a	17.9 *158*	n/a	n/a	n/a	NL?	Liu et al., 2007
	n/a	**PFMG1** 3QYL59	n/a	15.7 *136*	7.96	Outer epithelia of mantle	Calcium ion binding, nucleation of calcium components & nacre precipitatation	NL	Liu et al., 2007

Species	mRNA name & GeneBank™ accession no.	Protein name & UniProtKB accession no.	Solubility	MW kDA *(aa)*	IP theor.	Expression localisation	Putative function	Micro-structure	Reference
	Tyrosinase DQ112679	**OT47** Q287T6	?	47 445	9.4	Outer epithelium of the MF	Periostracum formation, metal-ion binding	P	Zhang et al., 2006
Pinctada fucata	***Priskilin-39*** EU921665	**Priskilin-39** C0J7L8	Insoluble	39.3 *406*	8.83	In prismatic & organic layers of the shell, extrapallial fluid, hemolymph, inner epithelial cells of the OF and the outer epithelial cells of the MF at the bottom of the periostracal groove	Crystal growth regulation (prismatic layer), involved in the chitinous framework building, chitin-binding, prob. Involved in organic framework construction & aragonitic-specific inhibition	PL	Kong et al., 2009
	CaM AY341376	**Calmodulin** Q6EEV2	Soluble	16.8 *149*	4.14	Highly expressed in gills & the inner epithelial cells of the OF, the outer epithelial cells of the MF & the IF. Lower expression in the gonad & adductor muscle	Involved in calcium uptake, transport & secretion, calcium-binding activity	n/a	Li et al., 2004
	GRMP AF516712	**MSI 7**	Insoluble	7 *76*	5.98	Outer epithelia of the DM and in MF & IF of the VM	Acceleration of nucleation & precipitation of $CaCO_3$	NL, PL	Zhang et al., 2003
	pfmg3 DQ104257	**PFMG3** Q3YL63	?	14.7 *121*	9.86	Outer epithelia of the DM	Enhancement of biomineralisation	NL?	Liu et al., 2007; Wang et al., 2011
Pinctada maxima	***N66*** AB032613	**N66 matrix protein** Q9NL38	Soluble	59.84 *568*	?	DM & VM	$CaCO_3$ synthesis, calcium concentrator	PL & NL	Kono et al., 2000
	n/a	**N14 matrix protein** JC7211	Soluble	13.734 *140*	?	DM	Involved in the formation of the nacreous layer	NL	Kono et al., 2000
Mytilus edulis	**n/a**	**Carbonic anhydrase** n/a	?	?	?	Mantle & gills	HCO_3^- synthesis Enhancement of HCO_3^- synthesis	n/a	Gaume et al., 2011; Medaković, 2000
Pinna nobilis	**n/a**	**Calprismin** P83631	Soluble	38 *61*	?	Mantle epithelium, location not specified (VM?)	Interaction with $CaCO_3$, crystal binding, involvement in cell-signalling or matrix-cell interactions	PL	Marin et al., 2005
	n/a	**Caspartin** P83631	Soluble	17 *61*	?	Mantle epithelium, location not specified (VM?)	Strong interaction with growing calcite crystals, role in prism formation	PL	Marin et al., 2005
	mcp AF145215	**Mucoperlin** Q9BKM3	Soluble	66.7 *636*	4.8	Localised around nacre tablets	May be involved in the lateral growth of the nacreous tablets, $CaCO_3$ inhibition? Calcium-binding?	NL	Marin et al., 2000
Patinopecten yessoensis	***Msp-1*** AB073617	**MSP-1** Q95YF6	Soluble	74.5 *840*	3.2	n/a	Calcium-binding?	FL	Sarashina and Endo, 2001

Species	mRNA name & GeneBank™ accession no.	Protein name & UniProtKB accession no.	Solubility	MW kDA *(aa)*	IP theor.	Expression localisation	Putative function	Micro-structure	Reference
GASTROPODA									
Haliotis tuberculata	**n/a**	**Alkaline phosphatase** n/a	?	?	?	Larval shell field, internal & external mantle epithelium, haemolymph	Ubiquitous enzyme involved in regulatory processes of mineralisation	n/a	Gaume et al., 2011
	n/a	**Carbonic anhydrase** n/a	?	?	?	Mantle epithelium & gills	HCO_3^- synthesis Enhancement of HCO_3^- synthesis	n/a	Gaume et al., 2011; Medaković, 2000
Haliotis rufescens	AF023459	**Lustrin A** O44341	Insoluble	142.2 *1428*	8.1	Pallial mantle epithelium (DM)	Multifunctional protein	NL	Shen et al., 1997
	AF225916	**AP7** Q9BP37	Soluble	7 *66*	5.17	n/a	Calcite-binding	NL	Michenfelder et al., 2003
	AF225915	**AP24** Q9BP38	Soluble	24 *171*	5.3		Calcite-binding	NL	
Haliotis laevigata	n/a	**Perlustrin** P82595	Soluble	9.3 *84*	8	n/a	IGF-binding, , cell interaction	NL	Weiss et al., 2001; Weiss et al., 2000
	n/a	**Perlucin** P82596	Soluble	18.2 *155*	7.2	n/a	Facilitation of $CaCO_3$ nucleation/ crystal growth, sugar-binding	NL	Weiss et al., 2000
	n/a	**Perlinhibin** P85035	Soluble	4.8 *41*	7.86	n/a	Binds to calcite crystals, inhibits $CaCo_3$ crystallisation	NL	Mann et al., 2007
Haliotis asinina	**Has-ubfm1** DW986191	**n/a**	n/a	n/a	n/a	Trochophora: edge of shell field; veliger; food primordia; juvenile: outer mantle epithelium	Operculum & shell construction	n/a	Jackson et al., 2007
Turbo marmoratus	***Nacrein*** AB073680	**Nacrein** Q8N0R6	Soluble	57.6 *538*	5.8	n/a	$CaCO_3$ inhibitor, carbonic anhydrase function, HCO_3^- synthesis	NL	Miyamoto et al., 2003

1.4 Impacts of Environmental Changes on Bivalves

Calcification in organisms such as bivalves can be affected by various factors such as changes in temperature and ocean acidification. In the next hundred years global climate changes are predicted to occur through increases in seawater temperature, water acidification and changes in seawater salinity (Nicholls et al., 2007). Increasing carbon dioxide concentrations in the atmosphere, caused by the burning of fossil fuels, have led to increased CO_2 uptake by the oceans over the past two centuries. Since the industrial revolution started in the 18th century, an estimated 30% of CO_2 released by human activity has been taken up by the oceans (Caldeira and Wickett, 2003; Feely, 2004). The dissolution of CO_2 in seawater will decrease carbonate ion (CO_3^{2-}) concentration and lower the pH by increasing levels of hydrogen (H^+), carbonic acid (H_2CO_3) and bicarbonate (HCO_3^-) ions. This process is termed "Ocean Acidification" (OA) (Caldeira and Wickett, 2003; Feely, 2004; Gazeau et al., 2007). Compared with pre-industrial values (~ pH 8.179), surface ocean pH has already declined by 0.1 units (~ pH 8.069) (Orr et al., 2005) and could, according to Caldeira and Wickett (2003) and Raven et al. (2005), decrease by the year 2100 by up to 0.5 units (~ pH 7.824). This acidification process will lead to a shift: simultaneously the carbonate ion concentrations will decrease while the aqueous CO_2 concentration will increase. These changes in seawater chemistry will potentially make it more difficult for marine calcifying organisms to precipitate calcium carbonate (Gazeau et al., 2007; Orr et al., 2005; Talmage and Gobler, 2009). Marine organisms that construct $CaCO_3$ structures, e.g. shells, are affected by the presence of carbonate and bicarbonate forms of dissolved carbon in seawater. If the surrounding seawater is under-saturated in respect to carbonate ions, the once formed $CaCO_3$ will potentially dissolve back into the water if not protected by an organic layer such as the periostracum of mollusc shells. Calcium carbonate also becomes more soluble with increasing pressure and decreasing temperature, and hence with ocean depth. A critical point is reached at depth, the 'saturation horizon', below which seawater is under-saturated and $CaCO_3$ will tend to dissolve and above which seawater is supersaturated and $CaCO_3$ will tend to be preserved. Due to the fact that calcite is less soluble than aragonite, the aragonite saturation horizon is shallower. Because anthropogenic CO_2 in the atmosphere dissolves in seawater and reduces its pH and also carbonate ion concentration, the saturation horizons will become shallower under future climate predictions (Raven et al., 2005).

As the planet warms due to increasing pCO_2 so does the ocean. It has been shown that mean global temperature has already increased by about 0.7 °C in the past 100 years and further increases of about 1.8 to 4 °C are expected by the end of the 21st century (Nicholls et al., 2007).

Rising sea surface temperatures (SSTs) can put entire ecosystems at risk, such as coral reefs by causing extensive coral bleaching. The frequency of coral bleaching events associated with El-Niño-Southern Oscillation (ENSO) events (Baker et al., 2008; Glynn, 2000) might become higher in response to atmospheric and sea water warming. However, the exact nature of future changes is difficult to predict. An increase of temperature could increase seawater evaporation and reduce rainfall, concentrating salt in the water and increasing the salinity. Alternatively, warming could lead to areas with increased rainfall, diluting the seawater and consequently reducing the salinity, especially in coastal regions and estuaries (Matozzo and Marin, 2011). Alterations in salinity, in combination with increased pCO_2, has been shown to affect the mechanical properties of oyster shells and to increase energy consumption and mortality (Dickinson et al., 2012). Other studies reported negative effects on immune and metabolic parameters in bivalves due to either very high or very low salinity levels (Hauton and Hawkins, 1998; Hauton et al., 2000; Heilmayer et al., 2008; Matozzo et al., 2006).
Ocean pH, $CaCO_3$ saturation state and pCO_2 co-vary and will change simultaneously with temperature, making it even more difficult to foresee future outcomes for marine biota. Nevertheless, many studies have investigated the impacts of environmental changes on calcifying organisms. A compilation of recent studies, which evaluate the effects of variations in abiotic factors such as temperature, pH and salinity on biological responses of molluscs, is shown in Table 2. Many of these studies have investigated the impacts of just a single stressor on marine biota, whereas multi-stressor approaches, such as the combined effects of water temperature and decreasing seawater pH (Anlauf et al., 2011; Byrne et al., 2009; Findlay et al., 2010; Lannig et al., 2010; Pansch et al., 2012; Parker et al., 2010b) are comparatively rare to date.

Comparing selected studies shown in Table 2, it is likely that not just the examined species may be affected by high pCO_2 in their development but also other marine bivalve species. By comparing clams, scallops, mussels and oysters, the latter seems to be less sensitive to environmental changes, which can be explained by the different microstructures of the shells. Parker et al. (2010b) described a negative impact of elevated pCO_2 on fertilisation of *Saccostrea glomerata* and *C. gigas*. In contrast, Havenhand and Schlegel (2009) and Kurihara et al. (2007 and 2008) found no evidence of a decline in fertilisation success and embryogenesis in *C. gigas* and *Mytilus galloprovincialis*. The reason for these different findings could be explained by intraspecific differences between populations of *C. gigas* and/or the factor temperature or the pCO_2 level used. While Havenhand and Schlegel (2009) and Kurihara et al. (2007 and 2008) used just ambient temperature for their studies, Parker et al. (2010b) tested four different temperatures in combination with four different levels of pCO_2. The latter study showed that at suboptimal temperatures, fertilisation success decreased significantly in both oyster species. In

all studies reviewed, larval development was strongly affected by decreased seawater pH, showing increased mortality, shell malformations, decreased growth rates and differences in shell microstructures compared to the controls. Calcification rates declined linearly and mortality increased in adult and juvenile bivalves with increasing pCO_2. For all developmental stages *Crassostrea spp.* seem to be more resistant to environmental changes compared to mussels (Gazeau et al., 2007), scallops and clams (Talmage and Gobler, 2009) and even the oyster *Saccostrea glomerata* (Parker et al., 2010a). The resistance of *Crassostrea spp.* to elevated pCO_2 can be explained in differences in shell mineralogy. Compared to the aragonitc shells of mussels, clams and scallops, the shell of *Crassostrea ssp.* consists mainly of calcite which is, as mentioned above, the most stable polymorph of calcium carbonate.

Whilst many studies has been investigated on the effects of OA on bivalve development including fertilisation success, shell growth and mineralogy (Gazeau et al., 2007; Kurihara et al., 2007) very few have investigated the effects of OA on the transcription of genes involved in biomineralisation combined with analyses on shell mineralogy. Therefore a key aim of this research has been to understand calcification processes at a molecular level in order to describe and compare changes in gene expression during development or environmental alterations, with possible correlated changes in shell microstructures.

Table 2: Compilation of recent studies investigating the effects of near-future OA scenarios on molluscs. According to availability, the tested parameters such as temperature, pCO_2, pH, salinity, O_2 saturation, duration of experiment, developmental stage tested and observed effects are given.

Species	T (°C)	pCO_2 levels/ pH	Salinity ‰	O_2 sat. (%)	Time	Developmental stage	Effects on development in treatment groups compared to the control group	Reference
Crassostrea gigas	23	pH 7.42 (348 µatm) pH 8.21 (2268 µatm)	33-34	97 ± 2.7 99 ± 1.3	48 h	Trochophora - veliger	No significant effects were observed at 2,3,8h after fertilisation (trochophora). At 24h, a significant decrease of 80% in normal larval development was observed which increased up to 91% at 48h after fertilisation (veliger).	Kurihara et al., 2007
Crassostrea gigas	19-20	pH 7.5, **8.15**	23-24	n/a	a) 100 s b) 1 h	Gametes	a) Sperm swimming: no significant impacts b) Fertilisation: no significant impacts	Havenhand and Schlegel, 2009
Crassostrea gigas	**15,** 25	**8.07**, 7.68	32		26-55 d	Adults	Negative effects on energy metabolism	Lannig et al., 2010
Saccostrea glomerata ***Crassostrea gigas***	**18, 22, 26,** 30	**375**, 600, 700, 1000 µatm	35	n/a	Various	Gametes, veliger & spat	Combined effects on elevated pCO_2 and temperature had significant negative effects on all developmental stages in both species, whereas *C.gigas* seemed to be less sensitive compared to *S. glomerata*	Parker et al., 2010b
Crassostrea virginica	21	pH 7.5 (3500 µatm), pH **8.2 (380 µatm)**	30	> 85 > 75	20 wks. 2 wks.	Juveniles Adults	Increase in mortality and metabolic rates and a decrease of growth and shell mass (40%) in juveniles. Changes in shell microstructures were detected in juveniles and adults. Up-regulation of CA mRNA expression in adult oysters.	Beniash et al., 2010
Crassostrea virginica ***Crassostrea ariakensis***	25	pH 8.16, **8.06**, 7.91, 7.76 pH 8.17, **8.08**, 7.92, 7.79 (280, **380**, 560, 800 ppm)	18	n/a	28 d	Veliger	*C. virginica*: 16% decrease in shell area & 42% reduction in calcium contend with increasing pCO_2 *C. ariakensis:* No significant effect on growth or calcification with increasing pCO_2	Miller et al., 2009
Saccostrea glomerata	26	pH 7.81, 7,64, **8.1**	32	n/a	8 d	Veliger	Survival decreased by 43% at pH 7.8 and by 72% at pH 7.6 and shell growth was retarded with decreasing pH, evidence of shell malformation/dissolution	Watson et al., 2009
Saccostrea glomerata	16, 22, **26**, 30	**375**, 600, 750, 1000 ppm	35	n/a	48 h	Gametes-D-veliger	Decreased fertilisation rates at elevated pCO_2 and elevated x decreased temperatures Percentage & size of D-veliger decreased with increased pCO_2. Increased mortality & shell malformations & reduced shell growth in response to increased pCO_2 and non-optimal temperatures.	Parker et al., 2009
Saccostrea glomerata	25	**375,** 1000 ppm	35	n/a	4 d	Spat	25% reduction in shell growth of the selectively bred population compared to a 64% reduction in shell growth of wild populations	Parker et al., 2010b
Mytilus edulis ***Crassostrea gigas***	20	pH 8.13-7.46 (421-2345 µatm) pH 8.7-7.55 (698-2774 µatm)	30	~ 100	2-3x 2 h incub./ day	Juveniles & adults	Calcification rates declined linearly with increasing pCO_2. Mussels seem to me more affected than oysters due to shell mineralogy.	Gazeau et al., 2007
Mercenaria mercenaria ***Argopecten irradians*** ***Crassostrea virginica***	24	pH 7.49, 7.84, **8.02** (350, 665, 1535 ppm)	28	~ 100	18 d 19 d 20 d	Veliger- juveniles	*M. mercendaria* & *A. irradians* showed a significant decline in survivorship and metamorphosis in the high and moderate treatments levels while survivorship, growth and metamorphosis in *C. viginica* was just affected in the highest CO_2 level.	Talmage and Gobler, 2009

Species	T (°C)	pCO_2 levels/ pH	Salinity ‰	O_2 sat. (%)	Time	Developmental stage	Effects on development in treatment groups compared to the control group	Reference
Crassostrea virginica	21	**400** µatm 700-800 µatm	**30** 15	n/a	11 wks.	Juveniles	High pCO_2 combined with low salinity: 1) significant increase in mortality & energy consumption (reduction of glycogen & lipid stores) 2) significant decrease in tissue growth & mechanical properties of the shell.	Dickinson et al., 2012
Mercenaria mercenaria ***Argopecten irradians***	24	pH 7.5, 7.8, 8.05, 8.2 (250, 390, 750, 1500 ppm)	28	~ 100	36 d 38 d	Veliger – spat	Decreased growth, metamorphosis, lipid accumulation and survival; reduced shell thickness; shell malformations	Talmage and Gobler, 2010
Mytilus edulis	16 -24	pH 6.7, 7.1, 7.4, 7.6, 8.1	21.4 - 28.3	> 50	44 d	Spat & adult	Mortality increased from day 23 to day 37 at pH 6.7 significantly in both, spat and adults and shell growth decreased. From day 37 to termination of the experiment, mortality seemed to correlate with increased water temperatures.	Berge et al., 2006
Mytilus galloprovincialis	13	pH 8.13, 7.42	35.5	< 90	6 d	Gametes- veliger	No effects on fertilisation & embryogenesis. Delay at trochophora stage and shell malformations at D-veliger stage.	Kurihara et al., 2008
Mytilus galloprovincialis	18	pH **8.05**, 7.3	32 ± 3.5	n/a	3 mo.	Juveniles	Reduced body-tissue growth & shell growth by 55%, metabolism-depression to 65%, reduction of haemolymph pH	Michaelidis et al., 2005
Mytilus californiaus	15	pH **8.06**, 7.96, 7.75 (**380**, 540, 970 ppm)	n/a	n/a	8d	Larvae	Larval shells were weaker, thinner & smaller	Gaylord et al., 2011
Ruditapes decussatus	21.6-23	pH 7.85, 7.67, **8.25**	30.6 – 31.6	50-100	75d	Juveniles	No differences in net calcification, size, weight and mortality were detected.	Range et al., 2011
SELECTED OTHER MOLLUSCS								
Sepia officinalis	**16.3**/16.3 **17.4**/17.4	~ pH **8**,7.2 (4000 ppm) ~ pH **8,** 7.1 (6000 ppm)	32-34	18-20 kPa	6 wks.	Juveniles	No negative effects on soft tissue growth or calcification rates	Gutowska et al., 2008
Haliotis coccoradiata	**20**, 22, 26	pH 7.6, 7.8 & **8.2**		36.9	6 wks.	Embryos-Juveniles	Unshelled veliger and abnormal juveniles	Byrne et al., 2011

1.5 Summary

Bivalve shell development has been of interest for many years as many bivalve species are economically very important. Global oyster aquaculture, for example, has increased within the past 60 years by 444% yielding a 1 262 608 USD market value in 2010. Even though oyster shell morphology is relatively well known, the mechanisms of calcification in molluscs remain unclear and are controversially discussed within the research community. Whilst many studies have focussed on proteins involved in shell development, little is known about the molecular mechanisms leading calcification during ontogeny. Oysters, as sessile marine animals, must cope with harsh and changing environmental conditions such as alterations in seawater pH, salinity or fluctuating temperature. Two major stressors, ocean acidification and ocean warming, have become a serious threat to marine calcifiers such as oysters. While the first line of self-protection in adult oysters is the thick calcified shell, early developmental stages of bivalves are known to react more sensitively to altered seawater conditions due to their shell mineralogy. Most studied species have shown increased mortality rates, reduced biomineralisation rates, shell malformations in response to ocean acidification. Whilst it is important to understand the impacts of these stressors on marine biota in isolation, it is vital to understand their combined effects, especially on the early life history stages of marine organisms.

1.6 Hypotheses, Aims and Objectives

Several studies have been published that have reported calcification mechanisms during ontogeny of bivalves, and the effects of ocean acidification on these mechanisms. However, the aim of this study is to close the gap between gene expression and mineralisation during ontogeny and to demonstrate the molecular processes of calcification during development and the corresponding changes in the microstructures and shell mineralogy of the Pacific oyster *Crassostrea gigas* in a changing environment. To my knowledge, this is the first study of the interactive effects of ocean warming and CO_2-driven acidification on bivalve growth, gene expression, shell development and mineralogy from the beginning of development to the benthic adult.

Hence, this work possessed the following hypotheses. It was predicted that a) changes in environment are reflected in changes in gene expression and ultimately in shell microstructures, b) development would be facilitated by warming up to a threshold, c) calcification would be impaired by decreasing pH, and d) due to temperature enhancement of metabolic processes,

increased temperature would antagonise the negative effects of decreased $CaCO_3$ saturation states on shell development.

The specific aims of this research were:

1. Identification of key molecular mechanisms involved in the calcification processes of larval, juvenile and adult *Crassostrea gigas*
2. Identification of possible impacts of changes in environmental conditions (seawater pH and temperature) on these molecular mechanisms
3. Identification of possible impacts of changes in seawater pH and temperature on (shell) larval development
4. Identification of shell microstructures and components of *C. gigas* in all shell- bearing life stages like veliger, juvenile and adult stage
5. Identification of how changes in these molecular mechanisms correlate with the expression of different biomineral microstructures in the forming bivalve shell
6. Identification of possible impacts of changes in environmental conditions (seawater pH and temperature) on shell microstructures, $CaCO_3$ precipitation and shell mineralogy.

1.7 Chapter outline

Within the framework of this study the impacts of multiple stressors on an entire life cycle of *C. gigas* on growth, gene expression and shell development were investigated for the first time. Chapter 1 has summarised the biology of *C. gigas*, the concepts of biomineralisation and the impacts of environmental changes on bivalves. In Chapter 2, experiments and methods applied in this research are described. In Chapter 3, the effects of elevated temperature and decreased pH on larval development and growth are discussed as well as the impacts of low pH on juvenile and adult growth. Chapter 4 focuses on the effects of temperature and pH on gene expression of biomineralisation genes in larvae, spat and adults. Chapter 5 investigates the impacts of pH and temperature on $CaCO_3$ precipitation, shell structure, composition and crystallinity during ontogeny. In Chapter 6 all results are discussed in the broad context of biomineralisation processes in *Crassostrea gigas* in a changing future oceans.

2 - Material and Methods

In the following material and methods for each experimental chapter will be presented, marked by subheadings matching Chapters 3-5.

2.1 The difficulties of growing up - Development of the Pacific oyster *Crassostrea gigas* under future ocean conditions (Chapter 3)

This study was performed to investigate the underlying mechanisms of biomineralisation in the Pacific oyster *Crassostrea gigas* during ontogeny. As already mentioned in Chapter 1, shell mineralogy changes during development, from ACC to aragonite in larval shells to mainly calcite in adult shells. The experiments designed and explained in the following were carried out to develop a deeper understanding of the basics of calcification and to understand how a changing environment could impact biomineralisation during a life span of an economically important bivalve species (Chapter 3). Molecular techniques were applied to understand which genes are involved in shell development (Chapter 4) and if/how these genes eventually are in charge of changes in shell mineralogy during ontogeny. To investigate changes in mineralogy and shell microstructures during development, shell morphology and shell crystallinity were examined and described (Chapter 5). Eventually it was investigated whether changes in environmental conditions were consistently reflected in both the molecular mechanisms as well as in mineralogical and microstructural changes of the developing shells (Chapter 6).

2.1.1 Responses of juveniles and adults to low pH – experiment 1

To investigate how and if growth and feeding rate of juvenile and adult oysters respond to decreased seawater pH at ambient seasonal water temperature, an initial experiment was conducted from January 26th to May 7th 2010 at Ifremer, Station d'Argenton, France. Growth and feeding rates of juvenile (< 1 yr.) and adult (> 2 yrs.) *C. gigas* were studied under controlled ambient conditions (pH 8.3 15°C) and compared with animals reared in seawater with decreased pH (pH 7.5 15°C) over a period of 3.5 months.

2.1.1.1 Animals

On 15th of January 2010 38 mature adult and 60 juvenile *C. gigas* were collected at Rade de Brest, Brittany, France and transferred into a 450 l tank at Ifremer, Station d'Argenton, France, containing 15°C 1 µm- filtered and UV-sterilised seawater (JBL AquaCristal UV-C, 9W, JBL GmbH & Co. KG Neuhofen, Germany). After several days of acclimation the animals were transferred into the experimental system on February the 2nd 2010.

2.1.1.2 Experimental system – experiment 1

The experimental system consisted of two tanks, each containing 19 adult and 30 juvenile oysters and a 20 l header tank without oysters in which the low pH seawater condition was pre-mixed (Figure 77). The seawater pH of 8.3 in the control tank simulated the seawater pH in natural conditions, while tank 2 simulated the expected seawater pH of 7.5 of the year 2100 (Caldeira and Wickett, 2003; Raven et al., 2005). Tank 1 and the header tank were connected to the general seawater supply system, which pumped 1 µm- filtered and UV- sterilised seawater (JBL AquaCristal UV-C, 9W, JBL GmbH & Co. KG Neuhofen, Germany) at 100 ml min^{-1} into the system. The temperature in both tanks was set to 15°C, simulating the ambient seasonal seawater temperature for northern Finistère, France; mean salinity was 34. The acidified seawater for tank 2 (treatment) was supplied by the header tank, which was bubbled with 100% CO_2 gas (160 bubbles min^{-1}, JBL ProFlora m2000, JBL GmbH & Co. KG Neuhofen, Germany) and regulated by a computerised pH and temperature control system (JBL ProFlora pH Control, JBL GmbH & Co. KG Neuhofen, Germany). To obtain a pH of 7.5 in tank 2, the pH in the header tank was set to 7.35 as preliminary tests showed a change in pH as the water flowed from the header tank to the experimental system. A possible explanation of the change in pH could be the outgassing of CO_2 from tank 2 as changes in pH already were observed at the beginning, when no animals were present. The oysters were fed with *Isochrysis T-ISO galbana* (T-ISO) algae with a flow-rate of 4-5 ml min^{-1} per tank and a concentration of approximately 67 T-ISO cells μl^{-1} seawater. Optimal phytoplankton concentrations were calculated by daily cell counts in the morning (in- and output of algae) using a Multisizer™ 3 COULTER COUNTER® (Beckmann Coulter Counter, France S.A.S, Villepinte, France).

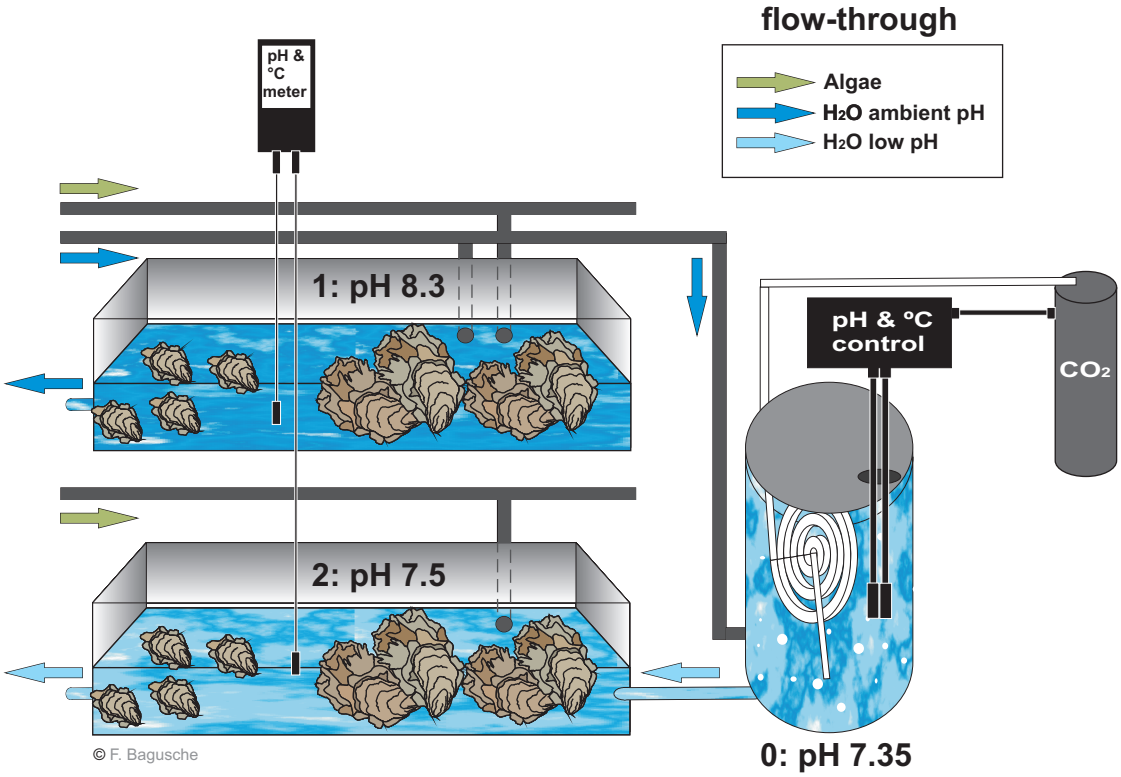

Figure 7: Experimental system to test the impacts of acidified seawater on growth and ingestion of juvenile and adult *C. gigas.* Tank 1 (control): pH 8.3 15°C; tank 2 (treatment): pH 7.5 15°C; tank 0: header tank to supply tank 2 with acidified seawater. The pH in the header tank was set to 7.35 and controlled by a computerised pH and temperature control system. Ambient seawater (pH 8.3 15°C) and algae were supplied via the general supply flow-trough system.

2.1.1.3 Measurements and sampling

1. Temperature, pH, oxygen and salinity measurements

Measurements of temperature, pH, O_2 and salinity were taken once per day in the morning. Temperature and pH were measured using a WTW pH3310 meter with a SenTix41-3 pH-electrode (WTW GmbH, Weilheim, Germany). Standard buffer solutions (pH= 4.0, pH= 7.0 and pH=10.01, L4998 SCHOTT® Instruments GmbH, Mainz, Germany) were used to calibrate the pH meter with an accuracy of 0.01 units. O_2 was measured using a handheld Dissolved Oxygen Meter (Oxi 340i, WTW GmbH, Weilheim, Germany) with a WTW CellOx®325 probe (WTW GmbH, Weilheim, Germany) and salinity was measured with a ProfiLineTM Cond 197i conductivity meter (WTW GmbH, Weilheim, Germany).

2. Consumption rate measurements

To study if there was a difference in algae consumption between oysters in ambient and oysters in low pH seawater, cell counts of the in- and output of algae were made each morning using the Multisizer^{TM} 3 COULTER COUNTER® as described above. The ingestion rate per oyster (10^3 µm^3 l^{-1} h^{-1}) was calculated.

3. Total wet weight measurements

To investigate if growth was affected by decreased pH, the total wet weight was measured of juveniles and adults on the following dates: 29th of January, 12th, 19th and 25th of February, 5th, 12th, 19th and 26th of March, 2nd, 9th, 16th and 30th of April and 7th of May 2010.

4. Tissue sampling

After termination of the experiment, tissue samples for qPCR analyses were taken from both, the left and the right mantle of juvenile and adult oysters. The oysters were carefully opened with an oyster knife to expose the mantle. After weighing the total flesh weight, approximately 5-10 mm of mantle margin was dissected using scalpel and scissors and immediately transferred into an 1.5 µl Eppendorf tube containing at least 1000 µl RNAlater®, (Ambion, Applied Biosystems, Cheshire, UK), a RNA stabilisation reagent. The tissue samples were completely submerged in RNAlater®, incubated at 4°C over night and then transferred into -20°C until further processing.

2.1.2 Larval responses to the combined effects of elevated temperature and low pH – experiment 2

A separate experiment was conducted during July 2011 to investigate the effects of elevated seawater temperature, low pH and the synergistic effects of elevated temperature*low pH on larval development, gene expression and shell development. Larvae were exposed to four different conditions and allowed to develop from PII veliger to post-metamorphosed larvae (spat) over a period of 20 days.

Environmental seawater pH and decreased seawater pH were tested in combination with ambient and elevated seawater temperature (Table 3 & Figure 8).

2.1.2.1 Animals

To produce embryos of the Pacific oyster *Crassostrea gigas*, nine mature male and thirty female individuals were collected on the 11th of July 2011 at Aber Benoît, Finistère, France. The oysters were transferred into a 450 l tank at Ifremer, Station d'Argenton, France, containing 1 µm-filtered and UV-sterilised seawater (JBL AquaCristal UV-C, 9W, JBL GmbH & Co. KG Neuhofen, Germany) at 15°C and kept there for nine days. After three days of acclimation the water was treated with 8 mg/l chloramphenicol (Sigma Aldrich, St. Quentin Fallavier, France).

After six days of antibiotic treatment, embryos were produced on the 20th July by strip spawning of the mature gonads. The quality of oocytes and sperm were determined by sperm-motility, the shape of the oocytes and the colour of the oocyte-cytoplasm. If the shape of the oocytes was round and the colour of the cytoplasm was dark, they were chosen for further *in-vitro*-fertilisation. The gametes were collected onto a 60 µm sieve, washed onto a 20 µm sieve and then transferred into 5 l beakers with filtered ambient seawater (20°C pH 8.1) for fertilisation with a concentration of less than 100 spermatozoa per oocyte. The observed fertilisation rate was about 90-100%. After two hours, approximately 50 million fertilized oocytes were transferred into a 150 l tank (herewith referred as treatment 0) with aerated and filtered seawater (20°C pH 8.1), without flow-though or algal supply. The fertilised embryos (14.6 million larvae in 150 l) were incubated in this fixed volume of seawater for 48 hours, until they had reached a size in excess of 40 µm. On the 22nd July, the PII veliger were then concentrated onto a 40 µm mesh, equally separated and transferred into twelve experimental tanks with aerated and filtered seawater. The initial density of larvae per 5 l tank was 161 larvae ml^{-1}.

2.1.2.2 Experimental system – experiment 2

The conditions were pre-mixed in four tanks and then pumped into the experimental tubes (Figure 7). To obtain a pH of 7.4, the seawater was bubbled with 100% CO_2 gas (160 bubbles mn^{-1}, JBL ProFlora m2000, JBL GmbH & Co. KG Neuhofen, Germany) and adjusted by a pH control system (JBL ProFlora pH Control, JBL GmbH & Co. KG Neuhofen, Germany). The water temperature was down regulated to 20°C by an external water-cooling system (HC-1000A, AQUAVIE, Paris, France) to maintain seasonal ambient water temperature for northern Finistère. Elevated water temperature of 24°C was provided by the general water supply system. The average room temperature was 21.4°C.

Each condition was operated in triplicates of each 5 l, providing a continuous flow-through (87 ml mn^{-1}) of UV-treated (JBL AquaCristal UV-C, 9W, JBL GmbH & Co. KG Neuhofen, Germany), 1 µm-filtered and aerated (30 ml min^{-1}) seawater. Depending on the larval size and the developmental stage, the outlet of each tube was sealed with a 40 µm or 60 µm mesh to prevent the larvae being washed out from the experiment.

Table 3: Treatment ID, corresponding pH and temperature tested. Control in bold.

Treatment	pH	Temperature (°C)
1	7.4	24
2	7.4	20
3	**8.1**	**20**
4	8.1	24

In order to provide the larvae with food, a 50:50 mixture of *Isochysis T-ISO galbana* (T-ISO) & *Chaetocerus gracilis* (CG) algae was injected into the system from day two onwards. The optimal concentration of ~1500 μm^3 μl^{-1} algae was calculated by cell counts (in- and output of algae) twice a day as described before. By manual adjustments of the control unit of a pump (ISMATEC Reglo ISM827B, IDEX Health & Science GmbH, Wertheim, Germany) connected to the general algae supply system of the institute, the optimal concentration of algae was maintained twice a day.

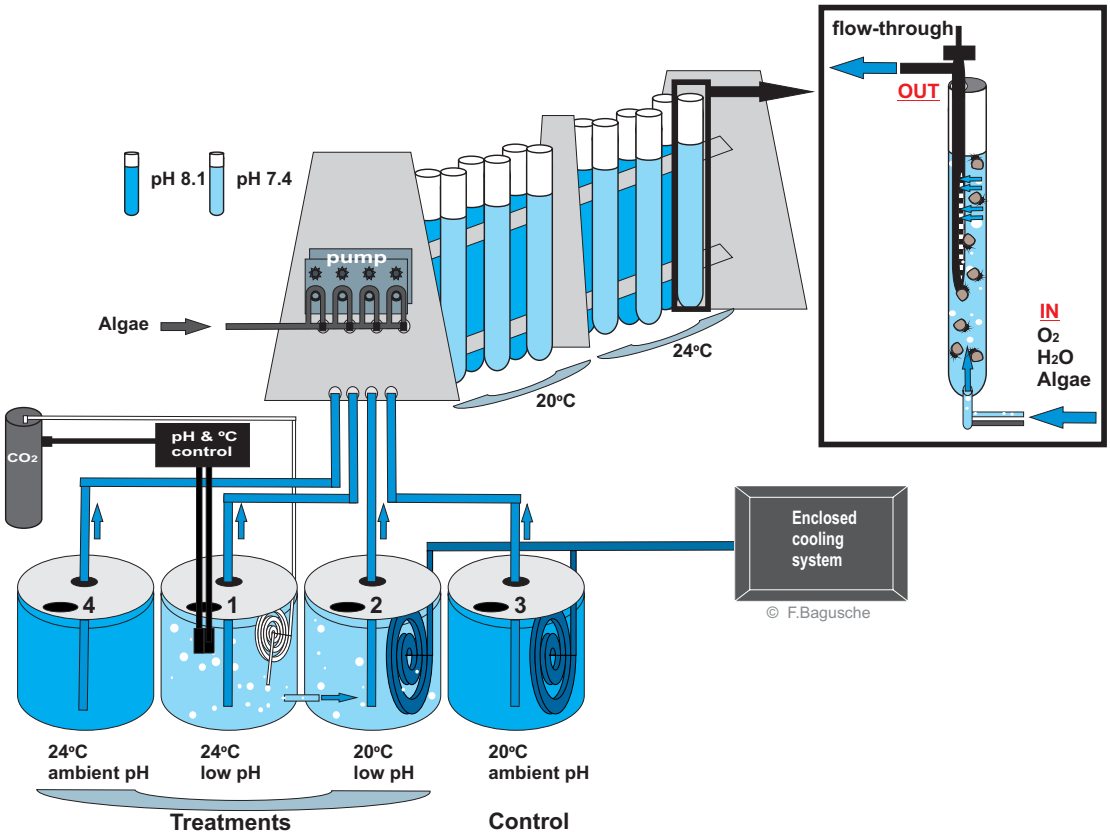

Figure 8: Experimental system to test the effects of temperature and pH on larval development of *C. gigas*. Treatments and control were pre-mixed in tanks and then pumped into the experimental tubes. Each treatment (24°C pH 8.1; 24°C pH 7.4; 20°C pH 7.4) and the control (20°C pH 8.1) consisted of three replicate tubes containing larvae and were supplied *via* a flow-though system with O_2, filtered and UV-sterilised seawater. Algae were injected into the system and concentrations were daily adjusted.

2.1.2.3 Measurements and sampling

1. Temperature, pH, oxygen and salinity

Seawater pH, temperature, oxygen and salinity were measured twice a day throughout the entire experiment in both, tanks and experimental tubes as described before.

2. Carbonate chemistry

Samples for the determination of Dissolved Inorganic Carbon (DIC), Total Alkalinity (TA) and nutrient analyses for each condition were taken on day 1, 6, 19 and 22 of the experiment corresponding to the sampled developmental stages of larvae (Table 4).

Following the protocol of Dickson et al. (2007) and Dumousseaud et al. (2011), a piece of Tygon Tubing (R1000, 6.4 mm x 1.6 mm, Fisher Scientific, Leicestershire, UK) attached to the outlet of the tanks and prepared with a 40 µm mesh, was inserted at the bottom of a 250 ml borosilicate glass bottle (Duran, Fisher Scientific, Leicestershire, UK). The water was left to overflow by at least half of the volume of the bottle to prevent any air bubbles being trapped in the sample. After inserting the glass stopper to remove the stopper volume and after removing an additional 2.5 ml of water to allow water expansion, the samples were immediately fixed with 50 µl of a saturated mercuric chloride solution. The labelled bottle was then sealed with an airtight glass stopper prepared with Apiezon grease (AP101, Fisherbrand, Fisher Scientific, Leicestershire, UK) and stored in the dark at 4°C until analysis.

Dissolved Inorganic Carbon (DIC) and Total Alkalinity (TA) were measured at the Carbonate Facility at the National Oceanography Centre, Southampton by Dr. Cynthia Dumousseaud using an Apollo SciTech DIC infrared analyser (AS-C3) (Apollo SciTech, Inc., Bogart, GA 30622 USA) and an Apollo SciTech AS-ALK2 Alkalinity Titrator (Apollo SciTech, Inc., Bogart, GA 30622 USA). Certified Reference Materials provided by A. G. Dickson (Scripps Institution of Oceanography, University of California San Diego, U.S.A) were used as standards to calibrate the system prior each measurement. The parameters of the carbonate system were calculated with the CO_2SYS program (Lewis et al., 1998) using the thermodynamic constants of Mehrbach et al. (1973) refitted by Dickson and Millero (1987). Nutrients were measured by Dr. Mark Stinchcombe at the National Oceanography Centre, Southampton, UK on a Skalar San+ auto analyser (Skalar Analytical B.V., Netherlands) calibrated for the expected range of nutrient concentrations.

3. Sampling of larvae

Samples of larvae for developmental studies (see Chapter 3), quantitative real-time PCR (qPCR) (see Chapter 4), Scanning Electron Microscopy (SEM) and Fourier Transform Infrared (FTIR) spectroscopy (see Chapter 5) were taken corresponding to the main developmental steps which were trochophora, PI veliger, PII veliger, eyed pediveliger and spat.

3.a) Sampling for developmental studies (Chapter 3)

To analyse and compare larval growth in different environments, samples were taken from each condition on day 3, 5, 7, 8, 12, 14, 15 and 17 of the experiment and imaged with a Sony 3CCD

Color Video Camera (DXC-930P, Sony Cooperation, Japan) mounted onto a LEICA DMIL microscope (Leica Microsystems, Wetzlar, Germany) and using the IMAQ^{TM} Vision Builder software (Version 6.0, National Instuments, Austin, Texas, USA). Shell widths, or dorso-ventral measurements (DVM) of at least 50 larvae per condition were measured for statistical analyses at Ifremer using the Macnification software (Version 2.0, Orbicule Inc., Leuven, Belgium).

3.b) Sampling for qPCR (Chapter 4), SEM and FTIR analyses (Chapter 5)

To investigate, if the genes of interest show different expression profiles during development when reared in different treatments, samples of larvae were taken on the dates listed in Table 4, fixed in RNAlater® and stored in -20°C until further analysis. Samples for shell growth, shell microstructure (SEM) and shell composition (FTIR) analyses were taken on the same dates, fixed in 70% ethanol to preserve the shells and stored at room temperature until further analysis. To obtain a similar amount of larvae for all treatments per sample (~150.000 larvae/1.5 ml microcentrifuge tube), 500 ml of stirred water was filtered onto a 20 µm mesh from which the larvae were collected using a pipette. Then, the larvae were transferred into a 1.5 ml microcentrifuge tube containing either RNAlater® or ethanol 70%. From each of the four conditions, a maximum of six samples (two of each replicate) per sampling day per 5 l tube were taken – three for qPCR analyses and three for SEM and FTIR studies. Individuals of spat were collected by hand, carefully removed from the experimental tubes and then fixed as described above.

Table 4: Treatment, sampling dates, developmental stages and age of larvae sampled for qPCR, SEM and FTIR analyses. For each treatment approximately ~150000 larvae/1.5 ml tube were fixed in RNA®later for qPCR analyses and in 70% ethanol for SEM and FTIR studies. Treatment 0: Batch condition: 20.8°C, pH 8.1; Treatment 1: 20.8°C, pH 8.1; Treatment 2: 20.8°C, pH 7.4; Treatment 3 (control): 20.8°C, pH 8.1; Treatment 4: 24°C, pH 8.1. Individuals of spat were collected by hand and transferred into the fixation reagent.

Experimental day	Sampling date	Developmental stage	Time after fertilisation (af)	Treatment
0	**Fertilisation 20th August 2011**			
1	21st August 2011	Trochophora	17 h	0
1	21st August 2011	PI veliger	24 h	0
6	26th August 2011	PII veliger	6 d	1-4
19	08th September 2011	Eyed pediveliger	19 d	1-4
22	11th September 2011	Spat	22 d	4
22	**Termination 11th September 2011**			

2.2 Molecular mechanisms of biomineralisation during ontogeny of the Pacific oyster *Crassostrea gigas* under future ocean scenarios

Biomineralisation mechanisms during ontogeny on a molecular level are largely undiscovered in molluscs contrary to other marine invertebrates such as in echinoderms (Hammond and Hofmann, 2012; Killian et al., 2010; Livingston et al., 2006; Martin et al., 2011). This study was carried out to discover some of the molecular mechanisms underlying biomineralisation in *C. gigas* during ontogeny and to analyse if/how these mechanisms are affected by altered environmental conditions.

2.2.1 Identification of Candidate and Endogenous Reference Genes for Gene Expression Studies

To identify genes that are possibly involved in biomineralisation processes of *Crassostrea gigas* three different methods were applied. The first approach was to search EST databases and publications to create a list of possible target genes involved in biomineralisation that have been isolated and sequenced in *Crassostrea gigas*. Secondly, degenerate primers were designed for additional genes of interest and, lastly, a technique of differential display was employed, making use of a commercially available GeneFishing^{TM} kit (Seegene, Seoul, South Korea).

2.2.1.1 Searching EST-databases and Literature

To create an initial list of target genes an EST database of *Crassostrea gigas* (http://www.ifremer.fr/GigasBase/) (Gueguen et al., 2003), the database of the National Center for Biotechnology Information (NCBI, http://www.ncbi.nlm.nih.gov/) and existing publications were searched.

The chosen genes of interest (GOI), putatively known to be involved in biomineralisation processes with sufficient sequence data were human dentin sialophosphoprotein (Accession number: Q9NZW4) here referred as dentin, and perlucin (*Haliotis laevigata;* Accession number: *P82596).* Perlucin was first purified from the nacreous layer of *Haliotis laevigata* by Weiss and co-workers (2000). *In vitro* experiments suggested that perlucin could accelerate

calcium carbonate precipitation and direct the morphology of the crystals. Perlucin is a functional C-type lectin showing a calcium-dependent carbohydrate binding activity with galactose and mannose specificity (Mann et al., 2000). C-type lectin domains are, by definition, calcium-dependent carbonate-recognition domains, which have been found in different calcifying systems like some sea urchin spicule matrix proteins, and others. In precipitation assays with saturated calcium carbonate solution perlucin also shows nucleating activity (Mann et al., 2000). Dentin sialophosphoprotein (DSPP), a highly phosphorylated protein in *Homo sapiens* that belongs to the family of small integrin-binding ligand N-linked glycoproteins (SIBLINGs) (Suzuki et al., 2012), is cleaved into two chains, namely dentin phosphoprotein (DPP) and dentin sialoprotein (DSP). The function of DSP is still not clear, but it may play an important role in dentinogenesis in humans, whereas DPP may bind high amounts of calcium and facilitates initial mineralisation of dentin matrix collagen by playing a direct role in the nucleation of hydroxyapatite onto dentin matrix collagen. DPP may also regulate the size and shape of the hydroxyapatite crystals (Butler, 1998; Gu et al., 2000; Veis et al., 1998).
Commonly used endogenous reference (ER) genes for quantitative real-time PCR chosen for this study were β-actin (*C. gigas;* Accession number: O17320), α-tubulin (*C. gigas;* Accession number: *AB185494*), cyclophilin (*C. gigas;* Accession number: *AY551095*) and 18S ribosomal RNA (rRNA) (*C. gigas;* Accession number: *AB064942*). Actins are highly conserved proteins that are involved in cell motility, structure, and integrity and are ubiquitously expressed in all eukaryotic cells. Tubulins are a major constituent of microtubules, with its most common members α-tubulin and β-tubulin. Cyclophilins are a family of proteins that facilitate protein folding and are involved in immune system regulation and 18S rRNA is a part of small eukaryotic ribosomal subunit (40S) and a basic component of all eukaryotic cells (Alberts et al., 2007).

2.2.1.2 Degenerate Polymerase Chain Reaction

To add additional informative candidate biomineralisation related genes, degenerate primers were designed for calmodulin, nacrein and ubiquitin-like fold modifying protein based on possible biomineralisation roles identified in published literature.
Calmodulin (*CaM*) is known as a pivotal calcium metabolism regulator in nearly all organisms, is highly conserved among the molluscan phyla and is thought to play an important role in the shell formation mechanism (Li et al., 2004). Calmodulin has been isolated from *Pinctada fucata* (Accession number: Q6EEV2) where the corresponding mRNA (AY341376) showed its highest expression level in the gill, a key organ involved in calcium uptake in oysters. Strong *in situ*-hybridization signals were also detected in the mantle folds and the outer epithelial cells of the

dorsal mantle region, suggesting that *CaM* is involved in regulation of calcium transport and secretion (Li et al., 2004).

The matrix protein nacrein is a significant component in the water-soluble matrix and is conserved in bivalves and gastropods (Miyamoto et al., 1996; Miyamoto et al., 2003). Although nacrein was first isolated from the matrix of nacreous layer of *Pinctada fucata* (Accession number: protein: Q27908*,* gene: D83523), it was also found in the prismatic layer (Miyashita et al., 2002). According to Miyashita (Miyashita et al., 2002) and Miyamoto (Miyamoto et al., 2005), nacrein mRNA is expressed in both the mantle edge and mantle pallial, suggesting that it is involved in prism and nacre mineralisation. The characteristic feature of nacrein is its carbonic-anhydrase (CA)-like structure with the repetitive domain Gly-Asn-Asn (Glycine-Asparagine-Asparagine), and Gly-Asp-Asn (Glycine-Asparic acid-Asparagine). Carbonic anhydrase catalyses the reversible hydration of carbon dioxide to form bicarbonate (HCO_3^-) ions (Gaume et al., 2011). CA also supports the maintenance of carbonate oversaturation and thus is the driving force towards mineral deposition. It also supports pH regulation in both calcified and non-calcified tissues. Miyamoto and co-authors (Miyamoto et al., 2003; Miyamoto et al., 2005) suggested in their studies that nacrein has the ability to bind Ca^{2+} and also detected a carbonic anhydrase activity. Therefore, it is plausible that nacrein would function both as a calcium concentrator and as an enzyme required for production of carbonate ions, which are assembled to $CaCO_3$ at mineralisation sites. Miyamoto et al. (Miyamoto et al., 2003; Miyamoto et al., 2005) demonstrated that in absence of the repeat domain, the inhibitory effect of nacrein on $CaCO_3$ crystallization was suppressed, which suggested that the repeat domain acted as a regulator for the negative function of nacrein in mineralisation.

Has-ubfm or *Haliotis asinina* ubiquitin fold-like modifier (Accession number: *DW986191*), expressed from trochophora to adult stage in the abalone *Haliotis asinina,* encoded an open reading frame (ORF) similar to ubiquitin fold-like modifying proteins from various organisms (Jackson et al., 2007). In trochophora larvae, *Has-ubfm* was expressed exclusively in the ectodermal cells of the expanding shell field, while in pre-torsional veliger, *Has-ubfm* was found in the foot primordia adjacent to the newly forming operculum suggesting an involvement in shell construction. In post-torsional veliger, expression of *Has-ubfm* was restricted to ectodermal cells associated with the digestive gland, while in juveniles *Has-ubfm* was expressed in various tissues, especially in the anterior edge of the outer mantle fold (Jackson et al., 2007).

Primers for calmodulin (as an example of the procedure, Figure 9), nacrein and ubiquitin-like fold modifying protein were designed based on conserved regions identified from protein sequence alignments (see Table 5 for sequences used and Accession numbers) by the CLUSTALW2- Multiple Sequence Alignment tool (EMBL-EBI, European Bioinformatics

Institute, http://www.ebi.ac.uk/Tools/msa/clustalw2/) using the default settings. The protein sequences of conserved regions were identified as potential primer sites. Conserved primer sequences were translated into a degenerate nucleotide sequence and a minimum of two primers of both, forward and reverse were designed (Table 6). The designed primers were synthesised by Eurofins MWG Operon, Ebersberg, Germany. The PCR cycle parameters performed are shown in Table 7.

Table 5: Sequences used for alignments to design degenerate primers. Listed are the protein names and the corresponding sequences the primers were based on, described by species names and Accession numbers.

Protein name	Species names and Accession numbers
Calmodulin	*Pinctada fucata (AAQ20043), Lumbricus rubellus (Q9GRJ1), Aplysia californica (AAK61380), Hyriopsis cumingii (A4UUE2), Hyriopsis schlegelii (B6E135), Homo sapiens (AAH06182), Ciona intestinalis (CAA73906), Mus musculus (NP_033920), Schistosoma japonicum (AAW27335), Metridium senile (BAB61794,), Patinopecten sp. (P02595)*
Nacrein	*Crassostrea nippona (A0ZSF7), Pinctada fucata (A0ZSF2), Pinctada maxima (A0ZSF3), Mizuhopecten yessoensis (A0ZSF4), Crassostrea nippona (A0ZSF6)*
Ubiquitin fold modifier	*Has-ubfm (DW986191), Strongylocentrotus purpuratus (XP_783597), Danio rerio (AAQ94583), Homo sapiens (AAH05193.1), Xenopus tropicalis (NP_001016988.1), Caenorhabditis elegans (NP_498705.1), Arabidopsis thaliana (NP_177894.1), Chlamydomonas incerta (AAV71156.1)*

Table 6: Forward (F) and reverse (R) degenerate primers for ubiquitin fold modifier (*ubfm*), calmodulin (*CaM*) and nacrein (*nac*). Melting temperature (T_mºC), primer length and the expected size of PCR product amplicon length in nucleotide basepairs (bp) are listed. Representations for sequence positions which can have alternative bases are: N=A,C,G,T; V=G,A,C; D=G,A,T; B=G,T,C; H=A,T,C; W=A,T; M=A,C; R=A,G; K=G,T; S=G,C; Y=C,T (International Union of Pure and Applied Chemistry, IUB). The successful working primers are in bold.

Gene/Primer name	Primer Sequence 5 to 3'	Primer length (bp)	T_m (°C)	Amplicon length (bp)
ubfm				
ubfm F2a	ACNCCNTTYACNGCNGT	17	54	
ubfm F2b	GCNCCNTTYACNGCNGT	17	56.4	
ubfm R2a	GYTTYAARAANACRTTNCCNGC	22	57.5	
ubfm R2b	GYTTNAGRAANACRTTNCCNGC	22	59.3	
CaM				
Cam F3a	GCNGAYCARCTNACNGARGA	20	59.4	
Cam F3b	GCNGAYCARTTRCANGARGA	20	57.3	244
Cam R3	TCGNRTCNGTRTCYTTCATYTT	22	56.5	
nacrein				
Nac F1	CAYGAYCAYTAYATGGAYAAYG	22	56.5	
Nac R1	GTNACYTTRTTYTTYTGNGTNGG	23	58	
Nac R2	CCRTCYTTRTANCCYTCNAC	20	57.3	

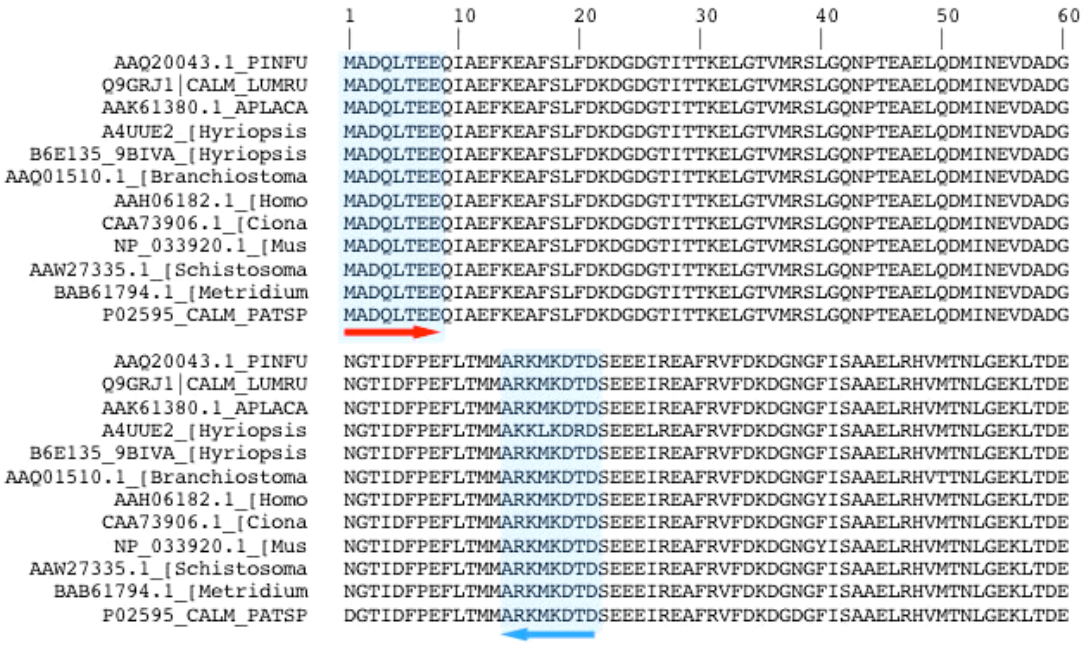

Figure 9: CLUSTALW2- Multiple Sequence alignment. Calmodulin primers, forward (red arrow) and reverse (blue arrow), are located in highly conserved regions of the sequence alignment of: *Pinctada fucata (AAQ20043), Lumbricus rubellus (Q9GRJ1), Aplysia californica (AAK61380), Hyriopsis cumingii (A4UUE2), Hyriopsis schlegelii (B6E135), Homo sapiens (AAH06182), Ciona intestinalis (CAA73906), Mus musculus (NP_033920), Schistosoma japonicum (AAW27335), Metridium senile (BAB61794), and Patinopecten sp. (P02595)*

Table 7: Degenerate PCR cycle parameters. Steps, temperature (°C) and duration of each step as well as the number of cycles are listed. XX denotes the annealing temperature of each pair of degenerate primers – this was empirically determined in each case.

Step	°C	Time	Number of cycles
Initial Denaturation	95	5 min	x 1
Denaturation	95	30 sec	x 30
Annealing	XX	30 sec	
Extension	72	1 min	
Final Extension	72	7 min	x 1

Degenerate PCR results

Degenerate PCR successfully identified calmodulin (*CaM)* to be used in this study as a target gene. The primers for *CaM* gave satisfying results with 24 h and 48 h larvae as well as with the adults. The successful annealing temperature for calmodulin was 50°C. The purified PCR products of *CaM* were cloned and sequenced following the protocols described in section 2.2.1.4. To confirm the identity of calmodulin, the sequence fragment of 244 basepairs (consensus of four sequences) was searched against the NCBI database using the BLASTX function in Geneious™. The analyses showed an overall pairwise identity of 98.8 % (Figure 10) with calmodulin from the African claw frog *Xenopus laevis* (Accession number: *AAH5370*, E-value = $1.68e^{-50}$), the common rat *Rattus norwegicus* (*EDL51715*, E-value = $5.47e^{-49}$), the Pacific oyster *Crassostrea gigas* (*AEA30980*, E-value = $7.14e^{-49}$), the Atlantic salmon *Salmo salar* (*ACI68592*, E-value = $8.48e^{-49}$) and the house mouse *Mus musculus* (*AAA65934*, E-value = $10e^{-49}$) as the top five hits.

Neither the designed primers for *ubfm*, nor those for *nac* worked for a range of melting temperatures combined with veliger and adult stages of *C. gigas*. Annealing temperatures of 45, 48 and 50°C for *nac* and 40, 45, 48 and 50°C for *ubfm* did not result in any amplification. Neither the PCR cycle parameters nor the primers for *nac* and *ubfm* were further optimised, as GeneFishing™ (section 2.2.1.3) seemed to be the more appropriate method to identify more informative gene sequence fragments more efficiently.

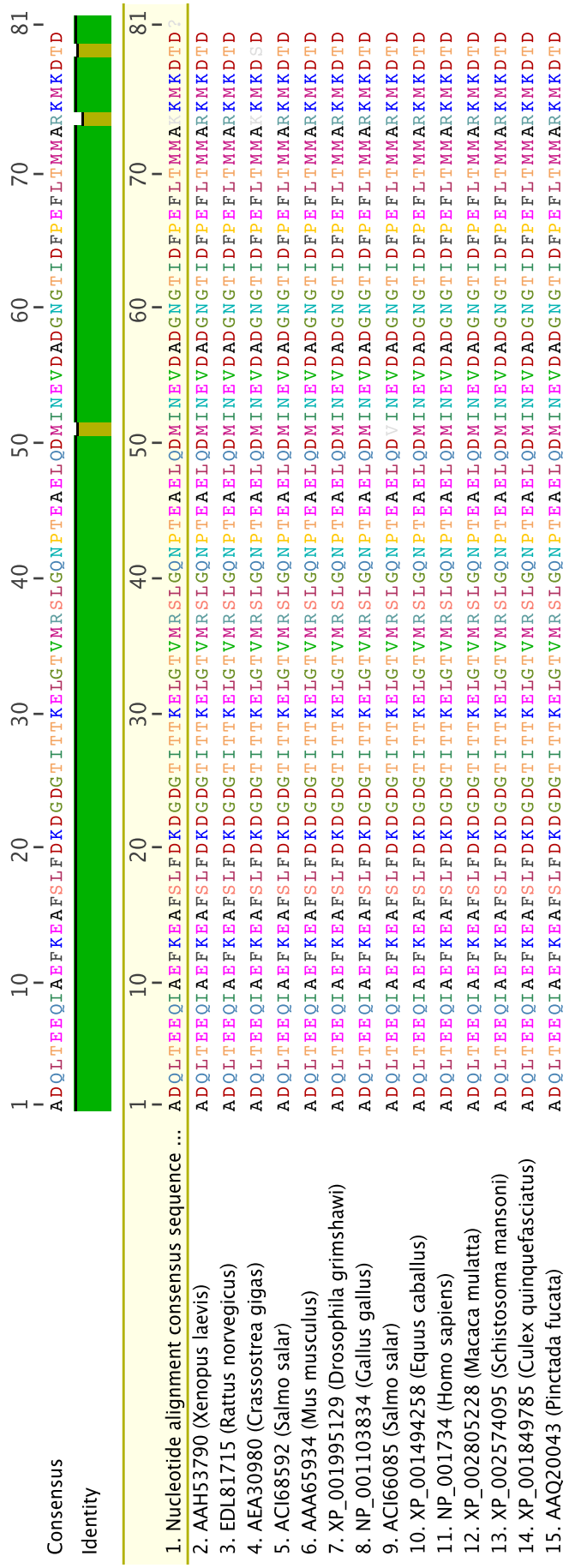

Figure 10: Calmodulin BLASTX alignment. The generated sequence fragment (consensus of four individual sequences) identified by degenerate PCR and highlighted in yellow (1), was searched against the NCBI database using the BLASTX function in Geneious™ to confirm the identity of calmodulin. Overall pairwise identity was 98.8 %. E-values are given in the following: (2) $1.68e^{-50}$ (3) $5.47e^{-49}$ (4) $7.14e^{-49}$ (5) $8.48e^{-49}$ (6) $1.10e^{-48}$ (7) $1.25e^{-48}$ (8) $1.53e^{-48}$ (9) $1.63e^{-48}$ (10) $1.68e^{-48}$ (11) $1.80e^{-48}$ (12) $1.81e^{-48}$ (13) $1.93e^{-48}$ (14) $2.09e^{-48}$ (15) $2.19e^{-48}$.

2.2.1.3 GeneFishing™

GeneFishing™, (Seegene, Seoul, South Korea) a method to identify only 'differentially expressed genes' (DEGs) in two or more nucleic acid samples, was used in all developmental stages (trochophora, veliger, juvenile and adult) of *Crassostrea gigas* as well as in both the right and the left mantle margin of adults. The method is based on arbitrary annealing control primers (ACP) with a tripartite structure (Figure 11), which bind in a two-stage PCR so specific to the template that just the target products are amplified (Figure 11). The tripartite structure of an ACP consists of a core sequence at the 3'end which anneals at the 1st PCR stage (Figures 11 & 12.3b, 12.4), a regulating part (regulator) with a universal sequence in the middle and a universal sequence at the 5'end which anneals at the 2nd PCR stage (Figures 11, 12.5a, 12.5b, 12.6). Thirty different primers from two kits (GeneFishing™ DEG101 Premix (K1001) and GeneFishing™ DEG103 & 104 Premix Kit (K102) were used to increase the coverage of the complete transcriptome of differentially expressed gene targets (GeneFishing™ user manual, version 5.1).

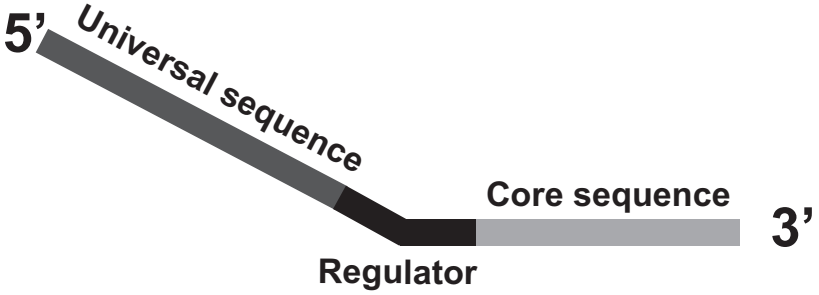

Figure 11: Annealing Control Primer (ACP). The tripartite structure consists of a core sequence at the 3' end, which is connected to the 5' universal sequence by a regulator. Both, universal and core sequence are designed to anneal under different thermal conditions, while the regulator plays a key role in controlling the annealing of each portion to the template. The core sequence is designed to anneal during the first PCR stage and the universal sequence to anneal during the second PCR stage.

cDNA synthesis for GeneFishing™ differential display

During reverse transcription the dT-ACP1 anneals with its poly-T region to the poly-A- tail of the mRNA, which results in a cDNA template with an universal sequence at the 5'-end (Figure 12.1 & 12.2).

The manufacturer's instructions (Seegene, Seoul, South Korea) were followed to reverse transcribe total RNA from each life stage to first-strand cDNA. For each sample, 3 µl of total RNA (100 ng/µl), 10 µl dT-ACP1 and 4.5 µl of RNase-free water was mixed gently and incubated for 3 min at 80°C in a PCR tube. After cooling the samples for 2 min on ice the following reagents were added: 4 µl 5X RT buffer, 5 µl 2 mM dNTP, 0.5 µl RNase inhibitor (40

U μl^{-1}), and 1 µl M-MLV reverse transcriptase (200 U μl^{-1}). The tubes then were incubated at 42°C for 90 min, heated at 94°C for 2 min, and chilled on ice for 2 minutes. The cDNA was then diluted by adding 80 µl of DNase free water and stored at -20°C until ready for use in the GeneFishing™ PCR.

GeneFishing™ PCR

To amplify differentially expressed genes, the following reagents were added on ice to a PCR tube: 3 µl cDNA (100 ng μl^{-1}), 2 µl 5 µm ACP primer, 1 µl 10 µM dt-ACP2, 4 µl Milli-Q™ water and 10 µl 2x SeeAmp ACP Mastermix. The tubes were then placed in a 94°C preheated thermal cycler and following the manufacturer's PCR programme, products were amplified.

PCR stage 1: In the 1st stage of a two-step PCR the first-strand cDNA was denatured at 94°C for 5 min, the 3'-end core portion of the ACP annealed at 50°C to a specific side of the template and by increasing the temperature to 72°C the second-strand cDNA extended in just one cycle (Figure 12.3a-4).

PCR stage 2: In the 2nd stage of the PCR the second-strand cDNA was amplified. The following steps, listed in Table 8, were performed. Due to this two-stage PCR only target PCR products were amplified (Figure 12.5a-6).

Table 8: GeneFishing™ PCR-cycle parameters. Steps, temperatures (°C), times and number of cycles are listed.

PCR Step	°C	Time	Number of cycles
Denaturation	94	5 min	x 40
Annealing of the universal sequence of the dt-ACP and the arbitrary ACP	65	40 sec	
Extension	72	40 sec	
Final Extension	72	5 min	x 1

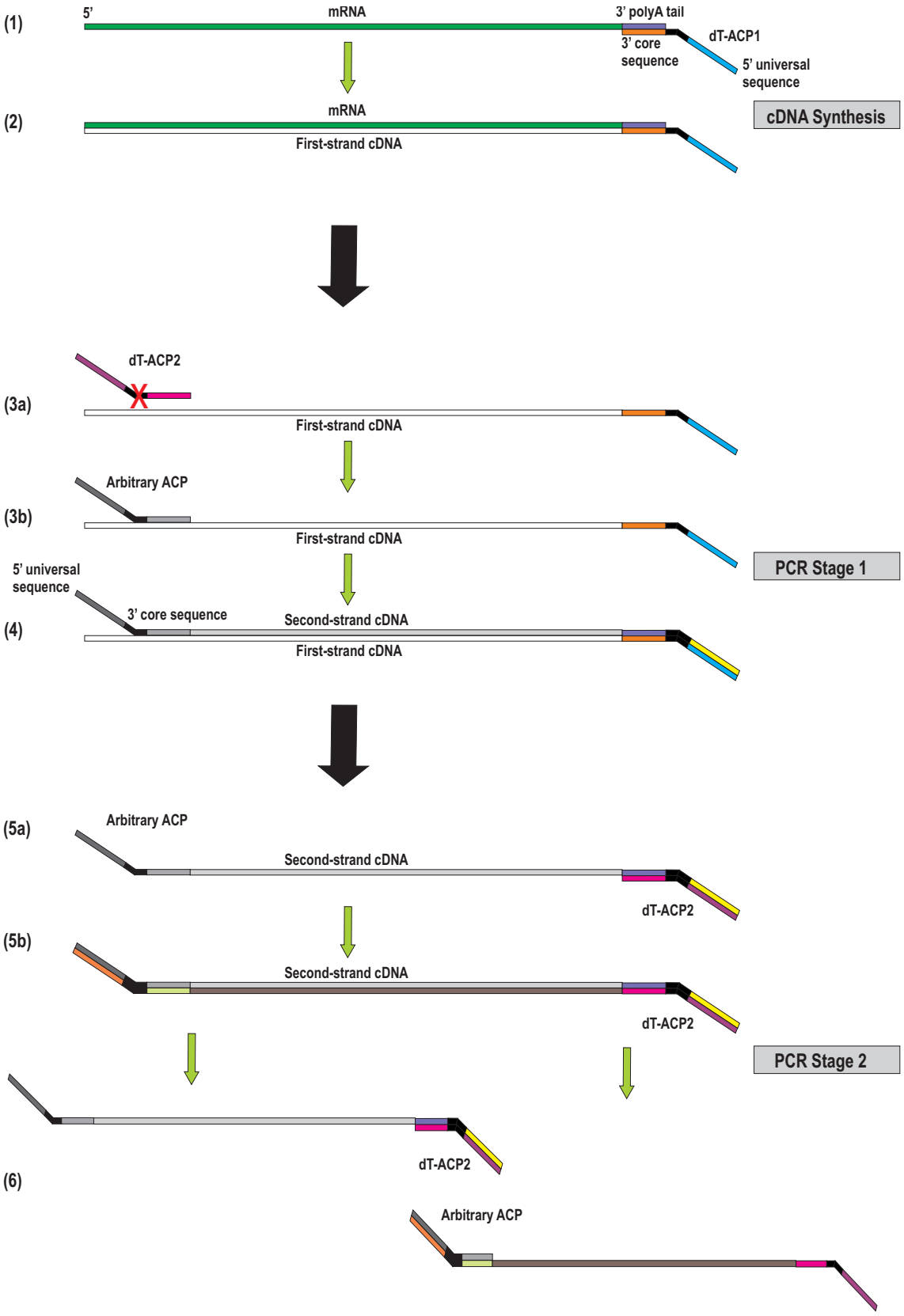

Figure 12: cDNA synthesis and GeneFishing™ PCR flow-chart. (1) & (2): cDNA is synthesized by reverse transcription using dT-ACP1. (3a)-(4): First-stage PCR for second strand cDNA synthesis using conditions optimal for the target sequence of the arbitrary ACPs only. (5a)-(6): Second-stage PCR for amplifying the second-strand cDNA using annealing control conditions optimal for the universal regions of the arbitrary ACPs and dT-ACPs. Figure based on the GeneFishing™ Manual, Version 5 (2005).

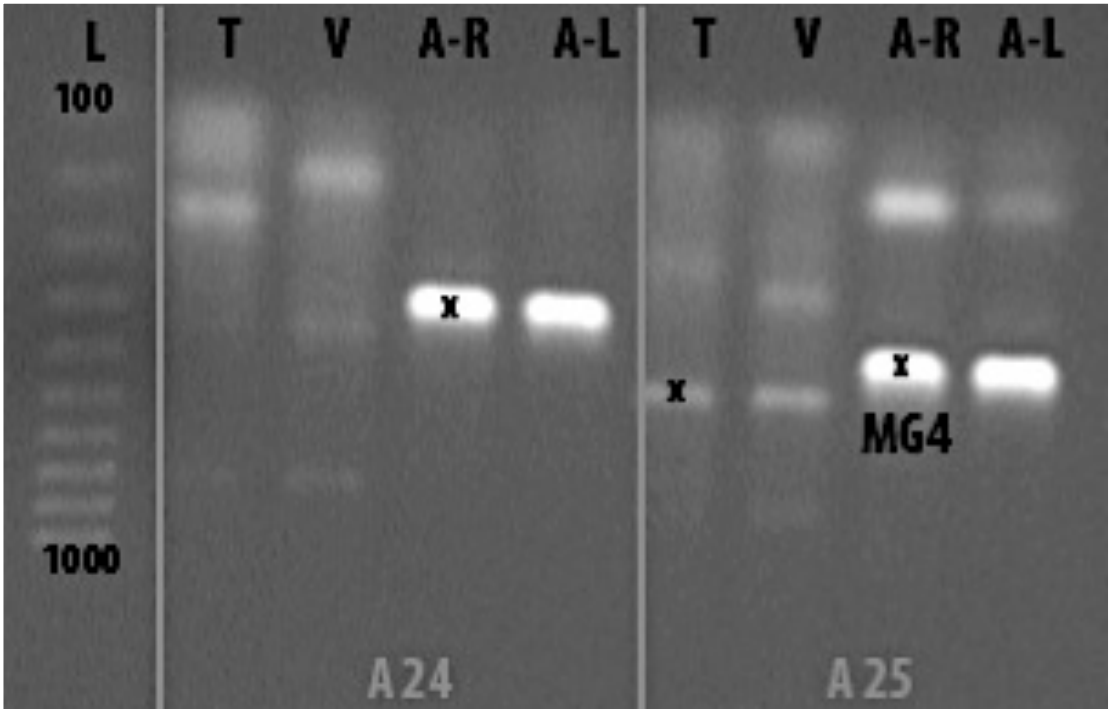

Figure 13: Electrophoresis gel image of GeneFishing™ PCR products. Annealing Control Primer (A) 24 and 25 were tested with each, trochophora (T) larvae, veliger (V) larvae, adult right mantle (A-R), and adult left mantle (A-L) and compared against a 100-basepair ladder (L) (Sigma-Aldrich). Products, which were over 200 basepairs and differentially expressed in different developmental stages (marked with a x), were gel-purified, cloned and sequenced. From the three sequenced genes marked, only mantle gene 4 (*MG4*) was successfully identified as a potential gene of interest.

Analyses of PCR products

The amplified PCR products were then separated and visualised. Using a 2% agarose gel made in TAE buffer containing 6 µl ethidium bromide (10 mg ml^{-1}). Images of gels (Figure 13) were taken using a Gel Doc™ UV transilluminator (Bio-Rad Laboratories Inc., Hemel Hempstead, UK). Products that were differentially expressed in different developmental stages and which were larger than 200 basepairs were purified by gel extraction using a QIAquick®gel extraction kit (Section 2.2.1.4 and Appendix 7.1.1) (Qiagen Ltd., Crawley, UK) for subsequent cloning (Section 2.2.1.4 and Appendix 7.1.2 and 7.1.3).

GeneFishing™ results

GeneFishing™ identified several differentially expressed genes, shown in Table 9. Only *P. fucata* mantle gene 4 (*PFMG4*) was chosen for in this study as it belongs to *PFMG* family, known to be involved in calcification processes in *P. fucata* (Liu et al., 2007; Wang et al., 2011). *PFMG1* is believed to be a calcium-binding protein, responsible for the nucleation of calcium compounds and may participate in nacre formation (Liu et al., 2007) whereas *PFMG3* is thought to enhance biomineralisation in *P. fucata* (Wang et al., 2011). *CGMG4* was expressed

in the right mantle of adult *C. gigas*. A band of the same size visualised in an electrophoresis gel, indicated an expression of *CGMG4* in the left mantle of adult *C. gigas* (Figure 13).

Table 9: GeneFishing™ BLASTX hits of differentially expressed genes. Top hit with lowest E-value, pairwise identity, score value, putative function and developmental stage the gene was expressed at are given. A-R: Adult right mantle; V: Veliger; T: Trochophora. Please refer to section 1.1.5 for explanations on sequence analyses

Top BLAST hit (*Accession no*)	**E-value**	**Pairwise Identity (%)**	**Score**	**Identified in dev. stage**	**Putative function**
C-type lectin 2 like protein (*C. gigas*) (*CAE18170*)	$2.44e^{-17}$	83.3	203	A-R	Carbohydrate binding
Cavortin (*C. gigas*) (*AAT44352*)	$4.32e^{-59}$	79.6	571	A-R	Metal-ion binding; Superoxide dismutase activity
Ubiquitin/ribosomal protein S27 (*C. gigas)* (*AFI80900)*	$9.36e^{-14}$	100	170	V	n/a
Mantle gene 4 (*P. fucata*) (*AAZ76258*)	$4.08e^{-08}$	31.5	147	A-R	Possibly involved in biomineralisation
ATP synthase F0 subunit 6 (*C. gigas*) (*ACD35416*)	$6.87e^{-32}$	89.9	352	T	Hydrogen ion trans-membrane transporter activity
Serine protease inhibitor-1S (*Chlamys farreri*) (*ABB58759*)	$3.46e^{-20}$	64.3	229	A-R	Protease inhibitor
Cadherin (*Aedes aegypt*) (*XP_001658290*)	$7.60e^{-02}$	32	93	V	Calcium ion binding

2.2.1.4 Cloning and sequencing

Cloning and sequencing was carried out using well-established methods. In this study, the positive PCR bands, obtained by degenerate PCR (see Section 2.2.1.2) and GeneFishing™ (see Section 2.2.1.3) were cut from the agarose gel using a sterile razor blade and transferred into a 1.5 ml microcentrifuge tube. DNA was then extracted from the gel using a QIAquick® Gel Extraction Kit (Qiagen Ltd., Crawley, UK) following the manufacturer's protocol (Appendix 7.7.1). After the extraction, the fragments were cloned using a TOPO TA Cloning® Kit for Sequencing (Invitrogen, Paisley, UK). Briefly, the purified PCR products of interest were ligated into 1 µl pCR®4-TOPO®vector (LifeTechnologies™, Paisley, Scotland) to obtain clonally amplified fragments of a gene for sequencing (see Appendix 7.1.2). Following the manufacturer's instructions the cloning reaction was added into the TOP10 OneShot® Chemically Competent *Escherichia coli*. Transformed *E. coli* were grown overnight on Luria Bertrani (LB) agar plates containing 50 µg ml^{-1} ampicillin. An M13-primed colony PCR

(LifeTechnologies™, Paisley, Scotland) following the manufacturer's protocol confirmed the presence of a PCR insert of the correct size. Eight to ten colonies were then picked for each sample and cultured overnight in LB broth with 100 µg ml^{-1}ampicillin. Plasmids were extracted using QIAprep®spin miniprep kit (Qiagen Ltd., Crawley, UK) following the manufacturer's instructions (Appendix 7.1.3) and sequenced by SourceBioscience http://www.lifesciences.sourcebioscience.com/genomic-services/sanger-sequencing-service.aspx (Department of Biochemistry, University of Oxford, UK) using vector-specific M13 primers. SourceBioscience uses Sanger sequencing technology on an Applied Biosystems 3739 DNA Analyzer.

2.2.1.5 Sequence analyses

Using Geneious Basic™ software version 5.3.4 – 5.6.3 (Biomatters Ltd., Auckland, New Zealand) the sequences were uploaded and excised from the vector sequence (see Appendix 7.1.2, Figure 41 for vector map). The chromatograms for each sequence were inspected for reading errors, and alignments for each clone were made to generate the full fragment length. Where available, multiple clones were aligned to generate a consensus sequence and the resulting sequences were searched against the National Centre for Biotechnology Information (NCBI, http://www.ncbi.nlm.nih.gov/) database using BLASTX via Geneious™.

BLAST (Basic Local Alignment Search Tool) is the umbrella term for a vast range of world wide used programs to analyse biological sequence data. BLAST can be used for several purposes, which include identifying species, locating domains, establishing phylogeny, DNA mapping, and comparison. To run, BLAST requires a query sequence to search for, and a sequence to search against (target sequence) or a sequence database containing multiple such sequences. BLAST will find sub-sequences in the database that are similar to sub-sequences in the query. BLASTX is used to compare a nucleotide query sequence with other amino acid sequences stored in protein sequence databases.

The resulting BLASTX alignments were then analysed by pairwise identity or sequence identity, score (S) and E-values. Score values are calculated from the number of gaps and substitutions associated with each aligned sequence - the higher the score, the more significant the alignment. Each score links to the corresponding pairwise alignment between query sequence and hit sequence. An E-value or 'Expect value' describes the number that can be "expected" to see by chance when searching a database. The lower the E-value (the closer it is to zero), the more significant the match is.

2.2.1.6 Summary

Applying these different approaches, including searching EST databases and literature, performing degenerate PCRs and GeneFishing™, identified four possible genes of interest and four possible endogenous reference genes to be used in this study.

Searching EST databases identified two genes of interest – *CGDent* and *CGPerl*. *CGDent* was chosen for this study as dentin is thought to play an important role in hard tissue formation in humans, which made it an interesting novel candidate gene for biomineralisation studies in *C. gigas*. Dentin in humans is cleaved into the two chains DPP and DSP. It is suggested that DPP may bind calcium and facilitates initial mineralisation and DSP may play an important role in dentinogenesis (Butler, 1998; Gu et al., 2000; Veis et al., 1998). *CGPerl* was chosen as a target gene as perlucin is involved in biomineralisation in abalone and may accelerate $CaCO_3$ precipitation and regulate crystal morphology (Mann et al., 2000; Weiss et al., 2000).

Degenerate PCR successfully identified *CGCaM* used in this study as a target gene as calmodulin is thought to regulate calcium transport and secretion in *P. fucata* (Li et al., 2004).

The fourth gene of interest, *CGMG4*, was identified by GeneFishing™ and chosen as members of the *PFMG* family (*PFMG1* and *PFMG3*) are thought to be involved in biomineralisation processes in the pearl oyster (Liu et al., 2007; Wang et al., 2011).

For this study an EST- database search identified *CGAct, CGCyclo, CGTub* and *CG18S* as potential endogenous reference genes. β-actin, cyclophilin, α-tubulin and 18S rRNA are widely used as internal references in qPCR research as they are constitutively expressed and minimally regulated.

2.2.2 Quantitative Real-Time PCR (qPCR)

Quantitative real-time PCR, referred in this study as qPCR (Bustin et al., 2009), remains the most sensitive method to characterise and compare simultaneous measurements of gene expression in different samples (Vandesompele et al., 2002). In this study gene expression between all developmental stages, from trochophora to adult stage, was measured and compared as well as between the different conditions the animals were exposed to.

2.2.2.1 Introduction

In 1989, conventional polymerase chain reaction (PCR) was announced as the "major scientific development of the year" (Guyer and Koshland, 1989). With this ground-breaking technique specific nucleic acid (target) sequences are exponentially amplified, using two specific oligonucleotide primers and a DNA polymerase (Lie and Petropoulos, 1998), which was proclaimed as the "molecule of the year 1989" (Guyer and Koshland, 1989). The so-called *Taq*-polymerase is a thermo-stable enzyme, originating from the thermophile bacterium *Thermus aquaticus* Brock & Freeze, 1969 (A Chien, 1976). By repeated cycles of heating and cooling, even minute amounts of DNA or cDNA can be amplified in presence of buffer, dNTPs, primer, *Taq* and sterile ultrapure water, generating thousands to millions of copies of the desired DNA fragment. The PCR process can be divided into three steps: (1) Exponential amplification, where the amount of product is doubled at every cycle, assuming 100% reaction efficiency; (2) Levelling off stage, at which the reaction slows as the reagents become limited and (3) Plateau phase, where no more product accumulates due to exhaustion of reagents and enzyme (McPherson and Moller, 2006). Conventional (end-point) PCR is a qualitative assessment, where the results are visualised by gel electrophoresis and image analyses, making it a useful tool to identify if genes are present, but this method neither accurately quantifies the amplified products nor measures changes in gene expression.

Since its introduction 16 years ago (Heid et al., 1996), quantitative PCR has become the standard method for quantification of nucleic acid sequences. qPCR follows the same principles as end-point PCR, but detects and quantifies the amount of copies of the amplified cDNA in real-time at an early stage of the PCR. In qPCR, intercalating fluorescent dyes (e. g. SYBR green) or dye labelled probes that bind to PCR products, are used to quantify the amplified products. Probes fluoresce only when cleaved, while dyes fluoresce when bound to double-stranded (ds) DNA. The increase of fluorescence, proportional to the amount of DNA, is measured in each reaction. The output from a real-time PCR reaction in the form of a graph at the end of each reaction known as amplification plot shows the number of PCR cycles against fluorescence. The resulting plots for all the samples are then set with their background

fluorescence at a common starting point (a process known as baseline correction). Then, a threshold level of fluorescence is set above the background but always within the exponential phase of amplification for all the plots (Bustin, 2000). The cycle number at which an amplification plot crosses this threshold fluorescence level is called the "C_q" or quantification cycle (Bustin et al., 2009; Lefever et al., 2009). The term C_q was used according to the Real-time PCR Data Markup Language (RDML) (http://www.rdml.org/) (Lefever et al., 2009) instead of cycle threshold value (C_t), take off point (TOP) or crossing point (C_p). The C_q value can be directly correlated to the starting target concentration of the sample. The greater the amount of initial cDNA template in the sample, the earlier (lower) the C_q value for that sample (Gibson et al., 1996). To determine fold-changes in experimental and control samples two basic quantification methods, each suitable for different applications, can be used: "Absolute quantification" *aka* "standard curve" and "relative quantification" (see Section 2.2.2.5). Absolute quantification relates the PCR signal to a standard curve that is prepared from a dilution series of template of known concentration, to determine the copy number of the transcript of interest. The standard curve approach is used when it is important to the experimental design and objective of the project to measure the exact level of template in the samples (e.g. monitoring the viral load in a sample). However, the majority of scientific questions regarding gene expression can be answered with the relative quantification method by measuring the gene expression of the gene of interest based an endogenous reference sample, also known as a calibrator (Livak and Schmittgen, 2001). Using this approach, differences in C_q value between the GOI and calibrator are expressed as fold-changes (i.e. up- or down-regulated) relative to the calibrator sample.

In recent years qPCR has become a well-established method, the "gold standard" (Bustin, 2004), for studying gene expression in medical and biological science. This has raised the need for standardised sample handling, assay-conditions and data analyses to provide quantitative and reliable outcomes. These issues have been addressed by a set of guidelines that propose a **M**inimum standard for the provision of **I**nformation for **Q**PCR **E**xperiments (''MIQE") (Bustin et al., 2009). The guidelines cover all aspects of qPCR that may affect the downstream results and focus on four key areas of standardisation that define any qPCR experiment: (1) study design, (2) technical detail, (3) analysis methods and (4) statistics (Bustin, 2010). In the following, the methods used for gene expression studies in this project will be described, covering the essential key points of the MIQE guidelines including sample handling (see Section 2.2.2.2), assay optimisation and design (see Sections 2.2.2.3 and 2.2.2.4) and data analyses (see Section 2.2.2.5 and Chapter 4).

2.2.2.2 Sample handling

Sample acquisition and purification of RNA mark the initial step of every qPCR assay, as the quality of the template is perhaps the most important factor for the reproducibility and biological relevance of downstream qPCR results (Bustin and Nolan, 2004). Therefore great care was taken whilst processing the samples by following the essential key points of the MIQE guidelines including sample storage, RNA extraction and storage, cDNA synthesis, and DNA purification and storage.

Samples

Samples of larvae, juveniles and adult *C. gigas* were generated at Ifremer as described before and fixed in RNAlater® (Ambion, Applied Biosystems, Cheshire, UK) for molecular analyses following the manufacturer's recommendations. The samples were stored at -20°C until further processing.

RNA extraction

To isolate total RNA from the mantle tissue samples of adult and juvenile and from pooled larvae samples of *C. gigas*, RNA extractions were performed as described below.
Total RNA was extracted from juvenile and adult right and left mantle tissue samples, previously fixed in RNAlater® applying the TRI Reagent® (Sigma-Aldrich, Dorset, UK) method by following the manufacturer's instructions. After removing the RNAlater®, up to 100 mg of tissue was homogenised in 1ml TRI Reagent® per 50-100 mg tissue in order to limit RNase activity in the sample, using a sterile polypropylene tissue pestle. Then, the sample was incubated for about one hour prior to further processing. After adding 0.2 ml chloroform (Sigma-Aldrich, Dorset, UK) per 1 ml TRI Reagent® the sample was allowed to stand at room temperature for approximately 15 minutes.
Phases of total RNA, DNA and proteins were then separated by centrifuging the mixture at 12 000 *g* for 15 min at 4ºC. The clear aqueous layer containing RNA was then transferred into a new microcentrifuge tube and 0.5 ml isopropanol was added per 1 ml of TRI Reagent® used to precipitate the RNA. The mixture was incubated at -20ºC for about two hours and eventually centrifuged for 10 minutes at 12 000 *g* at 4ºC producing a pellet at the bottom of the tube. The isopropanol supernatant was carefully removed and the remaining RNA pellet was washed in 75% molecular grade ethanol (1 ml minimum per 1 ml TRI Reagent®) freshly prepared in diethyl polycarbonate DEPC-treated ultrapure water, mixed and centrifuged for 5 min at 7 500 *g* at 4ºC. The ethanol was removed and the RNA pellet air-dried for about 5-10 minutes. After rehydrating the RNA pellet with DEPC-treated ultrapure water, purity and quantity of total RNA were determined.

As initial total RNA isolations of larvae samples with the TRI Reagent® method were disappointing in terms of RNA yield and integrity, total RNA was extracted following the NucleoSpin® RNA II protocol (Machery-Nagel GmbH & Co KG, Düren, Germany) with several modifications.

As in the most of the larvae samples crystallisation of the RNAlater® made it impossible to spin down the larvae and to remove the RNAlater® without losing too much of the sample, the crystals had to be re-dissolved first. After incubating the samples at 37ºC for 10 min, the samples were immediately transferred onto ice and ice-cold 0.1 M phosphate buffered saline, PBS (2-4 times more PBS than RNAlater®) was added. The PBS was made with sterile DEPC-treated ultrapure water. As the density of the RNAlater® decreased by adding the PBS, the larvae settled or pelleted at the bottom of the tube after centrifugation. The RNAlater® was then carefully aspirated and 700 ml lysis buffer RA1 together with 7 µl β-Mercaptoethanol (β-ME) to inhibit RNase activity were added to the sample and carefully disrupted as described before. Following the filtration of the lysate using a NucleoSpin® Filter at 11 000 *g* for 1 min, 700 µl of 70% ethanol was added to the lysate to adjust the RNA binding conditions and mixed by pipetting up and down 5 times. Then, the lysate was loaded onto a NucleoSpin® RNAII Column, placed into a collection tube and centrifuged at 11 000 *g* for 30 seconds to bind the RNA to the column membrane. To desalt the silica membrane 350 µl MDB (Membrane Desalting Buffer) was applied onto the column, incubated for <5 minutes at room temperature and then centrifuged at 11 000 *g* for 1 min to dry the membrane. This step was repeated once and the eluate was discarded. To digest genomic (g)DNA, each time fresh rDNase mixture was prepared in a 1.5 ml Eppendorf tube by adding 10 µl rDNase to 90 µl rDNase reaction buffer per sample and mixed by flicking the tube. 95 µl rDNase mixture was then directly applied onto the centre of each silica membrane and incubated for 15-30 minutes at room temperature. To wash the silica membrane, four steps were performed. In the first step, 200 µl Buffer RA2 was added and centrifuged for 30 seconds at 11 000 *g*. Afterwards, the NucleoSpin® RNAII Column was placed into a new 2 ml collection tube. In the second wash 600 µl Buffer RA3 was applied onto the column and centrifuged for 30 seconds at 11 000 *g*. The flow-trough was discarded and the NucleoSpin® RNAII Column was placed back into the collection tube. In the third wash, 250 µl ethanol-based Buffer RA3 was added to the NucleoSpin® RNAII Column and centrifuged at 11 000 *g* for 2 min to dry the membrane completely. This step was repeated once. The NucleoSpin® RNAII Column was then placed into a nuclease-free 1.5 ml collection tube. Finally the RNA was eluted in 40 µl RNase-free H_2O, supplied in the kit, and centrifuged at 11000 *g* for 1 min. This step was repeated once using 20 µl RNase-free H_2O to elute the RNA remaining in the silica membrane. Quality, quantity and RNA integrity by RQI were determined as described below.

RNA quality and quantity

High quality RNA plays a major role in the generation of accurate quantitative results from gene expression analyses (Bustin and Nolan, 2004) as cDNA made from degraded RNA will not be as faithfully amplified as cDNA derived from intact RNA (Gingrich et al., 2006).
In this study the purity of RNA was measured by analysing the A_{260}/A_{280} ratio using a ND-1000 spectrophotometer (NanoDrop®, Thermo Scientific, Wilmington, USA). Absorbance at 260 nm (A260) gives an indication of RNA concentration and the ratio A_{260}/A_{280} is an indicator of the purity of the RNA (Denisov et al., 2008). An A_{260}/A_{280} ratio of 2.0 for 'pure' RNA is recommended by Thermo Scientific using the NanoDrop® system, with lower values indicating contamination with proteins or phenols that may inhibit downstream protocols. However, this method does not give any information about RNA integrity and has been criticised for low accuracy (Bustin and Nolan, 2004).

Samples with suitable A_{260}/A_{280} (> 1.7) ratios were then analysed for integrity and quantity using an automated capillary electrophoresis system (Experion™ Bio-Rad Laboratories, Inc., Hemel Hempstead, UK) with StdSens chips and reagents (Experion™ Bio-Rad Laboratories, Inc., Hemel Hempstead, UK). For each run, the RNA StdSens protocol settings for Eukaryotic total RNA were used. Electrophoresis with the Bio-Rad Experion™ system is conducted in channels of microchips and can be performed with as little as 100 pg of RNA. The system provides a measure of RNA degeneration using the ratio of the two large ribosomal RNA molecules (28S/18S rRNA), which are displayed in an electropherogram as two distinct peaks. By visual inspection of the electropherogram the quality of RNA can be assessed, while the integrity is determined by comparing the area of the peaks. To standardise and quantitate the RNA, the Bio-Rad Experion™ software compares the electropherogram of the samples with a series of standardised degraded RNA samples and returns the RNA Quality Indicator (RQI) value. The RQI determines the integrity of RNA and outputs a number between 10 (intact RNA) and 1 (highly degraded RNA) for each eukaryotic RNA sample (Denisov et al., 2008). Ideally samples with an RQI above 7.5 were further processed to cDNA, but due to difficulties of RNA extraction in the larval samples (see troubleshooting at the end of this section), RNA with a lower integrity had to be processed (> 2) as some samples were very limited.

In all analysed *C. gigas* samples just a minor 28S rRNA peak was present. These observations are in agreement with the findings of Dheilly et al. (2011) and can be explained by a breaking point in the rRNA structure that converts 28S into two hydrogen-bounded fragments. These fragments then migrate at the same size as the 18S rRNA during gel electrophoresis and display one large and district peak at 18S and just a minor 28S rRNA peak (Figure 14) (Dheilly et al., 2011).

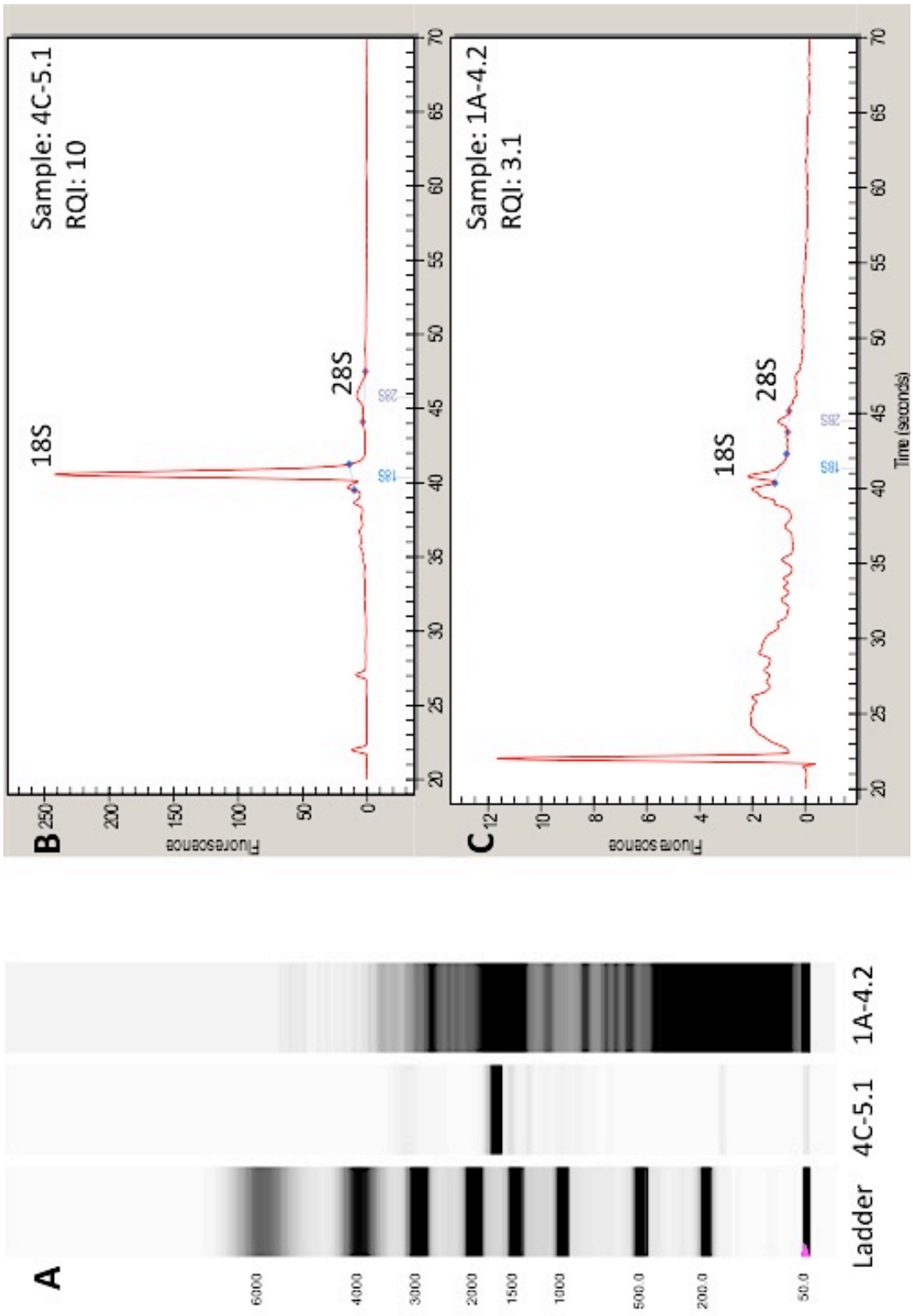

Figure 14: Comparison of intact (4C-5.1) and degraded (1A-4.2) RNA samples. The Experion™ electropherogram for sample 4C-5.1 (B) showed high quality RNA indicated by a distinct 18S peak and visualized by one distinct band on the virtual gel image (A). Sample 1A-4.2 was degraded, indicated by a decreased 18S peak in the electropherogram (C) and smeared bands in the virtual gel image (A). RQI values: Sample 4C-5.1 = 10; Sample 1A-4.2 = 3.1. A260/280 (NanoDrop®) values: Sample 4C-5.1 = 2.11; Sample 1A-4.2 = 1.79. Developmental stage and treatment: Sample 4C-5.1: Spat, cultured at 24°C pH 8.3; Sample 1A-4.2: Pediveliger, cultured at 24°C pH 7.4 (see Chapter 2).

Troubleshooting RNA extraction

In the following the most common problems occurred during this study will be summarised and the discovered and applied solutions will be presented.

The extraction of total RNA can be a difficult process as RNA quantity; quality and integrity can vary from one extraction to another, between developmental stages, between different samples and even between the same samples. Table 10 summarises the problems and applied solutions during the RNA extraction process.

Table 10: Total RNA extraction troubleshooting. Problems and applied solutions during the RNA isolation process are listed.

Method	Problem	Solution
Total RNA extraction	**Crystallised RNAlater® in larval samples** Larvae are surrounded by crystals of RNAlater® and won't form a pellet after spinning	Dissolve crystals by incubating the samples at 37ºC/10 min maximum, vortex and add ice-cold 0.1M PBS (2-4 times more PBS than RNAlater®) to dissolve the remaining crystals and to reduce the density of the RNAlater®, larvae will form a pellet after spinning and the supernatant of RNAlater® can easily be removed
	Genomic DNA in RNA gDNA amplifies in qPCR	Add additional DNase treatment to remove the contaminating DNA either during the RNA extraction protocol or afterwards
	Degraded RNA/ low RNA integrity Poor RQI values	Always work on ice, maintain a sterile working environment, avoid repeated defrosting of RNA, efficient RNA extraction, reduce exposure to RNases by homogenising sample in TRI®Reagent or lysis buffer with β-Mercaptoethanol
	Low yields of RNA	Homogenise in lysis reagent in gentle bursts of 30-45 seconds with 30 seconds of rest until all tissue is in lysis and incubate for <30min on ice. If using spin columns, repeat elution step to release more RNA from the membrane
	Inhibitors in the RNA 1. Low 260/230 measurements due to guanidine salt carry-overs or organic inhibitors 2. Low 260/280 measurements due to protein contaminations	1. More washes with ethanol/washing buffer to desalt the sample/column 2. Use less sample

Purification of RNA Samples and Complementary DNA (cDNA) Synthesis

Prior cDNA synthesis, the RNA samples were cleaned again of traces of gDNA using the Promega DNase treatment kit (Promega Ltd, Southampton UK) following the manufacturer's instructions. The use of the Promega DNase treatment kit was necessary as it was found that the column digestion during RNA extraction using the NucleoSpin® kit did not produce complete removal of contaminating gDNA.

Double reactions of DNase digestion were set up containing 16 µl RNA, 2 µl RQ1 RNase-Free DNase 10X Reaction Buffer and 2 µl RQ1 RNase-Free DNase and were incubated at 37ºC for

30 minutes. To terminate the reaction, 1 µl of RQ1 DNase Stop Solution was added followed by 10 minutes of incubation at 65ºC to inactivate the DNase. The purified RNA samples were stored at -80ºC until cDNA synthesis.

Following the manufacturer's protocol (LifeTechnologies™, Paisley, Sotland) RNA was transcribed into cDNA using SuperScript III Reverse Transcriptase (200 U μl^{-1}). Per reaction 2 µl of 10 ng μl^{-1} Ambion random decamers (Applied Biosystems, Cheshire, UK), 22 µl RNA, 2 µl dNTPs (LifeTechnologies™, Paisley, Sotland) each 10 mM, were mixed in a PCR tube and heated to 65ºC for 5 minutes using a PCR machine. Then, the reactions were placed immediately on ice for at least one minute, followed by brief centrifugation to collect the contents. The following reagents (all from LifeTechnologies™, Paisley, Sotland) were added, mixed by pipetting up and down and incubated at 55ºC for 60 minutes: 8 µl 5X First-Strand Buffer, 2 µl 0.1 M DTT, 2 µl RNase OUT™ Recombinant RNase Inhibitor (40 U μl^{-1}) and 2 µl SuperScript III Reverse Transcriptase (200 U μl^{-1}). Heating at 70ºC for 15 minutes inactivated the reaction. The cDNA was then stored at -20°C until needed.

2.2.2.3 qPCR assay design

Detection chemistry

qPCR fluorescent reporting chemistries can be divided into two categories, specific and nonspecific detection. Specific reporter molecules are sequence-specific probes comprised of an oligonucleotide labelled with a fluorescent dye plus a quencher (e.g., TaqMan® probes (hydrolysis probes), Molecular Beacons and Scorpions), while nonspecific detection is based on intercalating dyes, such as SYBR® Green I, that fluoresce when bound to double-stranded DNA (Bustin and Nolan, 2004). Depending on the budget available to support the project in designing and optimising qPCR assays, the most appropriate detection chemistry must be chosen.

Specific detection: Compared to non-specific chemistries, a higher level of detection specificity is provided by using an internal probe to detect the target gene. In the absence of a specific target sequence in the reaction, the fluorescent probe is not hybridized, remains quenched, and does not fluoresce. After hybridisation with its complementary target, the reporter dye is no longer quenched and a fluorescence signal is generated. The level of fluorescence detected is directly related to the amount of amplified target in each PCR cycle.

A significant advantage of probe-based chemistry compared to DNA-binding dyes is that no nonspecific signal will be generated due to mispriming or primer–dimer artifacts, reducing the need for sequence analysis, or melt curves to confirm the identity of the amplicon. Furthermore, multiple probes can be labelled with different reporter dyes and combined, allowing the

detection of more than one target sequences in a single reaction, referred to as multiplex qPCR (Bustin and Nolan, 2004; Wong and Medrano, 2005).

Nonspecific detection: Nonspecific detection uses intercalating fluorescent DNA-binding dyes, which, when free in solution display relatively low fluorescence, but when bound to double-stranded DNA, the fluorescence increases proportionally to DNA concentration. DNA-binding dyes have two major advantages over probe-based assays, as they can be easily used in already optimised and well-established protocols and the costs are significantly lower, making them very useful for optimising qPCR assays (Bustin and Nolan, 2004). One limitation of assays based on DNA-binding dye chemistry is the indiscriminate binding to nonspecific targets such as primer-dimers. This can result in signal contamination, resulting in artificially early C_q values, which gives an inaccurate representation of the true target concentration. Although signals from nonspecific binding can occur, it is possible to evaluate the amount of nonspecific binding from the desired signal by assessing the melt curve and analysing the sequences.
In present study, the nonspecific fluorescence detection method using SYBR® Green was chosen, taking advantage of its ease handling and lower costs.

Assay method and instrumentation

Assays were run according to the sample maximisation method where as many samples were analysed in the same run rather than using the gene maximisation method, in which multiple genes are analysed in one run and samples are spread across runs if required (Hellemans et al., 2007). Following the sample maximisation method, run-to-run variations between the samples were minimised. To remove the run-to-run differences corrections or calibration factors were calculated on a gene per gene basis between runs.
Each qPCR was performed following the cycling conditions shown in Table 11. Duplicate cDNA templates and no-template controls (NTCs) were run in each reaction (total volume 50 µl). Each reaction contained 4 µl of cDNA, forward primer, reverse primer, sterile ultrapure water, and 25 µl Precision 2x qPCR master mix pre-mixed with SYBR® green I, *Taq* DNA polymerase, dNTPs and buffer (Primer Design Ltd., Southampton, UK). The reactions were divided into two 23 µl volumes in 0.1 ml strip-tubes (Qiagen Ltd., Crawley, UK), designed for the 72-well rotor of the thermal cycler.

All qPCR assays were carried out using a Corbett Rotor-Gene 3000 (Corbett Life Science, Qiagen Ltd., Crawley, UK) and analysed with the Rotor Gene Q series software version 2.0.2 (Corbett Life Science, Qiagen Ltd., Crawley, UK).

Table 11: Cycling conditions for qPCR assays. PCR steps, temperatures (°C), times and number of cycles are listed.

PCR step	Temperature (°C)	Time	Number of cycles
Initial denaturation	95	10 min	x 1
Denaturation	95	10 sec	x 40
Annealing	60	40 sec	
Extension	60	20 sec	

Normalisation and calibration of qPCR data

When performing gene expression experiments, there are two categories of events that influence the results, which are (1) biological differences between samples and (2) technical variability (Bustin, 2010). The goal of expression studies is to quantify the level of biological change and to eliminate any effects caused by technical variability.

There are a number of steps that can reduce experimental errors including (1) normalisation to sample size by sampling similar tissue volume or weight; (2) accurate quantitation of RNA and RNA quality assessment; (3) purification of RNA; (4) input of similar quantities of RNA in reverse transcription and (5) normalising to internal reference genes (Huggett et al., 2005).

The process of inter-run calibration is very similar to normalisation. Normalisation removes the sample specific non-biological variation, while inter-run calibration removes the technical run-to-run variation between samples analysed in different runs. Inter-run calibrators (IRC) are identical samples that are tested in each run. By measuring the difference in quantification cycle or between the IRCs in all runs, it is possible to calculate a correction or calibration factor to remove the run-to-run differences, and proceed as if all samples were analysed in the same run. Inter-run calibration was run on a gene per gene basis (Hellemans et al., 2007).

2.2.2.4 Assay optimisation

Primer design

As it is one of the most important factors in qPCR, a good primer design is essential. qPCR primers are gene specific and must meet certain criteria to be as efficient as possible. The primers used in this study were designed based on the cDNA sequences supplied by degenerate PCR, GeneFishing™, and EST library search (see Section 2.2.1).

With the Primer Express® software (Applied Biosystems, Cheshire, UK) using the settings TaqMan Probe & Primer Design, qPCR primers were designed according to the following guidelines recommended by Primer Express®. Each primer had a minimum of nine and a maximum of 40 bases, a melting temperature (T_m) between 58-60°C but with maximum 2ºC difference in each primer pair, a GC-content of 30-80% with maximum two G/C residues in the last five nucleotides at the 3'-end. The amplicon length did not exceed 150 basepairs as short

amplicons can be amplified more effectively and are less likely to form secondary structures. A minimum of two primer pairs of each gene was designed.

Using an additional primer analyses software (NetPrimer, PREMIER Biosoft International, http://www.premierbiosoft.com/netprimer/index.html) secondary structures such as hairpins, self and cross dimers were analysed as they significantly affect the primer efficiency and therefore the success of a PCR reaction. The designed qPCR primers are listed in Table 13. The primers were synthesised by Eurofins MWG Synthesis GmbH (Ebersberg, Germany).

All primers were checked for their specificity by using the BLAST tool via Geneious Basic™ software version 5.3.4 – 5.6.3 to ensure that they were specific to the GOI and would not be misprime onto other genes.

The gene-specific lyophilised primers were rehydrated in sterile Milli-Q™ water to a stock solution with a concentration of 100 µM. For the use in qPCR, aliquots were diluted to 5 µM and stored at -20°C.

Melt curve analyses and initial primer check

Analysing the melt curve for each primer pair is crucial as it ensures if a single product was amplified. A melt curve, also known as dissociation curve, is used to differentiate between specific and non-specific amplicons based on the melting temperature (T_m) of the products. The melting temperature is the characteristic temperature at which the DNA molecule melts; the temperature is dependent on both size and nucleotide composition of the molecule. The T_m is defined as the temperature where 50% of the helical structure is denatured (Nolan et al., 2006). During melting curve analysis for this study, all products generated during the qPCR were melted at 95°C, eventually annealed at 60°C and then exposed to gradually increasing heating (from 72°C to 95°C), while fluorescence from the dye was monitored. The generated amplification plots were inspected for proper exponential amplification (Figure 15 A) and the melt curves were analysed for a single product in template positive samples (Figure 15 B), and a negative result for the NTC. Additional peaks or large wavy humps showed non-specific products (Figure 15 C). By analysing the NTCs, possible contamination and detection limits of the assay were identified. Before using valuable reagents on full titrations, an initial concentration of 300 nM for both, forward and reverse primer for each gene was tested to ensure that the primers amplified the target sequences correctly. If possible, for each gene at least two primer pair combinations were tested. After choosing the best working primer-pair for each gene, primer titrations provided information about the optimal primer concentration used in the final qPCRs.

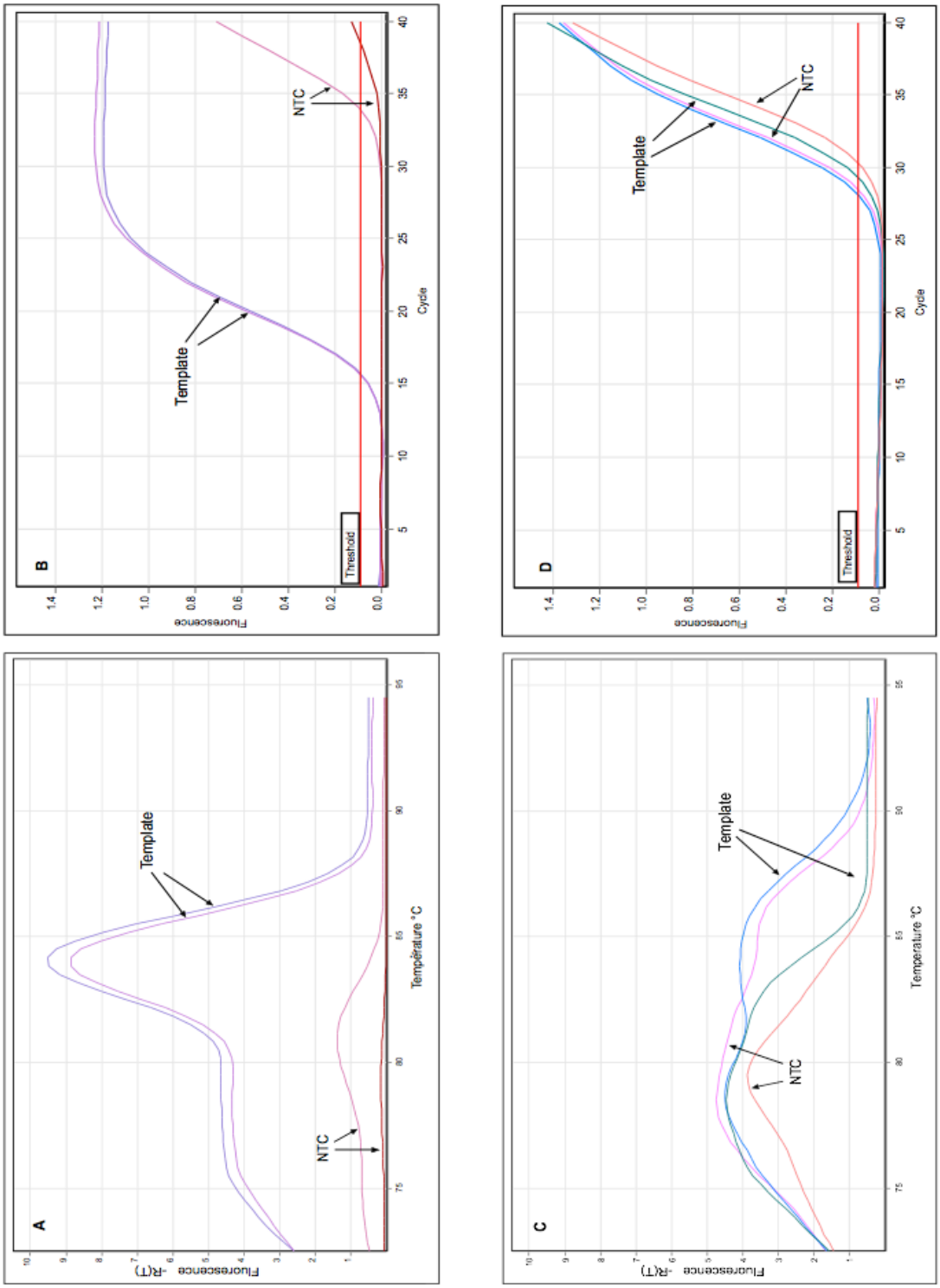

Figure 15: Melt curve (A) and amplification plot (B) for *Nephros norvegicus* (Crustracea) showing a single target product (purple lines) and a small amount of contamination in one of the NTCs (pink lines). The melt curve (C) and amplification plot (C) for *N. norvegicus cct7* shows multiple products in both the target samples (blue lines) and NTCs (pink lines), indicating a lack of specificity. Courtesy of J. Hoppes © 2011.

Primer titration

Testing different primer concentrations following the primer matrix shown in Table 12 identified the optimal primer concentration for each primer pair. Each reaction contained the same amount of target sample, but a different primer concentration. The final selection of primer concentration was based on the greatest C_q value difference between template and NTC and no indication of primer-dimers of contamination. The best concentration for all primers tested was 50 nM forward primer combined with 50 nM reverse primer and was therefore used in the qPCR essays.

Table 12: Primer titration matrix for optimizing primer concentrations in SYBR® Green I assays.

Reverse Primer (nM)	**Forward Primer (nM)** **50**	**300**	**900**
50	50/50	50/300	50/900
300	300/50	300/300	300/900
900	900/50	900/300	900/900

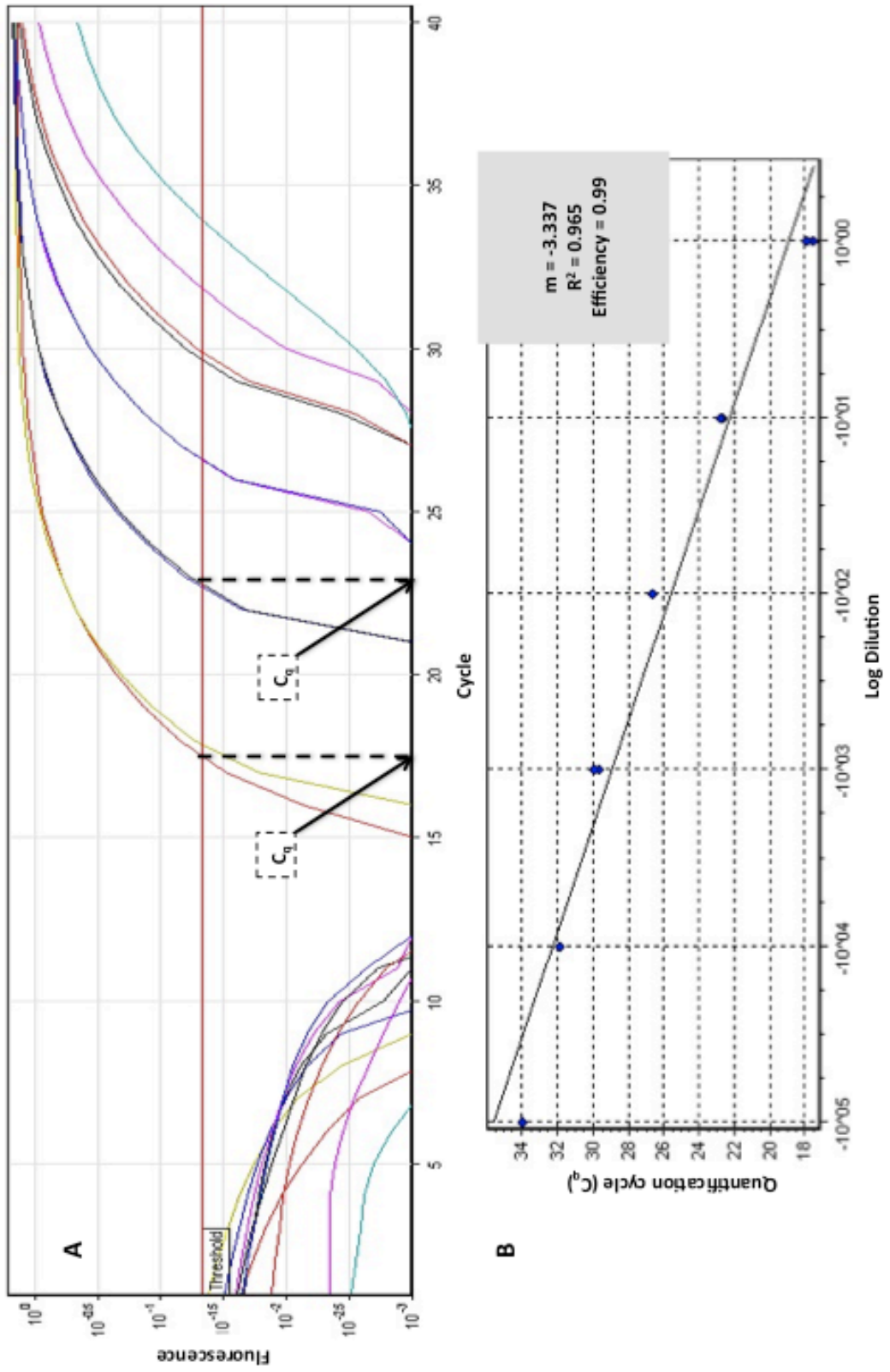

Figure 16: cDNA standard curve for *CGAct*. A: Amplification plot in semi-logarithmic scale with threshold and indicated C_q values. B: Linear regressions plot. Values (blue dots) are corresponding to the C_q values in A. Slope (m = -3.337), R^2 (= 0.965), and amplification efficiency (E = 0.99) values are all close to the ideal values of m = -3.32, R^2 = 1 and E = 1 (Nolan et al., 2006) and therefore well within the accepted range.

Table 13: qPCR primer. All designed gene specific qPCR primers are listed. Primer names, primer sequences, melting temperatures (T_m) in °C from Primer Express®, primer lengths (P. l.) and amplicon lengths (A. l.) of each primer pair in basepairs (bp), as well as the identification method of the template-cDNAs the primers were designed of, are listed. The successful primers, selected in melt curve analyses and finally used in this study, are highlighted in bold. Customary curve optimisation results of the successful primer pairs are given: slope, E = amplification efficiency, R^2 = correlation coefficient.

Identified by	Gene name	Primer sequence (5' to 3')	T_m (°C)	P.l (bp)	A.i (bp)	Slope	E	R^2
Degenerate PCR	*CGCaM*	**F1: GAGGCAGAGCTTCAAGACATGA**	58	22	76	- 3.898	0.81	0.986
		R1: TGAGGAATTCTGGGAAATCGA	58	21				
		F2: ACAGAGGCAGAGCTTCAAGACAT	58	23	79			
		R2: TGAGGAATTCTGGGAAATCGA	58	21				
Gene Fishing™	*CGMG4*	**F1: TGCTTACAACAGCGGCAATT**	58	20	72	- 3.919	0.8	0.999
		R1: GCAATGCTCCAAGAGAAGACATAC	58	24				
		F2: TCGCACTGCTCTTCTGGTTATC	58	22	72			
		R2: GACTTGATCGTGTTTGTTCAGAATG	59	25				
		F3: TCGCACTGCTCTTCTGGTTATC	58	22	75			
		R3: CCAGACTTGATCGTGTTTGTTCA	59	23				
EST database search	*CGDent*	F1: TGAACACCCTCAAATGGGAAA	59	21	72			
		R1: CCCGGGTTGTTGGTACCTTT	60	20				
		F2: CATTCCTGAGGGCGACACA	59	19	78	- 3.732	0.86	0.953
		R2: CCCGTCTTTTCGAGATTTCG	58	20				
	CGPerl	**F1: GATTCTGGGCGGCTGGTA**	58	18	64	- 3.738	0.85	0.996
		R1: TGCTTATTGGTCACCCATTTCC	60	22				
	CGAct	F1: TCACACAGTCCCATCTACGAA	59	22	66			
		R1: CCAGCGAGATCCAATCTCATG	59	21				
		F1: ACAGTCCCCATCTACGAAGGTTAC	59	24	111	- 3.337	0.99	0.966
		R2: GTATCCACGTTCTGTGAGGATTTTC	59	25				
	CGTub	**F1: CGGAGTCCAGATGGGCAAT**	59	19	106	- 3.840	0.82	0.976
		R1: GTCGTCCCCTCCTCCAATG	59	19				
		F2: GGTCAGATTGTGAGCTCCATCA	59	22	71			
		R2: AACTCGGTCAAGTCCACATTGAG	59	23				
	CGCyclo	F1: AATGTCGTCAAAGCGATGGAA	59	21	69			
		R1: TTCGATCTTGATTGGCTTGGA	59	21				
		F2: GATGGCATGAATGTCGTCAAA	58	21	77	- 3.663	0.87	0.998
		R2: TCGATCTTGATTGGCTTGGAT	58	21				
	CG18S	F1: TGTCCTGGCCCGAAAGG	59	17	101			
		R1: CGCGCTTACTGGGAATTCC	59	19				
		F2: CGCGCTACACTGAAGGAATCA	60	21	73	- 3.683	0.87	0.987
		R2: GAAGGAGGTTCAACGGGTTACC	60	22				

Standard Curves for Analysis of qPCR Assay Performance

The next step was to test sensitivity and efficiency of the qPCR assays for all target and reference genes by performing a standard curve. In a standard curve, a dilution series (10-fold over 7 log for this study) of the template is plotted against the C_q for each dilution. The more dilution points and the wider the range (dilution factor), the more precisely the PCR efficiency can be determined (Hellemans et al., 2007). Amplification efficiency (E) was calculated based on the slope of the linear regression line of the standard curve (Pfaffl, 2004) according to equation 2.1:

$$E = (10 - 1^{/slope}) - 1 \qquad \text{(Equation 2.1)}$$

The ideal linear regression of a plot of C_q vs. log dilution would have a slope of -3.32 indicating an exact doubling of the reaction and therefore 100% efficiency. Efficiencies less than 90% can be a result of poor primer design, whilst efficiencies above 110% can indicate nonspecific amplification (Pfaffl, 2004). For this study, the acceptable range of the slope was between -3.3 and -3.8. The concentration of the most diluted sample, which fitted to the standard curve and maintained a valid efficiency, was used in the qPCR assays. The correlation coefficient (R^2) is the fit of all data to the standard curve plot, with $R^2 = 1.00$ if all data lie perfectly on the line. R^2 values are recommended to be greater that 0.98 (Nolan, 2004). For each target and reference gene used in this study, amplification efficiencies and R^2 values were evaluated (Table 13).

2.2.2.5 Relative qPCR quantification

As the aim of this study was to analyse changes in gene expression of the GOI during development and to compare these changes between the treatments, the relative quantification method was chosen.

In relative quantification, gene expression levels of the gene of interest are compared to expression levels of an internal RNA control sample, the endogenous reference gene (Livak and Schmittgen, 2001; Nolan et al., 2006; Pfaffl, 2004). The internal endogenous reference gene ideally should not change expression between the various treatment groups and thus the relative difference between target and reference genes can be used to detect changes in gene expression. Contrary to the absolute quantification method, no external standard curve is generated, as the target and reference genes can be either amplified in the same tube (multiplex run) or in different tubes (Brisson et al., 2004), as done for this study. Therefore, relative quantification does not require standards with known concentrations and the reference gene can be any transcript with known sequence (Bustin, 2002).

For this study four reference genes *CGAct, CGTub, CGCyclo* and *CG18S* were chosen, based on sequences taken from EST-databases. β-actin, α-tubulin, cyclophilin and 18S rRNA are commonly used as internal control genes in qPCR research. However, as shown in various studies, the expression of reference genes can vary between different treatments (the ER can be regulated by the experimental conditions) or tissues (Blomberg et al., 1987; Dheda et al., 2004; Glare et al., 2002). To avoid misinterpretation of study findings, appropriate validation of internal reference genes was crucial. Therefore, the stability of ER genes had to be validated first to demonstrate that the selected ER genes were suitable for this study.

Evaluation of the Expression Stability of the Endogenous Reference Genes using NormFinder©

Evaluation of the expression stability is of particular importance as if a reference gene is regulated by the experimental condition it can result in altered findings (Huggett et al., 2005). The selected endogenous reference genes were evaluated using NormFinder© software (Molecular Diagnostic Laboratory, Dept. of Molecular Medicine, Aarhus University Hospital Skejby, Denmark), http://www.mdl.dk/publicationsnormfinder.htm (Andersen et al., 2004). NormFinder© uses an algorithm that ranks ER gene stability among a set of candidates. The software categorises the set of candidate normalisation genes according to their expression stability in a given sample set and a given experimental design, by combining the estimated intragroup variation with the intergroup variation. The highest ranked and therefore most stable genes should then be used as normalisation genes for relative quantification.

The logarithmic C_q values were transformed to linear scale expression quantities or relative linear values (RLV), following equation 2.2, as the input data for Normfinder had to be expressed on a linear scale.

$$RLV = \text{Amplification Efficiency}^{\text{IRC Cq} - \text{Sample Cq}} \qquad \text{(Equation 2.2)}$$

IRC C_q is the C_q value for an inter-run calibrator sample and Sample C_q represents each individual C_q value.

The NormFinder© results for the 1st and 2nd experiment are listed in Tables 14-16. For each combination tested, the best combination of two ER genes was used as normalisation genes in REST© 2009.

NormFinder© results of the 1st experiment (spat and adults)

By comparing the stability values of the three ERs of spat in pH 8.3 and pH 7.5, the most stable expressed gene was *CGCyclo* with a stability value of 0.148 (Table 14). The best combination of two ER genes was *CGAct* and *CGTub* with a stability value of 0.216. *CGAct* and *CGTub* were therefore used in REST©2009 as normalisation genes.

Assessing the most stable expressed ER gene of adults in pH 8.3 and pH 7.5, revealed *CGCyclo* as the best gene with a stability value of 0.017 and *CGAct* and *CGCyclo* as the best combination of two ERs with a stability value of 0.02 (Table 14). *CGAct* and *CGCyclo* were therefore used in REST©2009 as normalisation genes.

The most stable expressed ER gene comparing spat and adults in pH 8.3 was *CGCyclo* with a stability value of 0.098 and the best combination of two ER genes was *CGAct* and *CGTub* with a stability value of 0.184 (Table 14). *CGAct* and *CGTub* were therefore used in REST©2009 as normalisation genes.

To visualise the NormFinder© results of adults and spat in pH 8.3 and pH 7.5 and to allow a straightforward comparison of the expression stability of the three ER genes, intra-group and inter-group variation data were plotted in Figure 17.

Table 14: Evaluation of the Expression Stability of the Endogenous Reference Genes of the 1st experiment (testing the impacts of pH on gene expression in spat and adults). Stability values, intragroup and intergroup variations, best EG gene and best combination of two ER genes were assessed using NormFinder©

Spat at pH 8.3 *vs.* pH 7.5		Intragroup variation		Intergroup variation	
	Stability value	pH 7.5	pH 8.3	pH 7.5	pH 8.3
CGAct	0.277	0.030	0.226	0.143	-0.143
CGCyclo	0.148	0.004	0.015	0.097	-0.097
CGTub	0.420	0.047	0.822	-0.240	0.240
Best gene			*CGCyclo*		
Stability value			0.148		
Best combination of two genes			***CGAct & CGTub***		
Stability value for best combination of two genes			**0.216**		
Adults at pH 8.3 *vs.* pH 7.5		Intragroup variation		Intergroup variation	
	Stability value	pH 7.5	pH 8.3	pH 7.5	pH 8.3
CGAct	0.035	0.014	0.011	-0.003	0.003
CGCyclo	0.017	0.004	0.002	0.009	-0.009
CGTub	0.058	0.003	0.099	-0.005	0.005
Best gene			*CGCyclo*		
Stability value			0.017		
Best combination of two genes			***CGAct & CGCyclo***		
Stability value for best combination of two genes			**0.020**		
Spat vs. Adults at pH 8.3		Intragroup variation		Intergroup variation	
	Stability value	Spat	Adults	Spat	Adults
CGAct	0.257	0.226	0.011	-0.157	0.157
CGCyclo	0.098	0.015	0.002	-0.050	0.050
CGTub	0.387	0.822	0.099	0.207	-0.207
Best gene			*CGCyclo*		
Stability value			0.098		
Best combination of two genes			***CGAct & CGTub***		
Stability value for best combination of two genes			**0.184**		

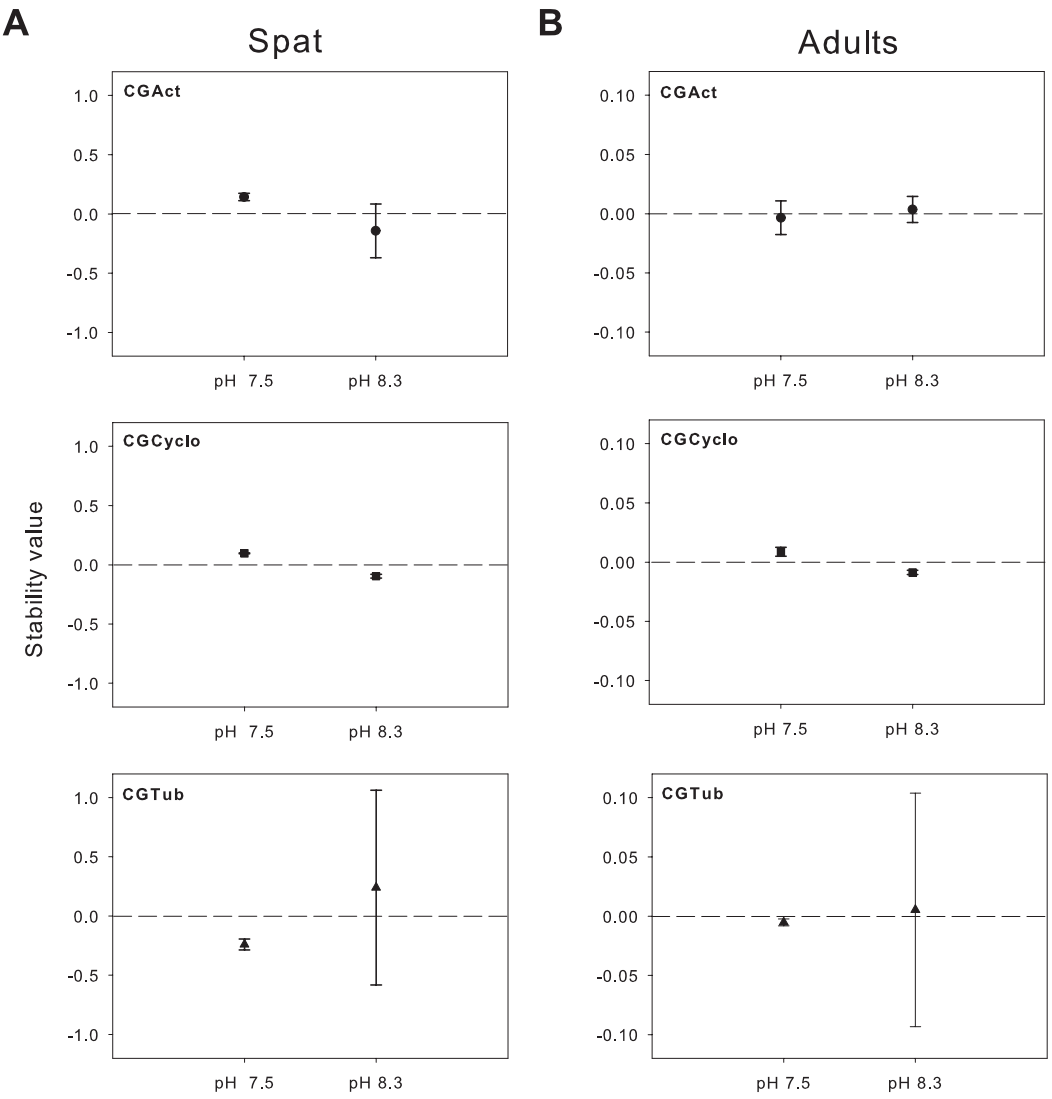

Figure 17: Comparative stability between the ERs of both control (pH 8.3) and experimental groups (pH 7.4) of the 1st CO_2 experiment, testing the impacts of pH on spat (A) and adult (B) *C. gigas*. Data are based on the inter-group variations (symbols) and the intra-group variations (error-bars) calculated by NormFinder® (see Table 14).

NormFinder© results of the 2nd experiment (larvae)

As mentioned before, stable expressed ER genes are crucial for robust essays. Using NormFinder©, the expression stability of *CGAct, CGCyclo* and *CGTub* over an entire larval cycle at ambient conditions (20°C pH 8.1) was evaluated (Table 15). As illustrated in Figure 18, ER gene expression was not stable during larval development, questioning the use of any of the endogenous reference genes for relative quantification analyses between different developmental stages. To provide robust assays in downstream analyses, only two developmental stages within the same condition were therefore compared (Table 16).

Table 15: Evaluation of the Expression Stability of the Endogenous Reference Genes of an entire larval cycle at ambient conditions. Stability values, intragroup and intergroup variations, best EG gene and best combination of two ER genes were assessed using NormFinder©

Trochophora – Pediveliger at ambient conditions (20°C pH 8.1)				
	Stability value			
CGAct	0.131	Best gene: *CGTub*		
CGCyclo	0.176	Stability value: 0.113		
CGTub	0.113	**Best combination of two genes: *CGCyclo & CGTub***		
		Stability value for best combination of two genes: 0.096		
	Trochophora	**PI veliger**	**PII veliger**	**Pediveliger**
Intragroup variation				
CGAct	0.002	0.026	0.006	0.007
CGCyclo	0.000	0.002	0.004	0.000
CGTub	0.004	0.014	0.001	0.002
Intergroup variation				
CGAct	-0.111	-0.054	0.098	0.066
CGCyclo	0.24	0.077	-0.124	-0.193
CGTub	-0.129	-0.022	0.026	0.126

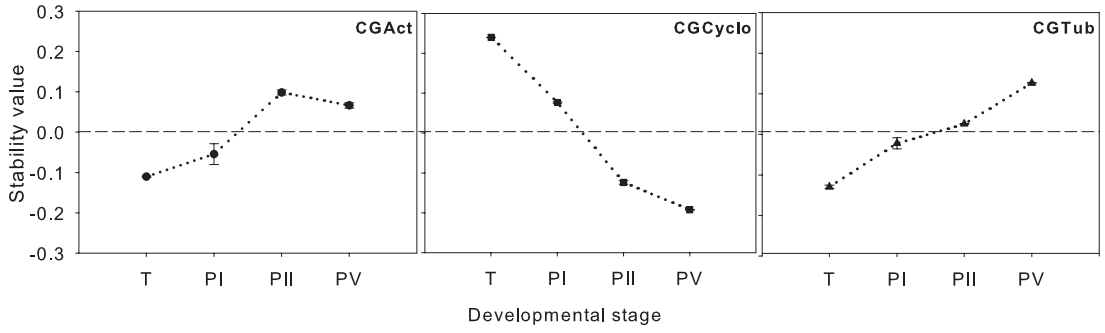

Figure 18: Illustration of the expression stability of the three ER genes during an entire larval cycle at ambient conditions (20°C pH 8.1). Data are based on the intergroup variations (symbols) and the intragroup variations (error bars) calculated by NormFinder® (see Table 15). T: Trochophora, PI: Prodissoconch I, PII: Prodissoconch II, PV: Pediveliger.

Table 16: Evaluation of the Expression Stability of the Endogenous Reference Genes of the 2nd experiment (testing the impacts of pH and temperature on gene expression in larvae). Stability values, intragroup and intergroup variations, best EG gene and best combination of two ER genes were assessed using NormFinder©

Trochophora *vs.* PI veliger at 20°C pH 8.1 (condition 0)		Intragroup variation		Intergroup variation	
	Stability value	Trochophora	PI veliger	Trochophora	PI veliger
CGAct	0.085	0.002	0.026	-0.028	0.028
CGCyclo	0.098	0.000	0.002	0.082	-0.082
CGTub	0.104	0.004	0.014	-0.054	0.054
Best gene			*CGAct*		
Stability value			0.085		
Best combination of two genes			***CGCyclo & CGTub***		
Stability value for best combination of two genes			**0.063**		
PII veliger *vs.* Pediveliger at 20°C pH 8.1 (control)		Intragroup variation		Intergroup variation	
	Stability value	PII veliger	Pediveliger	PII veliger	Pediveliger
CGAct	0.050	0.006	0.007	0.016	-0.016
CGCyclo	0.050	0.004	0.000	0.034	-0.034
CGTub	0.065	0.001	0.002	-0.050	0.050
Best gene			*CGAct*		
Stability value			0.05		
Best combination of two genes			***CGCyclo & CGTub***		
Stability value for best combination of two genes			**0.028**		
PII veliger *vs.* Pediveliger at 24°C pH 7.4 (treatment 1)		Intragroup variation		Intergroup variation	
	Stability value	PII veliger	Pediveliger	PII veliger	Pediveliger
CGAct	0.317	0.009	0.121	0.231	-0.231
CGCyclo	0.091	0.002	0.004	-0.067	0.067
CGTub	0.234	0.013	0.040	-0.165	0.165
Best gene			*CGCyclo*		
Stability value			0.091		
Best combination of two genes			***CGAct & CGTub***		
Stability value for best combination of two genes			**0.112**		
PII veliger *vs.* Pediveliger at 20°C pH 7.4 (treatment 2)		Intragroup variation		Intergroup variation	
	Stability value	PII veliger	Pediveliger	PII veliger	Pediveliger
CGAct	0.121	0.009	0.003	0.084	-0.084
CGCyclo	0.065	0.001	0.002	-0.042	0.042
CGTub	0.067	0.006	0.000	-0.043	0.043
Best gene			*CGCyclo*		
Stability value			0.065		
Best combination of two genes			***CGAct & CGTub***		
Stability value for best combination of two genes			**0.057**		
PII veliger *vs.* Pediveliger at 24°C pH 7.4 (treatment 4)		Intragroup variation		Intergroup variation	
	Stability value	PII veliger	Pediveliger	PII veliger	Pediveliger
CGAct	0.044	0.016	0.011	0.008	-0.008
CGCyclo	0.021	0.002	0.005	0.009	-0.009
CGTub	0.033	0.018	0.001	-0.017	0.017
Best gene			*CGCyclo*		
Stability value			0.021		
Best combination of two genes			***CGCyclo & CGTub***		
Stability value for best combination of two genes			**0.021**		

The most stable expressed ER gene comparing trochophora and PI veliger in ambient conditions (20°C pH 8.1) was *CGAct* with a stability value of 0.085 and the best combination of two ER

genes was *CGCyclo* and *CGTub* with a stability value of 0.063 (Table 16). *CGCyclo* and *CGTub* were therefore used in REST©2009 as normalisation genes.

Assessing the most stable expressed ER gene of PII veliger *vs.* pediveliger at ambient conditions (20°C pH 8.1), revealed *CGAct* as the best gene with a stability value of 0.05 and *CGCyclo* and *CGTub* as the best combination of two ERs with a stability value of 0.028 (Table 16). *CGCyclo* and *CGTub* were therefore used in REST©2009 as normalisation genes.

By comparing the stability values of the three ERs of PII veliger *vs.* pediveliger in treatment 1 (24°C pH 7.4), the most stable expressed gene was *CGCyclo* with a stability value of 0.091. The best combination of two ER genes was *CGAct* and *CGTub* with a stability value of 0.112 (Table 16). *CGAct* and *CGTub* were therefore used in REST©2009 as normalisation genes.

The most stable expressed ER gene comparing PII veliger and pediveliger in treatment 2 (20°C pH 7.4), was *CGCyclo* with a stability value of 0.065 and the best combination of two ER genes was *CGAct* and *CGTub* with a stability value of 0.057 (Table 16). *CGAct* and *CGTub* were therefore used in REST©2009 as normalisation genes.

Accessing the most stable expressed genes of PII veliger *vs.* pediveliger in treatment 4 by comparing the stability values of the three ER genes, revealed *CGCyclo* as the most stable expressed gene with a stability value of 0.021 and *CGCyclo* and *CGTub* as the best combination with a stability value of 0.021. *CGCyclo* and *CGTub* were therefore used in REST©2009 as normalisation genes.

Statistical Analyses of qPCR data using REST© 2009

Finally, relative expression data were analysed using the Relative Expression Software Tool REST© 2009 V20.1.3 http://www.gene-quantification.de/rest-2009.html (Qiagen, Ltd., Crawley, UK) (Pfaffl et al., 2002) to address variability in gene expression. REST© 2009 applies a mathematical model that takes into account the different PCR efficiencies of the genes of interest and reference genes. Applying Pair Wise Fixed Reallocation Randomisation Tests and bootstrapping methods, the statistical significance of gene expression ratios was analysed by the software. For each GOI and each reference gene, the calibrated C_q values were entered into the software as well as the efficiency values calculated from the standard curves (see Section 2.2.2.4). Relative expression was calculated based on equation 2.3. Relative expression values of 1 indicated no change in gene expression, whereas values of >1 meant up-regulation and values <1 down-regulation of the GOI.

$$\text{Relative expression ratio} = \frac{(E_{target})^{\Delta Cq\ target\ (MEAN\ control - MEAN\ sample)}}{(E_{ref})^{\Delta Cq\ ref\ (MEAN\ control - MEAN\ sample)}} \qquad \text{(Equation 2.3)}$$

2.2.2.6 Summary

To study the expression of genes involved in biomineralisation during ontogeny of *C. gigas* and to examine if the expression of these genes was affected by altering environmental conditions, the candidate genes *CGCaM, CGPerl, CGMG4* and *CGDent* were identified by searching EST-databases, degenerate PCR and GeneFishing™. To ensure high quality assay performance, great care was taken during storage, preparation and processing of the samples, following the MIQE guidelines. Extensive assay optimisation was carried out in preparation for gene expression studies using the relative quantification method. Melt curve analyses and primer titrations identified the best primer-pairs, primer and cDNA concentrations used in the qPCR assays. After initial qPCR runs *CG18S* was excluded, as it was amplified too early within each qPCR run due to its high expression. Thus, it was difficult to compare it to the other genes. To confirm that expression of the three remaining endogenous reference genes, *CGAct, CGTub* and *CGCyclo*, were not influenced by the experimental conditions, expression stability was evaluated using the NormFinder© software. The best combination of two ER genes assessed by NormFinder© (Tables 14, 15 and 16), was used in REST©2009 analyses to identify variability in gene expression between each of the compared parameters. Overall, robust assays were developed for gene expression studies in *C. gigas*, which will be described in Chapter 4.

2.3 Impacts of changing environmental conditions on size, microstructures and crystal disorder of the developing shell of *Crassostrea gigas*

To get a deeper understanding of biomineralisation in *C. gigas* during ontogeny and the corresponding mineralogical changes during shell development, Scanning Electron Microscopy (SEM) and Fourier Transform Infrared spectroscopy (FTIR) were carried out to characterise and analyse microstructures and the extent of crystal disorder of the developing shell. A key aim was to determine whether or not shell development, morphology, mineralogy and crystallinity were affected by varying environmental conditions during the life cycle.

Shell development of *C. gigas* is characterised by changes in shell mineralogy during ontogeny, ranging from amorphous calcium carbonate at the onset of shell mineralisation in early PI veliger larvae to aragonite in mature veliger larval shells (PI and PII veliger) to mainly calcite in post-metamorphosed shells. Shell development in bivalves has been described in detail in Chapter 1, Section 1.3.2.1. For more information about changing shell morphology in *C. gigas*, including changes in shell mineralogy, microstructures and crystallinity during ontogeny, please refer to Chapter 5.

2.3.1 Scanning Electron Microscopy (SEM)

Scanning electron microscopy is a useful tool to study, compare and analyse shell size and shell microstructures on a nanometre scale. As there is not much data available describing shell microstructures during an entire life cycle of the Pacific oyster, a catalogue of images was developed allowing deeper insights of changes in shell size and shell microstructures during ontogeny. Imaging entire larval shells and shell microstructures of larvae reared in different environmental conditions, allowed conclusions of how a changing environment could impact on shell development. With scanning electron microscopy the surface of a sample can be scanned using a small focussed beam of electrons. Interactions of electrons with the atoms of the sample produce the signals that can contain information about samples topography/external morphology, chemical composition and crystalline structure. Resolutions of down to 5 nm with magnifications of up to 300,000 times can be obtained. For this study high-resolution 2-dimensional images of selected areas and microstructures were produced.

2.3.1.1 The impacts of pH and temperature on larval shell development

A multi-stressor approach was set-up to investigate how temperature and pH influence larval shell development in terms of size, microstructures and crystal disorder. Veliger larvae of *C. gigas* were exposed to different conditions until metamorphosis and three different treatment groups (24°C pH 7.4; 20°C pH 7.4 and 24°C pH 8.3) were tested against one control group (20°C pH 8.3) over a period of 20 days. For details of the experimental set-up, measurements and sampling please refer to Section 2.1.2. Replicate samples were taken at selected times corresponding to the main stages of shell development (PI veliger, PII veliger, pediveliger and spat), fixed in 70% ethanol and stored at room temperature until further analyses.

Sample preparation

To measure the shell sizes and to identify shell microstructures of larval shells previously fixed in 70% ethanol, larval tissue had to be removed first. After replacing the ethanol with ultrapure water, four additional washings of 30 seconds with gentle shaking were performed. Following the protocol of Weiss et al. (2002), larval tissue was dissolved by treating the larval shells with 2.5% sodium hypochlorite (NaOCl) whilst gently shaking for 2-5 minutes. After washing the shells thoroughly (five times) with ultrapure water, they were dried for at least 12 h at 37°C and then mounted onto aluminium stubs with carbon tabs (Agar Scientific, Stansted, UK) and dried again overnight at 37°C. Then, the samples were placed into the chamber of a sputter coater (Hummer VI-A, ANATECH LTD., Alexandria, Vancouver, Canada) and coated with a 20 nm thick layer of gold according to the following protocol: by turning on the argon gas supply, a near-argon vacuum was created and the pressure was set to 60-80 millitorr (mTorr) with a current of approximately 10 milliampere (mA) for four minutes at seven volts. The coated samples were dried at 30°C for about 2 hours before analysis by SEM. Gold coating provides a conductive path for the electrons to return to earth, without which the sample would "charge up" and confound attempts to image the surface.

Imaging and image analyses

Images of entire shells to measure shell size and images of shell fractures to determine microstructures were taken using a LEO 1450 VP (variable pressure) tungsten filament SEM (LEO Electron Microscope Ltd., Cambridge, UK) with a PGT light element detector. Samples were carefully placed on a sample stage, aligned in the SEM chamber and a vacuum was initiated before switching on the electron beam. A vacuum was required to prevent any electrical discharges occurring due to the high voltages that are used to generate the beam and to prevent the electron beam being diffused or absorbed by the gas molecules (LEO 1400 series –

Operational Notices). The desired settings were adjusted using the Smart SEM™ V05.01.08 software (Carl Zeiss Ltd., Hertfordshire, UK) running on an attached PC.
Images were analysed using the Macnification software, version 1.8 (Orbicule Inc., Leuven, Belgium). Length, height and perimeter of the larval shells of all four conditions were measured, statistically analysed and compared.

2.3.1.2 Adult and juvenile shells

Random shell samples of adult and juvenile *C. gigas* were used to investigate shell microstructures using scanning electron microscopy.

Sample preparation

Samples were prepared by fracturing different parts of both valves of adult and juvenile *C. gigas*. Pieces of the shells were then cleaned in an ultrasonic bath (FB-11021, Fisherbrand™, Singen, Germany) for about five minutes at ambient temperature, oven dried for at least 24 hours at 30°C, aligned and mounted on aluminium stubs laminated with carbon tabs and further processed as described before.

Imaging and image analyses

Images were taken as described above. Using the Macnification software, the different shell microstructures were measured and compared.

2.3.2 Fourier Transform Infrared Spectroscopy (FTIR)

FTIR spectroscopy is a common and well-established method for obtaining information on the molecular structures of crystalline and amorphous/disordered materials as well as organic materials. FTIR thus can be used to identify minerals and to characterise their states of atomic disorder (Chu et al., 2008; Regev et al., 2010; Weiner, 2010). Characterisation of the extent of atomic disorder, also referred to as crystallinity, provides information on the stability of the mineral and hence the solubility of the mineral (Asscher et al., 2011). By comparison with for example X-ray diffraction (XRD) analyses, FTIR spectroscopy is relatively rapid and takes about 2 min per analysis. Furthermore, when compared to an X-ray diffractometer, an FTIR is inexpensive, costing about $40,000, and more sensitive to carbonates (Ji et al., 2009). For this study, FTIR spectroscopy was used to determine amorphous, poorly crystalline and crystalline carbonates during ontogeny of the Pacific oyster and to analyse if changes in crystallinity occur whilst exposing the animals/shells to different environmental conditions.

FTIR spectroscopy is based on the manner in which radiation interacts with molecules of the sample in the infrared (IR) range, 4000 to 250 cm^{-1} (cm^{-1}: wavenumber). A wavenumber defines the number of waves per unit length (the reciprocal of wavelength) and is influenced by differing interactions of the C-O bonds (Hsu, 1997; Regev et al., 2010). By positioning a sample in the path of an IR beam, the absorption of light energy at different IR frequencies by specific molecular bonds within the sample are measured (Hsu, 1997) and recorded as a series of peaks in the infrared absorbance spectrum. Thus, FTIR spectroscopy reflects the molecular composition of a sample, and the geometry of absorption peaks reflects the spatial bonding environment at a molecular level. The set of absorbance peaks that make up the IR spectrum of a specific material are characteristic for that material. Variations in peak position, shape and height are indicative of disorder or compositional changes of the material (Weiner, 2010). In carbonate minerals, the carbonate ion produces three major infrared absorption peaks (Figure 19) corresponding to: out-of-plane bending (ν_2), asymmetric stretching (ν_3), and in-plane-bending (ν_4). The three calcium carbonates, ACC, aragonite and calcite, found in *C. gigas* to date differ in terms of the positions of the peaks in their spectra (Lee and Choi, 2007b; Lee et al., 2011; Weiss et al., 2002). The infrared spectrum of calcite has three characteristic peaks in the range between 400-4000 cm^{-1} wavenumbers. In calcite (Figure 19), the first peak (ν_3) is at around 1420 cm^{-1}, the second (ν_2) at about 874 cm^{-1} and ν_4 as the last peak is at around 713 cm^{-1} (Regev et al., 2010). The IR spectrum of aragonite differs from that of calcite most noticeably in terms of peak positions as the ν_3 peak shifts to 1477 cm^{-1}, the ν_2 to 858 cm^{-1} and the ν_4 peak appears as doublet at about 713 cm^{-1} and 700 cm^{-1}. Additionally, a peak at 1083 cm^{-1} is prominent in aragonite (Jones and Jackson, 1994). Compared to aragonite and calcite, the peaks of ACC appear very broad and weak due to its unstable and less crystalline nature. The most

notable feature of ACC spectra are two main carbonate absorptions near 1450 cm^{-1} (ν_3), namely at around 1420 cm^{-1} and 1474 cm^{-1}, as compared to a single absorption for aragonite and calcite, and broadened peaks at around 866 cm^{-1} and 1080 cm^{-1}. The ν_4 peak of ACC shows a broad and weak absorption at 710 cm^{-1} rather than appearing as a distinct peak at 713 cm^{-1} as in calcite and aragonite (Addadi et al., 2003; Raz et al., 2002; Weiss et al., 2002). Absence of a peak at 713 cm^{-1} indicates that well ordered calcite and/or aragonite are not present, but only ACC (Addadi et al., 2003). Broad peaks that are not well separated from each other and are usually found at 2900 cm^{-1} indicate organic macromolecules such as proteins and polysaccharides (Weiner, 2010).

To identify variance within mineral crystallinity (the extend of atomic disorder) and/or between different shell samples, the intensity ratio of the ν_2/ν_4 peak heights is commonly used (Addadi et al., 2003; Beniash et al., 2010; Chu et al., 2008; Politi, 2004). Generally, the more crystalline the material the lower the ν_2/ν_4 intensity ratio (Figure 19) (Gueta et al., 2007).
As FTIR spectroscopy requires powdered samples and previous studies have shown that the amount of grinding affects peak widths and heights (Figures 19 and 20), normalisation of the ν_2/ν_4 peak heights ratio to the ν_3 peak height is required. The relationship between the ν_2/ν_4 intensity ratio and the full width at half maximum (FWHM) height through sequential grinding of the same sample separates the confounding effects of crystal size and crystal order (Asscher et al., 2011; Poduska et al., 2011; Regev et al., 2010), which means that peak width is influenced by the extent of the order of the sample and the size of the crystals (Figure 19). More disorder causes a broadening of the peak, while smaller particle size will narrow the peak (Asscher et al., 2011). Thus, the measurement of peak width in an IR spectrum provide a measure of a combination of atomic disorder and particle size. A sample can be re-ground and re-pressed repetitively before the FWHM reaches a limiting value, which varies among different sources of calcite specimens (Poduska et al., 2011).

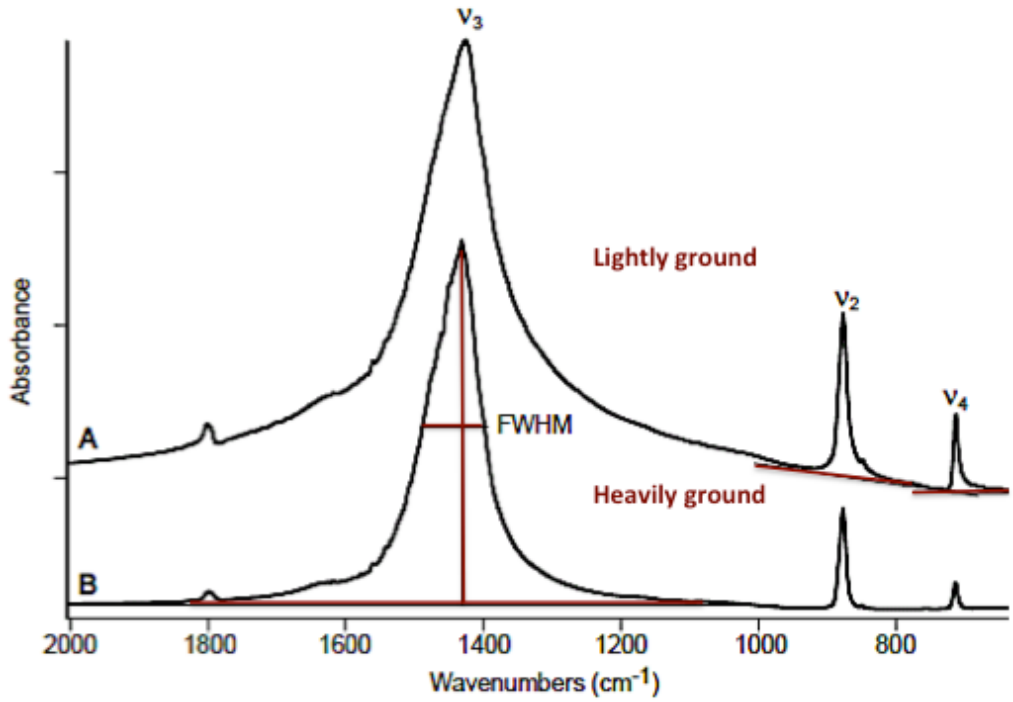

Figure 19: FTIR spectra of calcite for a lightly ground sample (A) and a heavily ground sample (B) showing its characteristic peaks at around 1420 cm^{-1} (ν_3), 874 cm^{-1} (ν_2) and 713 cm^{-1} (ν_4). Note that IR peaks sharpen to yield both higher intensities and smaller FWHM values when heavily ground. Following the method of Chu et al. (2008), baselines (in red) were drawn between the peak minima of ν_3, ν_2 and ν_4 to measure the peak heights and to calculate the FWHM values. After Regev et al. (2010).

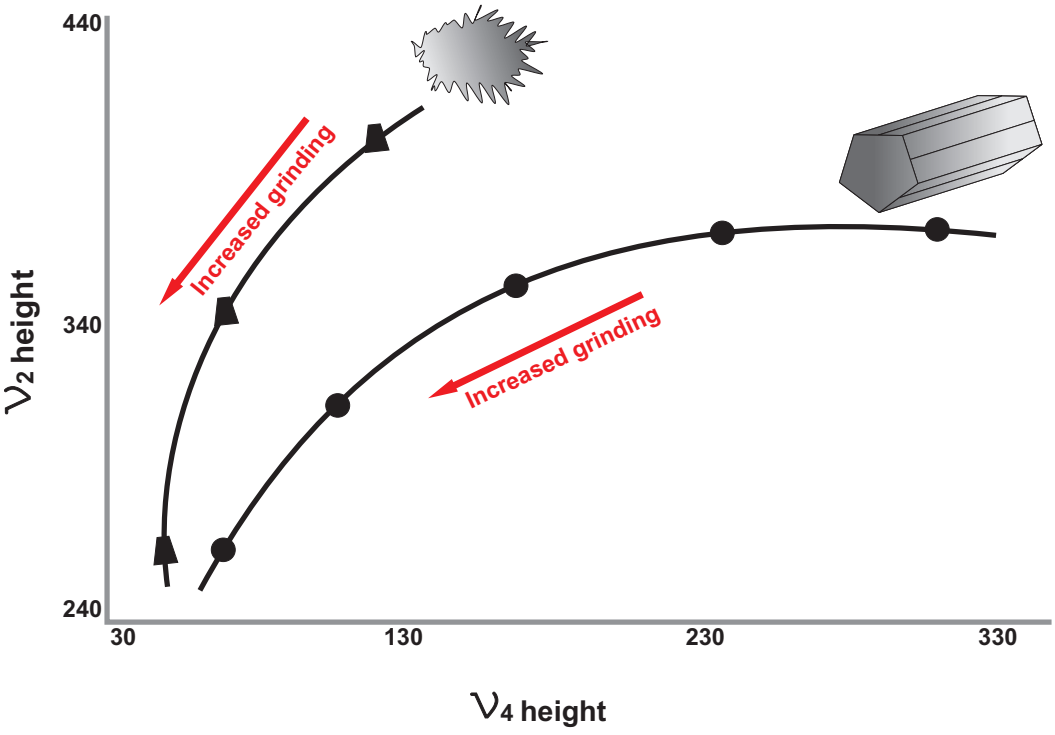

Figure 20: Schematic illustration to show the variation in the ν_2 and ν_4 peak heights when normalised to ν_3 with increased grinding of a highly disordered sample (as for example ACC) against a highly ordered, large crystal (such as calcite). Note that the slope of calcite is shallower compared to the slope of ACC, indicating a higher atomic order (Regev et al, 2010) ©F. Bagusche

2.3.2.1 The impacts of pH and temperature on crystal disorder on larval shell development

It was investigated whether or not changes in temperature and pH influence mineralogy and crystal disorder during larval shell development. Therefore larvae of *C. gigas* were exposed to multiple stressors during an entire larval cycle until metamorphosis. For details of the experimental set-up and sampling please refer to Section 2.1.2.

Sample preparation

Shell samples for FTIR analyses, previously fixed in 70% ethanol, were prepared by Sarah Long according to the following procedure. Special focus was laid on the complete removal of larval tissue as initial analyses had shown that traces of ethanol within the tissue distorted the spectra. As trochophora and PI veliger were floating in the ethanol, the samples had to be centrifuged first in order to form a pellet at the bottom of the tube, before removing the ethanol by pipetting. Ethanol from PII, pediveliger and spat samples was simply removed by pipetting, followed by 3-5 washing steps with ultrapure water whilst gently shaking. To separate and clean the shells of larval tissue, NaOCl was added and processed as described above. This treatment is known not to affect amorphous calcium carbonate in other organisms (Lowenstam, 1989). The cleaned shell samples were then dried at for at least 12 h at 37°C. Following trials of FTIR analysis, another 10 ultrapure washing steps were carried out to remove remaining anomalous peaks. Therefore in total these samples were washed 20 times with ultrapure water. Using pestle and mortar a few micrograms of the dry shell samples were lightly ground and mixed with approximately 50 mg ultra-pure potassium bromide (KBr) powder (Thermo Spectra-Tech, Fisher Scientific, Leicestershire, UK). KBr is used as a carrier for mounting samples in the beam as it does not absorb in the IR spectrum. After transferring the mixture into a special dye, translucent discs were formed using a hand-operated press with a pressure of approximately 2 tonnes. The discs were then transferred into the sample chamber of a Protégé 460 MAGNA-IR® and positioned in the path of the IR beam. Before the spectra were collected, a background was taken with an empty sample holder. This was repeated every 30 minutes or when necessary to remove the carbon dioxide peaks at 2360, 2342, and 668 cm^{-1} as well as the sharp water vapour peaks at around 1600 cm^{-1}. Using the default settings of the OMNIC E.S.P. 5.2 software (Nicolet, Wisconsin, USA) 32 scans were taken with a resolution of 4 cm^{-1}. For repetitive measurements the same KBr pellet was re-ground using a mortar and pestle. Typically 20 seconds of re-grinding was applied to the sample, up to a maximum of four times.

Measurements & sample analyses

To calculate the ratios of v_2/ v_3 and v_4/ v_3 and to work out the FWHM values, the height of v_3, v_2, and v_4 peaks were measured by drawing baselines between the minima on each side of v_3, v_2, and v_4 following Chu et al. (2008) (Figure 19). To determine peak ratios the v_2 and v_4 heights were normalized to the height of the v_3 peak, by dividing the height of the v_2 peak by the height of the v_4 peak. Each peak height was measured three times and an average was calculated. Data were analysed using the statistical computing program R, Version 2.14.2, http://www.R-project.org.

2.3.2.2 Mineralogy of adult shells

To get an overall picture of mineralogical changes in *C. gigas* during ontogeny, spectra of random adult shell samples were collected to determine if differences in the mineralogy of right and left valves occur and to identify the mineralogy of the different microstructures. Therefore adult *C. gigas* samples were collected from Rade de Brest, France, in August 2009. By scraping off the tissue using a scalpel, the shells were cleaned, rinsed with Milli-Q^{TM} water and stored in 70 % ethanol until analysis. To prepare samples for the four dominant microstructures (prismatic layer, foliated layer, chalk and myostractum), the shells were dried at 50°C for 48 hours and then cut to reveal a longitudinal section of the layers. Using a magnifying glass and scalpel, the target area of the shell was then separated and homogenised into a powder. The preparation procedure outlined before was then followed to investigate the mineral composition of these microstructures.

Sample preparation & measurements

Shell samples, previously fixed in 70% ethanol were prepared and processed for FTIR measurements as explained earlier. Measurements were carried out using the same settings as described in 2.3.2.1 and analysed as explained previously.

3 - The difficulties of growing up – Development of the Pacific oyster *Crassostrea gigas* under future ocean conditions

"It is not the strongest of the species that survives, nor the most intelligent that survives. It is the one that is the most adaptable to change."

Charles Darwin (1859)

3.1 Introduction

As sessile marine animals living in estuarine and intertidal regions, oysters must cope with harsh and changing environmental conditions such as alterations in seawater pH, salinity or fluctuating temperature. However, acidification of the ocean has become a serious threat to marine calcifiers such as oysters and most studied bivalve species showed increased mortality and metabolic rates (Beniash et al., 2010; Berge et al., 2006; Dickinson et al., 2012; Watson et al., 2009), decreased growth (Beniash et al., 2010; Berge et al., 2006; Talmage and Gobler, 2010), reduced body tissue growth (Dickinson et al., 2012; Michaelidis et al., 2005), decreased metamorphosis (Talmage and Gobler, 2009), decreased shell mass and calcification rates (Gaylord et al., 2011), and increased shell malformations (Beniash et al., 2010; Kurihara et al., 2008; Miller et al., 2009; Talmage and Gobler, 2009) in response to elevated pCO_2 (see Table 2, Section 1.4). Recent studies have shown that early life history stages of estuarine and marine species are more sensitive to elevated CO_2 stress than adults, including gametes, embryos and particularly larvae (Havenhand et al., 2008; Parker and Ross, 2009). Despite the fact that temperature is a controlling factor in bivalve development, most studies on the impacts of climate change on life histories have focused on ocean acidification as a single stressor (Beniash et al., 1997; Miller et al., 2009; Watson et al., 2009). However, according to the predictions for 2100 (Nicholls et al., 2007), benthic marine species, such as the Pacific oyster, have to face simultaneous warming and acidification from the onset of development. According to the "business-as usual" scenario for global change (Nicholls et al. 2007) an increase in surface ocean pCO_2 from present levels of about 380 ppm to 700-1000 ppm by 2100 and 2000 ppm by 2300 can be expected, resulting in a decrease of surface ocean pH of 0.14-0.41 units and 0.3-0.7 units, respectively (Caldeira and Wickett, 2003; Nicholls et al., 2007). The estimate for increase in mean sea surface temperature is predicted to lie between 1.8 and 4 °C by 2100 (Nicholls et al., 2007). It has been shown that marine calcifiers are particularly vulnerable to increasing pCO_2 as the ocean becomes undersaturated in respect to carbonate ions, making it more difficult for marine calcifying species to precipitate calcium carbonate (Gazeau et al., 2007; Orr et al., 2005; Talmage and Gobler, 2009).

Within the framework of this study, a key objective was to test if suboptimal temperature and pH and the combination of both would negatively influence tissue growth, shell growth and food consumption during ontogeny of the Pacific oyster.

3.2 Material and Methods

Two different experiments were designed and conducted at Ifremer, Station d'Argenton, France. The first experiment was performed to test the effects of pH on adult and juvenile development over a period of 3.5 months. This first experiment also served to confirm that it was possible to maintain the water chemistry parameters over this long duration. With the second experiment the synergistic effects of elevated temperature and decreased pH on larval development were investigated.

3.2.1 Responses of juveniles and adults to low pH

The experimental system and sampling is described in Section 2.1.1. To monitor the influence of pH, the total wet weight of 30 juvenile and 19 adult oysters per experimental tank was measured weekly until termination of the experiment. In- and output of algae per tank was measured daily to calculate the consumption rates of animals in the low pH treatment (pH 7.5) and control (pH 8.3) conditions (see Figure 7, Section 2.1.1.2). Due to an undetermined disease outbreak the mortality rate of juveniles increased towards the end of the experiment in both pH 8.3 (n=15) and pH 7.5 (n=20). As shown in Figure 21, the measured water parameters, temperature, pH and oxygen concentration, of control and low pH treatment were stable throughout the 3.5-months experiment. Using the software Statistica (Version 10, StatsSoft, Inc. Tulsa, OK, USA) an ANOVA of Co-Variance (ANCOVA) was performed to test for differences in total wet weight of juveniles and adults in the treatment compared to the control (Table 17). Additionally the consumption rates of algae were compared between the treatment and control tank (Table 17), containing both juveniles and adults.

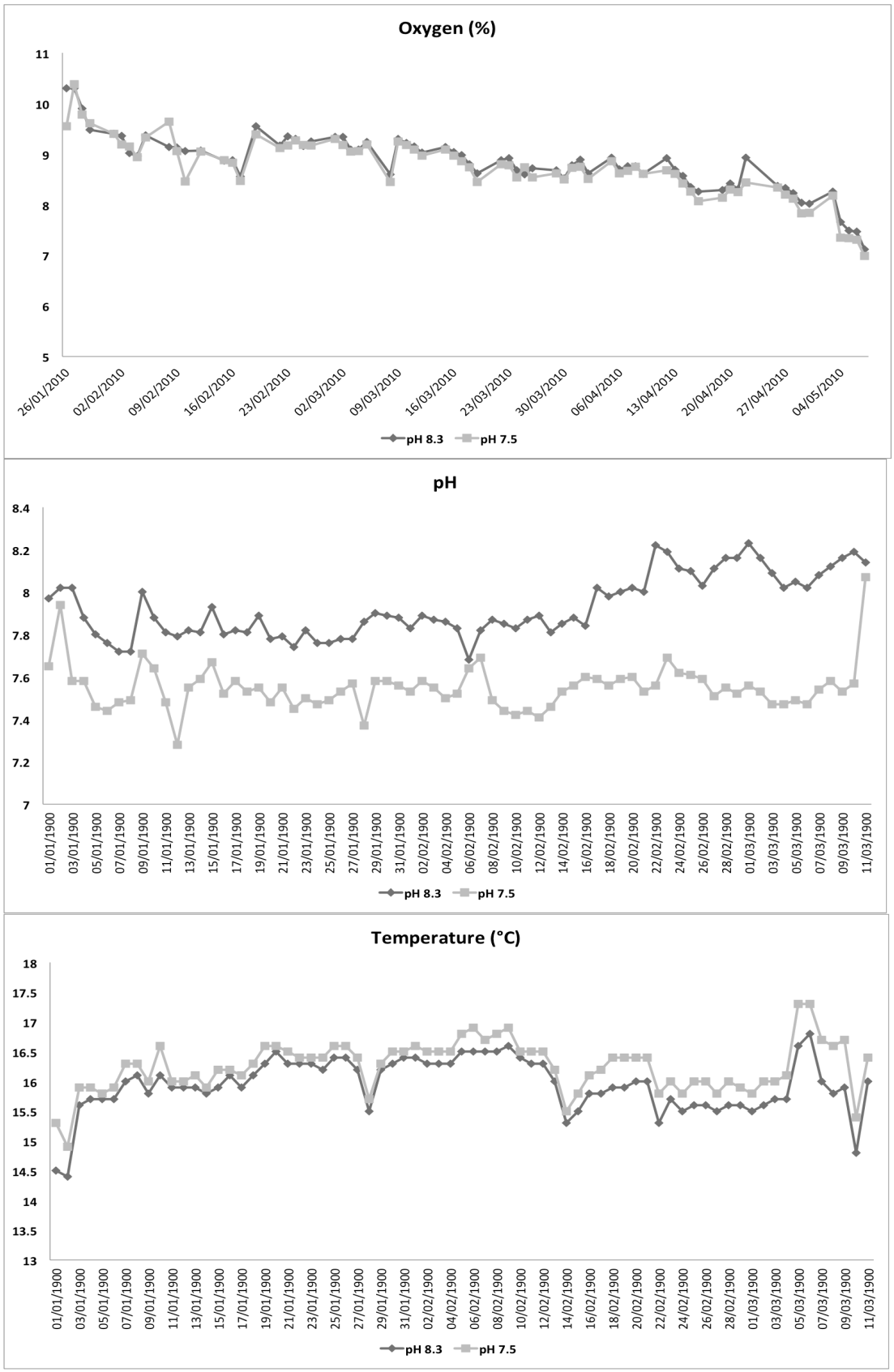

Figure 21: Measured water chemistry parameters of the first experiment at Ifremer testing the impacts of decreased pH on juvenile and adult *C. gigas* development. Oxygen concentration (%,), pH and temperature (°C) are shown in the control tank (pH 8.3) and the treatment tank (pH 7.5) containing 19 adult and 30 juvenile oysters each.

3.2.2 Larval responses to the combined effects of elevated temperature and low pH

The production of larvae, experimental system, measurements and sampling, are described in detail in Section 2.1.2. For an illustration of the experimental system, please refer to Figure 7, Section 2.1.2.2. The measured and calculated parameters for carbonate chemistry are listed in Table 18. As seen in Figure 22, temperature and pH remained constant over the experiment. The oxygen concentration was sufficient for animal survival over the period of the experiment (Figure 22); however, there was a slight decrease of 4% within the first eight days of the experiment. After this initial decrease the oxygen concentrations remained stable in all conditions apart from occasional deviations that were attributed to technical errors in measurement.

As already described in Section 2.1.2, animals were reared from embryo to the PII veliger stage at ambient conditions. Eventually the PII veliger were transferred into the experimental system to continue growing. As described before, samples were taken at regular intervals to measure larval shell growth during development. To analyse the influence of the experimental conditions on larval shell growth, two different approaches were performed. On-site, shell width measurements of sampled larvae over a period of two weeks were used to monitor larval development in real-time during the experiment. Shell width was defined as dorso-ventral measurements (DVM) of the widest part of the shell. After termination of the experiment, larval shells were imaged using a scanning electron microscope as explained in Section 2.3.1.1 and shell perimeter, shell width and shell length were measured. Shell length was defined as antero-posterior measurements (APM). Complete data sets were obtained for the two developmental stages, PII veliger and pediveliger, and therefore statistical analyses focused on these two stages to compare shell growth in all experimental conditions.

All statistical analyses were performed using Statistica. To distinguish differences between treatments, t-tests for normal distributed datasets were performed and Kruskal-Wallis one way ANOVAs on Ranks were conducted for non-normal distributed datasets. A two-way ANOVA was applied for each of the variables to test for a significant effect of the treatment factors: low pH, elevated temperature and the interacting effect low pH*elevated temperature.

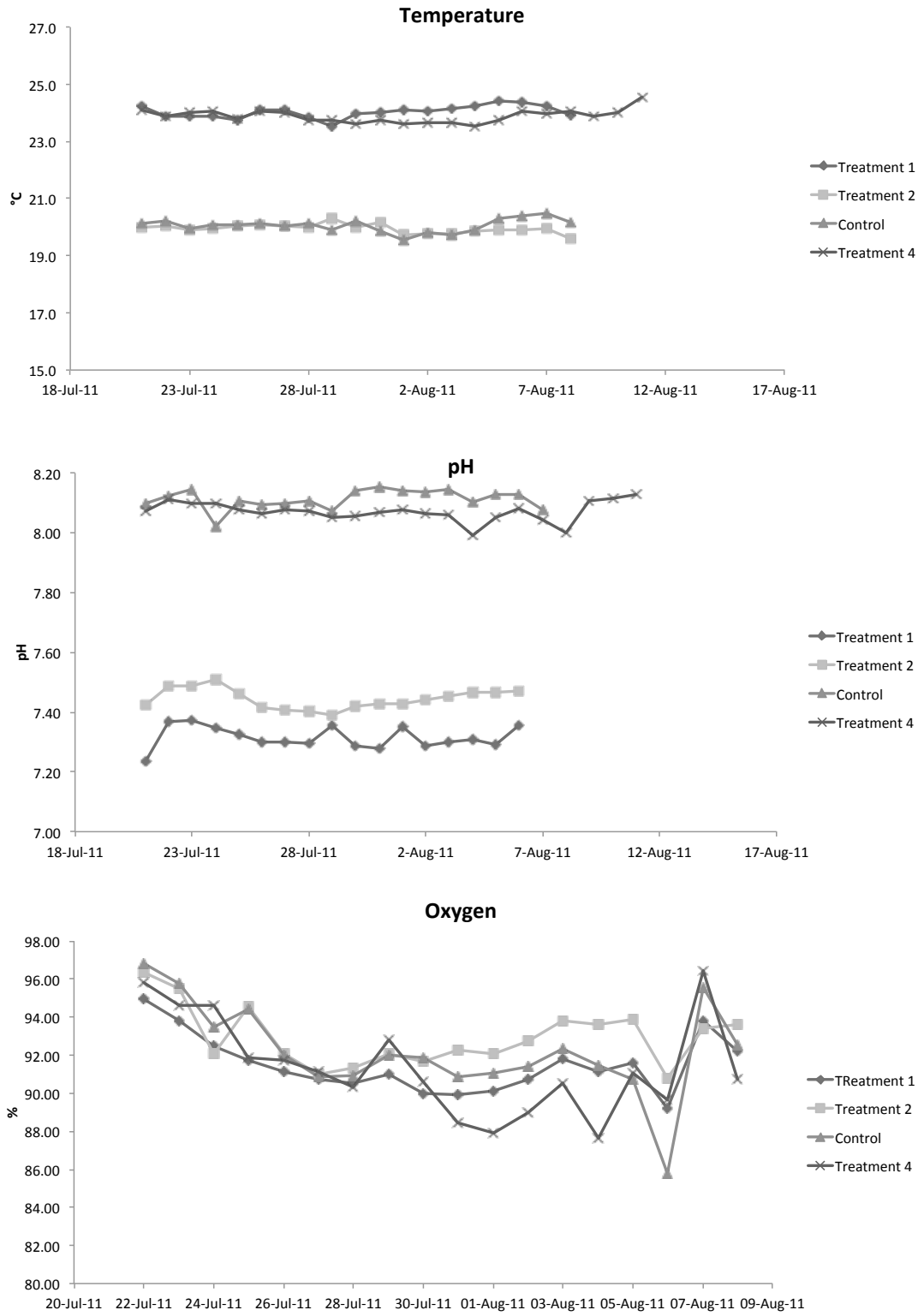

Figure 22: Water chemistry of treatment 1 (24°C pH 7.4), treatment 2 (20°C pH 7.4), control (20°C pH 8.1) and treatment 4 (24°C pH 8.1). Temperature, pH and oxygen were measured as explained in Section 2.1.2.3.

3.3 Results

Within the framework of this study it was shown that changes in pH and temperature affect the growth of *C. gigas* during ontogeny.

3.3.1 Responses of juveniles and adults to low pH

Algae consumption rates and total wet weight for spat and adults were compared between treatment and control over the 3.5-month rearing period. There was no significant difference in the algal consumption rates of juveniles or adults between pH 7.5 and pH 8.3 ($p>0.05$, ANCOVA, Table 17, Figure 23). However, comparing the consumption rates between sampling days, the ANCOVA indicated a significant effect ($p<0.01$), but showed no pattern over time (Table 17, Figure 23). At pH 7.5 the increase in total wet weight of juveniles and adults over the 3.5 months was significantly lower compared to pH 8.3 ($p<0.01$) for juveniles and $p<0.05$ for adults (ANCOVA, Table 17 and Figure 22). Never the less, and as expected, total wet weight changed significantly over time in both juveniles ($p<0.01$, ANCOVA, Table 17 and Figure 23) and adults ($p<0.01$, ANCOVA, Table 17 and Figure 23).

Due to the increased power of the multifunctional ANCOVA analyses, the adverse effect of low pH on juvenile and adult development was proven.

Table 17: Differences between algae consumption rate and total wet weight for juveniles and adults reared at pH 8.3 (control) and pH 7.5 (treatment). One Way ANCOVA testing over a period of 3.5 month using time as covariate. DF: Degrees of freedom, MS: Mean square

Source of Variation	DF	MS	F-value	p-value	Significant?
Consumption rates (pH 8.3 vs. pH 7.5)					
Time	1	4.862	8.90	0.0034	Yes
Treatment	1	0.000024	0.000044	0.9947	No
Error DF	125				
Total wet weight of juveniles (pH 8.3 vs. pH 7.5)					
Time	1	424.90	1.4272	0.0000	Yes
Treatment	1	14.11	1.4272	0.0049	Yes
Error DF	21				
Total wet weight of adults (pH 8.3 vs. pH 7.5)					
Time	1	732.24	13.65	0.00025	Yes
Treatment	1	351.93	6.56	0.0107	Yes
Error DF	457				

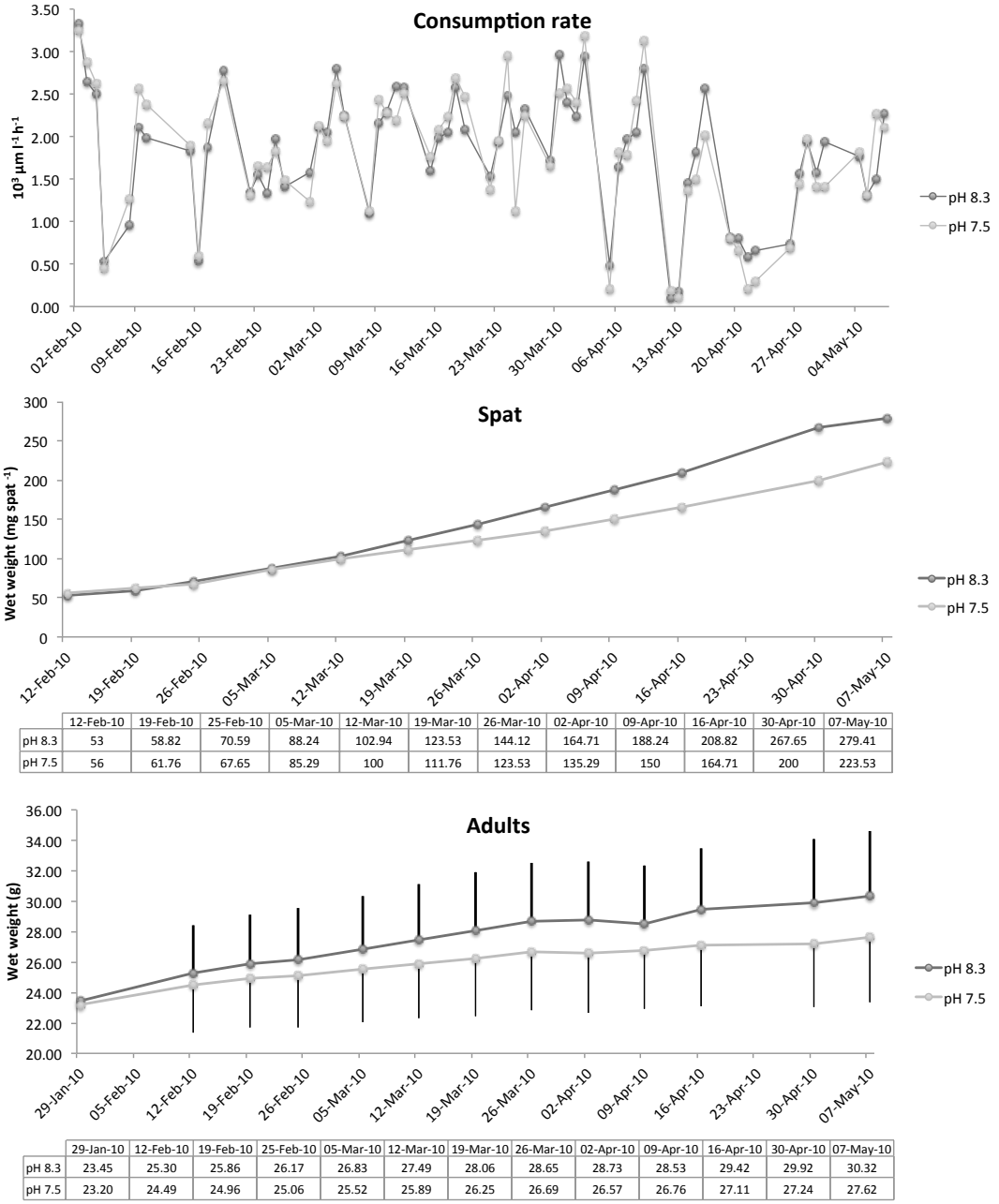

	12-Feb-10	19-Feb-10	25-Feb-10	05-Mar-10	12-Mar-10	19-Mar-10	26-Mar-10	02-Apr-10	09-Apr-10	16-Apr-10	30-Apr-10	07-May-10
pH 8.3	53	58.82	70.59	88.24	102.94	123.53	144.12	164.71	188.24	208.82	267.65	279.41
pH 7.5	56	61.76	67.65	85.29	100	111.76	123.53	135.29	150	164.71	200	223.53

	29-Jan-10	12-Feb-10	19-Feb-10	25-Feb-10	05-Mar-10	12-Mar-10	19-Mar-10	26-Mar-10	02-Apr-10	09-Apr-10	16-Apr-10	30-Apr-10	07-May-10
pH 8.3	23.45	25.30	25.86	26.17	26.83	27.49	28.06	28.65	28.73	28.53	29.42	29.92	30.32
pH 7.5	23.20	24.49	24.96	25.06	25.52	25.89	26.25	26.69	26.57	26.76	27.11	27.24	27.62

Figure 23: Consumption: calculated consumption rate animals in control (pH 8.3) and treatment (pH 7.5) group. Spat: Total wet weight over a period of 3.5 months in treatment and control groups. Adults: Mean weight (grammes; n=19) of individual adult *C. gigas* over a period of 3.5 months in treatment and control groups. SD shown as error bars.

3.3.2 Larval responses to the effects of elevated temperature and low pH

According to the protocol described in Section 2.1.2.3 water samples were taken to analyse the saturation states of aragonite and calcite during the experiment. Total alkalinity and salinity showed no clear change between the treatments throughout the experiment. However, pH, pCO_2, and saturation states for aragonite and calcite differed between different pH levels. Treatment 1 and treatment 2 were under-saturated ($\Omega<1$) with respect to aragonite, and treatment 1 was also under-saturated with respect to calcite (Table 18).

Table 18: Summary of water chemistry parameters during experimental exposure of *C. gigas* larvae. Temperature, salinity, alkalinity and DIC were measured as described in Section 2.1.2.3. HCO_3, CO_3, pCO_2, pH, Ω_{Ca} and Ω_{Ar} were calculated using co2sys software. Data are presented as means ± SD.

Treatment	0 (20°C pH 8.1)	1 (24°C pH 7.4)	2 (20°C pH 7.4)	Control (20°C pH 8.1)	4 (24°C pH 8.1)
Measured Parameters					
Temperature (°C)	20.9	24.13 ± 0.4	19.83 ± 0.21	20.17 ± 0.31	23.9 ± 0.18
Salinity	35.4	35.57 ± 0.06	35.5	35.5	35.5
A_T (µmol/kg)	2257.4	2259.53 ± 6.87	2263.33 ± 12.19	2256.3 ± 8.7	2249.38 ± 15.99
DIC (µmol/kg)	2046.8	2303.93 ±36.24	2269.77 ± 13.38	2054.83 ± 60.91	2041.65 ± 48.54
Computed parameters					
HCO_3 (µmol/kg)	1876.5	2167.8 ± 20.44	2151.93 ± 11.94	1888.03 ± 90.13	1870.43 ± 69.45
CO_3 (µmol/kg)	153.9	37.3 ± 8.13	45.07 ± 3.19	148.6 ± 36.6	153.33 ± 27.12
pCO_2	521.5	3431.37 ± 860.3	2249.23 ± 180.12	567.23 ± 219.75	615.58 ± 174.34
pH	7.94	7.20 ± 0.1	7.36 ± 0.03	7.92 ± 0.14	7.89 ± 01
Ω_{Ca}	3.67	0.89 ± 0.19	1.07 ± 0.08	3.54 ± 0.87	3.67 ± 0.65
Ω_{Ar}	2.39	0.59 ± 0.13	0.7 ± 0.05	2.3 ± 0.57	2.41 ± 0.43

Shell width measurements of PII veliger over time

ANCOVA analyses of shell width (as an indicator of larval shell growth) over a period of two weeks (Figure 24; Table 25 in Section 7.2.1.1) showed that, as expected, time had a significant influence ($p<0.01$) on shell growth. All factors, temperature, pH and the interactive effects of temperature*pH had a significant influence on shell growth (each $p<0.01$; Table 25 in Section 7.2.1.1). As shown in Figure 24, elevated temperature promoted shell growth at ambient pH (24°C pH 8.1), whereas decreased pH at ambient temperature (20°C pH 7.4) had a significant negative effect on larval shell growth and shells were significantly smaller. However, elevated temperature had a compensatory effect on shell growth at low pH in the interactive treatment (24°C pH 7.4) and shells grew larger and faster compared with the control within the time frame investigated.

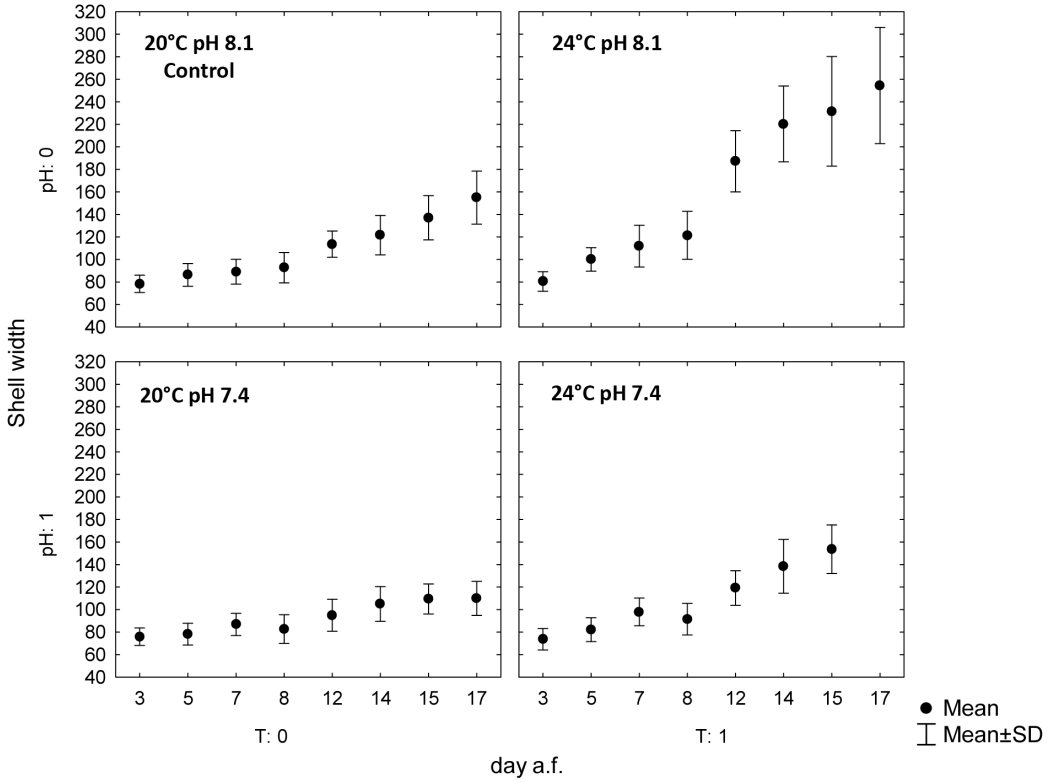

Figure 24: On-site measurements of larval shell widths of PII veliger over a period of two weeks in the control (20°C pH 8.1) and in the three treatments (treatment 1: 24°C pH 7.4, treatment 2: 20°C pH 8.1, treatment 4: 24°C pH 8.1). day a.f.: day after fertilisation; pH 0: 8.1; pH 1: 7.4; T 0: 20°C; T 1: 24°C.

Shell perimeter in PII veliger and pediveliger

PII veliger

Data for shell perimeter did not meet the assumptions of equal variance. Therefore a non-parametric Kruskal-Wallis ANOVA was performed. Elevated temperature (24°C pH 8.1) had a significant effect ($p<0.01$) on shell perimeter compared to the control (20°C, pH 8.1); the shells were significantly larger at the higher temperature (Figure 25; Table 19; Table 26 in Section 7.2.1.2).

Pediveliger

A 2-way ANOVA identified that each of the factors temperature, pH and temperature*pH had a significant ($p<0.01$) influence on shell perimeter (Figure 25; Table 19; Table 30 in Section 7.2.1.3) compared to the control. As expected, shell perimeter growth was increased at 24°C pH 8.1 and decreased at low pH*ambient temperature compared to the control. However, elevated temperature seemed to lightly compensate for low pH at 24°C pH 7.4 (Figure 25).

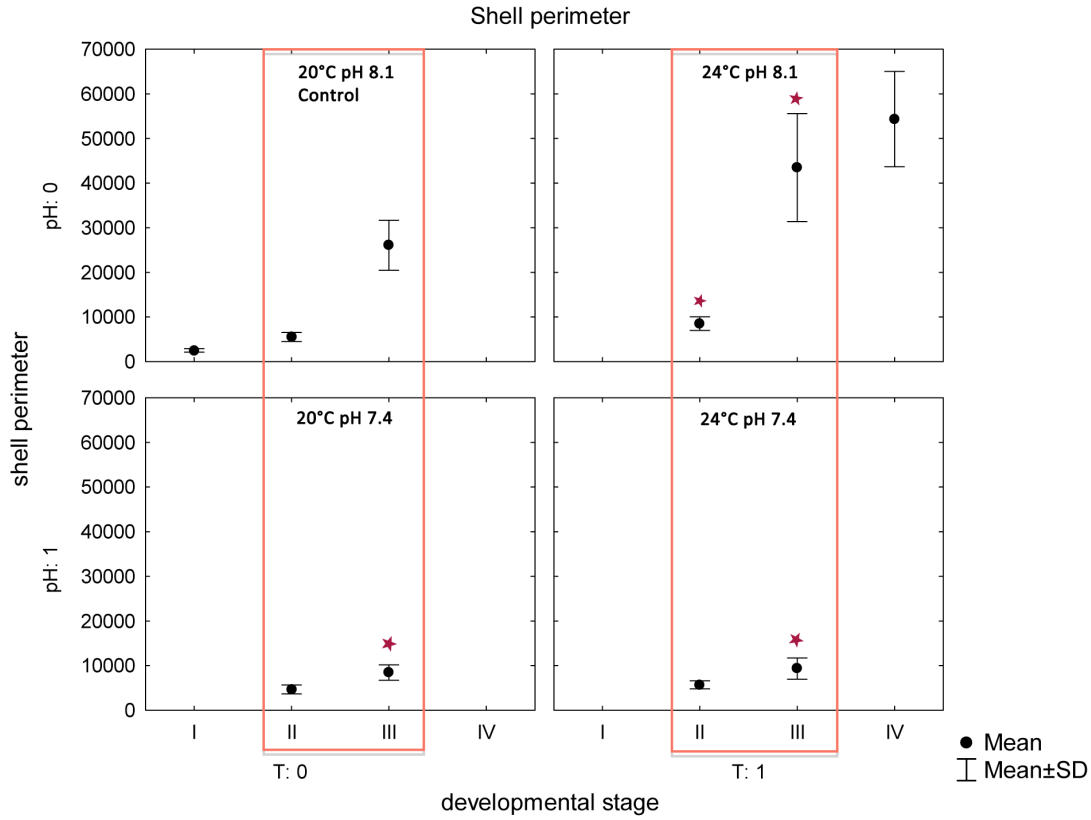

Figure 25: Larval shell perimeter in 24-h (after fertilisation, a.f.) old PI veliger (I), 6-d (a.f.) old **PII veliger (II)**, 19 d (a.f.) old **pediveliger (III)** and 22 d (a.f.) old spat (IV) in the control (20°C pH 8.1) and the three treatments. Significant differences compared to the control are marked with an asterisk. pH 0: 8.1; pH 1: 7.4; T 0: 20°C; T 1: 24°C. PII veliger and pediveliger are highlighted with red boxes.

Shell width in PII veliger and pediveliger

PII veliger

Data for shell width did not meet the assumption of equal variance. Therefore a non-parametric Kruskal-Wallis ANOVA was performed. Temperature had a significant effect on the shell width of the PII veliger reared at 24°C pH 8.1, which were significantly ($p<0.05$) larger than those in the control (20°C pH 8.1) (Figure 26; Table 19; Table 27 in Section 7.2.1.2).

Pediveliger

In pediveliger each of the tested factors temperature (24°C pH 8.1), pH (20°C pH 7.4) and temperature*pH (24°C pH 7.4) had a significant influence ($p>0.01$) on shell width as shown by a 2-way ANOVA (Table 19; Table 30 in Section 7.2.1.3). Compared to the control, shell width was reduced at low pH, whereas shell width increased at elevated temperature. Again, elevated temperature compensated for low pH in terms of increased shell size (Figure 26).

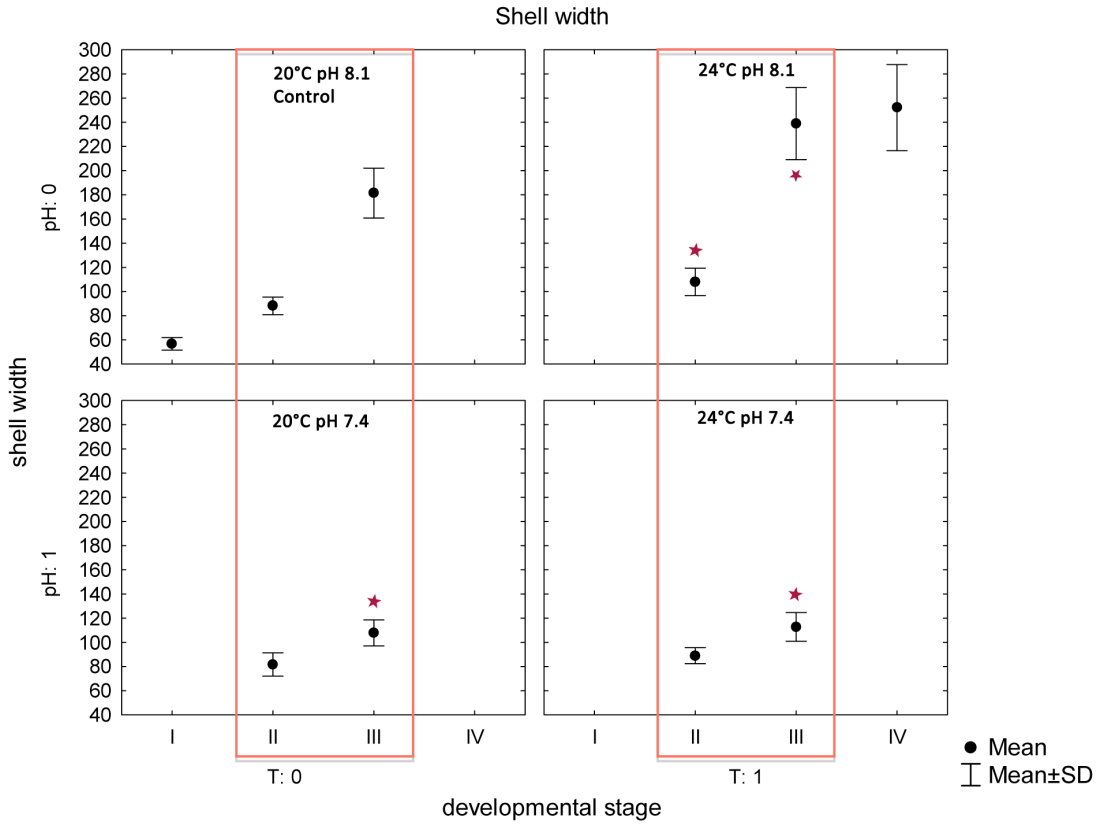

Figure 26: Larval shell width in 24-h (after fertilisation, a.f.) old PI veliger (I), 6-d (a.f.) old **PII veliger (II)**, 19 d (a.f.) old **pediveliger (III)** and 22 d (a.f.) old spat (IV) in the control (20°C pH 8.1) and the three treatments. Significant differences compared to the control are marked with an asterisk. pH 0: 8.1; pH 1: 7.4; T 0: 20°C; T 1: 24°C. PII veliger and pediveliger are highlighted with red boxes.

Shell length in PII veliger and pediveliger

PII veliger

Parametric ANOVA tests were applied as data for shell lengths met the assumptions of normal distribution and equal variances. Only an increase in temperature (24°C pH 8.1) had a significant effect ($p<0.01$) on shell length and shells were significantly longer compared to the control (Figure 27; Table 19; Tables 28 and 29 in Section 7.2.1.2).

Pediveliger

Shell length was significantly influenced by the factors: temperature, pH and temperature*pH ($p<0.01$) in pediveliger, as shown by a 2-way ANOVA (Table 19; Table 30 in Section 7.2.1.3). Elevated temperature had a positive influence on shell length at both ambient and low pH, whereas shell length in low pH (20°C pH 8.1) was lower than the control (Figure 27).

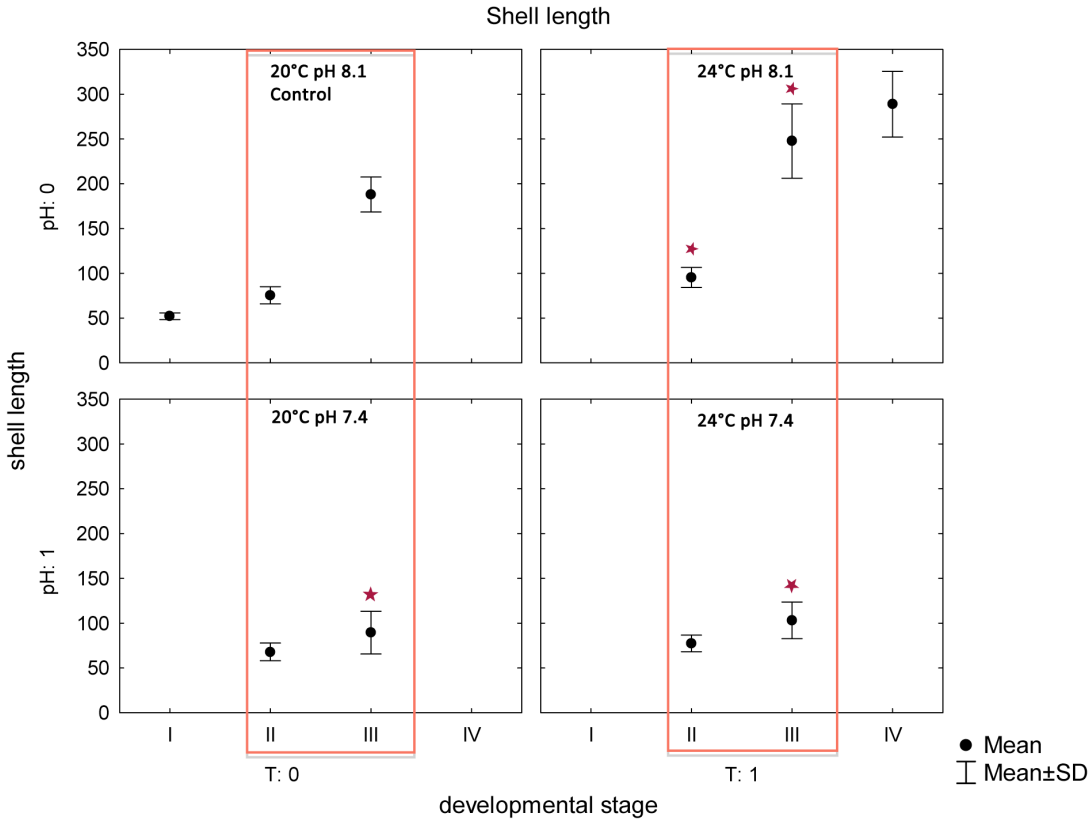

Figure 27: Larval shell length in 24-h (after fertilisation, a.f.) old PI veliger (I), 6-d (a.f.) old **PII veliger (II)**, 19-d (a.f.) old **pediveliger (III)** and 22-d (a.f.) old spat (IV) in the control (20°C pH 8.1) and the three treatments. Significant differences compared to the control are marked with an asterisk. pH 0: 8.1; pH 1: 7.4; T 0: 20°C; T 1: 24°C. PII veliger and pediveliger are highlighted with red boxes

Table 19: Shell sizes of PII veliger and pediveliger. Data are presented as means ± SD.

	Control (20°C pH 8.1)	**(24°C pH 7.4)**	**(20°C pH 7.4)**	**(24°C pH 8.1)**
PII veliger (6 days old)				
Shell length	75.44 ± 9.63	77.34 ± 9.27	67.91 ± 9.9	95.42 ± 11.21
Shell width	88.11 ± 7.3	89.07 ± 6.65	81.7 ± 9.69	108.02 ± 11.36
Shell perimeter	5522.25 ± 1014.95	5683.69 ± 897.08	4659.8 ± 1002.92	8535.27 ± 1526.52
Pediveliger (19 days old)				
Shell length	188.07 ± 19.52	103.14 ± 20.48	96.08 ± 11.12	247.69 ± 41.47
Shell width	181.42 ± 20.65	112.87 ± 11.89	107.84 ± 10.79	238.92 ± 29.85
Shell perimeter	26084.85 ± 5602.98	9359.44 ± 2376.85	8448.04 ± 1715.11	43465.94 ± 12090.26

3.4 Discussion

It is well documented that a decrease in seawater pH negatively impact various life stages of many bivalves and because of their shell mineralogy the larval stage has been reported to be the most vulnerable stage of all (see Table 2, Section 1.4).

The present study demonstrated that the predicted future pH of 7.4 (Nicholls et al., 2007) is likely to impair larval shell growth in the Pacific oyster as with increasing pCO_2 the water becomes under-saturated in respect to aragonite and calcite (Table 18), subsequently reducing the ability of the animals to precipitate calcium carbonate. It was shown that low pH at ambient temperature had a negative effect on larval shell growth as the shells were significantly smaller compared to the control (Figure 24; Table 25 in Section 7.2.1.1). The majority of studies that have investigated the effects of decreased pH on bivalve development showed that low pH was responsible for increased mortality rates, retarded growth and decreased metamorphosis (see Table 2) confirming the results of the present study.

However, according to the predictions for future oceans, the oceans will simultaneously warm as they become more acidic. It is well known that a moderate increase in temperature has beneficial effects on larval development with faster growth, larger size and reduced planktonic larval duration. Kheder et al. (2010) and Rico-Villa et al. (2009) showed that elevated temperatures (≤ 32°C) led to faster larval growth and increased metamorphosis rates in the Pacific oyster *C. gigas*. The favourable effects of elevated temperature were confirmed with the present study, showing that PII veliger larvae reared at 24°C grew faster and larger over time at pH 8.1 and even at pH 7.4 (Figure 24, Table 25 in Section 7.2.1.1), diminishing the effects of decreased pH. The fact that moderate warming is able to compensate the effects of decreased pH was also shown in the sea urchin *Heliocidaris erythrogramma* by Byrne et al. (2011), where an increase in seawater temperature of +2°C (to 24°C) led to normal spine development in the low pH treatments (pH 7.8 and pH 7.6). However, at +4°C (26°C) and low pH the thermal tolerance was breached and development failed. In contrast, development of the abalone *Haliotis coccoradiata* was already significantly affected by a moderate increase of +2°C and low pH treatments (pH 7.8 and pH 7.6) resulting in abnormal embryos, unshelled larvae and increased mortality (Byrne et al., 2011). With a temperature increase of +4°C development failed. Parker and Ross (2009) investigated the synergistic effects of OA and temperature on the development of *Saccostrea glomerata* and showed that at 1000 µatm (~ pH 7.7) and sub-optimal temperatures (18°C and 30°C) development of veliger larvae decreased and malformations and mortality increased. Parker et al. (2010b) also compared fertilisation success and development of *S. glomerata* and *C. gigas* under future ocean scenarios. It was shown that overall the Pacific oyster was less sensitive to perturbation compared to the Sydney rock oyster.

Still, the number of abnormal 48-h old D-veliger of *C. gigas* was greatest at extreme temperatures (18°C and 30°C) and elevated pCO_2 (1000 µatm), while growth was most affected at 18°C and 1000 µatm showing a significant decrease in shell size. Growth of pediveliger showed a significant decrease at temperatures 18°C and 22°C and elevated pCO_2 (600-1000 µatm) and spat was mostly affected by elevated pCO_2 at 30°C. By comparing all developmental stages tested, Parker et al. (2010b) found the greatest tolerance to elevated pCO_2 during the pediveliger stage of *C. gigas*.

With regards to the present study, development of *C. gigas* larvae was facilitated by an increase in temperature but decreased pH lowered the developmental success (Figures 24-27). As environmental stressors such as temperature and pH are unlikely to act independently it can be concluded that larval development in *Crassostrea gigas* in waters that become simultaneously warmer and more acidic, will not be affected in terms of shell size, at least within the PII veliger stage (Figure 24). It is important to note that mortality rates were not monitored in this experiment because of technical limitations of the rearing system that meant that during periodic "overflows" from the system larvae were washed out; this artificially decreased the number of animals in each treatment. However, estimated macroscopic numbers of larvae for the low pH treatments were smaller compared to larvae in ambient pH conditions. Thus, it can be speculated that just the fittest larvae developed into the PII veliger stage and grew larger at elevated temperature*low pH compared to the control.

The different reactions to the synergistic effects of elevated temperature and low pH highlight that the response to future sea water conditions is highly species specific and can even differ between developmental stages of the same species as shown by Parker et al. (2010b) and in the present study. Parker et al. (2010b) reported that pediveliger of *C. gigas* showed the greatest tolerance to elevated pCO_2 at all tested temperatures (18, 22, 26 & 30 °C) compared to D-veliger and spat, which stands in conflict to the results of the present study. By comparing just two developmental stages, six-days old PII veliger and 19-days old pediveliger, it was shown that pediveliger were more sensitive to decreased pH (Figures 24-26), likely as a result of the longer exposure times in the later stage and subsequent dissolution of the shells. While pediveliger shells in low pH treatments were significantly smaller in terms of shell perimeter, width and length, shell size of PII veliger was not significantly different to the control. For both developmental stages an increase in temperature of 4°C at ambient pH had a significant positive effect on shell growth as shells were significantly larger compared to the control (pH 8.1, 20°C). The dissimilarity in results of the present study and the findings of Parker et al (2010b) could be either accredited to differences in methodology as the tested pH in the present study was lower (pH 7.4) compared to pH 7.7 in Parker et al. (2010b), possibly resulting in higher sensitivity of

pediveliger. Another reason may be due to adaptive capacity of species to climatic conditions, which may differ between populations with a large geographic distribution.
Even though the aragonitic shells of larvae are more susceptible to dissolution due to their mineralogy, it was shown that development of juvenile and adult oysters was also negatively affected by low pH conditions. While no difference in the algae consumption rates of combined juveniles and adults between treatments and control was observed (Table 17, Figure 23), a significant difference in total wet weight between treatment and control over a period of 3.5 months was monitored. In both juveniles and adults the increase of total wet weight was significantly lower at low pH compared to the control, indicating decreased growth rates. These findings are in agreement with other studies showing reduced growth and calcification rates (Beniash et al., 2010; Gazeau et al., 2007; Miller et al., 2009), an increase in mortality and energy consumption (Beniash et al., 2010; Dickinson et al., 2012) and a significant decrease in tissue growth (Dickinson et al., 2012) in juvenile and adult *Crassostrea spp.* in response to low pH. Other mollusc species such as the blue mussel *Mytilus edulis* were also affected by decreased pH showing a significant decrease in shell growth and high mortality rates (Gazeau et al., 2007; Michaelidis et al., 2005). In contrast, juveniles of the grooved carped shell *Ruditapes decussatus* (Range et al., 2011) and the common cuttlefish *Sepia officinalis* (Gutowska et al., 2008) were not affected by decreased pH/increased pCO_2, showing that the impacts of OA are species-specific.

Thus, it can be concluded that overall, changing environmental conditions such as CO_2-driven acidification and elevated temperatures and their interactive effects are likely to impact development of *C. gigas*, with reduced growth as a long-term consequence. Therefore it is vital to develop a deeper understanding on the molecular mechanism of calcification, which will be presented in the following Chapter.

4 - Molecular mechanisms of biomineralisation during ontogeny of *Crassostrea gigas* under future ocean scenarios

"One of the major challenges in the field of biomineralisation is to understand the mechanisms by which biological systems determine which polymorph will precipitate. This is genetically controlled and it's almost always achieved with 100% fidelity"

Weiner and Dove (2003)

4.1 Introduction

Molluscan shell formation is under strict biological control, a process that is largely unknown. According to the widely accepted BCM hypothesis or organic matrix mediated biomineralisation (Lowenstam and Weiner, 1989; Lowenstam, 1981), calcification in molluscs takes place in an enclosed environment, the extrapallial space (Lowenstam and Weiner, 1989; Marin and Luquet, 2004; Veis, 2003; Weiner and Dove, 2003). The extrapallial space in larvae is the enclosed space between the periostracum and the shell field (see Section 1.3.2.1), while in adults the space is bounded by the growing shell, the periostracum and the mantle epithelium (Figure 3, Section 1.3.2.1) (Marin and Luquet, 2004). Within this space, epithelial cells of the mantle elaborate the organic matrix (Addadi et al., 2006; Levi-Kalisman et al., 2001; Lowenstam, 1981), which is thought to be the controller of shell mineralisation (Gong et al., 2008; Sudo et al., 1997; Takeuchi and Endo, 2006; Zhang and Zhang, 2006). Within this organic framework, the mineral phase is precipitated as explained in Section 1.3.2. Organic matrices are composed mainly of proteins, glycoproteins, proteoglycans and chitin (Addadi et al., 2006; Joubert et al., 2010; Marin and Luquet, 2004) and show a great diversity in molecular weight and amino acid composition across the species and within the different microstructures of species (Kobayashi and Samata, 2006) (see Table 1, Section 1.3.4). As many studies have investigated the composition and function of the organic matrices, as little is known about genes involved in calcification in molluscs. However, the number of studies investigating biomineralisation in molluscs on a molecular level has increased in the past six years (Fang et al., 2011; Gardner et al., 2011; Joubert et al., 2010; Miyazaki et al., 2010; Takeuchi and Endo, 2006; Takeuchi et al., 2012; Zhang and Hare, 2012; Zippay and Hofmann, 2010). Predicted changing environmental conditions such as OA and increasing SSTs (Nicholls et al., 2007) emphasises the need to fully understand the complexity of calcification processes, as OA is widely believed to impact biomineralisation in marine calcifiers (Table 2, Section 1.4).
To date, very few studies have investigated the impacts of multiple stressors on molecular level in marine invertebrates (Beniash et al., 2010; Gaume et al., 2011; Miyazaki et al., 2010; Sussarellu et al., 2010; Takeuchi and Endo, 2006; Zhang and Hare, 2012; Zippay and Hofmann, 2010). Therefore, a key objective of this study was to analyse if the combined effects of changing seawater temperature and altering pH impact the expression of the biomineralisation genes *CGCaM, CGDent, CGPerl* and *CGMG4* during ontogeny of *Crassostrea gigas*. By using quantitative real-time PCR the response of the Pacific oyster to two environmental stressors during ontogeny was quantified.

4.2 Material and Methods

To study the impacts of changing environmental conditions on gene expression levels of the biomineralisation genes *CGCaM, CGDent, CGPerl* and *CGMG4* of different life stages of *C. gigas*, two different experiments were designed and conducted at Ifremer, Station d'Argenton, France as explained in Section 2.1.

4.2.1 Molecular responses of juveniles and adults to low pH

As already described in Section 2.1.1, 38 adult (> 2 yrs.) and 60 juvenile (< 1 yr.) *C. gigas* were exposed to acidified (pH 7.5) and ambient seawater (pH 8.3) over a period of 3.5 months (Figure 7, Section 2.1.1.2). Temperature in both tanks was set to 15°C, simulating ambient seasonal seawater temperature and mean salinity was 34. Daily measurements of temperature, pH, O_2 and salinity were taken as described in Section 2.1.1.3. After termination of the experiment tissue samples were taken from both, the left and the right mantle of juvenile and adult oysters, fixed in RNAlater® and processed for relative qPCR according to the methods described in Section 2.2.

4.2.2 Molecular responses of larvae to the combined effects of elevated temperature and low pH

Embryos of the Pacific oyster were produced by strip-spawning of mature gonads of nine mature male and thirty females individuals as described in Section 2.1.2.1. As explained in Section 2.1.2.1, the embryos were transferred into a 150 l tank (treatment 0) with aerated and filtered ambient seawater (20°C pH 8.1) to develop into PI veliger within 48 hours. Once the larvae had reached a size in excess of 40 µm they were equally divided and transferred into the experimental system, described in Section 2.1.2.2. To simulate predicted future ocean conditions, three different treatments (treatment 1: 24°C pH 7.4, treatment 2: 20°C pH 7.4 and treatment 4: 24°C pH 8.3) were tested against one control (20°C pH 8.1). Each treatment was operated in triplicate. Temperature, pH, oxygen and salinity were measured regularly as described in Section 2.1.2.3. Corresponding to the sampled developmental stages, water samples for DIC and TA were taken following the protocol described in Section 2.1.2.3. As listed in Table 4 (Section 2.1.2.3) larvae samples for qPCR analyses were taken on particular dates, corresponding to the main developmental stages trochophora, PI veliger, PII veliger, pediveliger and spat and fixed in RNAlater® as described before. The samples were processed

for quantitative real-time PCR analyses as described in Section 2.2. As development was delayed and mortality rates were high in treatments 1 and 2, larvae did not develop into spat during the time span of the experiment. Therefore full sample sets were just available for the developmental stages trochophora, PI, PII and pediveliger.

4.3 Results

Due to the molecular approach of this study it was possible to capture changes in gene expression in response to CO_2-driven seawater acidification of juvenile and adult *C. gigas*. Changes in gene expression in response to the combined effects of ocean acidification and ocean warming on the developing oyster larvae were also monitored.

4.3.1 Molecular responses of juveniles and adults to low pH

In spat, the relative expression level of *CGCaM* was significantly lower at pH 7.5 ($p<0.05$) compared to the control condition (pH 8.3) as *CGCaM* was down-regulated by a mean factor of 0.248. *CGDent* ($p>0.05$) and *CGMG4* ($p>0.05$) showed no significant changes in expression levels at pH 7.5 compared to pH 8.3, whereas *CGPerl* was significantly down-regulated ($p<0.05$) by a mean factor of 0.21 at pH 7.5 (Table 20, Figure 28).
The relative expression level of *CGCaM* in adults showed a significant down-regulation by a mean factor of 0.626 ($p<0.05$) at pH 7.5 compared to pH 8.3, whereas *CGDent* showed no significant difference in expression at pH 7.5 ($p>0.05$) as well as *CGPerl* ($p>0.05$). *CGMG4* was significantly up-regulated in adults by a mean factor of 3.97 ($p<0.05$) at pH 7.5 compared to the control condition (pH 8.3) (Table 20, Figure 28).

Comparing the expression levels of the GOI of spat and adults at ambient pH (pH 8.3), none of the GOI did vary significantly in expression in adults compared to spat (all $p>0.05$) (Table 20).

Table 20: REST©2009 results of qPCR data testing the impact of pH on gene expression of spat and adults. For each analysis the best two ER genes evaluated by NormFinder© were used (see Section 2.2.2.5). Expression, standard error and p-value for each GOI are given.

Testing spat at pH 8.3 *vs.* pH 7.5				
Best combination of two ER genes: *CGCGAct & CGTub*				
GOI	**Relative expression**	**Std. Error**	**p-value**	**Significant result**
CGCaM	0.248	0.029 - 1.713	0.044	DOWN-regulated at pH 7.5
CGDent	0.645	0.221 - 1.955	0.446	/
CGPerl	0.21	0.030 - 0.924	0.032	DOWN-regulated at pH 7.5
CGMG4	0.693	0.085 - 3.969	0.66	/
Testing adults at pH 8.3 *vs.* pH 7.5				
Best combination of two ER genes: *GCAct & CGCyclo*				
GOI	**Relative expression**	**Std. Error**	**p-value**	**Significant result**
CGCaM	0.626	0.389 - 1.015	0.009	DOWN-regulated at pH 7.5
CGDent	0.663	0.262 - 1.636	0.226	/
CGPerl	0.879	0.212 - 4.155	0.765	/
CGMG4	3.97	0.667 - 38.000	0.042	UP-regulated at pH 7.5
Testing spat *vs.* adults at pH 8.3				
Best combination of two ER genes: *CGAct & CGTub*				
GOI	**Relative expression**	**Std. Error**	**p-value**	**Significant result**
CGCaM	0.325	0.047 - 1.858	0.121	/
CGDent	0.835	0.081 - 5.503	0.815	/
CGPerl	0.776	0.314 - 1.974	0.511	/
CGMG4	1.078	0.170 - 7.467	0.931	/

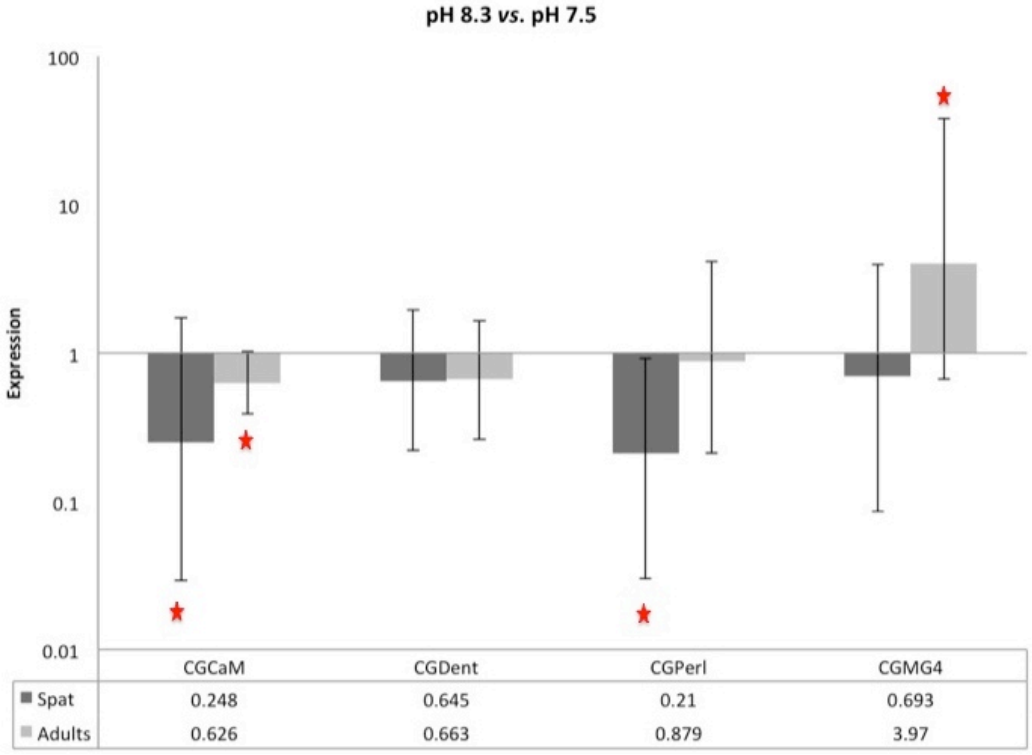

Figure 28: REST©2009 results comparing gene expression of the GOI in spat and adults in pH 8.3 and pH 7.5. Significant results are marked with a red asterisk. Bars indicate standard errors.

4.3.2 Molecular responses of larvae to the combined effects of elevated temperature and low pH

To determine the molecular response of early life history stages of *C. gigas* to altered seawater pH in combination with different temperatures, relative gene expression levels of *CGCaM, CGDent, CGPerl* and *CGMG4* were measured and analysed (Table 21 and Figure 29).
As described in Section 2.1.2.2, embryos were initially reared in ambient batch condition at 20°C pH 8.1 until PI veliger stage (treatment 0). Comparing PI veliger and trochophora at 20°C pH 8.1, neither *CGCaM* ($p>0.05$) nor *CGDent* ($p>0.05$) and *CGMG4* ($p>0.05$) showed a significant difference in expression levels. On the contrary, *CGPerl* was up-regulated by a mean factor of 1.775 ($p<0.05$) in PI veliger compared to trochophora.
Comparing PII veliger and pediveliger at ambient conditions (20°C pH 8.1), *CGCaM* was significantly up-regulated by a mean factor of 1.306 ($p<0.05$), *CGDent* showed no significant difference in expression levels between the two developmental stages ($p<0.05$), whereas *CGPerl* was up-regulated by a mean factor of 2.189 ($p<0.05$). The relative expression of *CGMG4* in pediveliger compared to PII veliger was significantly increased by a mean factor of 5.959 ($p<0.05$).
Comparisons of expression levels in pediveliger and PII veliger of treatment 1 (24°C pH 7.4), showed that *CGCaM* was significantly up-regulated by a mean factor of 3.017 ($p<0.05$). Neither the relative expression levels of *CGDent* ($p<0.05$) nor *CGPerl* ($p<0.05$) in pediveliger were significantly different to the expression levels in PII veliger. *CGMG4* on the contrary was significantly up-regulated by a mean factor of 33,572.75 ($p<0.05$) in pediveliger compared to PII veliger.
Comparing the relative expression levels of pediveliger and PII veliger in treatment 2 (20°C pH 7.4) identified that *CGCaM* was down-regulated in pediveliger by a mean factor of 0.628 ($p<0.05$) whereas the expression levels did not vary significantly in *CGDent* ($p<0.05$). On the contrary, *CGPerl* was up-regulated by a mean factor of 1.696 ($p<0.05$) as well as *CGMG4*, which was significantly up-regulated by a mean factor of 12,575.84 ($p<0.05$) in pediveliger compared to PII veliger.
Comparisons of expression levels in pediveliger and PII veliger of treatment 4 (24°C pH 8.1), showed that just *CGDent* was significantly different ($p<0.05$) in pediveliger compraed to PII veliger as it was down-regulated by a mean factor of 0.604. The expression levels of *CGCaM*. *CGPerl* and *CGMG4* in pediveliger did not vary significantly (all $p<0.05$) to the expression levels of PII veliger.

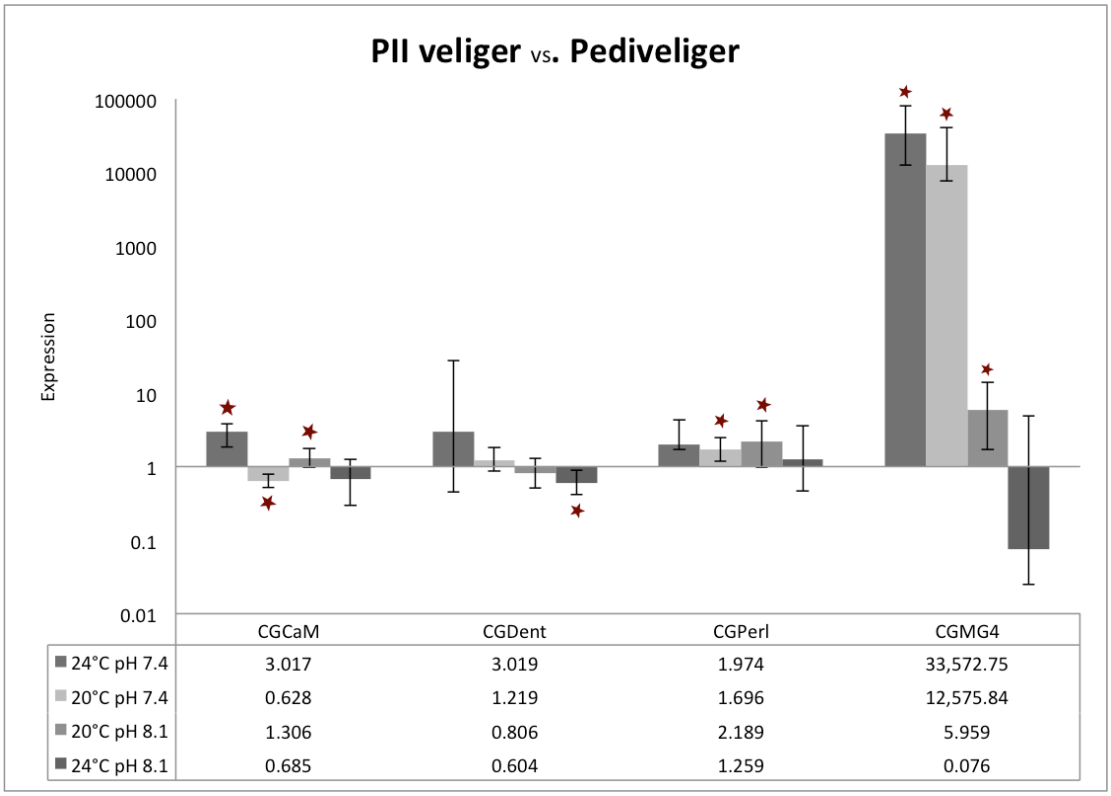

	CGCaM	CGDent	CGPerl	CGMG4
24°C pH 7.4	3.017	3.019	1.974	33,572.75
20°C pH 7.4	0.628	1.219	1.696	12,575.84
20°C pH 8.1	1.306	0.806	2.189	5.959
24°C pH 8.1	0.685	0.604	1.259	0.076

Figure 29: REST©2009 results comparing gene expression of the GOI of PII veliger *versus* pediveliger larvae in the control condition (20°C pH 8.1), at 24°C pH 7.4, 20°C pH 7.4 and 24°C pH 8.1. Significant results are marked with a red asterisk. Bars indicate standard errors.

Table 21: REST©2009 results of qPCR data testing the impact of pH and temperature on gene expression of larvae. For each analysis the best two ER genes evaluated by NormFinder© were used (see Section 2.2.2.5). Expression, standard error and p-value for each GOI are given.

Testing Trochophora *vs.* PI veliger at 20°C pH 8.1 (condition 0)				
Best combination of two ER genes: *CGCyclo & CGTub*				
GOI	**Relative expression**	**Std. Error**	**p-value**	**Significant result**
CGCaM	0.748	0.566 - 1.026	0.146	/
CGDent	0.765	0.472 - 1.199	0.378	/
CGPerl	1.775	1.364 - 2.172	0.009	UP-regulated in PI veliger compared to Trochophora
CGMG4	0.748	0.566 - 1.026	0.146	/
Testing PII veliger *vs*. Pediveliger at 20°C pH 8.1 (Control)				
Best combination of two ER genes: *CGCyclo & CGTub*				
GOI	**Relative expression**	**Std. Error**	**p-value**	**Significant result**
CGCaM	1.306	0.972 - 1.757	0.003	UP-regulated in PV compared to PII veliger
CGDent	0.806	0.509 - 1.297	0.121	/
CGPerl	2.189	0.966 - 4.160	0.001	UP-regulated in PV compared to PII veliger
CGMG4	5.959	1.700 - 13.798	0.002	UP-regulated in PV compared to PII veliger
Testing PII veliger *vs*. Pediveliger at 24°C pH 7.4 (treatment 1)				
Best combination of two ER genes: *CGAct & CGTub*				
GOI	**Relative expression**	**Std. Error**	**p-value**	**Significant result**
CGCaM	3.017	1.846 - 3.848	0.000	UP-regulated in PV compared to PII veliger
CGDent	3.019	0.448 - 27.897	0.11	/
CGPerl	1.974	1.685 - 4.260	0.388	/
CGMG4	33,572.75	12,580.935 - 81,136.702	0.000	UP-regulated in PV compared to PII veliger
Testing PII veliger *vs*. Pediveliger at 20°C pH 7.4 (treatment 2)				
Best combination of two ER genes: *CGAct & CGTub*				
GOI	**Relative expression**	**Std. Error**	**p-value**	**Significant result**
CGCaM	0.628	0.520 - 0.797	0.008	DOWN-regulated in PV compared to PII veliger
CGDent	1.219	0.870 - 1.841	0.329	/
CGPerl	1.696	1.184 - 2.504	0.022	UP-regulated in PV compared to PII veliger
CGMG4	12,575.84	7,649.714 - 41,069.399	0.004	UP- regulated in PV compared to PII veliger
Testing PII veliger *vs*. Pediveliger at 24°C pH 8.1 (treatment 4)				
Best combination of two ER genes: *CGCyclo & CGTub*				
GOI	**Relative expression**	**Std. Error**	**p-value**	**Significant result**
CGCaM	0.685	0.297-1.256	0.207	/
CGDent	0.604	0.417-0.895	0.006	DOWN-regulated in PV compared to PII veliger
CGPerl	1.259	0.462-3.598	0.563	/
CGMG4	0.076	0.025-4.869	0.397	/

4.4 Discussion

Although an increasing number of studies have investigated molecular mechanisms of biomineralisation in marine invertebrates, our understanding concerning molecular mechanisms in *C. gigas* is still very poor. However, just recently a study of Zhang and co-workers (2012) took molecular *C. gigas* research one step further as they were the first to sequence the whole genome of the Pacific oyster. This ground-breaking study predicted a total of 28,027 genes (encoding 50 amino acids or more) of which 8,654 genes are specific to oysters. 278 genes were highly expressed in the mantle and 214 genes were mantle-specific, providing support for their possible roles in shell formation in oysters. The list of genes expressed in the mantle of *C. gigas,* contained some well-known genes that have been reported to play important roles in shell formation in molluscs such as *Pif177*, which is thought to initiate aragonite crystallisation in the nacreous layer of *P. fucata* (Suzuki et al., 2009), alkaline phosphatase (AP), an ubiquitous enzyme involved in biomineralisation in mammals and in *Haliotis tuberculata* (Gaume et al., 2011), perlucin, a sugar-binding protein thought to accelerate calcium carbonate precipitation and direct the morphology of crystals in *Haliotis laevigata* (Weiss et al., 2000), and *PFMGs* including *PFMG4.* As already mentioned in Section 2.2.1.3, members of the PFMG family are involved in calcification processes in *P. fucata*, such as *PFMG3*, which is thought to enhance biomineralisation (Wang et al., 2011).

As for many of the known shell related genes, no homologues in the oyster genome were found (Zhang et al., 2012). The authors suggested that due to strong selection pressure genes related to shell formation showed a great diversity in oysters. Nevertheless, Zhang et al. (2012) identified 39 oyster genes with conserved domain structures, that were highly expressed in the mantle and which were homolog to known shell formation related genes including *CaM,* nacrein*, PFMG1* and *engrailed* (Zhang et al., 2006). These 39 oyster homologues are likely to be important for shell formation in *C. gigas.* As mentioned in Section 2.2.1.2, *CaM* regulates calcium metabolism in nearly all organisms and is highly conserved among the molluscan phyla. It was first isolated from *P. fucata* (Li et al., 2004) where it was highly expressed in the gills and the outer epithelium of the dorsal mantle, suggesting its involvement in calcium transport and secretion. Nacrein, a matrix protein highly conserved in bivalves and gastropods, was first isolated from the organic matrix of the nacreous layer in *P. fucata*, but was also found in the prismatic layer of the same species (Miyamoto et al., 1996; Miyamoto et al., 2003; Miyamoto et al., 2005). Its high expression in both the mantle edge and the mantle pallial supported its possible involvement in both prisms and nacre formation (Miyamoto et al., 2005; Miyashita et al., 2002). *PFMG1* is believed to be a calcium-binding protein, responsible for the nucleation of calcium carbonate compounds and is possibly involved in nacre formation (Liu et al., 2007).

The homeobox protein *engrailed* was found in almost all shell-bearing classes of the molluscan phylum including Scaphopoda (Wanninger and Haszprunar, 2001), Polyplacophora (Jacobs et al., 2000), Bivalvia (Jacobs et al., 2000; Kin et al., 2009), Gastropoda (Iijima et al., 2008; Moshel et al., 1998; Nederbragt et al., 2002) and Cephalopoda (Baratte et al., 2007). Even though *engrailed* was discovered in evo-devo research (evolutionary developmental biology), there is increasing evidence that it could play an important role in shell formation. Without going into too much detail, it has been suggested that *engrailed* might be involved in the development of the embryonic shell of the gastropods *Ilyanassa obsolenta* (Moshel et al., 1998) and *Haliotis rufescens* (Zippay and Hofmann, 2010), the clam *Transennella tantilla* (Jacobs et al., 2000), the chiton *Lepidochitona caverna* (Jacobs et al., 2000) and the scaphopod *Antalis entails* (Wanninger and Haszprunar, 2001).

However, biomineralisation mechanisms during ontogeny in *C. gigas* on a molecular level contain more questions than answers. To investigate some of the molecular mechanisms involved in shell development in the Pacific oyster, four genes of interest, *CGCaM, CGPerl, CGMG4* and *CGDent*, were chosen for this study. OA and increasing SSTs are known to impact gene expression in other marine calcifying organisms (Liu et al., 2012; Zippay and Hofmann, 2010). The present study demonstrated that a decrease in seawater pH affected the expression of *CGCaM* and *CGPerl* in spat, though expression of *CGDent* and *CGMG4* were not affected (Table 20, Figure 28). In adult *C. gigas* the expression of *CGCaM* and *CGMG4* were significantly changed by low pH, while no significant differences in gene expression of *CGDent* and *CGPerl* were observed (Table 20, Figure 28). These results suggest that ocean acidification directly changes the gene expression of skeletogenesis-related genes. It can be concluded that the down regulation of *CGCaM* eventually results in decreased Ca-binding activity. Thus, reduced calcium uptake may lead to decreased calcification rates and a decrease in shell growth in both juvenile and adult *C. gigas* under future ocean conditions. In spat *CGPerl* was down regulated at pH 7.5 in contrast to the adults, where no significant change in expression levels at pH 7.5 compared to pH 8.3 was observed.

Down-regulation of *CGPerl* in juveniles (Table 20, Figure 28) could possibly result in a decrease in calcium carbonate precipitation and malformed crystals. According to these data it can be concluded that juveniles are more sensitive to OA compared to adults on a molecular level. In adults, *CGMG4* showed an increase in expression levels at pH 7.5. Members of the PFMG family are believed to play important roles in shell development in *P. fucata*, such as calcium carbonate nucleation and enhancement of biomineralisation. Increased expression of *CGMG4* could indicate a mechanism to compensate for possible shell dissolution. To confirm the negative impact of lowered pH on gene expression in adults and juveniles, gene expression levels of adults at pH 8.3 were tested against gene expression in spat at pH 8.3 and no

significant change in expression levels was observed. These results show that expression levels of the GOI were not changed by developmental stage in post-metamorphosed animals.

Significant differences in gene expression levels were identified when examining the synergistic effects of pH and temperature on larval development (Table 21, Figure 29). As mentioned before, from embryo to PI veliger, larvae were reared at ambient conditions until they were transferred into the experimental system. To analyse which genes are involved in initial shell development at ambient conditions, gene expression levels of PI veliger and trochophora were compared. Apart from *CGPerl* none of the other GOI showed a significant difference in expression levels, suggesting that they are expressed consistently throughout larval development. However, according to the results *CGPerl* becomes more important during the prodissoconch I shell formation in *C. gigas* larvae. Further analyses showed that *CGPerl* seems to play an important role in shell formation throughout the entire life cycle of *C. gigas* as it was significantly up-regulated in pediveliger compared to PII veliger at ambient conditions (20°C pH 8.1). Comparing *CGPerl* expression levels of pediveliger and PII veliger of treatment 1 and treatment 2, the results showed that at 24°C and pH 7.4 (treatment 1) no significant difference in gene expression levels was present, whereas at 20°C and pH 7.4 (treatment 2) *CGPerl* was up-regulated in pediveliger. This result could indicate that a decrease in seawater pH does not significantly affect gene expression of *CGPerl*, but shows that elevated temperature effects *CGPerl* expression levels. However, it should be considered that even if *CGPerl* was up-regulated by a mean factor of 1.969 in treatment 2, the relative expression level was lower compared to *CGPerl* expression levels of the control where *CGPerl* was up-regulated by a mean factor of 2.189. This result suggests that reduced pH lowers gene expression of *CGPerl,* eventually resulting in retarded larval shell growth.

According to the results, *CGCaM* seems to be involved in larval shell formation as expression levels in pediveliger increase by a mean factor of 1.306 compared to PII veliger in the control condition. Temperature appears to compensate for decreased pH as *CGCaM* is up-regulated by a mean factor of 3.017 in treatment 1, whereas in treatment 2 *CGCaM* is down-regulated by a mean factor of 0.628. The down-regulation of *CGCaM* in treatment 2 could possibly result in reduced calcium uptake and ultimately in a decrease of shell growth.

Even though the relative expression levels of *CGDent* increased by exposing the animals to decreased pH at ambient temperature (relative expression=1.219) and decreased pH at increased temperature (relative expression=3.019) compared to the control (relative expression=0.806), statistical analyses could not confirm a significant difference in gene expression of pediveliger compared to PII veliger. However, a statistical significant difference was confirmed for

pediveliger at 24°C and ambient pH where *CGDent* was down-regulated by a mean factor of 0.604 as a possible response to elevated temperature.
CGCM4 was significantly up-regulated at ambient conditions in pediveliger compared to PII veliger by a mean factor of 5.959, confirming a possible involvement in shell development. Both low pH and increased temperature*low pH enhanced *CGMG4* expression, with a relative expression of 12575.84 in treatment 2 and 33572.75 in treatment 1. Thus, it can be concluded that neither low pH as a single factor nor the interactive effects of low pH and elevated temperature negatively influences the expression of *CGMG4* in *C. gigas*. It is possible that these stressors positively affect gene expression, potentially as a means to compensate for reduced aragonite saturation states (Table 18, Section 3.3.2) to ensure shell development continues. Overall, the results show that different genes respond differently to environmental stressors as also shown in other studies. Zhang et al. (2012) tested the transcriptomic response of adult *C. gigas* to environmental stressors such as salinity, temperature exposure to air and heavy metals. Their results showed that 5844 genes were differentially expressed under at least one stressor and genes responding to different stressors showed significant overlap. The expansion of key defence genes and the complex transcriptomic response to stress highlight the sophisticated genomic adaptions of oysters to sessile life in a highly stressful intertidal environment. A recent study of Liu et al. (2012) showed that acidified and warm seawater induced significant down-regulation of four shell formation related genes, namely *aspein, calmodulin, nacrein* and *she-7-F10*, in adult pearl oysters. They also demonstrated that the synergistic effects of low seawater pH and elevated temperature caused up-regulation of the heat-shock protein *hsp70* in *P. fucata* in reaction to stress. The down-regulation of *calmodulin* in *P. fucata* is contrary to the results of this study where elevated temperature *low pH caused an up-regulation of *CGCaM* in *C. gigas* larvae. The differences in expression patterns of *CGCaM* could be explained by species-specific reactions to altering environmental stressors and the different developmental stages investigated. Furthermore, differences in experimental set-up have to be taken into account. Zippay and Hofmann (2010) investigated the effects of acidified seawater on the ability of red abalone larvae to tolerate thermal stress and how the expression of two genes involved in biomineralisation was influenced. They showed that low pH did not affect the expression patterns of *engrailed* and *ap24* at any time of larval development in *Haliotis rufescens*, but negatively influenced the thermal tolerance of some developmental stages.

Summing up, the effects of ocean acidification on the expression of biomineralisation-related genes seem to be species-specific and depended on developmental stage. As for example sea urchin larvae of the species *Lytechinus pictus* showed a significant decrease in expression of energy metabolism and skeletogenesis-related genes in response to ocean acidification, possibly

resulting in a reduction in skeleton formation (O'Donnell et al., 2010), whereas expression was changed in just two of seven genes investigated in sea urchin larvae of the species *Strongylocentrotus purpuratus* (Hammond and Hofmann, 2012). Generally, temperature seems to balance the effects of OA until a certain threshold is reached, specific for each species. Relating to gene expression in *C. gigas*, juveniles seem to be the most sensitive developmental stage compared to adult and larval stages with regards to the four GOI investigated. Counter-mechanisms such as the up-regulation of genes, for example *CGMG4*, seem to compensate for the effects of OA (Figure 29 & Table 21). Each gene appears to react differently to environmental stressors. In *C. gigas,* the expression of *CGCaM* was most affected by decreased pH throughout the entire development (Tables 20 & 21), but the negative effects are reduced at elevated temperature. *CGPerl* seems to play an important role in shell growth during the entire development. Significant up-regulation of *CGPerl* in PI and pediveliger veliger (Table 21) suggests an involvement in shell development from the onset of biomineralisation, confirmed by a continuous expression throughout the larval stages to post-metamorphosed animals.

To get a comprehensive picture of the effects of temperature and pH on shell development, shell microstructures and shell mineralogy throughout ontogeny, the results will be discussed in the following Chapter.

5- Impacts of changing environmental conditions on size, microstructures and crystal disorder of the developing shell of *Crassostrea gigas*

"The shape of a crystal reflects the nature of the environment in which it grows"
Weiner and Dove (2003)

5.1 Introduction

Calcium carbonates are the most abundant biogenic minerals, both in terms of quantities produced and their widespread distribution among many different taxa (Lowenstam and Weiner, 1989). Of the three known polymorphs of $CaCO_3$ to be found in the Pacific oyster, two are crystalline, calcite and aragonite, and one is amorphous, ACC. It has been observed that ACC plays an important function as a precursor phase for aragonite in larval shells, subsequently becoming more crystalline and transforming into aragonite as the larval shell matures (Lee et al., 2006a; Weiss et al., 2002). The onset of shell mineralisation in bivalve molluscs occurs during the trochophora stage (Figure 2, Section 1.2), eventually transforming into the prodissoconch I shell and enlarges during development into the prodissoconch II shell (Lee et al., 2006a; Weiss et al., 2002). Recent work of Weiss et al. (2002) identified three different larval shell layers for *C. gigas* including an inner prismatic layer, overlain by a homogenous layer with globular structures and an irregular distributed outer prismatic layer adjacent to the periostracum. As the shell matures it transforms after metamorphosis into the so-called dissoconch (Figure 2) and is in *C. gigas*, mostly calcitic (see Section 1.3.2.1). In adult oyster shells four distinct microstructures have been described so far (Bøggild, 1930; Carriker et al., 1980; Higuera-Ruiz and Elorza, 2009; MacDonald et al., 2010). The calcitic prismatic layer, adjacent to the periostracum, the inner lamellar or foliated layer consisting of calcitic elongated laths, porous calcitic lenses embedded randomly into the foliated layer and lastly the myostracum, aragonitic needle-like prisms (see Section 1.3.2.1).

Among bivalve molluscs adult oysters produce one of the thickest shells, which provides vital protection against predation, desiccation and wave action. Due to their mineralogy, larval shells of oysters are more vulnerable to OA compared to juveniles and adults as aragonite is known to be more soluble than the calcite (Feely, 2004; Mucci, 1983). Ocean warming, acidification, decreased carbonate saturation and their interactive effects are likely to impair skeletogenesis of marine calcifiers (see Table 2, Section 1.4), resulting in for example shell malformations (Parker and Ross, 2009; Talmage and Gobler, 2010; Watson et al., 2009), retarded shell growth (Watson et al., 2009), increased dissolution of the shells (Gaylord et al., 2011; Talmage and Gobler, 2010), decreased mechanical properties of the shells (Chan et al., 2012; Dickinson et al., 2012) and unshelled veliger (Byrne, 2011).

This chapter will focus on the shell development and the corresponding mineralogical changes that characterise the life cycle of *C. gigas,* and how this could be affected by varying environmental conditions.

5.2 Material and Methods

To get a comprehensive picture of the differences in shell size and microstructures during ontogeny, and to investigate the impacts of elevated temperature and low pH and their synergistic effects on larval shell development scanning electron microscopy analyses were performed. The mineralogical changes during shell development and the effects of environmental changes on larval shell growth were studied using Fourier Transform Infrared spectroscopy.

5.2.1 SEM & FTIR sample preparation

To give an overview on the different shell microstructures and their differences in mineralogy in adult and juvenile shells, random shell samples were prepared and processed for SEM and FTIR studies as explained in Sections 2.3.1 and 2.3.2.
Shell samples of larvae, produced as described in Section 2.1.2, were prepared for SEM analyses as explained in Section 2.3.1.1. To get an idea of the shell morphology of the two main larval shell types Prodissoconch I and Prodissoconch II, grown at ambient conditions, shell eidonomy and anatomy were compared. Furthermore, shell morphology of larvae reared in the experimental system was compared to investigate the impacts of environmental changes.
For FTIR analyses, samples of larvae were prepared as described in Section 2.3.2.1 and analysed using the program RStudio 2009-2012 (Version 0.97-312, Boston, MA, USA, http://www.rstudio.org/).

5.3 Results

5.3.1 Adult and juvenile shells

5.3.1.1 Shell morphology

Shell microstructures in oysters are already well described in the existing literature (Bøggild, 1930; Checa et al., 2007; Higuera-Ruiz and Elorza, 2009; Lee et al., 2011; MacDonald et al., 2010) and with regards to *C. gigas* shell microstructures have been described in Section 1.3.2.1. However, to complete the picture of shell morphology in *C. gigas* for the present study, the different microstructures are presented below in plates.

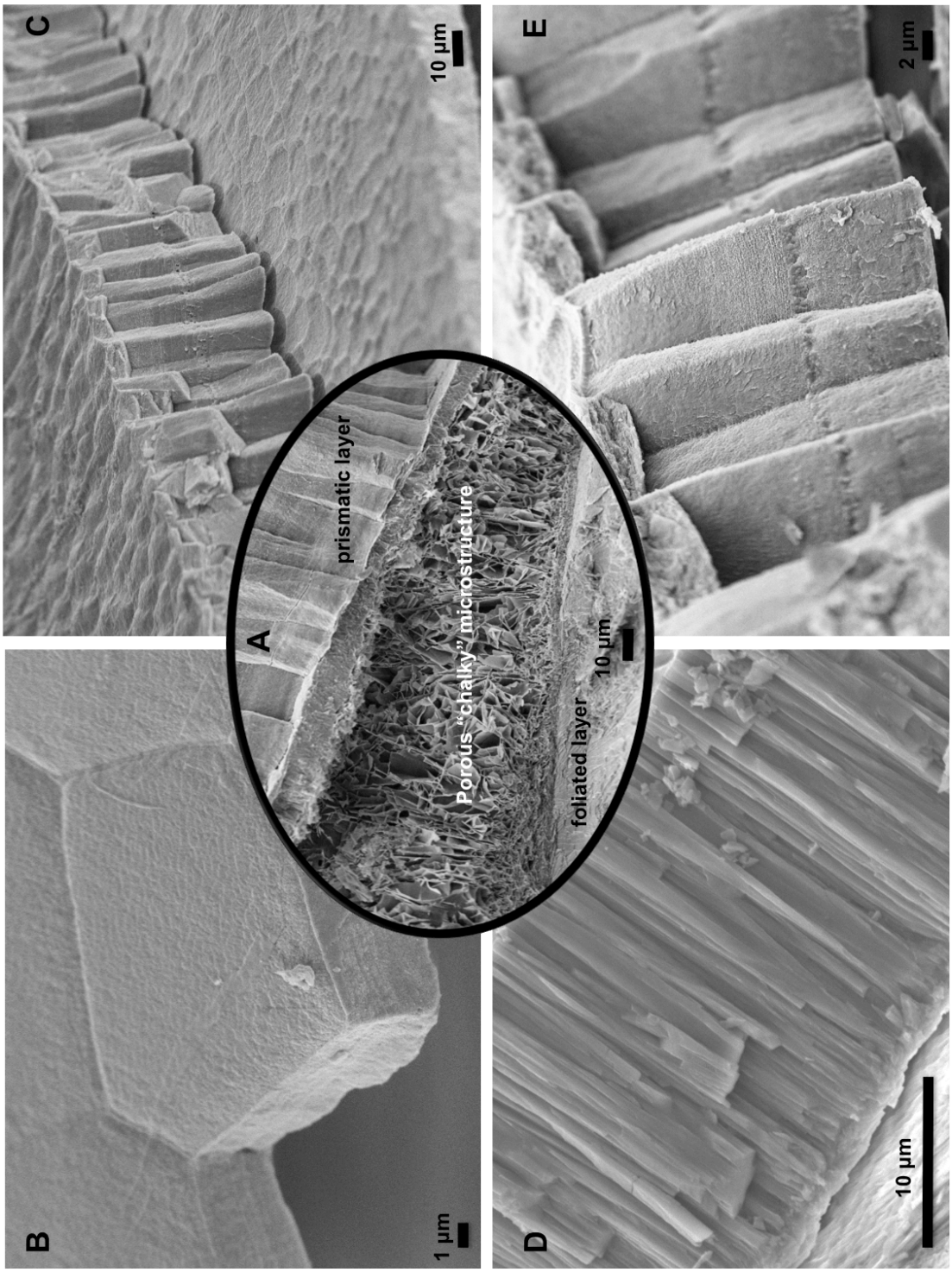

Figure 30: SEM images of shell microstructures in juvenile (A, B,C, E) and adult (D) *C. gigas*. A: Longitudinal fraction showing three microstructures; B: Surface of the calcitic prismatic layer; C: Prismatic layer; D: Aragonitic myostracum; E: Prisms. Scale bars as indicated.

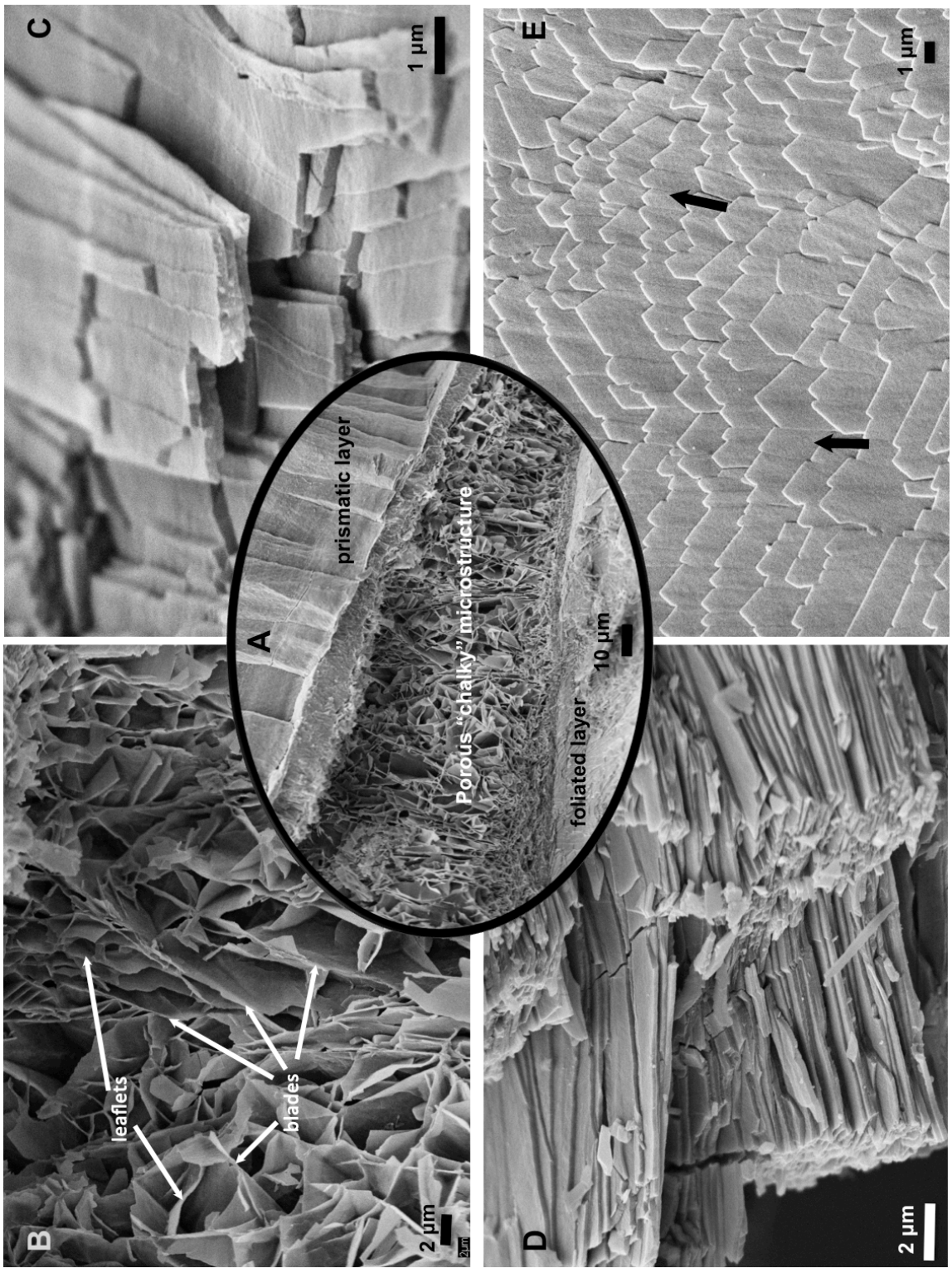

Figure 31: SEM images of shell microstructures in juvenile *C. gigas*. A: Longitudinal fraction showing three microstructures; B: Porous "chalky" microstructure (calcitic) consisting of blades and leaflets; C: Surface of the foliated layer showing elongated calcitic laths; D: Lateral view of the foliated layer; E: Surface of foliated layer showing the endings of the laths; arrows indicate growth directions. Scale bars as indicated.

5.3.1.2 Shell mineralogy

Mineralogy of the four principal microstructures in shells of juvenile and adult *C. gigas*, consisting predominantly of calcite with a minor area of aragonite, have been confirmed by the obtained IR spectra (see Table 31 in Section 7.3.1 and Appendix DVD), presented in the following.

The most abundant microstructure in spat and adult *C. gigas*, the foliated layer, showed distinct peaks at 1421 cm^{-1} (ν_3), 877 cm^{-1} (ν_2) and 713 cm^{-1} (ν_4), all characteristic for calcite (Figure 32 a). Samples of the prismatic layer from both spat and adult shells displayed very similar peak positions to the foliated layer but were not as well defined (Figure 32 b). The measured peak positions were 1421 cm^{-1}, 876 cm^{-1} and 713 cm^{-1}, confirming the calcitic nature of the prisms. The mineral composition of the myostracum differed in terms of peak positions as the peaks were at 1472 cm^{-1}, 1083 cm^{-1}, 858 cm^{-1}, 713 cm^{-1} and 700 cm^{-1}, all characteristic for aragonite (Figure 32 c). The final microstructure, the "chalky" lenses were composed of calcite with the carbonate peaks ν_3 at 1418 cm^{-1}, ν_2 at 878 cm^{-1} and ν_4 at 713 cm^{-1} (Figure 32 d).

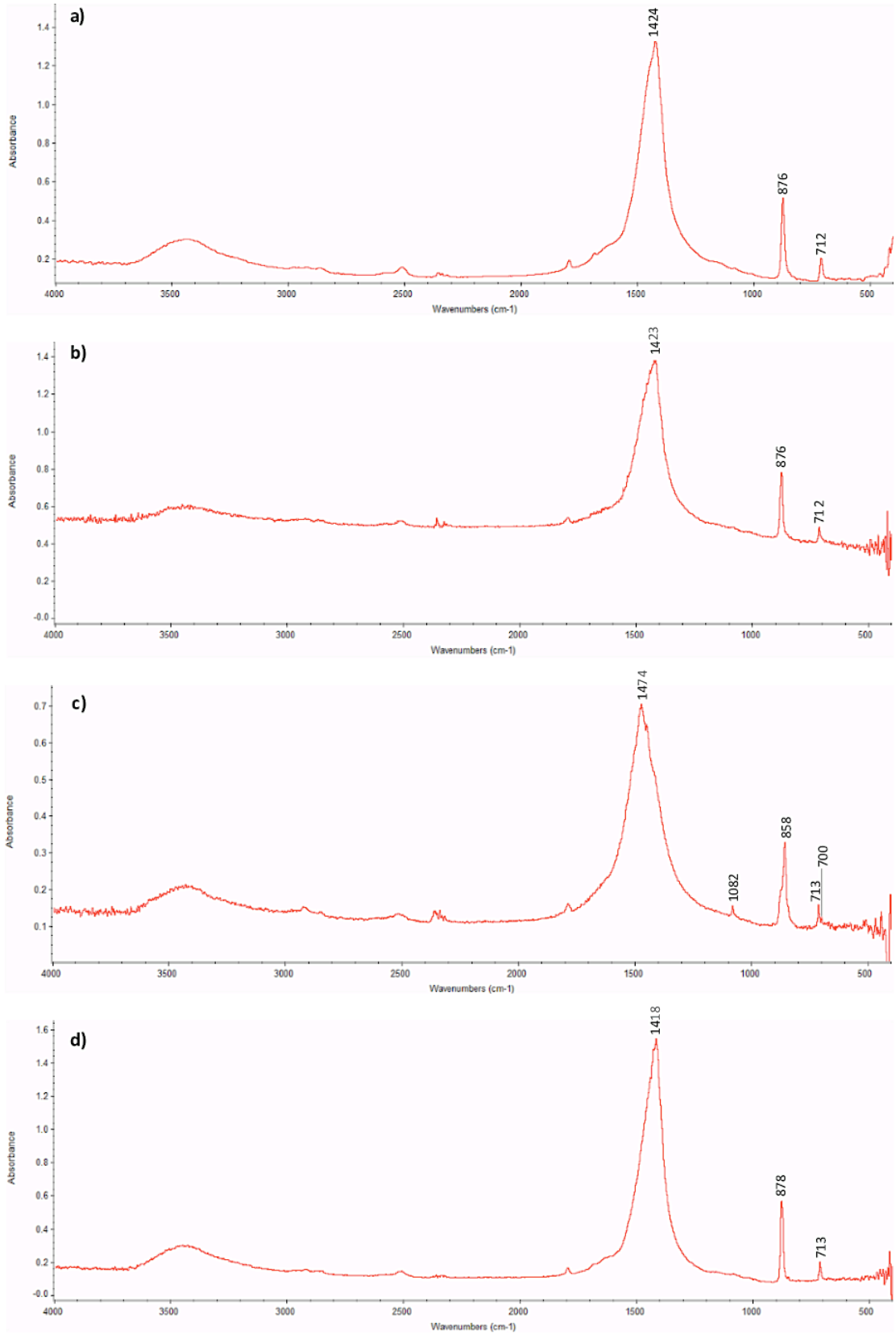

Figure 32: FTIR spectra of the four mineralised microstructures of adult (a, b, d) and juvenile (c) *C. gigas* shells. Peak positions are indicated. a) Foliated layer, right valve, calcite (sample A27-Rb1); b) Prismatic layer, left valve, calcite (sample A1-Ld2); c) Myostracum, right valve, aragonite (sample J2-R1); d) Chalky microstructure, left valve, calcite (sample A1-La). Courtesy of S. Long

5.3.2 The impacts of pH and temperature on development, morphology and crystal disorder of larval shells

Larval development was monitored throughout the experiment. It was shown that a temperature of 24°C and ambient pH the first trochophora developed at 12 hours after fertilisation (a. f.) (Figure 2). Eight hours later (20 h a. f.) the first D-veliger, referred to as PI-veliger, were monitored which eventually developed into PII veliger 48 hours after fertilisation. Four days after fertilisation the shells developed an umbo, hence called umboned veliger. The first eyed pediveliger developed 16 days after fertilisation. Three days later, the first pediveliger began to search for appropriate substrate to settle down and to transform into spat.

Within the framework of this study it was shown that low pH, elevated temperature and the synergistic effects of low pH*elevated temperature had a significant negative effects on larval shell development and crystal disorder of the shells.

5.3.2.1 Shell morphology

Morphology of PI and PII shells

As shown in Figure 33 a, the outer shell surface of a 24-h old Prodissoconch I shells appeared overall very smooth, but towards the centre lightly dented. The average shell perimeter for PI shells was 2502 µm ± 373.2 µm. Lateral shell fractures of the proximal part of the shell revealed poorly defined prisms, arranged perpendicular to the shell surface (Figure 33 A). Towards the distal part/shell margin globular structures were detected and the prismatic layer became less defined. Average thickness of proximal prismatic layer was 0.5 µm ± 0.1 µm, with decreasing shell thickness towards the shell edge.
As the shell matured a sharply defined transition between PI and PII shell could be identified. After five days (6 d a. f.) the prodissoconch II has enlarged to 5522.3 µm ± 1015 µm in perimeter and the outer shell surface was characterised by growth rings (Figure 33 b). Shell thickness was very variable, thinnest in the proximal (older) part of the shell (2.7 µm ± 0.3 µm) and greatest towards the outer shell edge (4.3 µm ± 0.7 µm). However, shell thickness again decreased at the shell margin (0.9 µm ± 0.04 µm). Shell microstructures were clearly defined in the proximal part of the shell, consisting of an outer and an inner prismatic layer with a granular layer sandwiched in-between (Figure 33 B). Towards the shell edge the microstructures became less defined and neither an outer nor an inner prismatic layer was detected and were instead replaced by a granular microstructure.

Environmental impacts on shells of PII veliger and pediveliger

For results on shell growth including shell length, shell width and shell perimeter in PII veliger and pediveliger please refer to Chapter 3, Section 3.3.2, Table 19.

PII veliger

The shell surface of six days old PII veliger in low pH treatments was clearly affected by pH (Figure 34 A & B) compared to PII shells in ambient pH (Figure 34 C & D). In both low pH treatments the shell surface appeared patchy, indicating a partly dissolved periostracum. Shell deposition of the PII shell was no longer smooth, but appeared pitted and deformed compared to the control. However, shell growth in the low pH treatments was greater at 24°C compared to shells reared at 20°C (see Section 3.3.2).

Shell surface of shells reared at ambient conditions were smooth, with no signs of dissolution and increased malformations and shell size were greatest at elevated temperature (Figure 34 C & D and Section 3.3.2).

Pediveliger

The shell surfaces of 19 days old pediveliger at low pH treatments (Figure 34 E & F) were severely affected compared to shells at ambient pH (Figure 34 G & H). Shells at 24°C pH 7.4 (Figure 34 E) were mostly affected showing frayed valve edges (PII), a rough shell surface particularly in the area of PI due to proceeding shell dissolution and increased shell malformations. The shells of larvae at ambient temperature and pH 7.4 (Figure 34 F) displayed also a rough shell surface of PI shell but the effects of dissolution were less pronounced compared to shells at elevated temperature. Also no distinct damages of the PII shell were observed at ambient temperature*low pH.

Pediveliger shells reared at ambient pH were normally developed with no signs of dissolution and increased malformations. At both temperatures, 20°C and 24°C, pediveliger had already developed an umbo, contrary to pediveliger in low pH treatments (Figure 34 G & H). Again, shell size was greatest at elevated temperature (see Section 3.3.2

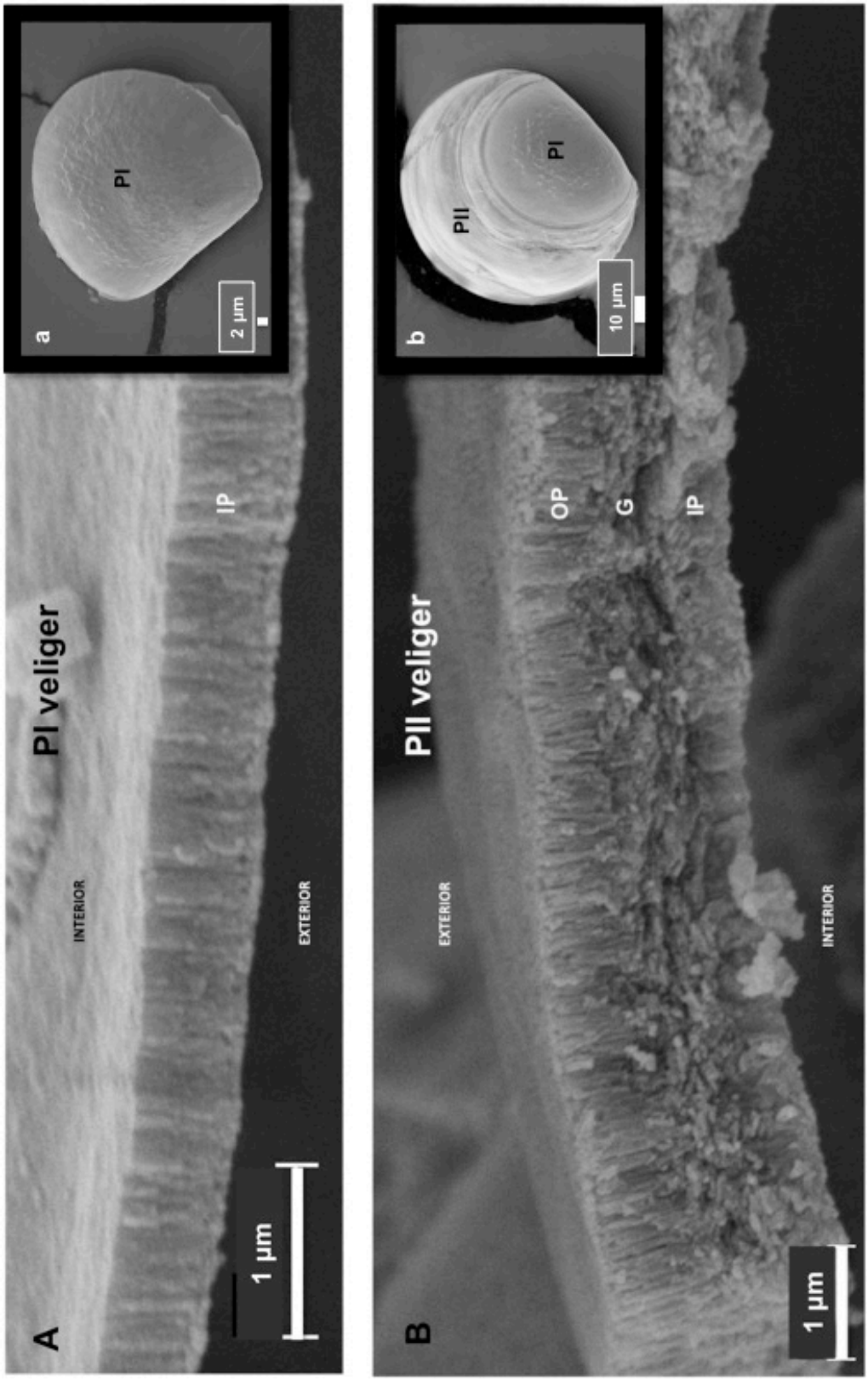

Figure 33: SEM images comparing microstructures in 24 hours old PI shells (A, a) and 6 days old PII (B, b) shells. A & B are lateral fractures of the proximal shell, where the periostracum was removed during the process of tissue dissolution. OP: Outer prismatic layer; G: Granular layer; IP: Inner prismatic layer. PI: Prodissoconch I, PII: Prodissoconch II. Scale bars as indicated.

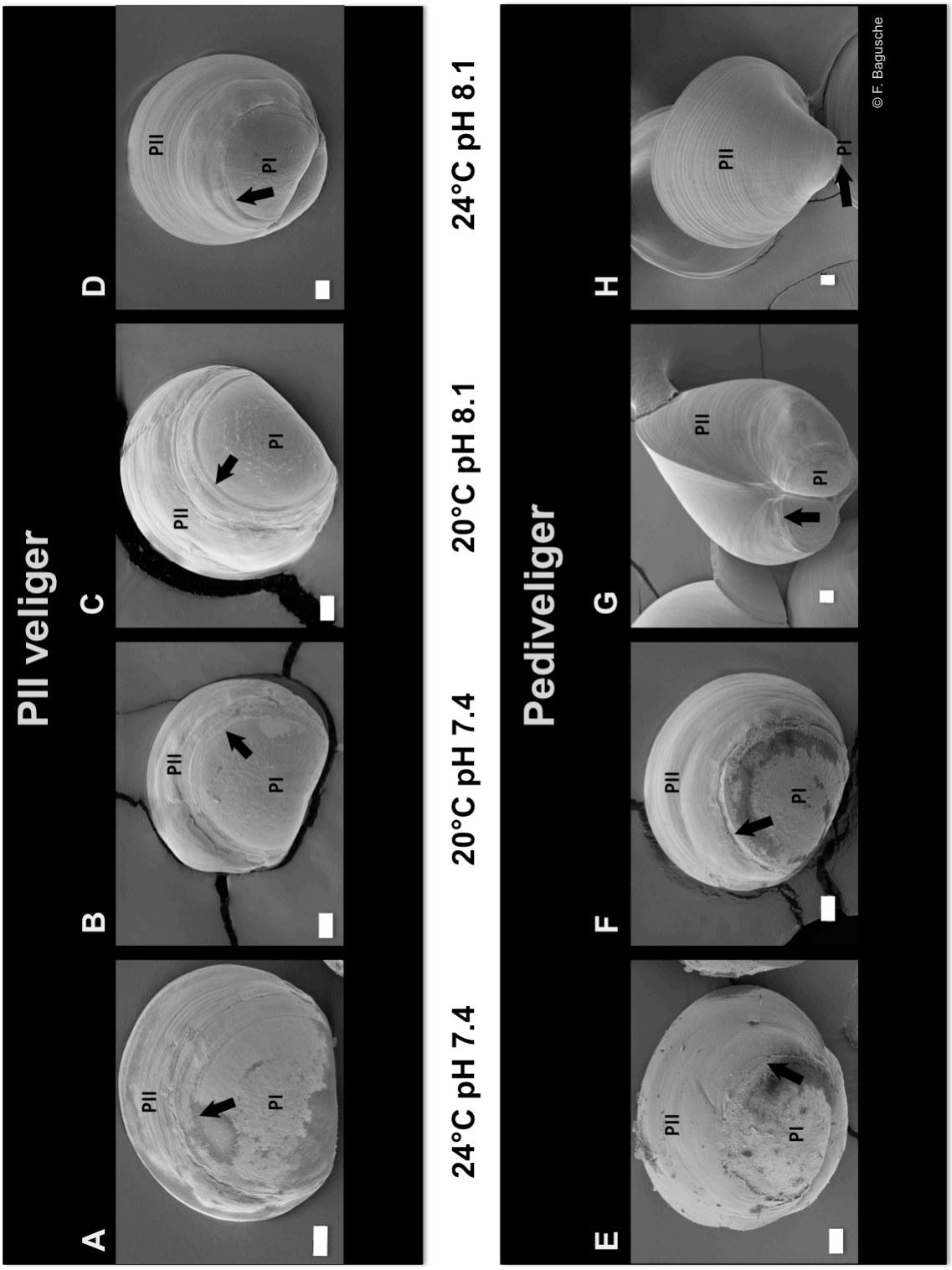

Figure 34: Comparison of larval *C. gigas* shells reared in different conditions. A-D: SEM images of 6 days old PII veliger. E-H: SEM images of 19 days old pediveliger. G & H: Pediveliger with developed umboned shells. Arrows mark transitions between PI and PII shells. PI: Prodissoconch I, PII: Prodissoconch II. Scale bars in all images: 10 µm.

5.3.2.2 Shell mineralogy

Effects of grinding

Through sequential grinding of the same sample the confounding effects of crystal size and crystal order were separated.

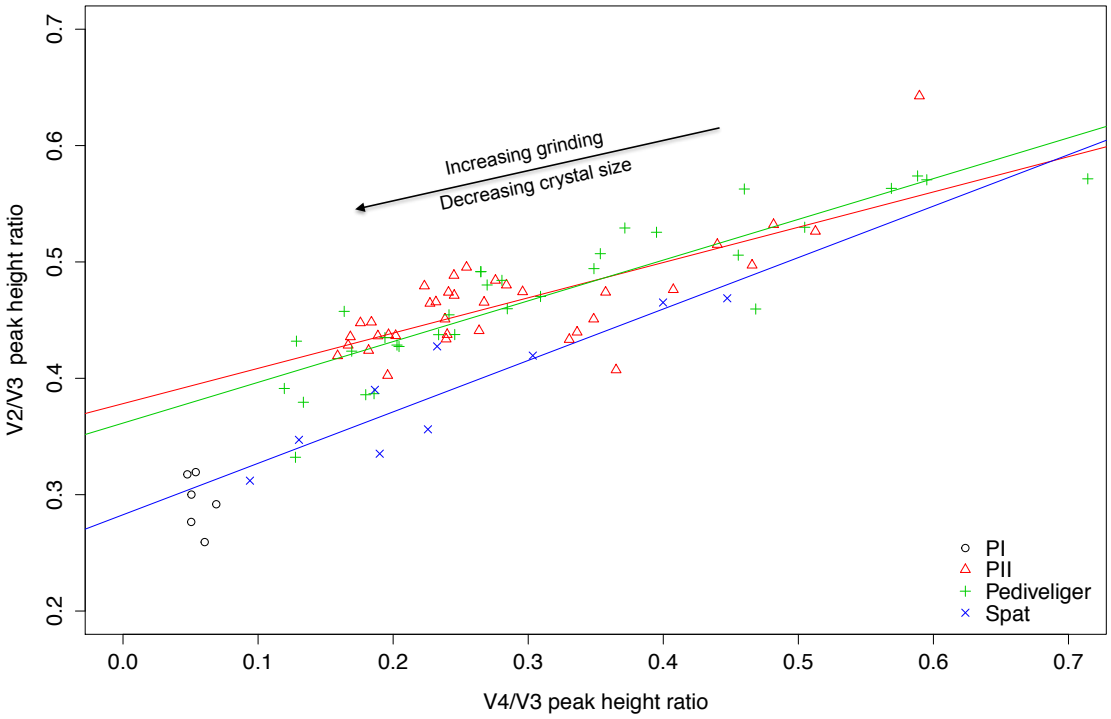

Figure 35: Plot of the ν_2 versus ν_4 peak heights of Prodissoconch I (PI), Prodissoconch II (PII), pediveliger and spat samples after each spectrum was normalised to the corresponding ν_3 peak height. With increasing grinding the relative ν_2 and ν_4 peak height decreased, as indicated by trend lines.

A consistent trend emerged between all developmental stages regardless of the temperature and pH conditions. IR peaks sharpened as samples were subjected to more grinding, yielding both higher intensities and smaller FWHM values (Table 32 in Section 7.3.2 and Appendix DVD). As the crystal size was reduced with grinding, peak heights of ν_2 and ν_4 varied, whereas peak height of ν_3 remained more or less constant. As a consequence, this was affecting the peak height ratios of $\nu_2/\ \nu_3$ and $\nu_4/\ \nu_3$.Through all experimental conditions, the $\nu_4/\ \nu_3$ peak height ratio decreased more rapidly than the $\nu_2/\ \nu_3$ ratio. This trend was constant through PII veliger, pediveliger and spat (Figure 35). Values for PI veliger did not show this well-defined trend, questioning the reliability of this dataset as very few samples were analysed (see Table 32 in Section 7.3.2 and spectra on Appendix DVD). Although the slopes of the PII veliger and pediveliger trend lines are fairly similar, a separation between the trend lines is evident showing

that the slope of pediveliger is lower indicating a higher atomic order (Regev et al., 2010) compared to PII veliger. Spat samples correspond to the shallowest slope and therefore the highest atomic order (Table 32 Section 7.3.2 and Appendix DVD).

Mineral composition during development

A clear mineral transformation can be seen through larval development of *C. gigas* by migration of the ν_3 peak (Figure 37 A-D; Table 32 Section 7.3.2). However, spectra obtained at the trochophora stage did not possess any peaks corresponding to carbonates. It was therefore assumed that no $CaCO_3$ was present in larval shells younger than 16 hours after fertilisation (Appendix DVD) or at least not enough to be detected. Shells of 24 hours old PI veliger showed peaks characteristic for ACC, represented by the doublet of the ν_3 peak at 1473 cm^{-1} and 1450 cm^{-1}. Yet an additional doublet of the ν_4 peak pointed towards the presence of aragonite, as ACC does not have distinct peaks in this lattice frequency region (Figure 36). These observations were consistent with PI larval shells containing in addition to ACC, a less crystalline aragonite phase (Figure 37 A; Table 32 Section 7.3.2). Subsequently, the ACC transformed into aragonite post 24 hours after fertilisation within the PI veliger stage itself. Once the PII veliger stage was reached the shell was composed entirely of aragonite (Figure 37 B). This mineral phase matured into the pediveliger, where consistently well-defined aragonite peaks were visible at 1474 cm^{-1} and 860 cm^{-1} (Figure 37 C; Table 32 Section 7.3.2). Out of all samples, the PI shells contained the highest ν_2/ ν_4 ratio values, with an average of 5.4, suggesting a highly disordered aragonite compared to average value of 2 in pediveliger (Table 32 Section 7.3.2).

After the larvae transformed into spat, the shells were predominantly made of calcite, indicated by transition of the ν_3 peak to 1418 $cm^{-1}$and ν_2 peak to 877 cm^{-1} (Figure 37 D). However, a few samples remained aragonitic due to the early sampling time post metamorphosis (Table 32 Section 7.3.2 and Appendix DVD).

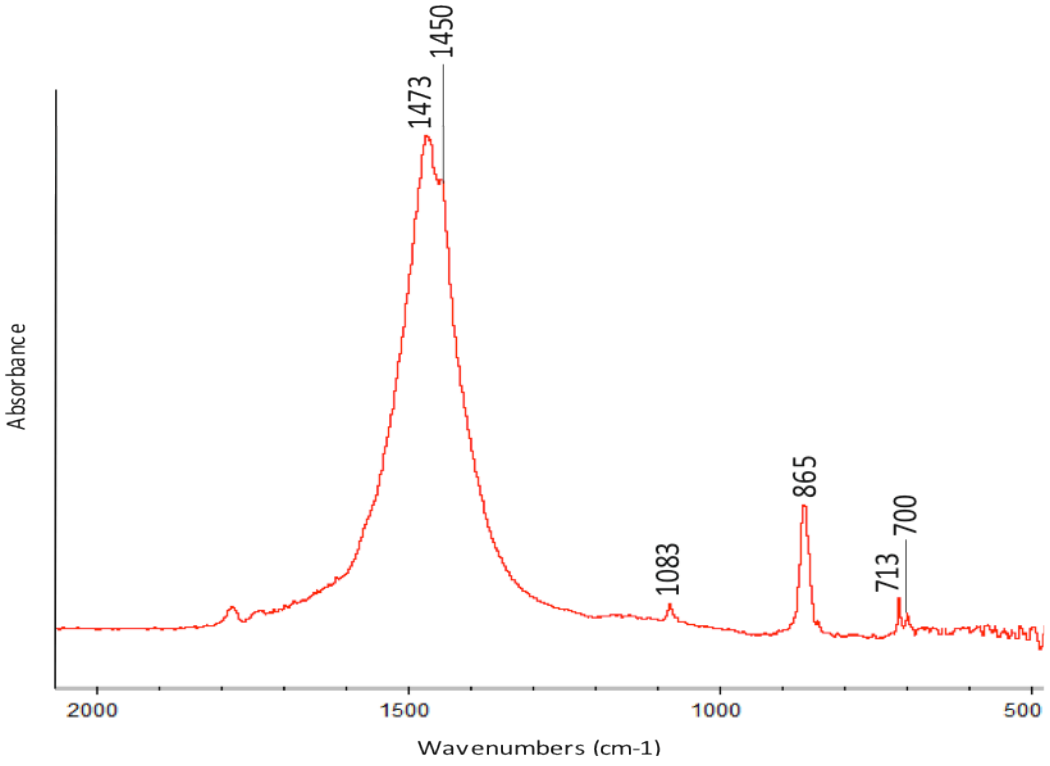

Figure 36: Spectrum of a PI shell (Spectrum Bb-2E.1, Appendix DVD) showing peaks of aragonite and a doublet of the v_3 peak, characteristic of ACC

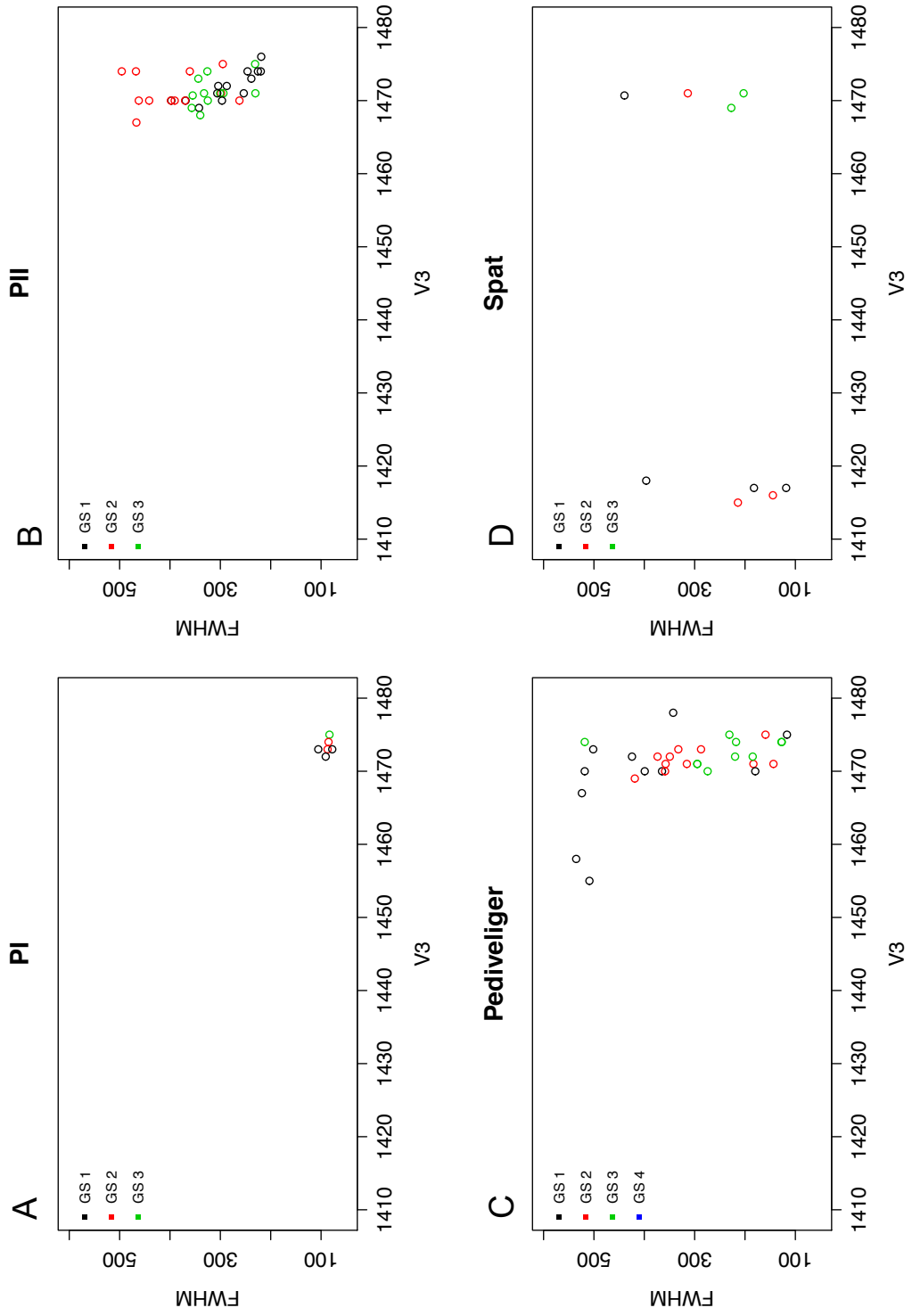

Figure 37: Shift of the ν_3 peak position (cm^{-1}) during development from PI veliger (A) to PII veliger (B) to pediveliger (C) to spat (D) indicating the change in $CaCO_3$ precipitation during a larval cycle. With each grinding stage (GS) the FWHM decreases.

Impacts of temperature and pH and their interactive effects on mineral order

Changing environmental conditions, regardless of the combination of pH and temperature, did not effect $CaCO_3$ polymorph precipitation from ACC to aragonite in larval shells to calcite in spat. At both low (7.4) and ambient (8.1) pH, and high (24°C) and ambient (20°C) temperatures, there was only very minor variability observed between the position of the carbonate IR spectra peaks, reflecting differences in grinding only (Figure 37; Table 32 in Section 7.3.2 and Appendix DVD).

However, mineral order of the shells was affected by changes in pH and temperature as shown by increased $\nu_2/\ \nu_4$ ratios and decreased FWHM values (Figures 38 and 39).
When evaluating the effects of pH and temperature as single stressors it can be seen that at pH 7.4 in both PII veliger (Figure 38 A) and pediveliger (Figure 38 C) an elevated state of mineral disorder was present compared to shells reared at pH of 8.1. With repetitive grinding a rising disorder was shown at 24°C in both PII veliger (Figure 38 B) and pediveliger (Figure 38 D). However, both elevated temperature and decreased pH had greater negative effect on pediveliger compared to PII veliger with higher $\nu_2/\ \nu_4$ ratios and lower FWHM values both are indicative for increasing disorder.

By investigating the interactive effects of pH and temperature it was shown that elevated temperature*low pH had the greatest negative effect compared to the control, reflected in increased $\nu_2/\ \nu_4$ ratios and decreased FWHM values (Figure 39). The synergistic effects of 24°C and pH 7.4 were most pronounced in pediveliger (Figure 39 B) compared to PII veliger (Figure 39 A). Contrary, the highest FWHM values and lowest $\nu_2/\ \nu_4$ ratios were seen in the control and at 24°C pH 8.1 in both PII veliger and pediveliger, suggesting a higher mineral order compared to the low pH treatments.

Summing up elevated temperature and low pH as single stressors as well as their interactive effects negatively influenced mineral order in both PII veliger and pediveliger, with a greater negative effect on mineral order in pediveliger.

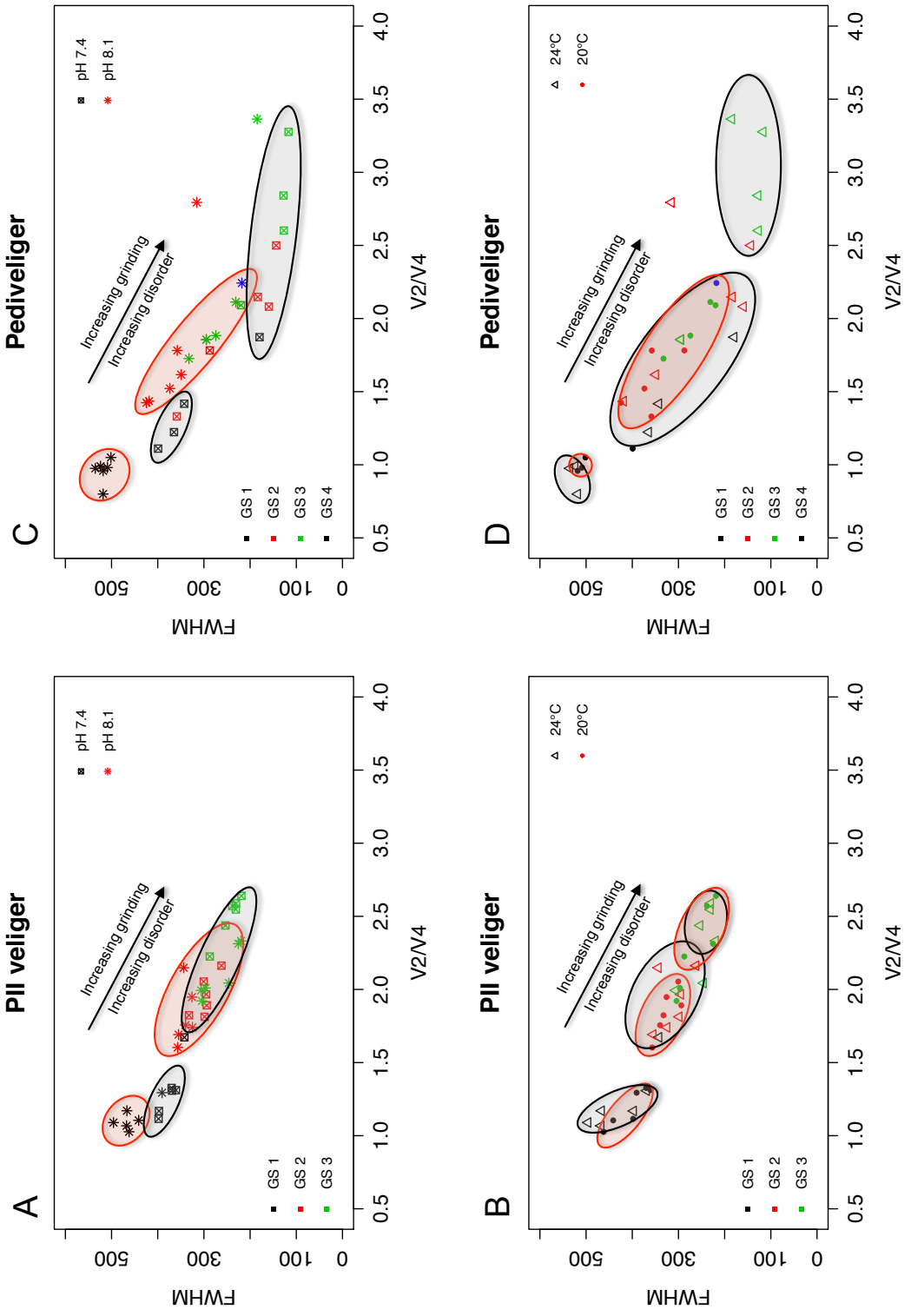

Figure 38: Comparison of the variation in the v_2/v_4 ratios in PII veliger (A, B) and pediveliger (C, D) both in different pH (A, C) and temperature (B, D) treatments. With repetitive grinding crystal size was reduced and crystal disorder increased indicated by decreased FWHM values and increased v_2/v_4 ratios. Each grinding stage (GS) is highlighted by a different colour. To highlight differences in disorder between the treatments, clusters of both pH 7.4 and 24°C are circled in black and clusters of both pH 8.1 and 20°C are circled in red.

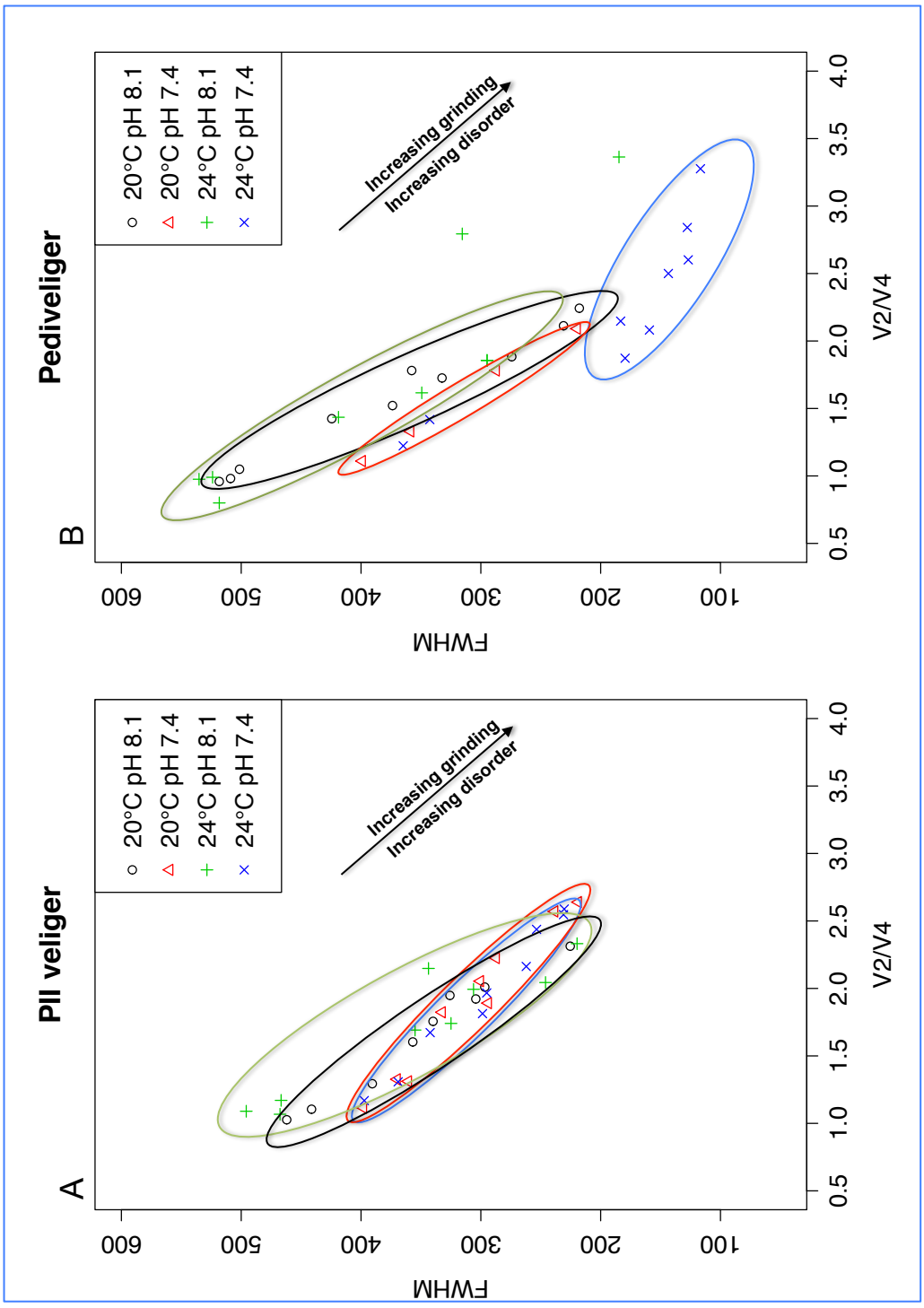

Figure 39: Comparison of the variation in the v_2/v_4 ratios in PII veliger (A) and pediveliger (B) between the control (20°C pH 8.1) and the three treatments (20°C pH 7.4, 24°C pH 8.1 and 24°C pH 7.4). With repetitive grinding crystal size was reduced and crystal disorder increased indicated by decreased FWHM values and increased v_2/v_4 ratios. To highlight differences in crystal disorder between the four conditions, the main clusters are encircled corresponding to the colour scheme of the conditions.

5.4 Discussion

Shell mineralogy and morphology during development

Of the known biominerals, carbonate polymorphs are the most abundant and are widely precipitated during calcification processes among many taxa. It is well known that in *C. gigas* precipitation of calcium carbonates is characterised by a switch in carbonate polymorphs during shell development, ranging from ACC to aragonite to calcite.
According to Lee et al. (2006a), shell development in *C. gigas* starts in the trochophora stage where organic tissue was detected, suggesting the presence of an organic matrix. From the middle trochophora stage to the early veliger stage X-ray diffraction (XRD) patterns exhibited that the fraction of organic tissue decreased exponentially during maturation while the percent of aragonite detected increased, eventually forming the prodissoconch I. Throughout the entire veliger stage the PII shells were predominantly composed of aragonite with traces of calcite. During the pediveliger stage the fraction of calcite slightly increased (< 1%), followed by a rapid increase (81%) after metamorphosis forming the early dissoconch. In *Ostrea edulis*, the European flat oyster, XRD detected organic tissue in the first gastrula stage, pointing towards the development of the periostracum and an organic matrix (Medaković et al., 1997). The beginning of shell formation in *Ostrea edulis* was indicated by the appearance of calcite (up 1-4 % of the total volume) followed by aragonite (2-7%) in the early veliger stage (PI shell). With maturation the part of calcite decreased as well as the organic fraction, replaced by a rapid increase of aragonite. In the PII shell, aragonite was dominant, with very small organic fractions and traces of calcite. After metamorphosis the amount of aragonite decreased, correlated to a rapid increase of calcite (Medaković et al., 1997). However, as with XRD is not possible to detect amorphous calcium carbonates, neither Lee et al. (2006a) nor Medaković et al. (1997) were able to pinpoint the initial deposition of calcium carbonate polymorphs in oysters.

Of various groups of calcifiers investigated there is evidence that crustaceans (Addadi et al., 2003; Roer and Dillaman, 1984), echinoids (Beniash et al., 1997; Politi, 2004) and molluscs (Hasse et al., 2000; Weiner et al., 2003; Weiss et al., 2002) utilise ACC as a precursor phase in skeletogenesis. However, it should be emphasised that there still is significant uncertainty over the extent to which marine calcifiers produce ACC as a precursor to their crystalline end-products (Ries, 2011). Using FTIR and RAMAN spectroscopy Weiss and co-authors (2002) showed that ACC was deposited as a precursor of aragonite in both *C. gigas* and *M. mercendaria* larvae. In both species ACC was present in the PI shell along with a poorly crystalline aragonite. The results of Weiss et al. (2002) are in agreement with the results of the present study, where carbonate mineralisation was first detected in PI shells. The results suggest

that either ACC in combination with a poorly crystalline aragonite is deposited first or that ACC subsequently transforms into a poorly crystalline aragonite. The transition between ACC to aragonite can be narrowed within the PI veliger stage itself, as spectra of six days old PII veliger are characteristically aragonitic. In contrast, Weiss et al. (2002) detected ACC in nine days old *C. gigas* PII veliger, suggesting variations in mineral deposition within the same species. It has to be taken into account that no information regarding the environmental conditions in which the larvae were reared was given. As it is well established that growth is influenced by nutrient supply and temperature, conclusions about timescales of mineral deposition must be drawn with caution.

Within the resolution of the present study, no calcite was detected during the larval stages, which does not agree with the results of Lee et al. (2006a), but supports the findings of Weiss et al. (2002). One possible explanation of this non-conformity regarding traces of calcite could be the different methods applied. Another possible explanation may be the limited amount of sample in the present study, which made it difficult to map mineral composition thoroughly during development. The results of the present study show that early post-metamorphosed shells exhibited both, calcite and aragonite, which is in agreement with the study of Lee et al. (2006a). FTIR analyses of juvenile and adult shells showed that the matured shells are composed almost entirely of calcite, which is already well established in the literature (Beniash et al., 2010).

Using scanning electron microscopy shell microstructures characteristic for the main shell types, prodissoconch I, prodissoconch II and dissoconch were identified. In agreement with Weiss et al. (2002), larval PI shells were composed of poorly defined prisms arranged perpendicular to the shell surface (Figure 33 A). The prismatic structure became less evident towards the distal part of the shells and was replaced by a globular structure. Weiss et al. (2002) suggested that the microstructures close to the shell edge are composed entirely of ACC as well as the poorly developed prismatic structures. As the shells matured a sharply defined transition between PI and PII shell could be identified. Microstructures in the PII shells were more developed compared to microstructures of the PI shells. Three distinct layers could be identified, a well-defined inner prismatic and an outer prismatic layer with the granular layer sandwiched in-between (Figure 33 B). Based on observations in *M. mercendaria* and *C. gigas* larvae, Weiss et al. (2002) suggested that the inner prismatic layer is initially formed by ACC, while in mature PII shells the granular layer at the shell edge is formed by deposited aragonite.

As already mentioned, the dissoconch of mature juveniles and adult *C. gigas* is composed mainly of calcite and can be differentiated into four distinct microstructures, namely the calcitic prismatic layer, the calcitic lamellar or foliated layer, lenses of a chalky appearance composed of calcite and finally the aragonitic myostracal prisms. No novelties were found regarding

microstructures in post-metamorphosed shells and the results presented in this study are in full agreement with the existing literature (Bøggild, 1930; Higuera-Ruiz and Elorza, 2009; Kobayashi and Samata, 2006; MacDonald et al., 2010).

Effects of pH and temperature on shell structure and mineral disorder

Although progress has been made investigating the effects of CO_2- induced OA on calcification rates of marine calcifying organisms, substantial uncertainties remain regarding impacts on shell/skeletal polymorph mineralogy. Few recent studies have made pioneering observations on crystallography of calcified structures produced at future ocean scenarios (Beniash et al., 2010; Chan et al., 2012; Cohen et al., 2009; Dickinson et al., 2012; Ries, 2011). According to these studies, OA impairs calcification rates, microstructures and crystallographic textures and limits the skeletal strength, which ultimately could reduce the survival rates of these calcifying organisms. Chan et al. (2012) investigated the effects of OA on juvenile serpulid tubeworms. Their results suggested that OA altered $CaCO_3$ precipitation in response to decreasing Ω_A. When Ω_A was below or close to 1, juvenile *Hydroides elegans* had a significantly higher proportion of calcite compared to tubeworms at ambient condition where the tube was primarily made of aragonite. Chan et al. (2012) proposed that the replacement of aragonite with calcite could be interpreted as a consequence of increased dissolution of the more soluble aragonite as well as the higher energetic costs of aragonite production. Additionally an interesting observation was made, showing that the content of ACC in the tubes increased by up to 30% at near or below aragonite saturation. As ACC is known as a precursor for both aragonite and calcite, Chan et al. (2012) suggested that the increase of ACC could be an attempt to elevate production of crystalline products. However, the results of the present study did not indicate an increase in ACC, pointing towards a species-specific reaction to OA. Furthermore, Chan et al. (2012) also found that the mechanical properties of the tubes were significantly affected when exposed to pH 7.4, resulting in reduced hardness (62%) and elasticity (72%). They assumed that the reduced mechanical properties could be either a result of the impaired microstructures of the tubes or the decreased aragonite content. Aragonite is known to be harder than calcite due to its higher packing density of calcium and carbonate ions (Weiner & Addadi, 1997), which results in higher mechanical properties of the skeletal structures.

Though OA, ocean warming and their interactive effects did not change $CaCO_3$ polymorph precipitation in *C. gigas* in the present study (Figure 37), a negative influence on shell structure and crystal disorder was observed. It was shown that mineral order in larval shells was affected by changes in pH and temperature resulting in increased ν_2/ν_4 peak height ratios and decreased

FWHM values. Both decreased pH and elevated temperature and the combined effects of low pH*elevated temperature had a negative effect on PII veliger (Figure 38 A & B, Figure 39 A) and pediveliger (Figure 38 C & D, Figure 39 B), resulting in increased crystal disorder with a greater effect on pediveliger shells. It can be assumed that an increase of crystal disorder under future ocean scenarios may lead to increased solubility (Asscher et al., 2011) of larval shells with greater impacts on late developmental stages. It is likely that shells with increased disorder are more vulnerable to dissolution through aragonite saturation states below 1 in OA scenarios. This assumption is supported by the SEM results, showing that both low pH and the interactive effects of high temperature*low pH had a negative impact on shell structures compared to the control (Figure 34). Again, the shells of pediveliger larvae were more strongly affected compared to shells of the PII larvae. Particularly shells of pediveliger larvae exposed to 24°C pH 7.4 showed a rough shell surface mostly in the area of the PI shell, frayed valve edges and an increase in malformations (Figure 34 E). These corroded shells are unlikely to provide sufficient protection from predators or further environmental perturbations. By correlating the aragonite saturation sates of the low pH treatments (Chapter 3, Table 18) with the results of this chapter, it is shown that at 24°C pH 7.4 the Ω_A is lower (0.59 ± 0.13) compared to 20°C pH 7.4 (Ω_A = 0.7 ± 0.05). Increased disorder and the severely corroded shells of pediveliger at 24°C pH 7.4 may be a result of the lower Ω_A making it more difficult for the larvae to precipitate aragonite.

Changes in mechanical properties and shell ultrastructure in response to elevated pCO_2 have also been reported elsewhere. Beniash et al. (2010) showed that a pH of 7.5 had negative effects on shell formation in juvenile *C. virginica* with increased thickness of the calcitic laths of the foliated layer and reduced hardness and fracture toughness of the shells. Beniash et al. (2010) also compared the ν_2/ ν_4 peak height ratios of control and treatment group and discovered a small shift of the ν_2 peak towards a higher frequency. They suggested that this shift might indicate small differences in the structural organisation of calcite crystals between treatment and control shells. However, as the crystallinity of calcite did not change significantly, Beniash et al. (2010) concluded that it was unlikely that the observed decrease in the mechanical strength of shells was associated with a change in the crystallographic characteristics of calcite mineral, but rather caused by changes in shell microstructures.
Similar effects on juvenile *C. virginica* were discovered by Dickinson et al. (2012) who investigated the synergistic effects of elevated pCO_2 (~700-800 µatm) and low salinity (15). The combined effects of these two stressors resulted in reduced hardness and fracture resistance of juvenile shells.

Summing up, changing environmental conditions and the corresponding decrease in $CaCO_3$ saturation states may have serious impacts on many marine calcifiers by impairing their skeletal microstructures and jeopardising their survival as a consequence. Species-specific changes in mineralogy are likely such as increased mineral disorder and altered $CaCO_3$ precipitation, putting survival of marine calcifying organisms at risk through increased dissolution of their skeletal structures.

6– Synthesis and future perspectives

The present on-going processes of ocean warming, CO_2-driven ocean acidification and the corresponding decreasing $CaCO_3$ saturation states have emphasised the need to understand the impacts on marine calcifiers. Changing environmental conditions may harm a wide range of marine organisms and the food webs that depend on them, changing entire marine ecosystems (Cooley and Doney, 2009; Fabry, 2008). Recent studies suggest that molluscs, such as oysters and mussels and especially their larval stages, are particularly sensitive to these changes as summarised in Table 2, Section 1.4. As a consequence OA and rising SSTs may affect humans through a variety of socio-economic connections, potentially beginning with reduced harvests of commercially important marine calcifying species (Cooley and Doney, 2009). As a commercially valuable species, harvested worldwide and supporting a global industry that has produced 662 513 metric tonnes in 2010 yielding a 1 262 608 USD market value (FAO, 2012), development of the Pacific oyster *Crassostrea gigas* may be at risk. Thus, it is important to fully understand the physiology of calcification of *C. gigas* during ontogeny from a molecular to a mineralogical level. Hence, the present study aimed to identify: a) the key molecular mechanisms involved in the calcification processes of larval, juvenile and adult *C. gigas;* b) the possible impacts of changes in environmental conditions on these molecular mechanisms; c) the possible impacts of changes in seawater pH and temperature on larval development; d) the shell microstructures and components of *C. gigas* in all shell- bearing life stages like veliger, juvenile and adult stage; e) how changes in these molecular mechanisms correlate with the expression of different biomineral microstructures in forming bivalve shells and; f) possible impacts of changes in environmental conditions on shell microstructures, $CaCO_3$ precipitation and shell mineralogy. To achieve these aims, the response to both low pH and elevated temperature and their interactive effects on development, gene expression, shell growth and shell mineralogy during ontogeny of *C. gigas* were studied using quantitative real-time PCR, SEM and FTIR spectroscopy.

The results presented in this thesis provide a significant step in understanding the molecular, microstructural and mineralogical changes that occur during the development of the Pacific oyster under future ocean conditions. This section will bring together the data from Chapters 3-5 placing in context with the effects of OA and rising SSTs on calcification processes in *C. gigas*.

6.1 *C. gigas* development at ambient conditions

Development of *C. gigas* is characterised by a larval pelagic life stage and a post-larval benthic life stage with both periods of life having a unique shell mineralogy (Figure 2). In larvae, $CaCO_3$ mineralisation was first detected in the early veliger or prodissoconch I stage. Using FTIR spectroscopy, it was shown that the first minerals precipitated in 24 h old PI veliger were ACC and a poorly crystalline aragonite (Figure 37, Section 5.3.2.2). It can be assumed that the ACC was deposited as a precursor and eventually transformed into aragonite as suggested by other authors (Addadi et al., 2003; Weiner et al., 2003; Weiss et al., 2002). The average shell perimeter of PI shells was 2502 (± 373.2) µm displaying a characteristically smooth shell surface, which became lightly dented towards the centre as shown by scanning electron microscope imaging (Figure 33 a, Section 5.3.2). A poorly defined prismatic layer in combination with granular structures was characteristic for microstructures in the PI shell (Figure 33 A, Section 5.3.2) and both are, according to Weiss et al. (2002) and confirmed with the present study, poorly crystalline indicated by high ν_2/ν_4 ratios (Table 32, Section 7.3.2 and Figure 35, Section 5.3.2.2). Quantitative real-time PCR showed an up-regulation of *CGPerl* in PI veliger compared to trochophora (Table 21, Section 4.3.2), suggesting that *CGPerl* might fulfil an important function in early shell formation processes in *C. gigas*. However, within the limitations of this study it was not possible to correlate ACC or aragonite precipitation to the expression of *CGPerl*.

With proceeding development the second larval shell or prodissoconch II was precipitated, separated by a distinct transition to the PI shell (Figure 33 b, Section 5.3.2). FTIR spectroscopy identified exclusively aragonite in six days old PII shells, narrowing ACC precipitation to PI development (Table 32, Section 7.3.2 and Figure 37, Section 5.3.2.2). However, results of Weiss et al. (2002) suggested a continuous but decreasing precipitation of ACC throughout PII development in *C. gigas*, indicating differences in growth within the same species as a possible result of the experimental system. The average PII shell of a six days old veliger had increased more than double in shell perimeter (5522.3 ± 1015 µm) and was characterised by growth rings (Figure 33 b, Section 5.3.2). Indication of a higher crystal order was given by lower ν_2/ν_4 ratios compared to the ratios of PI shells (Table 32, Section 7.3.2 and Figure 35, Section 5.3.2.2), reflected in the three clearly defined microstructural layers (Figure 33 B, Section 5.3.2).

With maturation the average shell perimeter of 19 days old pediveliger enlarged to 9350 ± 2377 µm and well-defined peaks at 1474 cm^{-1} and 860 cm^{-1} (Table 32, Section 7.3.2) confirmed the exclusive presence of aragonite. The up-regulation of *CGCaM*, *CGPerl* and *CGMG4* in pediveliger (Figure 29 and Table 21, Section 4.3.2 and Figure 40) suggests an increased expression of biomineralisation related genes with growth, allowing for the conclusion that

CGCaM and *CGMG4* could be involved in PII shell development, whereas *CGPerl* seemed to be involved in both PI and PII shell development.

After metamorphosis $CaCO_3$ precipitation was characterised by a switch, from ACC to aragonite in larval shells to predominantly calcite in juveniles and adult shells (Figure 31, Section 5.3.1.2 and Figure 37, Section 5.3.2.2). Adult and juvenile shells were characterised by four distinct microstructures (Figures 29 and 30, Section 5.3.1.1) of which the prismatic layer, the foliated layer and the "chalky" lenses were composed of calcite and the myostracum consisted of aragonite, showed by characteristic FTIR peak positions (Figure 31, Section 5.3.1.2).

6.2 *C. gigas* development in future oceans

By simulating predicted future ocean conditions (Nicholls et al., 2007) it was shown that, regardless of the combination of pH and temperature, $CaCO_3$ polymorph precipitation was not affected during development (Figure 37, Section 5.3.2.2), though effects on shell structure (Figure 34, Section 5.3.2.1), crystal disorder (Figures 38 & 39, Section 5.3.2.2) and gene expression (Tables 20 and 21, Sections 4.3.1 and 4.3.2) were observed.

However, elevated temperature (24°C) significantly promoted larval growth over time and even had a significant compensatory effect on growth at low pH (pH 7.4) (Table 27, Section 7.2.1.1). Despite the under-saturation with respect to aragonite (Table 18, Section 3.3.2), larvae grew faster and larger at 24°C pH 7.4 compared to the control condition (Figure 23, Section 3.3.2). It is well known that moderate warming has beneficial effects on development (Kheder et al.; 2010; Rico-Villa et al., 2009) as well as counterbalancing the effects of low pH (Byrne, 2011) up to a threshold, which is species-specific and can differ even between developmental stages of the same species as shown by Parker et al. (2010b) and in the present study.

By comparing growth of 6-day old PII veliger and 19-day old pediveliger it was shown that pediveliger were more sensitive to decreased pH than PII veliger. Growth in pediveliger, including measurements of shell perimeter, shell width and shell length was significantly reduced in low pH treatments, while growth of PII veliger was not significantly different to the control (Figures 24-26, Section 3.3.2). The different reaction of the two developmental stages to decreased pH could be accredited to increased dissolution rates as a consequence of longer exposure times of the pediveliger. SEM analyses revealed that shells of both PII veliger and pediveliger showed severe corrosions at low pH treatments with a greater negative effect on pediveliger shells (Figure 34, Section 5.3.2.1) due to the dissolution of the protective periostracum. In both developmental stages elevated temperature*low pH had a greater negative effect on shell structure than ambient temperature*low pH. This was supported by FTIR analyses showing higher ν_2/ν_4 ratios and lower FWHM values at 24°C pH 7.4 (Figure 39,

Section 5.3.2.2), which are both indications for an increased crystal disorder. It can be assumed that the increase in crystal disorder may be the reason for the observed increased dissolution of the pediveliger shells. Gene expression analyses of *CGPerl* indicated that decreased pH lowers its expression compared to the control (Table 21, Section 4.3.2, and Figure 40), although not significantly. However, as low pH seemed to affect expression levels of *CGPerl* in pediveliger, it possibly could lead to a decrease in $CaCO_3$ precipitation (Weiss et al., 2000) with increased malformations and decreased growth as a consequence. Low pH*ambient temperature had also a significant negative effect on *CGCaM* expression in pediveliger as *CGCaM* was down-regulated compared to the control (Figure 29 & Table 21, Section 4.3.2, and Figure 40). As a possible consequence, uptake of $CaCO_3$ could be reduced resulting ultimately in decreased shell growth.

However, elevated temperature seemed to have a compensatory effect as *CGCam* was significantly up-regulated in pediveliger at low pH*elevated temperature. Of the three GOI *CGMG4* showed the highest expression ratios in pediveliger exposed the low pH treatments where expression was more than two times higher at 24°C pH 7.4 compared to 20°C pH 7.4 (Figure 29 & Table 21, Section 4.3.2), suggesting a compensatory effect to increased dissolution due to decreased aragonite saturation states. The results of this study clearly showed that pediveliger were more sensitive to low pH and low pH*elevated temperature compared to PII veliger. Contrarily, Parker et al. (2010b) reported that pediveliger of *C. gigas* showed greater tolerance to elevated pCO_2 at all tested temperatures (18, 22, 26 & 30°C) compared to PII-veliger, which stands in conflict to the results of the present study. These dissimilarities could be accredited to differences in methodology and experimental system as the tested pH in the present study (pH 7.4) was lower compared to pH 7.7 in Parker et al. (2010b), possibly resulting in higher sensitivity of pediveliger. However, Parker et al. (2010b) focussed on mortality rates, growth and malformations rather than investigating shell structures and mineral composition. Another reason may be due to adaptive capacity of species to climatic conditions, which may differ between populations with a large geographical distribution.

The results suggest that changing environmental conditions affect not only larvae, but also juvenile and adult *C. gigas*. It was shown that in response to low pH the increase in total wet weight of juveniles and adults was significantly reduced over a period of 3.5 months (Figure 23 and Table 17, Section 3.2.1). Gene expression analyses showed that *CGCaM* was significantly down-regulated in low pH treatments in both juveniles and adults (Figure 40). Down-regulation of *CGCaM* could eventually result in decreased Ca-binding activity with reduced calcium uptake and ultimately decreased calcification rates and shell growth as a consequence. In spat, the down-regulation of *CGPerl* at low pH could possibly result in a decrease in $CaCO_3$ precipitation and malformed crystals, causing a decrease in shell growth. In adults, *CGMG4*

showed an increase in expression levels at pH 7.5, indicating a mechanism to compensate for possible shell dissolution.

Setting development of the Pacific oyster under future ocean scenarios in relation to other marine organisms, it is obvious that not just bivalves will be affected by changing environmental conditions. It was shown that other marine organism such as cephalopods (for example Dorney et al., 2012; Wolfe et al. 2012), gastropods (for example Byrne et al., 2011; Kimura et al., 2011), corals (for example Hoegh-Guldberg et al., 2007; Anlauf et al., 2010:), polychaetes (Chan et al., 2012), coralline algae (Kuffner et al., 2007), crustaceans (Arnold et al., 2009), echinoderms (O'Donnell et al., 2010; Kurihara et al., 2012), and fish (Baumann et al., 2012) react sensitive to environmental changes.
Changing environmental conditions such as OA impact not just calcification processes, but also other physiological mechanisms as shown for example in fish. A recent study of Douglas et al. (2013) with the tropical damselfish *Pomacentrus amboinensis* showed that predicted near-future CO_2 levels reduced the ability to learn the identity of predators in damselfish, as neurotransmitter function was impaired. Consequently, survival under future ocean scenarios could have a major influence on population recruitment due to impaired learning (Chivers et al., 2013). Another study on fish by Jutfeld et al. (2013) revealed that not just tropical fish are affected by high CO_2-leves, but also temperate fish such as the three-spined sickleback *Gasterosteus aculeatus* as with increased CO_2 concentrations severe behavioural disturbances, including effects on boldness, exploratory behaviour, lateralisation, and learning was shown.

As a complete listing of the impacts of OA on marine organisms would go far beyond the scope of this study I suggest the interested reader to sign up to the Ocean Acidification newsletter at http://oceanacidification.wordpress.com/ to receive regular updates on publications and other OA-related information.

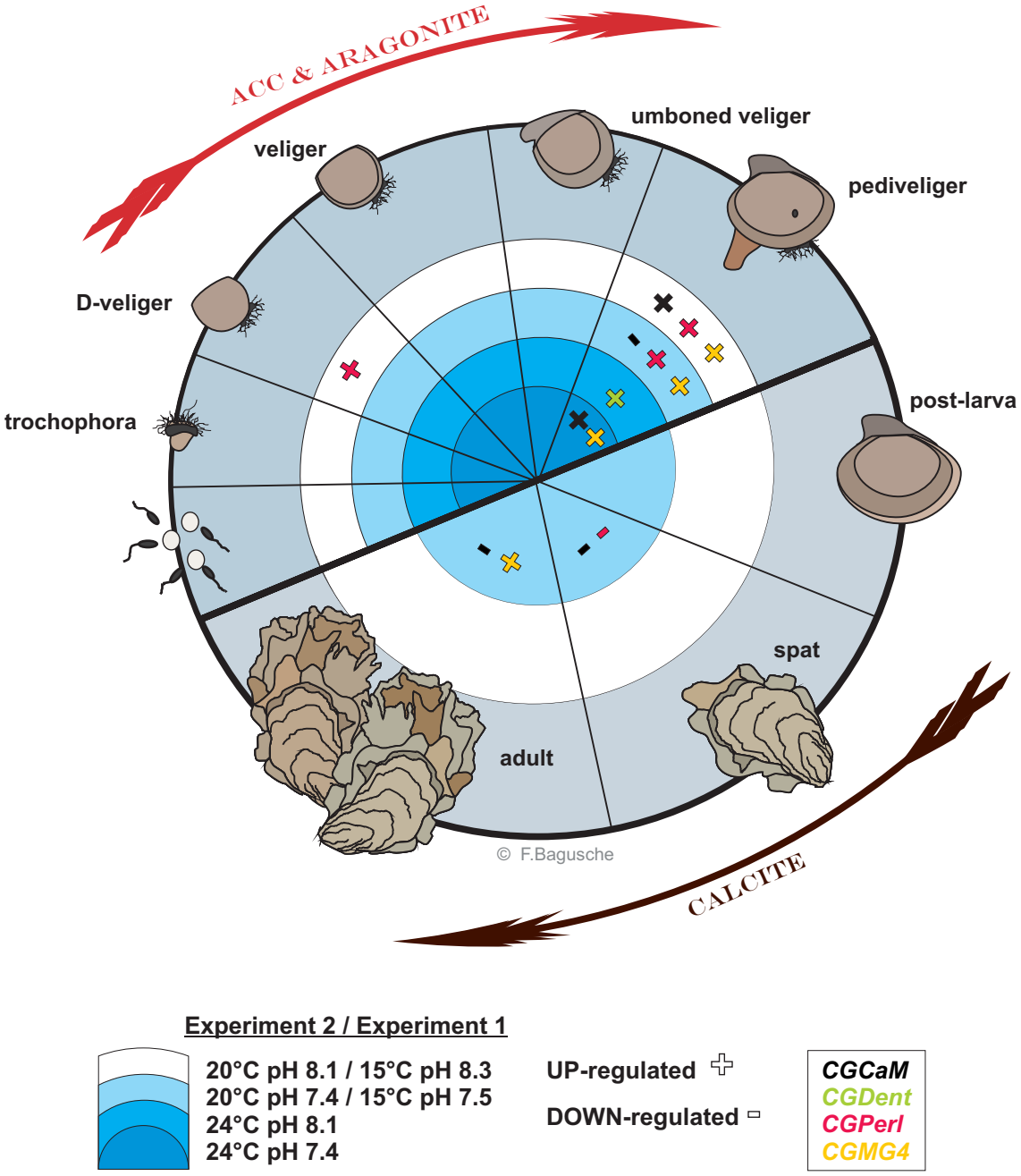

Figure 40: Life cycle of *C. gigas*. Expression of the GOI is correlated to the different treatments and developmental stages. Up-regulation is indicated by **+** and down-regulation by **-**. The GOI are color-coded. For details of gene expression levels please refer to Sections 4.3.1 (experiment 1) and 4.3.2 (experiment 2).

6.3 Conclusions

With the present study it was shown for the first time how the synergistic effects of ocean acidification and ocean warming affect biomineralisation processes in a commercially important bivalve species and the resulting implications on *C. gigas* development from a molecular to a mineralogical level.

This study demonstrates that the effects of temperature and pH, alone and in combination, have overall negative effects on *C. gigas* development, based on decreased growth rates, increased mineral disorder and altered gene expression of skeletogenesis-related genes. Under the conditions of this experiment, low pH is a greater single stressor than high temperature, whereas the combination of these two factors produces greater changes in physiology and shell properties in *C. gigas* than each of the factors alone. Impaired shell growth including corrosions, malformations and increased mineral disorder are likely to jeopardise the survival of larvae and may lead to reductions in both natural and commercial oyster populations. Furthermore, reduced growth of oysters following settlement may not only lower competitive ability and increase vulnerability to predation but may also increase the time taken for oysters to reach market size, thus impacting on the economic viability of important aquaculture industries.

6.4 Future research considerations

Even though this study marks an important step forward in our understanding of calcification processes under future ocean scenarios more research is required to uncover the molecular processes of mineralisation. With the recently published genome of *C. gigas* (Zhang et al., 2012) future projects can now investigate the cellular pathways of carbonate ion uptake and deposition in oysters using powerful genomic, transcriptomic and proteomic techniques in parallel with molecular biology and physiological studies. More specifically, RNA interference (Fire et al. 1998) could be used to knock-down gene expression of biomineralisation-related genes to suppress synthesis of biomineralisation proteins and to ultimately identify their specific function and relation to the different shell components/microstructures. As mentioned above, the mantle of bivalves is subdivided into different functioning zones as shown in Figure 2, Section 1.3.2 (Gardner et al., 2011) and each zone is thought to be specific to genes/proteins related to the different microstructures (Baronnet et al., 2008; Gardner et al., 2011; Kong et al., 2009; Takeuchi and Endo, 2006; Zhang et al., 2006). To validate and localise the expression of the GOI in the oyster tissue *in-situ* hybridisation (Jin and Lloyd, 1997) could be used.

One of the major unanswered questions in oyster research in relation to climate change is how oysters will adapt to ocean acidification. This deserves considerable research effort that should be based on collaborations between evolutionary biologists, molecular biologists, bio-

geochemists and the oyster producing industry. Studies should focus on understanding the genetic plasticity of oysters by assessing the genetic variability between geographically different *C. gigas* populations. Long-term culturing approaches are required combined with the latest genomic-based techniques to assess genetic adaption over many generations.

In order to understand the impacts of environmental stressors on oyster development it is essential that large integrated multi- disciplinary research efforts be undertaken. These should focus on multiple aspects of oyster biology from the cellular to population level working over a wide range of time- scales and concentrating on scaling cellular processes to ecosystem and global changes.

7 – Appendices

7.1 Molecular Protocols

7.1.1 Extraction of nucleic acids from agarose gel using Qiagen QIAquick® Gel Extraction kit

This protocol was used to extract and purify DNA from an agarose gel after electrophoresis using the Qiagen QIAquick® Gel Extraction kit. All centrifugation steps were carried out at 17 900 *g* at room temperature in a conventional tabletop microcentrifuge.

1) Using appropriate UV protection, the desired bands were identified using UV light and excised from the agarose gel using a clean, sharp blade. The gel fragments were then placed in individual sterile 1.5 ml microcentrifuge tubes.
2) 500 µl Buffer QG was added to each sample, which were then incubated at 50°C for 10 min. To ensure the gel completely dissolved samples were vortexed every 2-3 min. The yellow color of Buffer QG indicates a pH ≤ 7.5. In case the color turned orange or violet following incubation, 10 µl of 3M sodium acetate pH 5.0 had to be added and mixed.)
3) 200 µl of 2-propanol (Sigma-Aldrich, Dorset, UK) were added to each reaction and mixed.
4) The samples were then pipetted into individual spin columns in collection tubes and centrifuged at 17 900 *g* 1 min^{-1} to bind the DNA to the column. The flow through was discarded and the columns replaced in the collection tubes
5) 500 µl Buffer QG was added to each sample and centrifuged at 17 900 *g* 1 min^{-1} to wash the column. The flow-through was discarded and the column placed back into the collection tube.
6) To wash the columns again, 750 µl Buffer QG were added to each sample and allowed to stand for 5 minutes at room temperature.
7) The samples were then centrifuged at 17 900 *g* 1 min^{-1}, the flow-through discarded and the columns were tried by additional centrifugation at 17 900 *g* 1 min-1.
8) The QIAquick columns were then placed into clean 1.5 µl microcentrifuge tubes and the DNA eluted with 30 µl Buffer EB. Columns were allowed to stand for 1 min before being centrifuged at 17 900 *g* 1 min^{-1}.
9) Samples were stored at -20°C until needed.

7.1.2 Cloning PCR products using TOPO TA Cloning® Kit for Sequencing

This protocol was carried out to clone amplified PCR products using the TOPO TA Cloning® kit for Sequencing (LifeTechnologies™, Paisley, Scotland) following the manufacturers instructions.

TOPO® cloning reaction

1. For each cloning reaction the reagents described in Table 22 were combined in a thin-walled 500 µl tube and gently mixed without vortexing and incubated for 15 minutes.
2. The samples were incubated for 15 minutes at room temperature and afterwards immediately placed on ice.

Table 22: Components for TOPO® cloning reaction.

Component	Volume
PCR product	4 µl
Salt solution (1.2 M NaCl, 0.06 M $MgCl_2$)	1 µl
Sterile water	-
TOPO® vector	1 µl
Final volume	**6 µl**

1. Fifteen minutes prior to use, One Shot TOP10 chemically competent *E. coli* (one vial per reaction) was removed from -80°C storage and placed on ice to thaw.
2. 2 µl of the TOPO® cloning reaction was added to the 50 µl *E. coli* vial and the reaction was mixed by gentle flicking and incubated on ice for 15 minutes.
3. The *E. coli* cells were heat-shocked in a thermal-cycler for 30 seconds at 42°C without shaking and then immediately placed on ice.
4. 250 µl of room temperature S.O.C. medium (Super Optimal broth with Catabolic repression) was added and the tubes tightly capped.
5. The samples were horizontally placed in a shaking incubator (200 rpm) at 37°C for 1 hour.
6. Following the incubation, 30-50 µl transformation reaction were spread onto pre-warmed selective plates (Luria agar treated with 50- 100 µg ml^{-1} ampicillin sodium salts, 100 µl IPTG (100 mM) and 2- µl X-Gal, 50 mg/ml) and incubated at 37°C over night. Only *E. coli* containing the vector and insert can have ampicillin resistance. IPTG (isopropylthio-β-galactoside) is an inducer of β-galactosidase activity in bacteria and in combination with X-Gal (5-bromo-4-chloro-indolyl-β-D-galactopyranoside) used as a visual indication of whether a cell expresses a functional β-galactosidase enzyme in a technique called

blue/white screening. This method of screening is a convenient way of distinguishing a successful cloning product from other unsuccessful ones.

Selection of positive *E. coli* transformants

7. Following the incubation, 8-10 white or light-blue colonies, representing a successful ligation reaction, were selected from the plates for further analyses by colony PCR.
8. Colony PCR master mix was prepared by adding the components listed in Table 23 into a thin-walled 500 µl PCR tube.

Table 23: Components for colony PCR

Component	Volume
10X *Taq* PCR Reaction Buffer	2 µl
M13 Forward primer (0.5 µM)	0.5 µl
M13 Reverse Primer (0.5 µM)	0.5 µl
dNTP mix (10 µM)	0.4 µl
Sterile water	16.4 µl
Taq DNA Polymerase (0.05 unit μl^{-1})	0.2 µl
Final volume	**20 µl**

9. The selected colonies were picked from the plates using a sterile cocktail stick and swirled gently in the master mix. The remaining cells on the used toothpicks were then applied onto fresh Luria agar (master-) plates and incubated at 37°C over night.
10. The PCR tubes were place into a thermal cycler using the conditions listed in Table 24.
11. The resulting PCR products were then visualised on a 1% agarose gel containing 6 µl ethidium bromide (10 mg ml^{-1}).
12. Colonies containing fragments of the expected size were transferred with sterile cocktail sticks into 25 ml Falcon tubes containing 5 ml Luria broth and 100 µg ml^{-1} ampicillin in preparation for plasmid extraction.

Table 24: Colony PCR thermocycling conditions

Step	Temp (°C)	Duration	No. of cycles
Initial denaturation	95	10 min	1
Denaturation	95	30 sec	30
Annealing	55	30 sec	
Extension	72	30 sec	

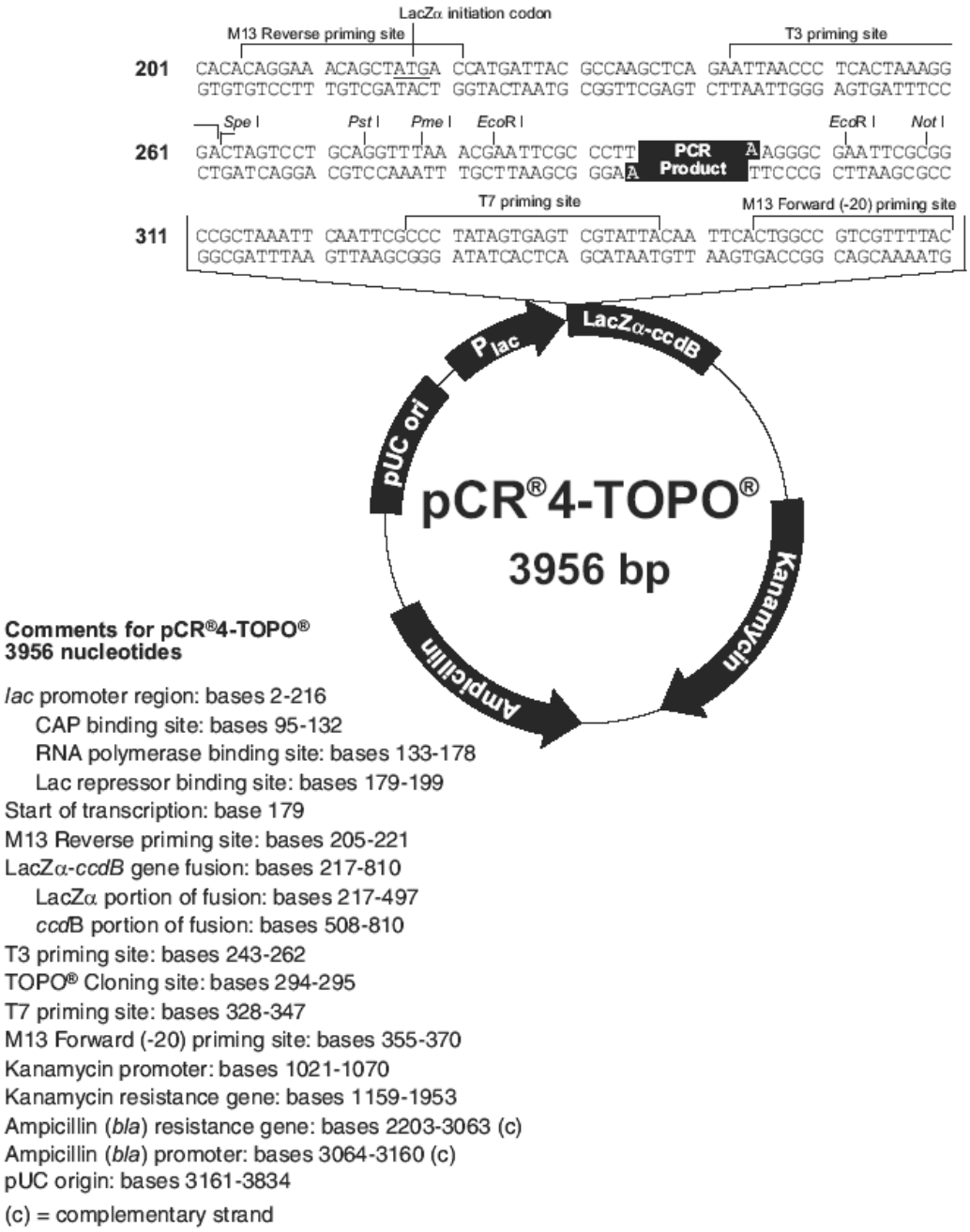

Comments for pCR®4-TOPO®
3956 nucleotides

lac promoter region: bases 2-216
  CAP binding site: bases 95-132
  RNA polymerase binding site: bases 133-178
  Lac repressor binding site: bases 179-199
Start of transcription: base 179
M13 Reverse priming site: bases 205-221
LacZα-*ccdB* gene fusion: bases 217-810
  LacZα portion of fusion: bases 217-497
  *ccd*B portion of fusion: bases 508-810
T3 priming site: bases 243-262
TOPO® Cloning site: bases 294-295
T7 priming site: bases 328-347
M13 Forward (-20) priming site: bases 355-370
Kanamycin promoter: bases 1021-1070
Kanamycin resistance gene: bases 1159-1953
Ampicillin (*bla*) resistance gene: bases 2203-3063 (c)
Ampicillin (*bla*) promoter: bases 3064-3160 (c)
pUC origin: bases 3161-3834
(c) = complementary strand

Figure 41: pCR® 4-TOPO® cloning vector map. Features of pCR® 4-TOPO® and the sequence surrounding the TOPO® Cloning site. Restriction sites are labeled to indicate the actual cleavage site. After TOPO TA Cloning® Kit for sequencing user manual, version O (April 2006)

7.1.3 Plasmid extraction using a QIAprep® Miniprep Kit

Plasmids containing the insert were extracted from the bacterial cells using a QIAprep® Miniprep Kit (QIAGEN Ltd., Crawley, UK) following the manufacturers instructions and sent for Sanger sequencing at Source Bioscience, Oxford, UK

1. Falcon tubes containing the *E. coli* cultures grown over night were removed from the incubator and centrifuged at 3000 *g* 10 min^{-1} at 25°C.
2. The Luria broth was removed from the cell pellet and transferred into the liquid culture waste bin designated for autoclaving before it was disposed of.
3. The cell pellet was gently re-suspended with 250 µl Buffer P1 containing RNase A and LyseBlue reagent and then transferred into a sterile 1.5 ml microcentrifuge tube.
4. Buffer P2 (250 µl) was added and carefully mixed by inverting the tube 4-6 times until the colour was homogeneous blue (due to the LyseBlue reagent). The lysis reaction was not allowed to proceed for more than 5 minutes.
5. 350 µl Buffer N3 was added and immediately mixed by inverting the tube 4-6 times until the suspension remained homogeneously colourless.
6. Samples were centrifuged at 17 900 *g* 10 min^{-1} in a tablet-op microcentrifuge at room temperature.
7. The supernatant from each sample was applied to individual QIAprep spin columns in 2 ml collection tubes by decanting and centrifuged at 17 900 *g* 1 min^{-1}.
8. After discarding the flow-through, the columns were washed by adding 0.5 ml Buffer PB and centrifuged again at 17 900 *g* 1 min^{-1}.
9. A second wash with 0.75 ml Buffer PB was performed and centrifuged at 17 900 *g* 1 min^{-1}. The flow-through was discarded and the samples centrifuged for another minute at 17 900 *g* to dry the column membrane and to remove residual wash buffer.
10. Finally, the QIAprep columns were placed in clean 1.5 ml microcentrifuge tubes. DNA was then eluted by adding 40 µl Buffer EB to each sample and allowed to stand for 1 minute at room temperature. Samples were then centrifuged at 17 900 *g* 1 min^{-1}.
11. Plasmid DNA was analysed for purity and quantity using a NanoDrop ND-1000 spectrophotometer and stored at -20°C until needed.

7.2 Statistical Analyses

7.2.1 Larval responses to the effects of elevated temperature and low pH

7.2.1.1 Shell width measurements over time

An ANCOVA was performed to test the influence of the factors time, temperature, pH and temperature*pH on shell width (growth). It was shown that all tested factors had a significant influence ($p<0.01$) on shell growth.

Table 25: ANCOVA to test the influence of pH, temperature and temperature*pH on shell width over a period of two weeks. Significant differences are highlighted red. F/R: Fixed/Random, DF: Degrees of Freedom, MS: Mean Square,

Sources	Effect (F/R)	DF Effect	MS Effect	DF Error	MS Error	F-value	p-value
day	Fixed	1	2186155	1445	2248.983	972.0637	0.000000
Temp	Fixed	1	482322	1445	2248.983	214.4622	0.000000
pH	Fixed	1	269311	1445	2248.983	119.7481	0.000000
Temp*pH	Fixed	1	98194	1445	2248.983	43.6615	0.000000

7.2.1.2 PII veliger

Data for shell perimeter and shell width were not meeting assumptions of equal variances. Therefore non-parametric Kruskal-Wallis ANOVAs were performed. It was shown that low pH and the interactive effects of elevated temperature*low pH had a significant influence on shell perimeter (Table 26). The interactive effects of elevated temperature*low pH had a significant effect on shell width, as shown in Table 27.

Data for shell lengths met assumptions for normal distribution and equal variances. Therefore parametric ANOVA tests were applied. It was shown that just temperature and pH had a significant effect on shell length, as shown in Tables 28 and 29.

Shell perimeter

Table 26: Multiple Kruskal-Wallis ANOVA comparisons between conditions of shell perimeters of PII veliger. Significant differences are highlighted red. Kruskal-Wallis test: H (3, N= 67) =34.23151, p=.0000.

Condition	20°C pH 7.4	20°C pH 8.1 (Control)	24°C pH 8.1
24°C pH 7.4	0.015106	1.000000	0.007970
20°C pH 7.4		0.357471	0.000000
20°C pH 8.1 (Control)			**0.000838**

Shell width

Table 27: Multiple Kruskal-Wallis ANOVA comparisons between conditions of shell widths of PII veliger. Significant differences are highlighted red. Kruskal-Wallis test: H (3, N= 67) =27.76826, p =.0000.

Condition	20°C pH 7.4	20°C pH 8.1 (Control)	24°C pH 8.1
24°C pH 7.4	0.065667	1.000000	0.013557
20°C pH 7.4		0.660754	0.000001
20°C pH 8.1 (Control)			**0.002494**

Shell length

Table 28: 2-way ANOVA to identify the influencing factors (temperature, pH and temperature*pH) on shell length. Significant differences are highlighted red. SS: Sum of Squares, MS: Mean Squares, DF: Degrees of Freedom.

Shell length	SS	MS	F-value	p-value	DF	
Temperature	3784.8	3784.8	42.523	0.000000	Temperature	1
pH	2245.1	2245.1	25.224	0.000004	pH	1
Temp*pH	308.8	308.8	3.470	0.067156	Temp*pH	1
Error	5607.4	89.0			Error	63
Total	11178.9				Total	63

Table 29: Unequal Turkey Honest Significance Test between conditions for shell length in PII veliger. Significant differences are highlighted red.

Condition	20°C pH 7.4	24°C pH 8.1	24°C pH 7.4
20°C pH 8.1 (Control)	0.138543	**0.00018**	0.728792
20°C pH 7.4		0.000154	0.00245
24°C pH 8.1			0.000852

7.2.1.3 Pediveliger

A 2-way ANOVA was performed to identify the influencing factors on shell perimeter, shell width and shell length in pediveliger. It was shown that each of the factors temperature, pH and temperature*pH had a significant ($p<0.01$) influence on shell perimeter, shell width and shell length (Table 30).

Table 30: 2-way ANOVA to identify influencing factors on shell perimeter, shell width and shell length. Significant differences are highlighted red. SS: Sum of Squares, MS: Mean Squares, DF: Degrees of Freedom

Log10 shell perimeter				
	SS	**MS**	**F-value**	**p-value**
Temperature	0.1725	0.1725	17.96	0.000099
pH	3.4413	3.4413	358.36	0.000000
Temp*pH	0.0812	0.0812	8.46	0.005444
Error	0.4705	0.0096		
Total	4.2414			

Log10 shell width				
	SS	**MS**	**F-value**	**p-value**
Temperature	0.0500	0.0500	21.75	0.000024
pH	0.7806	0.7806	339.50	0.000000
Temp*pH	0.0256	0.0256	11.16	0.001608
Error	0.1127	0.0023		
Total	0.9556			

Shell length				
	SS	**MS**	**F-value**	**p-value**
Temperature	13870	13870	23.996	0.000011
pH	152474	152474	263.795	0.000000
Temp*pH	5431	5431	9.396	0.003532
Error	28322	578		
Total	193411			

DF	
Temperature	1
pH	1
Temp*pH	1
Error	49
Total	52

7.3 FTIR spectra

7.3.1 Juveniles and Adults

Table 31: FTIR peak positions and measured peak heights for random juvenile and adult samples to determine the mineralogy of the four microstructures. Spectra were collected by S. Long.

Sample ID	Dev. stage	Valve	Shell region	Grinding sample ID	Dominant peaks - wavenumbers (cm^{-1})			
					v_3	v_2	v_4	1083
A27-Ra	Adult	R	Muscle scar	**A27-Ra**	1426	877	712	
				A27-Ra1	1426	876	712	
				A27-Ra2	1424	877	712	
				A27-Ra3	1427	877	713	
A27-Rb	Adult	R	Foliated layer	**A27-Rb**	1421	877	712	
				A27-Rb1	1424	877	712	
				A27-Rb2	1421	877	713	
				A27-Rb3	1420	877	713	
A27-Rc	Adult	R	Random	**A27-Rc**	1423	877	712	
				A27-Rc1	1421	877	713	
				A27-Rc2	1421	877	713	
				A27-Rc3	1426	877	713	
A28-Lb	Adult	L	Muscle scar	**A28-Lb**	1418	876	712	
				A28-Lb1	1422	877	713	
				A28-Lb2	1422	877	713	
A30-Rb	Adult	R	Muscle scar	**A30-Rb**	1420	876	712	
				A30-Rb1	1417	877	713	
				A30-Rb2	1417	877	713	
				A30-Rb3	1418	877	713	
A30-Rc	Adult	R	Random	**A30-Rc**	1423	876	713	
				A30-Rc1	1425	876	713	
				A30-Rc2	1427	876	713	
				A30-Rc3	1427	877	713	
A1-La	Adult	L	Chalk lens	**A1-Laa**	1415	880	713	
				A1-La1	1417	877	713	
				A1-La2	1418	878	713	
A1-Lb	Adult	L	Foliated layer	**A1-Lbb**	1419	877	711	
				A1-Lb1	1420	877	713	
				A1-Lb2	1419	877	713	
				A1-Lb3	1423	876	713	
A1-Ld	Adult	L	Prismatic layer	**A1-Ld**	1421	875	713	
				A1-Ld1	1418	876	713	
				A1-Ld2	1423	876	712	
S2-Ra	Spat	R	Random	**S2-Ra**	1417	876	713	
				S2-Ra1	1418	876	713	
				S2-Ra2	1420	876	713	
S2-Rb	Spat	R	Prismatic layer	**S2-Rb**	1421	875	713	
				S2-Rb1	1421	875	712	

Appendices

Sample ID	Dev. stage	Valve	Shell region	Grinding sample ID	Dominant peaks - wavenumbers (cm^{-1})			
					v_3	v_2	v_4	1083
				S2-Rb2	1423	876	713	
S2-Rc	Spat	R	Chalk lens	**S2-Rc**	1417	878	713	
				S2-Rc1	1418	877	712	
				S2-Rc2	1420	877	713	
S2-Rd	Spat	R	Myostracum	**S2-Rd**	1472	856	713	1082
				S2-Rd1	1474	858	713	1082
				S2-Rd2	1471	858	713	1082

7.3.2 Larvae

Table 32: FTIR peak positions and measured peak heights for larval samples of the 2nd experiment. FWHM: Full Width at Half Maximum. GS: Grinding Stage. Spectra were collected by S. Long.

Life Stage	pH	Temp. (°C)	Sample ID	GS	IR peaks - LEFT: peak position (cm^{-1}), RIGHT: measured peak height (mm)														FWHM (cm^{-1})	v2.v3	v4.v3	v2.v4
					1740 - 1780		1630 - 1650		1420 - 1480		1083		850 - 880		713		700					
									v3				v2		v4							
PI veliger	8.1	20	**Ba-2E.1**	1	1785	4.5	N/A	N/A	1473	132.3	1082	4.7	865	34.3	713	8.0	700	3.8	105.6	0.3	0.1	4.3
PI veliger	8.1	20	**Ba-2E.1a**	2	1786	3.0	N/A	N/A	1473	132.7	1083	3.8	863	36.7	713	6.7	700	2.7	87.0	0.3	0.1	5.5
PI veliger	8.1	20	**Ba-2E.1b**	3	1786	3.0	1630	5.3	1475	134.3	1083	3.2	863	40.3	713	6.8	700	2.5	83.3	0.3	0.1	5.9
PI veliger	8.1	20	**Bb-2E.1**	1	1786	4.0	N/A	N/A	1472	134.7	1083	4.8	864	39.3	713	9.3	700	4.5	90.7	0.3	0.1	4.2
PI veliger	8.1	20	**Bb-2E.1a**	2	1786	3.0	1635	4.0	1474	133.7	1082	3.8	863	42.7	713	7.2	700	3.7	85.2	0.3	0.1	5.9
PI veliger	8.1	20	**Bb-2E.1b**	3	1785	2.8	1633	8.0	1473	132.3	1083	3.3	862	42.0	713	6.3	700	3.3	77.8	0.3	0.0	6.7
PII veliger	7.4	24	**1A-3E.1**	1	1789	11.8	N/A	N/A	1469	110.0	1082	14.0	859	48.5	712	29.0	699	16.5	349.3	0.4	0.3	1.7
PII veliger	7.4	24	**1A-3E.1a**	2	1789	10.0	N/A	N/A	1470	106.5	1082	12.0	857	46.5	712	21.5	699	11.0	267.6	0.4	0.2	2.2
PII veliger	7.4	24	**1A-3E.1b**	3	1788	7.0	N/A	N/A	1471	101.0	1082	10.0	858	44.0	712	17.0	699	8.0	235.2	0.4	0.2	2.6
PII veliger	7.4	24	**1B-3E.2**	1	1789	17.0	N/A	N/A	1470	94.5	1082	18.5	866	45.0	712	38.5	700	18.0	405.6	0.5	0.4	1.2
PII veliger	7.4	24	**1B-3E.2a**	2	1788	12.0	N/A	N/A	1475	124.5	1082	16.5	858	59.0	712	30.0	700	15.5	301.4	0.5	0.2	2.0
PII veliger	7.4	24	**1B-3E.2b**	3	1788	9.0	N/A	N/A	1475	128.0	1082	13.0	858	57.3	712	22.5	700	11.0	231.0	0.4	0.2	2.5
PII veliger	7.4	24	**1C-3E.1**	1	1788	16.5	1652	4.0	1470	116.0	1083	17.0	860	51.0	712	39.0	699	18.3	369.0	0.4	0.3	1.3
PII veliger	7.4	24	**1C-3E.1a**	2	1789	12.0	N/A	N/A	1471	127.5	1082	16.0	858	55.3	712	30.5	699	12.0	298.6	0.4	0.2	1.8
PII veliger	7.4	24	**1C-3E.1b**	3	1789	11.0	N/A	N/A	1471	130.5	1082	11.8	859	58.5	712	24.0	700	11.5	253.5	0.4	0.2	2.4
PII veliger	7.4	20	**2A-3E.1**	1	1789	14.8	N/A	N/A	1470	96.0	1083	15.2	864	45.5	712	34.3	700	16.0	370.0	0.5	0.4	1.3
PII veliger	7.4	20	**2A-3E.1a**	2	1789	13.3	N/A	N/A	1471	125.0	1083	15.0	859	54.7	713	30.0	700	12.5	332.4	0.4	0.2	1.8
PII veliger	7.4	20	**2A-3E.1b**	3	1789	11.5	N/A	N/A	1472	128.7	1082	13.0	858	56.3	713	25.3	700	12.0	287.3	0.4	0.2	2.2
PII veliger	7.4	20	**2B-3E.1**	1	1789	14.7	N/A	N/A	1470	83.0	1083	11.3	854	33.8	713	30.3	700	17.7	398.1	0.4	0.4	1.1
PII veliger	7.4	20	**2B-3E.1a**	2	1789	12.5	N/A	N/A	1471	122.5	1082	13.3	858	49.3	713	24.0	700	10.8	300.5	0.4	0.2	2.1
PII veliger	7.4	20	**2B-3E.1b**	3	1788	9.0	N/A	N/A	1476	124.0	1082	9.7	857	52.0	712	19.7	700	8.8	218.8	0.4	0.2	2.6

Life Stage	pH	Temp. (°C)	Sample ID	GS	IR peaks - LEFT: peak position (cm^{-1}), RIGHT: measured peak height (mm)														FWHM (cm^{-1})	v2.v3	v4.v3	v2.v4
					1740 - 1780		1630 - 1650		1420 - 1480		1083		850 - 880		713		700					
									v3				v2		v4							
PII veliger	7.4	20	**2C-3E.1c**	1	1787	16.0	N/A	N/A	1474	102.0	1083	14.3	866	44.2	713	33.7	700	21.7	360.6	0.4	0.3	1.3
PII veliger	7.4	20	**2C-3E.1d**	2	1788	12.0	N/A	N/A	1471	112.0	1082	12.3	860	50.5	713	26.7	699	12.3	293.9	0.5	0.2	1.9
PII veliger	7.4	20	**2C-3E.1e**	3	1787	9.2	N/A	N/A	1473	123.0	1082	11.0	857	52.7	713	20.5	700	11.3	238.5	0.4	0.2	2.6
PII veliger	8.1	20	**3A-3E.1**	1	1789	21.7	N/A	N/A	1470	109.0	1083	20.7	870	58.0	712	52.5	699	24.3	441.3	0.5	0.5	1.1
PII veliger	8.1	20	**3A-3E.1a**	2	1788	15.0	N/A	N/A	1469	122.7	1082	17.0	860	58.2	712	36.3	699	15.0	356.8	0.5	0.3	1.6
PII veliger	8.1	20	**3A-3E.1b**	3	1788	11.7	N/A	N/A	1472	125.2	1082	14.7	858	59.0	712	30.7	699	12.7	304.2	0.5	0.2	1.9
PII veliger	8.1	20	**3B-3E.1**	1	1789	16.3	N/A	N/A	1470	95.0	1082	17.7	866	50.0	713	48.7	699	24.7	462.0	0.5	0.5	1.0
PII veliger	8.1	20	**3B-3E.1a**	2	1789	13.7	N/A	N/A	1468	123.3	1082	16.7	860	59.7	713	34.0	699	15.7	339.9	0.5	0.3	1.8
PII veliger	8.1	20	**3B-3E.1b**	3	1789	12.7	N/A	N/A	1470	129.5	1082	15.7	860	60.3	712	30.0	699	12.7	296.7	0.5	0.2	2.0
PII veliger	8.1	20	**3C-3E.1a**	1	1790	17.3	N/A	N/A	1470	94.7	1082	14.7	866	42.7	712	33.0	700	21.0	390.6	0.5	0.3	1.3
PII veliger	8.1	20	**3C-3E.1b**	2	1789	11.8	N/A	N/A	1474	98.3	1082	13.0	861	48.7	712	25.0	699	12.3	325.8	0.5	0.3	1.9
PII veliger	8.1	20	**3C-3E.1c**	3	1788	9.8	N/A	N/A	1474	120.3	1082	11.5	860	52.5	712	22.7	700	10.2	225.4	0.4	0.2	2.3
PII veliger	8.1	24	**4A-3E.1**	1	1787	18.0	N/A	N/A	1467	100.0	1082	19.0	866	51.5	712	44.0	699	26.0	466.7	0.5	0.4	1.2
PII veliger	8.1	24	**4A-3E.1a**	2	1789	15.0	N/A	N/A	1471	123.3	1082	17.0	860	59.2	712	35.0	700	21.0	354.9	0.5	0.3	1.7
PII veliger	8.1	24	**4A-3E.1b**	3	1788	12.3	N/A	N/A	1471	125.3	1082	15.0	858	61.2	712	30.7	700	14.0	306.1	0.5	0.2	2.0
PII veliger	8.1	24	**4B-3E.1**	1	1786	19.0	N/A	N/A	1474	88.7	1083	20.0	869	57.0	713	52.3	700	30.3	495.8	0.6	0.6	1.1
PII veliger	8.1	24	**4B-3E.1a**	2	1789	13.8	N/A	N/A	1473	121.0	1082	15.8	861	58.0	713	27.0	700	16.0	343.7	0.5	0.2	2.1
PII veliger	8.1	24	**4B-3E.1b**	3	1789	11.3	N/A	N/A	1474	130.7	1082	14.3	859	60.7	712	29.7	699	13.0	246.0	0.5	0.2	2.0
PII veliger	8.1	24	**4C-3E.1a**	1	1788	21.3	N/A	N/A	1474	108.0	1082	20.0	863	53.7	712	50.3	699	23.0	467.6	0.5	0.5	1.1
PII veliger	8.1	24	**4C-3E.1b**	2	1788	13.7	N/A	N/A	1470	119.7	1082	15.0	859	55.7	712	32.0	699	15.7	324.9	0.5	0.3	1.7
PII veliger	8.1	24	**4C-3E.1c**	3	1788	10.5	N/A	N/A	1474	121.0	1082	12.3	860	51.3	712	22.0	699	10.7	219.7	0.4	0.2	2.3
Pediveliger	7.4	24	**1C-4E.1**	1	1788	12.3	1655	2.5	1478	78.3	1083	11.0	863	38.7	713	27.3	700	15.8	342.6	0.5	0.3	1.4
Pediveliger	7.4	24	**1C-4E.1a**	2	1790	8.0	N/A	N/A	1471	90.7	1082	8.0	859	35.0	712	16.3	700	7.3	183.3	0.4	0.2	2.1
Pediveliger	7.4	24	**1C-4E.1b**	3	1787	7.0	N/A	N/A	1474	127.3	1082	9.0	860	48.3	713	17.0	700	7.2	127.7	0.4	0.1	2.8
Pediveliger	7.4	24	**1B-4E.1**	1	1786	13.3	N/A	N/A	1470	75.0	1082	13.8	865	42.2	713	34.5	700	22.8	364.8	0.6	0.5	1.2
Pediveliger	7.4	24	**1B-4E.1a**	2	1788	6.8	1621	8.3	1475	106.0	1082	8.2	861	41.0	713	19.7	700	7.5	159.3	0.4	0.2	2.1

Life Stage	pH	Temp. (°C)	Sample ID	GS	IR peaks - LEFT: peak position (cm^{-1}), RIGHT: measured peak height (mm)												FWHM (cm^{-1})	v2.v3	v4.v3	v2.v4
					1740 - 1780		1630 - 1650		1420 - 1480		1083		850 - 880		713		700					
									v3				v2		v4							
Pediveliger	7.4	24	**1B-4E.1b**	3	1789	5.8	1633	11.0	1474	112.0	1082	7.5	860	37.2	713	14.3	700	8.0	126.9	0.3	0.1	2.6
Pediveliger	7.4	24	**1A-4E.1**	1	1789	10.3	N/A	N/A	1470	104.0	1082	10.5	862	45.5	712	24.3	700	13.0	179.6	0.4	0.2	1.9
Pediveliger	7.4	24	**1A-4E.1a**	2	1789	7.0	N/A	N/A	1471	106.3	1083	8.7	861	45.0	713	18.0	700	8.3	143.5	0.4	0.2	2.5
Pediveliger	7.4	24	**1A-4E.1b**	3	1788	4.7	N/A	N/A	1475	103.0	1083	6.7	860	40.3	713	12.3	700	6.0	116.7	0.4	0.1	3.3
Pediveliger	7.4	20	**2A-4E.1**	1	1790	2.7	N/A	N/A	1470	50.0	1082	5.0	865	13.0	713	19.0	698	16.0	428.2	0.1	0.4	0.3
Pediveliger	7.4	20	**2B-4E.1**	2	1787	21.5	N/A	N/A	1470	115.7	1082	18.0	867	60.8	712	45.7	700	21.3	358.7	0.5	0.4	1.3
Pediveliger	7.4	20	**2B-4E.1a**	3	1788	11.8	N/A	N/A	1472	128.7	1082	12.3	860	55.0	712	26.3	700	11.5	219.7	0.4	0.2	2.1
Pediveliger	7.4	20	**2C-4E.1**	1	1788	21.3	N/A	N/A	1470	111.3	1082	20.8	864	56.3	713	50.7	699	25.0	399.1	0.5	0.5	1.1
Pediveliger	7.4	20	**2C-4E.1a**	2	1789	13.7	N/A	N/A	1473	125.0	1082	13.7	861	54.7	712	30.7	700	16.0	287.3	0.4	0.2	1.8
Pediveliger	8.1	20	**3A-4E.1**	1	1788	26.3	N/A	N/A	1474	102.0	1082	22.3	864	58.2	712	60.7	699	27.3	518.3	0.6	0.6	1.0
Pediveliger	8.1	20	**3A-4E.1a**	2	1780	16.5	N/A	N/A	1472	97.7	1082	14.7	857	51.7	712	36.3	699	19.0	424.4	0.5	0.4	1.4
Pediveliger	8.1	20	**3A-4E.1b**	3	1789	11.0	N/A	N/A	1473	110.5	1082	14.5	859	53.5	712	31.0	699	15.0	332.4	0.5	0.3	1.7
Pediveliger	8.1	20	**3A-4E.1c**	4	1789	10.0	N/A	N/A	1474	125.3	1082	12.3	859	54.5	712	24.3	700	10.7	217.8	0.4	0.2	2.2
Pediveliger	8.1	20	**3B-4E.1**	1	1788	24.0	N/A	N/A	1473	95.7	1082	20.3	867	50.7	713	48.3	700	27.3	501.4	0.5	0.5	1.0
Pediveliger	8.1	20	**3B-4E.1a**	2	1788	15.3	N/A	N/A	1472	119.7	1082	16.3	860	56.3	712	37.0	699	19.0	373.7	0.5	0.3	1.5
Pediveliger	8.1	20	**3B-4E.1b**	3	1789	12.0	N/A	N/A	1470	124.3	1082	14.3	860	56.5	712	30.0	699	13.7	274.2	0.5	0.2	1.9
Pediveliger	8.1	20	**3C-4E.1b**	1	1789	26.0	N/A	N/A	1455	112.5	1082	20.0	862	51.7	712	52.7	700	29.7	508.9	0.5	0.5	1.0
Pediveliger	8.1	20	**3C-4E.1c**	2	1789	15.0	N/A	N/A	1471	118.7	1082	15.0	859	57.0	712	32.0	700	16.0	357.7	0.5	0.3	1.8
Pediveliger	8.1	20	**3C-4E.1d**	3	1789	12.0	N/A	N/A	1475	126.7	1082	12.3	860	54.3	712	25.7	699	11.3	231.0	0.4	0.2	2.1
Pediveliger	8.1	24	**4A-4E.1**	1	1787	29.3	N/A	N/A	1467	106.0	1082	25.7	867	59.7	712	60.3	700	34.3	523.9	0.6	0.6	1.0
Pediveliger	8.1	24	**4A-4E.1a**	2	1789	14.7	1650	9.0	1472	83.3	1082	12.7	863	38.3	712	23.7	699	15.0	349.3	0.5	0.3	1.6
Pediveliger	8.1	24	**4A-4E.1b**	3	1789	14.0	1615	8.0	1471	125.7	1082	16.0	859	61.8	712	33.3	699	17.3	217.8	0.5	0.3	1.9
Pediveliger	8.1	24	**4B-4E.1**	1	1788	32.3	N/A	N/A	1458	111.0	1082	26.0	864	63.7	713	65.3	699	34.3	535.2	0.6	0.6	1.0
Pediveliger	8.1	24	**4B-4E.1a**	2	1789	17.0	1624	14.0	1469	119.7	1082	18.0	861	60.7	712	42.3	699	21.7	418.8	0.5	0.4	1.4
Pediveliger	8.1	24	**4B-4E.1b**	3	1789	14.0	1615	8.0	1471	125.7	1082	16.0	859	61.8	712	33.3	699	17.3	294.8	0.5	0.3	1.9
Pediveliger	8.1	24	**4C-4E.1**	1	N/A	N/A	N/A	N/A	1470	56.0	1082	13.5	860	32.0	712	40.0	699	25.0	518.3	0.6	0.7	0.8

Life Stage	pH	Temp. (°C)	Sample ID	GS	IR peaks - LEFT: peak position (cm^{-1}), RIGHT: measured peak height (mm)														FWHM (cm^{-1})	v2.v3	v4.v3	v2.v4
					1740 - 1780		1630 - 1650		1420 - 1480		1083		850 - 880		713		700					
									v3				v2		v4							
Pediveliger	8.1	24	**4C-4E.1a**	2	1788	8.5	1630	6.0	1471	97.7	1082	8.3	860	44.7	712	16.0	700	9.0	315.5	0.5	0.2	2.8
Pediveliger	8.1	24	**4C-4E.1b**	3	1789	9.0	1640	4.0	1472	128.5	1082	7.5	860	55.5	712	16.5	699	6.0	184.7	0.4	0.1	3.4
Spat	8.1	24	**4A-5E.1**	1	1788	21.7	N/A	N/A	1471	107.3	1082	20.3	864	50.3	712	48.0	700	24.3	439.4	0.5	0.4	1.0
Spat	8.1	24	**4A-5E.1a**	2	1789	10.5	N/A	N/A	1471	91.3	1082	11.8	860	38.3	713	27.7	700	12.0	313.6	0.4	0.3	1.4
Spat	8.1	24	**4A-5E.1b**	3	1789	11.7	540	1.3	1469	124.7	1082	12.3	861	53.3	712	29.0	699	12.3	227.2	0.4	0.2	1.8
Spat	8.1	24	**4B-5E.1**	1	1791	20.3	N/A	N/A	1418	113.3	1083	14.5	872	52.7	712	45.3	700	12.7	396.2	0.5	0.4	1.2
Spat	8.1	24	**4B-5E.1a**	2	1794	9.0	N/A	N/A	1415	122.7	1082	7.7	876	43.7	712	27.7	700	7.0	214.1	0.4	0.2	1.6
Spat	8.1	24	**4B-5E.1b**	3	1792	6.7	N/A	N/A	1471	111.0	1082	6.5	877	43.3	712	20.7	699	4.3	202.8	0.4	0.2	2.1
Spat	8.1	24	**4C-5E.1**	1	1798	9.3	N/A	N/A	1417	124.7	1083	5.0	877	41.8	713	23.7	N/A	N/A	182.2	0.3	0.2	1.8
Spat	8.1	24	**4C-5E.1a**	2	1798	6.0	N/A	N/A	1416	130.5	1083	3.5	878	45.3	713	17.0	N/A	N/A	144.6	0.3	0.1	2.7
Spat	8.1	24	**4C-5E.1b**	3	1796	4.2	N/A	N/A	1417	133.0	1082	2.0	878	41.5	713	12.5	N/A	N/A	118.3	0.3	0.1	3.3
Spat	8.1	24	**4C-5E.1c**	4	1794	3.0	N/A	N/A	1422	618.5	1083	1.8	878	34.0	713	8.3	N/A	N/A	105.6	0.1	0.0	4.1

References

A Chien, D. B. E. J. M. T. (1976). Deoxyribonucleic acid polymerase from the extreme thermophile Thermus aquaticus. *Journal of Bacteriology* **127**, 1550.

Addadi, L., Joester, D., Nudelman, F. and Weiner, S. (2006). Mollusk Shell Formation: A Source of New Concepts for Understanding Biomineralization Processes. *Chem. Eur. J.* **12**, 980–987.

Addadi, L., Raz, S. and Weiner, S. (2003). Taking Advantage of Disorder: Amorphous Calcium Carbonate and Its Roles in Biomineralization. *Adv. Mater.* **15**, 959–970.

Alberts, B., Johnson, A., Lewis, J., Raff, M., Roberts, K. and Walter, P. (2007). *Molecular Biology of the Cell*. 5(null) ed. Garland Science.

Almeida, M., Moura, G., Pinheiro, T., Machado, J. and Coimbra, J. (1998). Modifications in *Crassostrea gigas* shell composition exposed to high concentrations of lead. *Aquatic Toxicology* **40**, 323–334.

Andersen, C. L., Jensen, J. L. and Ørntoft, T. F. (2004). Normalization of real-time quantitative reverse transcription-PCR data: a model-based variance estimation approach to identify genes suited for normalization, applied to bladder and colon cancer data sets. *Cancer Res* **64**, 5245–5250.

Anlauf, H., D'Croz, L. and O'Dea, A. (2011). A corrosive concoction: The combined effects of ocean warming and acidification on the early growth of a stony coral are multiplicative. *Journal of Experimental Marine Biology and Ecology* **397**, 13–20.

Arnold, K. E., Findlay, H. S., Spicer, J. I., Daniels, C. L. and Boothroyd, D. (2009). Effect of CO_2-related acidification on aspects of the larval development of the European lobster, *Hommarus gammarus. Biogeosciences Discussions* **6**, 3078-3107.

Asscher, Y., Weiner, S. and Boaretto, E. (2011). Variations in Atomic Disorder in Biogenic Carbonate Hydroxyapatite Using the Infrared Spectrum Grinding Curve Method. *Adv. Funct. Mater.* **21**, 3308–3313.

Baker, A. C., Glynn, P. W. and Riegl, B. (2008). Climate change and coral reef bleaching: An ecological assessment of long-term impacts, recovery trends and future outlook. *Estuarine, Coastal and Shelf Science* **80**, 435–471.

Baratte, S., Andouche, A. and Bonnaud, L. (2007). *Engrailed* in cephalopods: a key gene related to the emergence of morphological novelties. *Dev Genes Evol* **217**, 353–362.

Baronnet, A., Cuif, J. P., Dauphin, Y., Farre, B. and Nouet, J. (2008). Crystallization of biogenic Ca-carbonate within organo-mineral micro-domains. Structure of the calcite prisms of the Pelecypod *Pinctada margaritifera* (Mollusca) at the submicron to nanometre ranges. *Mineral. Mag.* **72**, 617–626.

Baumann, H., Talmage, S. C., Gobler, C. J. (2012). Reduced early life growth and survival in a fish in direct response to increased carbon dioxide. *Nature Climate Change* **2**, 28-41.

Beniash, E., Aizenberg, J., Addadi, L. and Weiner, S. (1997). Amorphous calcium carbonate transforms into calcite during sea urchin larval spicule growth. *Proceedings of the Royal Society B: Biological Sciences* **264**, 461–465.

Beniash, E., Ivanina, A., Lieb, N., Kurochkin, I. and Sokolova, I. (2010). Elevated level of carbon dioxide affects metabolism and shell formation in oysters *Crassostrea virginica* (Gmelin). *Mar. Ecol. Prog. Ser.* **419**, 95–108.

Berge, J. A., Bjerkeng, B., Pettersen, O., Schaanning, M. T. and Øxnevad, S. (2006). Effects of increased sea water concentrations of CO_2 on growth of the bivalve *Mytilus edulis* L. *Chemosphere* **62**, 681–687.

Blomberg, J. J., Andersson, M. M. and Fäldt, R. R. (1987). Differential pattern of oncogene and beta-actin expression in leukaemic cells from AML patients. *Br J Haematol* **65**, 83–86.

Bøggild, O. B. (1930). The Shell Structure of the Mollusks. *Acad. Royale Sci. et Lett. Danemark.*

Bondad-Reantaso, M. G., Bondad-Reantaso, M. G., McGladdery, S. E., McGladdery, S. E., Berthe, F. C. J. and Berthe, F. C. J. (2007). Pearl Oyster Health Management. A manual. *FAO Fisheries Technical Paper* **503**.

Borowitzka, M. A. (1981). Photosynthesis and calcification in the articulated coralline red algae *Amphiroa anceps* and *A. foliacea*. *Mar Biol* **62**, 17–23.

Brennand, H. S., Soars, N., Dworjanyn, S. A., Davis, A. R. and BYRNE, M. (2010). Impact of Ocean Warming and Ocean Acidification on Larval Development and Calcification in the Sea Urchin *Tripneustes gratilla*. *PLoS ONE* **5**, e11372–e11372.

Brisson, M., Hall, S., Keith Hamby, R., Park, R. and Srere, H. K. (2004). Optimization of Single and Multiplex Real-Time PCR. In *A-Z of Quantitative PCR*, Intl Univ Line.

Brownlee, C., & Taylor, A. (2004). Calcification in coccolithophores: A cellular perspective. In H. R. Thierstein & J. Young (Eds.), Coccolithophores: from molecular processes to global impact. Berlin: Springer.

Buckwalter, J. A., Glimcher, M. J., Cooper, R. R. and Recker, R. (1995). Bone Biology. *The Journal of Bone and Joint Surgery* **77-A**.

Bustin, S. (2000). Absolute quantification of mRNA using real-time reverse transcription polymerase chain reaction assays. *Journal of Molecular Endocrinology* **25**, 169–193.

Bustin, S. A. (2002). Quantification of mRNA using real-time reverse transcription PCR (RT-PCR): trends and problems. *Journal of Molecular Endocrinology* **29**, 23–39.

Bustin, S. A. (2004). A-Z of Quantitative PCR. *International University Line.*

Bustin, S. A. (2010). Developments in real-time PCR research and molecular diagnostics. *Expert Rev Mol Diagn* **10**, 713–715.

Bustin, S. A. and Nolan, T. (2004). Pitfalls of quantitative real-time reverse-transcription polymerase chain reaction. *J Biomol Tech* **15**, 155–166.

Bustin, S. A., Benes, V., Garson, J. A., Hellemans, J., Huggett, J., Kubista, M., Mueller, R., Nolan, T., Pfaffl, M. W., Shipley, G. L., et al. (2009). The MIQE Guidelines: Minimum Information for Publication of Quantitative Real-Time PCR Experiments. *Clinical Chemistry* **55**, 611–622.

Butler, W. T. W. (1998). Dentin matrix proteins. *Eur. J. Oral Sci.* **106 Suppl 1**, 204–210.

Byrne, M. (2011). Impact of Ocean Warming and Ocean Acidification on Marine Invertebrate Life History Stages — Vulnerabilities and Potential for Persistence in a Changing Ocean. *Oceanography and Marine Biology* 1–42.

Byrne, M., Ho, M., Selvakumaraswamy, P., Nguyen, H. D., Dworjanyn, S. A. and Davis, A. R. (2009). Temperature, but not pH, compromises sea urchin fertilization and early development under near-future climate change scenarios. *Proceedings of the Royal Society B: Biological Sciences* **276**, 1883–1888.

Byrne, M., Ho, M., Wong, E., Soars, N. A., Selvakumaraswamy, P., Shepard-Brennand, H., Dworjanyn, S. A. and Davis, A. R. (2011). Unshelled abalone and corrupted urchins: development of marine calcifiers in a changing ocean. *Proceedings of the Royal Society B: Biological Sciences* **278**, 2376–2383.

Caldeira, K. and Wickett, M. E. (2003). Oceanography: anthropogenic carbon and ocean pH. *Nature* **425**, 365–365.

Carriker, M., Palmer, R. and Sick, L. (1980). Interaction of mineral elements in sea water and shell of oysters (*Crassostrea virginica* (Gmelin)) cultured in controlled and natural systems. *Journal of Experimental Marine Biology and Ecology* **46**, 279–296.

Cartwright, J. H. E. and Checa, A. G. (2006). The dynamics of nacre self-assembly. *Journal of The Royal Society Interface* **4**, 491–504.

Chan, V. B. S., Li, C., Lane, A. C., Wang, Y., Lu, X., Shih, K., Zhang, T. and Thiyagarajan, V. (2012). CO_2-Driven Ocean Acidification Alters and Weakens Integrity of the Calcareous Tubes Produced by the Serpulid Tubeworm, *Hydroides elegans*. *PLoS ONE* **7**, e42718.

Checa, A. G., Esteban-Delgado, F. J. and Rodríguez-Navarro, A. B. (2007). Crystallographic structure of the foliated calcite of bivalves. *Journal of Structural Biology* **157**, 393–402.

Checa, A. G., Okamoto, T. and Ramirez, J. (2006). Organization pattern of nacre in Pteriidae (Bivalvia: Mollusca) explained by crystal competition. *Proceedings of the Royal Society B: Biological Sciences* **273**, 1329–1337.

Chivers, D. P., MaCormick, M. I., Nilsson, G., Munday, P., Watson, S-A., Meekan, M. G., Mitchell, M. D., Corkill, K. C. and Maud, C. (2013). Impaired learning of predators under elevated CO_2: a consequence of neurotransmitter interference. *Global Chance Biology*. doi: 10.1111/gcb. 12291.

Chu, V., Regev, L., Weiner, S. and Boaretto, E. (2008). Differentiating between anthropogenic calcite in plaster, ash and natural calcite using infrared spectroscopy: implications in archaeology. *Journal of Archaeological Science* **35**, 905–911.

Cohen, A. L., McCorkle, D. C., de Putron, S., Gaetani, G. A. and Rose, K. A. (2009). Morphological and compositional changes in the skeletons of new coral recruits reared in acidified seawater: Insights into the biomineralization response to ocean acidification. *Geochemistry* **10**, 7005.

Cooley, S. R. and Doney, S. C. (2009). Anticipating ocean acidification's economic consequences for commercial fisheries. *Environ. Res. Lett.* **4**, 024007.

Cuif, J. P. and Dauphin, Y. (1996). Occurrence of mineralization disturbances in nacreous layers of cultivated pearls produced by *Pinctada margaritifera* var. *cumingi* from French Polynesia. Cornparison with reported shell alterations. *Aquat. Living Resour.* **9**, 187–193.

Dauphin, Y., Ball, A. D., Cotte, M., Cuif, J.-P., Meibom, A., Salomé, M., Susini, J. and Williams, C. T. (2008). Structure and composition of the nacre–prisms transition in the shell of *Pinctada margaritifera* (Mollusca, Bivalvia). *Anal Bioanal Chem* **390**, 1659–1669.

David, E., Tanguy, A., Pichavant, K. and Moraga, D. (2010). Response of the Pacific oyster *Crassostrea gigas* to hypoxia exposure under experimental conditions. *FEBS J.* **272**, 5635–5652.

Decker, G. and Lennarz, W. (1988). Skeletogenesis in the sea urchin embryo. *Development* **103**, 231–247.

Denisov, V., Strong, W., Walder, M., Gingrich, J. and Wintz, H. (2008). Development and Validation of RQI: An RNA Quality Indicator for the Experion™ Automated Electrophoresis System. *Bio-Rad Bulletin*.

Dheda, K., Huggett, J. F., Bustin, S. A., Johnson, M. A., Rook, G. and Zumla, A. (2004). Validation of housekeeping genes for normalizing RNA expression in real-time PCR. *BioTechniques* **37**, 112–119.

Dheilly, N. M., Lelong, C., Huvet, A. and Favrel, P. (2011). Development of a Pacific oyster (*Crassostrea gigas*) 31,918-feature microarray: Identification of reference genes and tissue-enriched expression patterns. *BMC Genomics* **12**, 468–468.

Dickinson, G. H., Ivanina, A. V., Matoo, O. B., Pörtner, H. O., Lannig, G., Bock, C., Beniash, E. and Sokolova, I. M. (2012). Interactive effects of salinity and elevated CO_2 levels on juvenile eastern oysters, *Crassostrea virginica*. *The Journal of Experimental Biology* **215**, 29–43.

Dickson, A. (1987). A comparison of the equilibrium constants for the dissociation of carbonic acid in seawater media. *Deep Sea Research Part A. Oceanographic Research Papers* **34**, 1733–1743.

Dickson, A. G., Sabine, C. L. and Christian, J. R. (2007). Guide to best practices for ocean CO_2 measurements. *3rd ed. IOCCP Report.*

Diederich, S. (2000). Verbreitung und Überlebensfähigkeit von eingeführten Pazifischen Austern *Crassostrea gigas* im Sylter Wattenmeer. 1–3.

Diederich, S. (2005). Differential recruitment of introduced Pacific oysters and native mussels at the North Sea coast: coexistence possible? *Journal of Sea Research* **53**, 269–281.

Diederich, S., Nehls, G., Beusekom, J. E. E. and Reise, K. (2004). Introduced Pacific oysters (*Crassostrea gigas*) in the northern Wadden Sea: invasion accelerated by warm summers? *Helgol Mar Res* **59**, 97–106.

Dorney, N. Melzner, F., Martin, S., Oberhaensli, F., Teyssine, J-L., Bustamante, P., Gattuso, J-P. and Lacoue-Labarthe, T. (2012). Ocean acidification and temperature rise: Effects on calcification during early development of the cuttlefish *Sepia officinalis*. *Marine Biology*. 1432-1793.

Dumousseaud, C., Achterberg, E. and Tyrell, T. (2011). *Practical guide – UK Ocean Acidification Research Programme (UKOARP). Carbonate Chemistry Facility*.

Enríquez-Díaz, M., Pouvreau, S., Chávez-Villalba, J. and Pennec, M. (2009). Gametogenesis, reproductive investment, and spawning behavior of the Pacific giant oyster *Crassostrea gigas*: evidence of an environment-dependent strategy. *Aquacult International* **17**, 491–506.

Erez, J. (2003). Chapter 5. The source of ions for biomineralization in foraminefera and their implications for paleoceanographic proxies. In *Biomineralization*, Reviews in Mineralogy and Geochemistry. In *Biomineralization*, *Reviews in Mineralogy and Geochemistry*. **54.**

Eyster, L. S. and Morse, M. P. (1984). Early shell formation during molluscan embryogenesis, with new studies on the surf clam, *Spisula solidissima*. *American zoologist* 871–882.

Fabry, V. J. (2008). Marine Calcifiers in a High-CO_2 Ocean. *Science* **320**, 1020–1022.

Fang, D., Xu, G., Hu, Y., Pan, C., Xie, L. and Zhang, R. (2011). Identification of Genes Directly Involved in Shell Formation and Their Functions in Pearl Oyster, *Pinctada fucata*. *PLoS ONE* **6** (7): e21860.

FAO (2012). Cultured Aquatic Species Information Programme. *FAO Fisheries and Aquaculture Department*.

Feely, R. A. (2004). Impact of Anthropogenic CO_2 on the $CaCO_3$ System in the Oceans. *Science* **305**, 362–366.

Findlay, H. S., Kendall, M. A., Spicer, J. I. and Widdicombe, S. (2010). Relative influences of ocean acidification and temperature on intertidal barnacle post-larvae at the northern edge of their geographic distribution. *Estuarine, Coastal and Shelf Science* **86**, 675–682.

Frankel, R. B. and Bazylinzki, D. A. (2003). Chapter 4. Biologically induced mineralization by bacteria. In *Biomineralization*, *Reviews in Mineralogy and Geochemistry*. **54.**

Galtsoff, P. S. (1964). The American oyster: *Crassostrea virginica* Gmelin. *Fishery Bulletin of the Fish and Wildlife Service*. **64**.

Gardner, L. D., Mills, D., Wiegand, A., Leavesley, D. and Elizur, A. (2011). Spatial analysis of biomineralization associated gene expression from the mantle organ of the pearl oyster *Pinctada maxima*. *BMC Genomics* **12**, 455.

Gaume, B., Fouchereau-Peron, M., Badou, A., Helléouet, M.-N., Huchette, S. and Auzoux-Bordenave, S. (2011). Biomineralization markers during early shell formation in the European abalone *Haliotis tuberculata*, Linnaeus. *Mar Biol* **158**, 341–353.

Gaylord, B., Hill, T. M., Sanford, E., Lenz, E. A., Jacobs, L. A., Sato, K. N., Russell, A. D. and Hettinger, A. (2011). Functional impacts of ocean acidification in an ecologically critical foundation species. *The Journal of Experimental Biology* **214**, 2586–2594.

Gazeau, F., Quiblier, C., Jansen, J. M., Gattuso, J.-P., Middelburg, J. J. and Heip, C. H. R. (2007). Impact of elevated CO_2 on shellfish calcification. *Geophys. Res. Lett.* **34**.

Gibson, U. E. U., Heid, C. A. C. and Williams, P. M. P. (1996). A novel method for real time quantitative RT-PCR. *Genes Dev* **6**, 995–1001.

Gilbert, S. (2000). Osteogenesis: The Development of Bones. *Developmental Biology. Sundeland (MA): Sinauer Associates* **6.**

Gingrich, J., Rubio, T. and Karlak, C. (2006). Effect of RNA degradation on the data quality in quantitative PCR and microarray experiments. *Bio-Rad Bulletin*.

Glare, E. M., Divjak, M., Bailey, M. J. and Walters, E. H. (2002). beta-Actin and GAPDH housekeeping gene expression in asthmatic airways is variable and not suitable for normalising mRNA levels. *Thorax* **57**, 765–770.

Glynn, P. W. (2000). El Nino-Southern Oscillation mass mortalities of reef corals: a model of high temperature marine extinctions? *Geological Society, London, Special Publications* **178**, 117–133.

Gong, N., Li, Q., Huang, J., Fang, Z., Zhang, G., Xie, L. and Zhang, R. (2008). Culture of outer epithelial cells from mantle tissue to study shell matrix protein secretion for biomineralization. *Cell Tissue Res* **333**, 493–501.

Gosling, E. (2003). Bivalve Molluscs. *Ecology and Culture. Fishing News Book. Blackwell Publishing Ltd.*

Grangeré, K., Ménesguen, A., Lefebvre, S., Bacher, C. and Pouvreau, S. (2009). Modelling the influence of environmental factors on the physiological status of the Pacific oyster *Crassostrea gigas* in an estuarine embayment; The Baie des Veys (France). *Journal of Sea Research* **62**, 147–158.

Gu, K., Chang, S., Ritchie, H. H., Clarkson, B. H. and Rutherford, R. B. (2000). Molecular cloning of a human dentin sialophosphoprotein gene. *Eur. J. Oral Sci.* **108**, 35–42.

Gueguen, Y., Cadoret, J.-P., Flament, D., Barreau-Roumiguière, C., Girardot, A.-L., Garnier, J., Hoareau, A., Bachère, E. and Escoubas, J.-M. (2003). Immune gene discovery by expressed sequence tags generated from hemocytes of the bacteria-challenged oyster, *Crassostrea gigas. Gene* **303**, 139–145.

Gueta, R. R., Natan, A. A., Addadi, L. L., Weiner, S. S., Refson, K. K. and Kronik, L. L. (2007). Local atomic order and infrared spectra of biogenic calcite. *Angew Chem Int Ed Engl* **46**, 291–294.

Gutowska, M., Pörtner, H. and Melzner, F. (2008). Growth and calcification in the cephalopod Sepia officinalis under elevated seawater pCO_2. *Mar. Ecol. Prog. Ser.* **373**, 303–309.

Guyer, R. and Koshland, D. (1989). The Molecule of the Year. *Science* **246**, 1543–1546.

Hammond, L. M. and Hofmann, G. E. (2012). Early developmental gene regulation in *Strongylocentrotus purpuratus* embryos in response to elevated CO_2 seawater conditions. *The Journal of Experimental Biology* **215**, 2445–2454.

Hasse, B. B., Ehrenberg, H. H., Marxen, J. C. J., Becker, W. W. and Epple, M. M. (2000). Calcium carbonate modifications in the mineralized shell of the freshwater snail *Biomphalaria glabrata*. *Chemistry* **6**, 3679–3685.

Hauton, C. and Hawkins, L. (1998). The use of the neutral red retention assay to examine the effects of temperature and salinity on haemocytes of the European flat oyster *Ostrea edulis* (L). *Comparative Biochemistry and Biochemistry and Physiology Part B* **119,** 619-623.

Hauton, C., Hawkins, L. E. and Hutchinson, S. (2000). The effects of salinity on the interaction between a pathogen (*Listonella anguillarum*) and components of a host (*Ostrea edulis*) immune system. *Comparative Biochemistry and Physiology, Part B* **127**, 203–212.

Havenhand, J. and Schlegel, P. (2009). Near-future levels of ocean acidification do not affect sperm motility and fertilization kinetics in the oyster *Crassostrea gigas*. *Biogeosciences* **6**, 3009–3015.

Havenhand, J. N., Buttler, F.-R., Thorndyke, M. C. and Williamson, J. E. (2008). Near-future levels of ocean acidification reduce fertilization success in a sea urchin. *Curr. Biol.* **18**, R651–R652.

Heid, C. A., Stevens, J., Livak, K. J. and Williams, P. M. (1996). Real time quantitative PCR. *Genome Research* **6,** 986-994.

Heilmayer, O., Digialleonardo, J., Qian, L. and Roesijadi, G. (2008). Stress tolerance of a subtropical *Crassostrea virginica* population to the combined effects of temperature and salinity. *Estuarine, Coastal and Shelf Science* **79**, 179–185.

Hellemans, J. J., Mortier, G. G., De Paepe, A. A., Speleman, F. F. and Vandesompele, J. J. (2007). qBase relative quantification framework and software for management and automated analysis of real-time quantitative PCR data. *CORD Conference Proceedings* **8**, R19–R19.

Higuera-Ruiz, R. and Elorza, J. (2009). Biometric, microstructural, and high-resolution trace element studies in *Crassostrea gigas* of Cantabria (Bay of Biscay, Spain): Anthropogenic and seasonal influences. *Estuarine, Coastal and Shelf Science* **82**, 201–213.

Hoegh-Guldberg, O., Mumby, P. J., Hooten, A. J., Steneck, R. S., Greenfield, P., Gomez, E., Harvell, C. D., Sale, P. F., Edwards, A. J., Caldeira, K., Knowlton, N. and Eakin, C. M. et al. (2007). Coral reefs under rapid climate change and ocean acidification. *Science* **318** (5857), 1737-1742.

Hsu, C. (1997). Infrared spectroscopy. *Handbook of Instrumental Techniques for Analytical Chemistry,* Chapter 15, 247-283.

Huggett, J., Dheda, K., Bustin, S. and Zumla, A. (2005). Real-time RT-PCR normalisation; strategies and considerations. *Genes Immun* **6**, 279–284.

Iijima, M., Takeuchi, T., Sarashina, I. and Endo, K. (2008). Expression patterns of *engrailed* and *dpp* in the gastropod *Lymnaea stagnalis*. *Dev Genes Evol* **218**, 237–251.

Jackson, D. J., Wörheide, G. and Degnan, B. M. (2007). Dynamic expression of ancient and novel molluscan shell genes during ecological transitions. *BMC Evol Biol* **7**, 160.

Jacobs, D. K., Wray, C. G., Wedeen, C. J., Kostriken, R., DeSalle, R., Staton, J. L., Gates, R. D. and Lindberg, D. R. (2000). Molluscan *engrailed* expression, serial organization, and shell evolution. *Evol. Dev.* **2**, 340–347.

Ji J., Ge Y., Balsam, W., Damuth, J. E. and Chen, J (2009). Rapid identification of dolomite using Fourier Transform Infrared Spectroscopy (FTIR): A fast method for identifying Heinrich events in IODP Site U1308. *Marine Geology* **258** (1), 60-68.

Jin, L. and Lloyd, R. V. (1997). *In situ* hybridization: methods and applications. *Journal of clinical laboratory analysis* **11**, 2–9.

Jones, G. C. and Jackson, B. (1994). Infrared Transmission Spectra of Carbonate Minerals. *Journal of Applied Crystallography* **27***,* 132.

Joubert, C., Piquemal, D., Marie, B., Manchon, L., Pierrat, F., Zanella-Cléon, I., Cochennec-Laureau, N., Gueguen, Y. and Montagnani, C. (2010). Transcriptome and proteome analysis of *Pinctada margaritifera* calcifying mantle and shell: focus on biomineralization. *BMC Genomics* **11**, 613–613.

Kádár, E. (2008). Haemocyte response associated with induction of shell regeneration in the deep-sea vent mussel *Bathymodiolus azoricus* (Bivalvia: Mytilidae). *Journal of Experimental Marine Biology and Ecology* **362**, 71–78.

Kádár, E., Lobo-da-Cunha, A. and Azevedo, C. (2009). Mantle-to-shell $CaCO_3$ transfer during shell repair at different hydrostatic pressures in the deep-sea vent mussel *Bathymodiolus azoricus* (Bivalvia: Mytilidae). *Mar Biol* **156**, 959–967.

Kheder, B. R., Moal, J. and Robert, R. (2010). Impact of temperature on larval development and evolution of physiological indices in *Crassostrea gigas*. *Aquaculture* **309**, 286–289.

Killian, C. E., Croker, L. and Wilt, F. H. (2010). SpSM30 gene family expression patterns in embryonic and adult biomineralized tissues of the sea urchin, *Strongylocentrotus purpuratus*. *Gene Expr. Patterns* **10**, 135–139.

Kimura, R., Tamaki, H., Ono, T., Onitsuka, T. and Nojiri, Y. (2011). Effects of elevated pCO_2 on the early development of the commercially important gastropod, Ezo abalone *Haliotis discus hannai. Fisheries Oceanography* **20** (5), 357-366.

Kin, K., Kakoi, S. and Wada, H. (2009). A novel role for dpp in the shaping of bivalve shells revealed in a conserved molluscan developmental program. *Developmental Biology* **329**, 152–166.

Kniprath, E. (1980). Larval development of the shell and the shell gland in Mytilus (Bivalvia). *Wilhelm Roux' Archiv* **188**, 201–204.

Kobayashi, I. (2008). Scanning electron microscopic structure of the prismatic layer in the Bivalvia. *Front Mater Sci China* **2**, 246–252.

Kobayashi, I. and Samata, T. (2006). Bivalve shell structure and organic matrix. *Materials Science and Engineering: C* **26**, 692–698.

Kong, Y., Jing, G., Yan, Z., LI, C., Gong, N., Zhu, F., Li, D., Zhang, Y., Zheng, G., Wang, H., et al. (2009). Cloning and Characterization of Prisilkin-39, a Novel Matrix Protein Serving a Dual Role in the Prismatic Layer Formation from the Oyster *Pinctada fucata. Journal of Biological Chemistry* **284**, 10841–10854.

Kono, M., Hayashi, N. and Samata, T. (2000). Molecular Mechanism of the Nacreous Layer Formation in *Pinctada maxima*. *Biochemical and Biophysical Research Communications* **269**, 213–218.

Kudo, M., Kameda, J., Saruwatari, K., Ozaki, N., Okano, K., Nagasawa, H. and Kogure, T. (2009). Microtexture of larval shell of oyster, *Crassostrea nippona*: A FIB-TEM study. *Journal of Structural Biology* 1–5.

Kuffner, I. B., Andersson, A., Jokiel, P. L., Rodgers, K. and Mackenzie, F. (2007). Decreased abundance of crustose algae during to ocean acidification. *Nature Geoscience* **1** (2), 114-117.

Kurihara, H., Asai, T., Kato, S. and Ishimatsu, A. (2008). Effects of elevated pCO_2 on early development in the mussel *Mytilus galloprovincialis*. *Aquat. Biol.* **4**, 225–233.

Kurihara, H., Kato, S. and Ishimatsu, A. (2007). Effects of increased seawater pCO_2 on early development of the oyster *Crassostrea gigas. Aquat. Biol.* **1**, 91–98.

Kurihara, H., Takano, Y., Kurokawa, D. and Akasaka, K. (2012). Ocean acidification reduces biomineralisation-related gene expression in the sea urchin *Hemicentrotus pulcherrimus. Marine Biology* **159** (12), 2819-2826.

LaBarbera, M. (1974). Calcification of the first larval shell of *Tridacna squamosa* (Tridacnidae: Bivalvia). *Mar Biol* **25**, 233–238.

Langdon, C. and Atkinson, M. J. (2005). Effect of elevated pCO_2 on photosynthesis and calcification of corals and interactions with seasonal change in temperature/irradiance and nutrient enrichment. *J. Geophys. Res.* **110**.

Lannig, G., Eilers, S., Pörtner, H. and Sokolova, I. (2010). Impact of Ocean Acidification on Energy Metabolism of Oyster, *Crassostrea gigas*—Changes in Metabolic Pathways and Thermal Response. *Marine Drugs* **8**, 2318–2339.

Lee, S. W. and Choi, C. S. (2007a). The correlation between organic matrices and biominerals (myostracal prism and folia) of the adult oyster shell, *Crassostrea gigas*. *Micron* **38**, 58–64.

Lee, S. W. and Choi, C. S. (2007b). High-Rate Growth of Calcium Carbonate Crystal Using Soluble Protein from Diseased Oyster Shell. *Crystal Growth & Design* **7**, 1463–1468.

Lee, S. W., Hong, S. M. and Choi, C. S. (2006a). Characteristics of calcification processes in embryos and larvae of the Pacific oyster, *Crassostrea gigas*. *B Mar Sci*. **78,** 309-317.

Lee, S. W., Jang, Y.-N. and Kim, J.-C. (2011). Characteristics of the Aragonitic Layer in Adult Oyster Shells, *Crassostrea gigas:* Structural Study of Myostracum including the Adductor Muscle Scar. *Evid-Based Compl Alt* **2011**, 1–10.

Lee, S. W., Kim, Y. M., Choi, H. S., Yang, J. M. and Choi, C. S. (2006b). Primary Structure of Myostracal Prism Soluble Protein (MPSP) in Oyster Shell, *Crassostrea gigas. Protein J* **25**, 288–294.

Lefever, S., Hellemans, J., Pattyn, F., Przybylski, D. R., Taylor, C., Geurts, R., Untergasser, A. and Vandesompele, J. (2009). RDML: structured language and reporting guidelines for real-time quantitative PCR data. *Nucleic Acids Res.* **37**, 2065–2069.

Levi-Kalisman, Y., Falini, G., Addadi, L. and Weiner, S. (2001). Structure of the nacreous organic matrix of a bivalve mollusk shell examined in the hydrated state using cryo-TEM. *JOURNAL OF STRUCTURAL BIOLOGY* **135**, 8–17.

Lewis, E., Wallace, D. and Allison, L. J. (1998). *Program Developed for CO_2 System Calculations*. Carbon Dioxide Information Analysis Center, Oak Ridge National Laboratory, U.S. Department of Energy, Oak Ridge, Tennessee.

Li, S., Xie, L., Zhang, C., Zhang, Y., Gu, M. and Zhang, R. (2004). Cloning and expression of a pivotal calcium metabolism regulator: calmodulin involved in shell formation from pearl oyster (*Pinctada fucata*). *Comp. Biochem. Physiol. B, Biochem. Mol. Biol.* **138**, 235–243.

Lie, Y. S. and Petropoulos, C. J. (1998). Advances in quantitative PCR technology: 5′ nuclease assays. *Current Opinion in Biotechnology* **9**, 43–48.

Liu, H.-L., Liu, S.-F., Ge, Y.-J., Liu, J., Wang, X.-Y., Xie, L.-P., Zhang, R.-Q. and Wang, Z. (2007). Identification and Characterization of a Biomineralization Related Gene PFMG1 Highly Expressed in the Mantle of *Pinctada fucata. Biochemistry* **46**, 844–851.

Liu, W., Huang, X., Lin, J. and He, M. (2012). Seawater Acidification and Elevated Temperature Affect Gene Expression Patterns of the Pearl Oyster *Pinctada fucata*. *PLoS ONE* **7**, e33679.

Livak, K. J. and Schmittgen, T. D. (2001). Analysis of Relative Gene Expression Data Using Real-Time Quantitative PCR and the 2−ΔΔCT Method. *Methods* **25**, 402–408.

Livingston, B. T., Killian, C. E., Wilt, F., Cameron, A., Landrum, M. J., Ermolaeva, O., Sapojnikov, V., Maglott, D. R., Buchanan, A. M. and Ettensohn, C. A. (2006). A genome-wide analysis of biomineralization-related proteins in the sea urchin *Strongylocentrotus purpuratus. Developmental Biology* **300**, 335–348.

Lopez, E., Milet, C., Lamghari, M., Pereira Mouries, L., Borzeix, S. and Berland, S. (2004). The Dualism of Nacre. *KEM* **254-256**, 733–736.

Lowenstam, H. (1989). Spicular Morphology and Mineralogy in Some Pyuridae (Ascidiacea). *B Mar Sci* **45**, 243–252.

Lowenstam, H. A. and Weiner, S. (1989). On Biomineralization. *Oxford University Press, New York.* 324

Lowenstam, H. A. H. (1981). Minerals formed by organisms. *Science* **211**, 1126–1131.

MacDonald, J., Freer, A. and Cusack, M. (2010). Alignment of Crystallographic c-Axis throughout the Four Distinct Microstructural Layers of the Oyster *Crassostrea gigas. Crystal Growth & Design* **10**, 1243–1246.

Mann, K., Siedler, F., Treccani, L., Heinemann, F. and Fritz, M. (2007). Perlinhibin, a Cysteine-, Histidine-, and Arginine-Rich Miniprotein from Abalone (*Haliotis laevigata*) Nacre, Inhibits In Vitro Calcium Carbonate Crystallization. *Biophysical Journal* **93**, 1246–1254.

Mann, K., Weiss, I. M., André, S., Gabius, H. J. and Fritz, M. (2000). The amino-acid sequence of the abalone (*Haliotis laevigata*) nacre protein perlucin. Detection of a functional C-type lectin domain with galactose/mannose specificity. *Eur. J. Biochem.* **267**, 5257–5264.

Marin, F. and Luquet, G. (2004). Molluscan shell proteins. *Comptes Rendus Palevol* **3**, 469–492.

Marin, F., Amons, R., Guichard, N., Stigter, M., Hecker, A., Luquet, G., Layrolle, P., Alcaraz, G., Riondet, C. and Westbroek, P. (2005). Caspartin and calprismin, two proteins of the shell calcitic prisms of the Mediterranean fan mussel *Pinna nobilis*. *Journal of Biological Chemistry* **280**, 33895–33908.

Marin, F., Corstjens, P., de Gaulejac, B., de Vrind-De Jong, E. and Westbroek, P. (2000). Mucins and Molluscan Calcification. *Journal of Biological Chemistry* **275**, 20667–20675.

Marsh, M. E., Chang, D. K. and King G. C. (1992). Isolation and characterization of a novel acidic polysaccharide and containing tartrate and glyoxylate residues from the mineralized scales of a unicellular coccolithophorid alga *Pleurochrysis carterae*. *Journal of Biological Chemistry* **267** (28), 20507-20512.

Marsh, M. E (2003). Regulation of $CaCO_3$ formation in coccolithophores. *Comparative Biochemistry and Physiology, Part B* **136**, 743-754.

Martin, S., Richier, S., Pedrotti, M.-L., Dupont, S., Castejon, C., Gerakis, Y., Kerros, M.-E., Oberhänsli, F., Teyssié, J.-L., Jeffree, R., et al. (2011). Early development and molecular plasticity in the Mediterranean sea urchin *Paracentrotus lividus* exposed to CO_2-driven acidification. *The Journal of Experimental Biology* **214**, 1357–1368.

Matozzo, V. and Marin, M. (2011). Bivalve immune responses and climate changes: is there a relationship? *ISJ* **8**, 70–77.

Matozzo, V., Monari, M., Foschi, J., Serrazanetti, G. P., Cattani, O. and Marin, M. G. (2006). Effects of salinity on the clam *Chamelea gallina*. Part I: alterations in immune responses. *Mar Biol* **151**, 1051–1058.

McPherson, M. J. and Moller, S. G. (2006). *PCR (THE BASICS (Garland Science))*. 2nd ed. Taylor & Francis.

Medaković, D. (2000). Carbonic anhydrase activity and biomineralization process in embryos, larvae and adult blue mussels *Mytilus edulis* L. *Helgol Mar Res* **54**, 1–6.

Medaković, D., Popović, S., Grzeta, B., Plazonic, M. and Hrs-Brenko, M. (1997). X-ray diffraction study of calcification processes in embryos and larvae of the brooding oyster *Ostrea edulis*. *Mar Biol* **129**, 615–623.

Mehrbach, C. (1973). Measurement of the Apparent Dissociation Constants of Carbonic Acid in Seawater at Atmospheric Pressure. *Limnology and Oceanography* **18** (6), 897-907.

Michaelidis, B., Ouzounis, C., Paleras, A. and Pörtner, H. O. (2005). Effects of long-term moderate hypercapnia on acid-base balance and growth rate in marine mussels *Mytilus galloprovincialis*. *Mar. Ecol. Prog. Ser.* **293**, 109–118.

Michenfelder, M. M., Fu, G. G., Lawrence, C. C., Weaver, J. C. J., Wustman, B. A. B., Taranto, L. L., Evans, J. S. J. and Morse, D. E. D. (2003). Characterization of two molluscan crystal-modulating biomineralization proteins and identification of putative mineral binding domains. *Biopolymers* **70**, 522–533.

Miller, A. W. A., Reynolds, A. C. A., Sobrino, C. C. and Riedel, G. F. G. (2009). Shellfish face uncertain future in high CO_2 world: influence of acidification on oyster larvae calcification and growth in estuaries. *CORD Conference Proceedings* **4**, e5661–e5661.

Minchin, D. and Gollasch, S. (2008). *Crassostrea gigas*. DAISIE Delivering Alien Invasive Species Inventories for Europe.

Miossec, L., Le Deuff, R. and Goulletquer, P. (2009). Alien species alert: *Crassostrea gigas* (Pacific oyster). *ICES Cooperative Research Report* No. **299,** pp 42

Miyamoto, H. H., Miyoshi, F. F. and Kohno, J. J. (2005). The carbonic anhydrase domain protein nacrein is expressed in the epithelial cells of the mantle and acts as a negative regulator in calcification in the mollusc *Pinctada fucata*. *Zoolog Sci* **22**, 311–315.

Miyamoto, H., Hamaguchi, M. and Okoshi, K. (2002). Analysis of genes expressed in the mantle of oyster *Crassostrea gigas*. *Fisheries Science* **68**, 651–658.

Miyamoto, H., Miyashita, T., Okushima, M., Nakano, S., Morita, T. and Matsushiro, A. (1996). A carbonic anhydrase from the nacreous layer in oyster pearls. *Proc. Natl. Acad. Sci. U.S.A.* **93**, 9657–9660.

Miyamoto, H., Yano, M. and Miyashita, T. (2003). Similarities in the structure of nacrein, the shell-matrix protein, in a bivalve and a gastropod. *Journal of Molluscan Studies* **69**, 87–89.

Miyashita, T., TAKAGI, R., Miyamoto, H. and Matsushiro, A. (2002). Identical carbonic anhydrase contributes to nacreous or prismatic layer formation in *Pinctada fucata* (Mollusca: Bivalvia). *The Veliger* **45**, 250–255.

Miyazaki, Y., Nishida, T., Aoki, H. and Samata, T. (2010). Expression of genes responsible for biomineralization of *Pinctada fucata* during development. *Comparative Biochemistry and Physiology, Part B* **155**, 241–248.

Moltschaniwskyj, N. (2006). Edible shellfish: biology and science. *Handbook of Food Science, Technology and Engeneering. CRC Press, Florida.* 1-36.

Moshel, S. M., Levine, M. and Collier, J. R. (1998). Shell differentiation and engrailed expression in the *Ilyanassa embryo*. *Dev Genes Evol* **208**, 135–141.

Mount, A. S., Wheeler, A. P., Paradkar, R. P. and Snider, D. (2004). Hemocyte-mediated shell mineralization in the eastern oyster. *Science* **304**, 297–300.

Moutahir-Belqasmi, F. and Balmain, N. (2001). Effect of water soluble extract of nacre (*Pinctada maxima*) on alkaline phosphatase activity and Bcl-2 expression in primary cultured osteoblasts from neonatal rat calvaria. *Journal of Materials Science: Materials in Medicine* **12** (1), 1-6.

Mucci, A. (1983). The solubility of calcite and aragonite in seawater at various salinities, temperatures, and one atmosphere total pressure. *American Journal of Science* **283**, 780–799.

Nakahara, H. (1991). Chapter 4.2. Nacre formation in bivalve and gastropod molluscs. *Mechanisms and phylogeny of mineralization in biological systems. Springer-Verlag, Tokyo.* 343-350.

Nederbragt, A. J., van Loon, A. E. and Dictus, W. J. A. G. (2002). Expression of *Patella vulgata* Orthologs of engrailed and dpp-BMP2/4 in Adjacent Domains during Molluscan Shell Development Suggests a Conserved Compartment Boundary Mechanism. *Developmental Biology* **246**, 341–355.

Nehls, G. and Büttger, H. (2007). Spread of the Pacific oyster *Crassostrea gigas* in the Wadden Sea. *Causes and Consequences of a Successful Invasion. BioConsult SH, Husum, on behalf of the Common Wadden Sea Secretariat, Wilhelmshaven, HARBASINS report, Husum, Germany*.

Nehls, G., Diederich, S., Thieltges, D. W. and Strasser, M. (2006). Wadden Sea mussel beds invaded by oysters and slipper limpets: competition or climate control? *Helgol Mar Res* **60**, 135–143.

Nicholls, R. J., Wong, P. P., Burkett, V., Codignotto, J., Hay, J., McLean, R. F., Ragoonaden, S. and Woodroffe, C. D. (2007). Coastal systems and low-lying areas. In *IPCC, 2007: Climate Change 2007: Impacts, Adaptation and Vulnerability. Contribution of Working Group II to the Fourth Assessment Report of the Intergovernmental Panel on Climate Change* (eds. Parry, M. L., Canziani, O. F., Palutikof, J. P., van der Linden, P. J., and Handson, C. E., pp. 315–356. Cambridge University Press.

Nolan, T. (2004). Chapter 13 - Getting Started - The Basics of Setting up a qPCR Assay. In *A-Z of Quantitative PCR*, Intl Univ Line.

Nolan, T., Hands, R. E. and Bustin, S. A. (2006). Quantification of mRNA using real-time RT-PCR. *Nat Protoc* **1**, 1559–1582.

Nudelman, F., Chen, H. H., Goldberg, H. A., Weiner, S. and Addadi, L. (2007). Spiers memorial lecture: Lessons from biomineralization: comparing the growth strategies of mollusc shell prismatic and nacreous layers in *Atrina rigida*. *Faraday Discuss* **136**, 9–25.

Orr, J. C., Fabry, V. J., Aumont, O., Bopp, L., Doney, S. C., Feely, R. A., Gnanadesikan, A., Gruber, N., Ishida, A., Joos, F., et al. (2005). Anthropogenic ocean acidification over the twenty-first century and its impact on calcifying organisms. *Nature* **437**, 681–686.

O'Donnell, M., Todgham, A., Sewell, M., Hammond, L., Ruggiero, K., Fangue, N., Zippay, M. and Hofmann, G. (2010). Ocean acidification alters skeletogenesis and gene expression in larval sea urchins. *Mar. Ecol. Prog. Ser.* **398**, 157–171.

Pansch, C., Nasrolahi, A., Appelhans, Y. S. and Wahl, M. (2012). Impacts of ocean warming and acidification on the larval development of the barnacle *Amphibalanus improvisus*. *Journal of Experimental Marine Biology and Ecology* **420-421**, 48–55.

Parker, L. M. and ROSS, P. M. (2009). The effect of ocean acidification and temperature on the fertilization and embryonic development of the Sydney rock oyster *Saccostrea glomerata*. *Global Change Biology* **15**, 2123–2136.

Parker, L. M., Ross, P. M. and O'Connor, W. A. (2010a). Populations of the Sydney rock oyster, *Saccostrea glomerata*, vary in response to ocean acidification. *Mar Biol* **158**, 689–697.

Parker, L. M., Ross, P. M. and O'Connor, W. A. (2010b). Comparing the effect of elevated pCO_2 and temperature on the fertilization and early development of two species of oysters. *Mar Biol* **157**, 2435–2452.

Pfaffl, M. W. (2004). Quantification strategies in real-time PCR. In *A-Z of Quantitative PCR*, pp. 87–112. Intl Univ Line.

Pfaffl, M. W., Horgan, G. W. and Dempfle, L. (2002). Relative expression software tool (REST) for group-wise comparison and statistical analysis of relative expression results in real-time PCR. *Nucleic Acids Res.* **30**, e36–e36.

Poduska, K. M., Regev, L., Boaretto, E., Addadi, L., Weiner, S., Kronik, L. and Curtarolo, S. (2011). Decoupling local disorder and optical effects in infrared spectra: differentiating between calcites with different origins. *Adv. Mater. Weinheim* **23**, 550–554.

Politi, Y. (2004). Sea Urchin Spine Calcite Forms via a Transient Amorphous Calcium Carbonate Phase. *Science* **306**, 1161–1164.

Politi, Y., Metzler, R. A., Abrecht, M., Gilbert, B., Wilt, F. H., Sagi, I., Addadi, L., Weiner, S., Gilbert, P. U. P. A. and Gilbert, P. (2008). Transformation mechanism of amorphous calcium carbonate into calcite in the sea urchin larval spicule. *Proceedings of the National Academy of Sciences* **105**, 17362–17366.

Range, P., Chícharo, M. A., Ben-Hamadou, R., Piló, D., Matias, D., Joaquim, S., Oliveira, A. P. and Chícharo, L. (2011). Calcification, growth and mortality of juvenile clams Ruditapes decussatus under increased pCO_2 and reduced pH: Variable responses to ocean acidification at local scales? *Journal of Experimental Marine Biology and Ecology* **396**, 177–184.

Raven, J. A., Caldeira, K., Elderfield, H., Hoegh-Guldberg, O., Liss, P., Riebesell, U., Sheperd, J. S., Turley, C. and Watson, S. A. (2005). Ocean acidification due to increasing atmospheric carbon dioxide. *The Royal Society.*

Raz, S. S., Testeniere, O. O., Hecker, A. A., Weiner, S. S. and Luquet, G. G. (2002). Stable amorphous calcium carbonate is the main component of the calcium storage structures of the crustacean Orchestia cavimana. *The Biological Bulletin* **203**, 269–274.

Regev, L., Poduska, K. M., Addadi, L., Weiner, S. and Boaretto, E. (2010). Distinguishing between calcites formed by different mechanisms using infrared spectrometry: archaeological applications. *Journal of Archaeological Science* **37**, 3022–3029.

Rico-Villa, B., Pouvreau, S. and Robert, R. (2009). Influence of food density and temperature on ingestion, growth and settlement of Pacific oyster larvae, *Crassostrea gigas*. *Aquaculture* **287**, 395–401.

Ries (2011). Skeletal mineralogy in a high-CO_2 world. *Journal of Experimental Marine Biology and Ecology* **403**, 11–11.

Roer, R. and Dillaman, R. (1984). The Structure and Calcification of the Crustacean Cuticle. *Integr Comp Biol* **24**, 893–909.

Salas, C., Marina, P., Checa, A. G. and Rueda, J. L. (2012). The Periostracum of Digitaria Digitaria (Bivalvia: Astartidae): Formation and Structure. *Journal of Molluscan Studies* **78**, 34–43.

Samata, T., Hayashi, N., Kono, M., Hasegawa, K., Horita, C. and Akera, S. (1999). A new matrix protein family related to the nacreous layer formation of *Pinctada fucata*. *FEBS Letters* **462**, 225–229.

Sarashina, I. and Endo, K. (2001). The Complete Primary Structure of Molluscan Shell Protein 1 (MSP-1), an Acidic Glycoprotein in the Shell Matrix of the Scallop *Patinopecten yessoensis. Mar. Biotechnol.* **3**, 362–369.

Shen, X., Belcher, A. M., Hansma, P. K., Stucky, G. D. and Morse, D. E. (1997). Molecular cloning and characterization of lustrin A, a matrix protein from shell and pearl nacre of *Haliotis rufescens*. *Journal of Biological Chemistry* **272**, 32472–32481.

Stenzel, H. B. (1964). Oysters: Composition of the Larval Shell. *Science* **145**, 155–156.

Stumpp, M., Dupont, S. and Thorndyke, M. (2011a). CO_2 induced seawater acidification impacts sea urchin larval development II: Gene expression patterns in pluteus larvae. *Comparative Biochemistry and Physiology - Part A: Molecular & Integrative Physiology* 320–330.

Stumpp, M., Wren, J., Melzner, F., Thorndyke, M. C. and Dupont, S. T. (2011b). CO_2 induced seawater acidification impacts sea urchin larval development I: elevated metabolic rates decrease scope for growth and induce developmental delay. *Comparative Biochemistry and Physiology - Part A: Molecular & Integrative Physiology* **160**, 331–340.

Sudo, S., Fujikawa, T., Nagakura, T., Ohkubo, T., Sakaguchi, K., Tanaka, M., Nakashima, K. and Takahashi, T. (1997). Structures of mollusc shell framework proteins. *Nature* **387**, 563–564.

Sussarellu, R., Fabioux, C., Le Moullac, G., Fleury, E. and Moraga, D. (2010). Transcriptomic response of the Pacific oyster *Crassostrea gigas* to hypoxia. *Mar Genomics* **3**, 133–143.

Suzuki, M. M., Murayama, E. E., Inoue, H. H., Ozaki, N. N., Tohse, H. H., Kogure, T. T. and Nagasawa, H. H. (2004). Characterization of Prismalin-14, a novel matrix protein from the prismatic layer of the Japanese pearl oyster (*Pinctada fucata)*. *CORD Conference Proceedings* **382**, 205–213.

Suzuki, M. M. and Hiromichi, N. (2007). The structure-function relationship analyses of Prismalin-14 from the Japanese pearl oyster, Pinctada fucata. *FEBS Journal* **274** (19), 5158-5166.

Suzuki, M., Saruwatari, K., Kogure, T., Yamamoto, Y., Nishimura, T., Kato, T. and Nagasawa, H. (2009). An acidic matrix protein, Pif, is a key macromolecule for nacre formation. *Science* **325**, 1388–1390.

Suzuki, S., Haruyama, N., Nishimura, F. and Kulkarni, A. B. (2012). Dentin sialophosphoprotein and dentin matrix protein-1: Two highly phosphorylated proteins in mineralized tissues. *Arch. Oral Biol.* **57**, 1165–1175.

Takeuchi, T. and Endo, K. (2006). Biphasic and Dually Coordinated Expression of the Genes Encoding Major Shell Matrix Proteins in the Pearl Oyster *Pinctada fucata. Mar. Biotechnol.* **8**, 52–61.

Takeuchi, T. T., Kawashima, T. T., Koyanagi, R. R., Gyoja, F. F., Tanaka, M. M., Ikuta, T. T., Shoguchi, E. E., Fujiwara, M. M., Shinzato, C. C., Hisata, K. K., et al. (2012). Draft genome of the pearl oyster *Pinctada fucata*: a platform for understanding bivalve biology. *DNA Res* **19**, 117–130.

Talmage, S. C. and Gobler, C. J. (2009). The effects of elevated carbon dioxide concentrations on the metamorphosis, size, and survival of larval hard clams (*Mercenaria mercenaria*), bay scallops (*Argopecten irradians*), and Eastern oysters (*Crassostrea virginica*). *Limnol. Oceangr.* **54**, 2072–2080.

Talmage, S. C. S. and Gobler, C. J. C. (2010). Effects of past, present, and future ocean carbon dioxide concentrations on the growth and survival of larval shellfish. *CORD Conference Proceedings* **107**, 17246–17251.

Tambutté, S., Holcomb, M., Ferrier-Pagès, C., Reynaud, S., Tambutté, É., Zoccola, D. and Allemand, D. (2011). Coral biomineralization: From the gene to the environment. *Journal of Experimental Marine Biology and Ecology* **408**, 58–78.

Taylor, A. R., Russel, M. A., Harper, G. M., Collins, T. T. and Brownlee, C. (2007). Dynamics of formation and secretion of heterococcoliths by *Coccolithus pelagicus* ssp. *braarudii. European Journal of Phycology* **42**, 125-136.

Tsukamoto, D., Sarashina, I. and Endo, K. (2004). Structure and expression of an unusually acidic matrix protein of pearl oyster shells. *Biochemical and Biophysical Research Communications* **320**, 1175–1180.

Vandesompele, J., De Preter, K., Pattyn, F., Poppe, B., Van Roy, N., De Paepe, A. and Speleman, F. (2002). Accurate normalization of real-time quantitative RT-PCR data by geometric averaging of multiple internal control genes. *Genome Biol.* **3**, research0034.1–0034.11.

Veis, A. (2003). Chapter 9. Mineralization in organic matrix frameworks. In Biomineralization, *Reviews in Mineralogy and Geochemistry*. **54.**

Veis, A. A., Wei, K. K., Sfeir, C. C., George, A. A. and Malone, J. J. (1998). Properties of the (DSS)n triplet repeat domain of rat dentin phosphophoryn. *Eur. J. Oral Sci.* **106**, 234–238.

Walne, P. (1979). Culture of Bivalve Molluscs, 50 years Experience at Conway. *Fishing News.*

Wang, X., Liu, S., Xie, L., Zhang, R. and Wang, Z. (2011). *Pinctada fucata* mantle gene 3 (PFMG3) promotes differentiation in mouse osteoblasts (MC3T3-E1). *Comp. Biochem. Physiol. B, Biochem. Mol. Biol.* **158**, 173–180.

Wanninger, A. and Haszprunar, G. (2001). The Expression of an Engrailed Protein During Embryonic Shell Formation of the Tusk-Shell, *Antalis entalis* (Mollusca, Scaphopoda). *Evol. Dev.* **3**, 312–321.

Watson, S. A., Southgate, P. C., Tyler, P. A. and Peck, L. S. (2009). Early larval development of the Sydney rock oyster Saccostrea glomerata under near-future predictions of CO_2-driven ocean acidification. *Jornal of Shellfish Research* **28**, 431–437.

Weiner, S. (2010). *Microarchaeology*. Cambridge University Press, Cambridge.

Weiner, S. and Dove, P. M. (2003). Chapter 1. An overview of biomineralization processes and the problem of the vital effect. In *Biomineralization*, *Reviews in Mineralogy and Geochemistry.* **54.**

Weiner, S., Levi-Kalisman, Y., Raz, S. and Addadi, L. (2003). Biologically formed amorphous calcium carbonate. *Connect Tissue Res* **44 Suppl 1**, 214–218.

Weiner, S., Traub, W. and Parker, S. B. (1984). Macromolecules in Mollusc Shells and Their Functions in Biomineralization [and Discussion]. *Philosophical Transactions of the Royal Society B: Biological Sciences* **304**, 425–434.

Weiss, I. M., Göhring, W., Fritz, M. and Mann, K. (2001). Perlustrin, a Haliotis laevigata (Abalone) Nacre Protein, Is Homologous to the Insulin-like Growth Factor Binding Protein N-Terminal Module of Vertebrates. *Biochemical and Biophysical Research Communications* **285**, 244–249.

Weiss, I. M., Kaufmann, S., Mann, K. and Fritz, M. (2000). Purification and Characterization of Perlucin and Perlustrin, Two New Proteins from the Shell of the Mollusc *Haliotis laevigata*. *Biochemical and Biophysical Research Communications* **267**, 17–21.

Weiss, I. M., Tuross, N., Addadi, L. and Weiner, S. (2002). Mollusc larval shell formation: amorphous calcium carbonate is a precursor phase for aragonite. *J. Exp. Zool.* **293**, 478–491.

Westbroek, P., de Jong, E. W., van der Waal, P., Borman, A. H., de Vrind, J. P. M., Kok, D., Bruijn, W. C. and Parker, S. B. (1984). Mechanisms of calcification in the marine alga *Emiliania huxleyi. Philosophical Transactions of the Royal Society of London, Series B* **304**, 435-443.

Wilt, F. (2002). Biomineralization of the Spicules of Sea Urchin Embryos. *Zoological Society of Japan.* **19** (3), 253-261.

Wolfe, K Smith, A.M., Trimby, P. and Byrne, M. (2012). Vulnerability of the paper nautilus (*Argonauta nodosa*) shell to a climate-change ocean: Potential for extinction by dissolution. *The Biological Bulletin* **223** (2), 236-244.

Wong, M. L. and Medrano, J. F. (2005). Real-time PCR for mRNA quantitation. *BioTechniques* **39**, 75–85.

Yano, M., Nagai, K., Morimoto, K. and Miyamoto, H. (2006). Shematrin: A family of glycine-rich structural proteins in the shell of the pearl oyster *Pinctada fucata. Comp. Biochem. Physiol. B, Biochem. Mol. Biol.* **144**, 254–262.

Young, J. R., Didymus, J. M.,Brown, P. R., Prins, B. and Mann S. (1992). Crystal assembly and phylogenetic evolution in heterococcoliths. *Nature* **256** (6), 516-518.

Young, J. R., Davis, S. A., Brown, P. R. and Mann, S. (1999). Coccolith ultrastructure and biomineralisation. *Journal of Structural Biology* **126** (3), 195-215.

Young, J. R., Henriksen, K. (2003). Biomineralization within vesicles: The calcite of coccoliths. *Reviews in Mineralogy and Geochemistry* **54**, 189-215.

Zhang, C. and Zhang, R. (2006). Matrix Proteins in the Outer Shells of Molluscs. *Mar. Biotechnol.* **8**, 572–586.

Zhang, C., Xie, L., Huang, J., Chen, L. and Zhang, R. (2006). A novel putative tyrosinase involved in periostracum formation from the pearl oyster (*Pinctada fucata*). *Biochemical and Biophysical Research Communications* 632–639.

Zhang, G., Fang, X., Guo, X., Li, L., Luo, R., Xu, F., Yang, P., Zhang, L., Wang, X., Qi, H., et al. (2012). The oyster genome reveals stress adaptation and complexity of shell formation. *Nature* **490**, 49-54.

Zhang, H. and Hare, M. P. (2012). Identifying and reducing AFLP genotyping error: an example of tradeoffs when comparing population structure in broadcast spawning versus brooding oysters. *Heredity (Edinb)*. **108** (6), 616-625.

Zhang, Y., Xie, L., Meng, Q., Jiang, T., Pu, R., Chen, L. and Zhang, R. (2003). A novel matrix protein participating in the nacre framework formation of pearl oyster, *Pinctada fucata. Comparative Biochemistry and Physiology, Part B* **135**, 565–573.

Zippay, M. L. and Hofmann, G. E. (2010). Effect of pH on gene expression and thermal tolerance of early life history stages of red abalone (*Haliotis rufescens*). *Jornal of Shellfish Research* **29**, 429–439.

And finally...

“The world’s my oyster”

After Shakespeare (1602)